Design and Performance Analysis of Distributed Space Time Coding Schemes for Cooperative Wireless Networks

Gbenga Owojaiye

A thesis submitted to the University of Hertfordshire in partial fulfilment of the requirements for the degree of Doctor of Philosophy

The programme of research was carried out in the Science and Technology Research Institute (STRI), University of Hertfordshire, United Kingdom.

June 2012

Acknowledgments

My sincere gratitude goes to my supervisor Prof Yichuang Sun for his guidance and continuous motivation. His technical advice and method of instruction have been exceedingly valuable and have helped to create a wonderful learning experience. His expertise, perceptiveness, and encouragement have helped me reach many academic milestones, and have helped to develop a solid foundation for my future endeavours.

I will also like to thank Dr. Fabien Delestre for taking time out of his busy schedule to assist me with some significant aspects of my work. I also want to thank my second supervisor Dr. David Lauder, my research office colleagues, and my dear friends for their kindness and encouragement.

I cannot express enough gratitude to my family for the love, affection, and support they have shown me all my life. They have stood by me all the way and have been there for me at all times, their affection means more than words can express. Finally, I thank the Almighty God for the grace and guidance He has granted me up till this point, and for the many future achievements He has planned for me. I hope the completion of this PhD will be a starting point for bigger things.

Abstract

In this thesis, space-time block codes originally developed for multiple antenna systems are extended to cooperative multi-hop networks. The designs are applicable to any wireless network setting especially cellular, adhoc and sensor networks where space limitations preclude the use of multiple antennas. The thesis first investigates the design of distributed orthogonal and quasi-orthogonal space time block codes in cooperative networks with single and multiple antennas at the destination. Numerical and simulation results show that by employing multiple receive antennas the diversity performance of the network is further improved at the expense of slight modification of the detection scheme. The thesis then focuses on designing distributed space time block codes for cooperative networks in which the source node participates in cooperation. Based on this, a source-assisting strategy is proposed for distributed orthogonal and quasi-orthogonal space time block codes. Numerical and simulation results show that the source-assisting strategy exhibits improved diversity performance compared to the conventional distributed orthogonal and quasi-orthogonal designs.

Motivated by the problem of channel state information acquisition in practical wireless network environments, the design of differential distributed space time block codes is investigated. Specifically, a co-efficient vector-based differential encoding and decoding scheme is proposed for cooperative networks. The thesis then explores the concatenation of differential strategies with several distributed space time block coding schemes namely; the Alamouti code, square-real orthogonal codes, complex-orthogonal codes, and quasi-orthogonal codes, using cooperative networks with different number of relay nodes. In order to cater for high data rate transmission in non-coherent cooperative networks, differential

distributed quasi-orthogonal space-time block codes which are capable of achieving full code-rate and full diversity are proposed. Simulation results demonstrate that the differential distributed quasi-orthogonal space-time block codes outperform existing distributed space time block coding schemes in terms of code rate and bit-error-rate performance. A multi-differential distributed quasi-orthogonal space-time block coding scheme is also proposed to exploit the additional diversity path provided by the source-destination link.

A major challenge is how to construct full rate codes for non-coherent cooperative broadband networks with more than two relay nodes while exploiting the achievable spatial and frequency diversity. In this thesis, full rate quasi-orthogonal codes are designed for non-coherent cooperative broadband networks where channel state information is unavailable. From this, a generalized differential distributed quasi-orthogonal space-frequency coding scheme is proposed for cooperative broadband networks. The proposed scheme is able to achieve full rate and full spatial and frequency diversity in cooperative networks with any number of relays. Through pairwise error probability analysis we show that the diversity gain of the proposed scheme can be improved by appropriate code construction and sub-carrier allocation. Based on this, sufficient conditions are derived for the proposed code structure at the source node and relay nodes to achieve full spatial and frequency diversity. In order to exploit the additional diversity paths provided by the source-destination link, a novel multi-differential distributed quasi-orthogonal space-frequency coding scheme is proposed. The overall objective of the new scheme is to improve the quality of the detected signal at the destination with negligible increase in the computational complexity of the detector.

Finally, a differential distributed quasi-orthogonal space-time-frequency coding scheme is proposed to cater for high data rate transmission and improve the performance of non-coherent cooperative broadband networks operating in highly mobile environments. The

approach is to integrate the concept of distributed space-time-frequency coding with differential modulation, and employ rotated constellation quasi-orthogonal codes. From this, we design a scheme which is able to address the problem of performance degradation in highly selective fading environments while guaranteeing non-coherent signal recovery and full code rate in cooperative broadband networks. The coding scheme employed in this thesis relaxes the assumption of constant channel variation in the temporal and frequency dimensions over long symbol periods, thus performance degradation is reduced in frequency-selective and time-selective fading environments. Simulation results illustrate the performance of the proposed differential distributed quasi-orthogonal space-time-frequency coding scheme under different channel conditions.

Table of Contents

List of Figures

List of Acronyms

ASTM: American Society for Testing and Material

AF: amplify and forward

BPSK: binary phase shift keying

BER: bit error rate

CSI: channel state information

CP: cyclic prefix

DF: decode-and-forward

DAF: differential amplify and forward

DDF: differential decode and forward

DPSK: differential phase shift keying

DOSTBC: distributed orthogonal space time block codes

DQSFC: distributed quasi-orthogonal space frequency codes

DQSTBC: distributed quasi-orthogonal space time block codes

DQSTFC: distributed quasi-orthogonal space time frequency codes

DSFC: distributed space frequency codes

DSTBC: distributed space time block codes

DSTBC-OFDM: DSTBC orthogonal frequency division multiplexing

DSTFC: distributed space time frequency codes

FFT: fast Fourier transform

ML: maximum likelihood

MIMO: multiple input multiple output

MISO: multiple input single output

PEP: pairwise error probability

PSK: phase shift keying

OFDM: orthogonal frequency division multiplexing

QAM: quadrature amplitude modulation

QPSK: quadrature phase shift keying

QSF: quasi-orthogonal space frequency

QSTBC: quasi-orthogonal STBC

SNR: signal-to-noise ratio

SISO: single input single output

SA: source assisting

SA-DOSTBC: source assisting distributed orthogonal space time block codes

SA-DQSTBC: source assisting distributed quasi-orthogonal space time block codes

SF: space frequency

ST: space time

STBC: space time block codes

STF: space time frequency

List of Important Symbols

$\boldsymbol{a}$: A bold-face lower case letter denotes a vector

$\mathbf{A}$: A bold-face upper case letter denotes a matrix

$|x|$: Absolute value of x

$(\cdot)^*$: Conjugate operation

$(\cdot)^H$: Conjugate-transpose operation

$det(\boldsymbol{S})$: Determinant of $\boldsymbol{S}$

$diag[s_1, s_2, \dots, s_N\ ]$: $N \times N$ Diagonal matrix with diagonal entries $s_1, s_2, \dots, s_N$

$\mathbb{C}^{T \times N}$: Dimension of a matrix of complex numbers

$E(\cdot)$: Expectation of a random variable

$\|\boldsymbol{X}\|_F$: Frobenius norm of the matrix $\boldsymbol{X}$

$\boldsymbol{a} \odot \boldsymbol{b}$: Hadamard product or entry-wise product of the vectors $\boldsymbol{a}$ and $\boldsymbol{b}$

$\boldsymbol{A} \odot \boldsymbol{B}$: Hadamard product or entry-wise product of the matrices $\boldsymbol{A}$ and $\boldsymbol{B}$

$\boldsymbol{I}_N$: $N \times N$ Identity matrix

$j = \sqrt{-1}$

$\boldsymbol{A} \otimes \boldsymbol{B}$: Kronecker product of the matrices $\boldsymbol{A}$ and $\boldsymbol{B}$

$\lfloor x \rfloor$: Largest integer smaller than x

$tr(\cdot)$: Trace function

$(\cdot)^T$: Transpose operation

$var(\cdot)$: Variance of a random variable

Declaration

The following papers have been published and parts of their material are included in this thesis:

Published Manuscripts

- Gbenga Owojaiye and Yichuang Sun, "Source Assisting Strategy for Distributed Space-time Block Codes", IEEE International Symposium on Wireless Communication Systems, York, Sep. 2010
- Gbenga Owojaiye, Yichuang Sun, Nandini Alinier and Pandelis Kourtessis "A Systematic Study of the Behaviour of PMEPR in Relation to OFDM Design Parameters", 12th Annual Postgraduate Symposium on the Convergence of Telecommunications, Networking and Broadcasting, Liverpool, Jun. 2011
- Gbenga Owojaiye and Yichuang Sun, "Generalized Differential Distributed Space-time Block Codes using Co-efficient Vectors", IEEE 8th International Wireless Communications and Mobile Computing Conference, Cyprus, 2012
- Gbenga Owojaiye and Yichuang Sun, "Differential Distributed Quasi-orthogonal Space-Time-Frequency Coding", IEEE Wireless Advanced Conference, London, 2012
- Fabien Delestre, Gbenga Owojaiye and Yichuang Sun, "An Iterative Joint Channel Estimation and Data Detection Technique for MIMO-OFDM Systems" IEEE 8th International Wireless Communications and Mobile Computing Conference, Cyprus, 2012

Manuscripts Submitted/Accepted for Publication

- Gbenga Owojaiye and Yichuang Sun, "Co-efficient Vector Based Distributed Quasi-orthogonal Codes in Cooperative Networks", manuscript submitted to IEEE International Performance Computing and Communications Conference, Illinois, 2012
- Gbenga Owojaiye and Yichuang Sun "Focal Design Issues Affecting the Deployment of Traffic Monitoring Wireless Sensor Networks" manuscript accepted by IET Intelligent Transport Systems Journal, 2012
- Gbenga Owojaiye and Yichuang Sun, "Differential and Multi-differential Distributed Quasi-orthogonal Space Time Block Codes", manuscript submitted to IEEE Transactions on Wireless Communications, 2012
- Gbenga Owojaiye, Fabien Delestre, and Yichuang Sun, "Quasi-orthogonal Space-frequency Coding in Non-coherent Cooperative Broadband Networks", manuscript submitted to IEEE Transactions on Communications, 2012
- Gbenga Owojaiye, Fabien Delestre, and Yichuang Sun, "Differential Distributed Space Time Frequency Coding using Quasi-orthogonal Codes", manuscript submitted to IEEE Transactions on Vehicular Technology, 2012
- Gbenga Owojaiye and Yichuang Sun "Focal Design Issues Affecting the Deployment of Wireless Sensor Networks for Pipeline Monitoring" manuscript submitted to Elsevier Adhoc Networks Journal, 2012
- F. Delestre, G. Owojaiye, and Y. Sun, "An Efficient SFBC Pilot-Aided Channel Estimation Method for MIMO-OFDM Systems over Mobile Frequency Selective Fading Channels", manuscript submitted to IEEE Transactions on Wireless Communications, 2012
- G. Owojaiye and Y. Sun, "Optimizing Capacity Gain and Power Efficiency in Wireless Multimedia Sensor Networks", manuscript submitted to IEEE ISM2012, 2012

1 Introduction

1.1 Background

Increasing interest in wireless applications has led to the continuous development of wireless technologies. Users of wireless applications now get more and more dependent on wireless devices that provide mobile data usage, real-time information processing, and multi-media sharing. Moreover, present-day convergence and interoperability of wireless technologies has further increased the amount of services that can be provided. Consequently, there has been a proportionate surge in research and development efforts which aim to ensure that wireless technologies meet the expectations of high quality of service. Existing conditions, specifically the nature of the wireless communication channel however poses a major challenge to the performance of these wireless technologies. Radio waves propagated through wireless channels are affected by static and mobile obstacles in the surrounding environment. These obstacles which may vary from buildings, hills, and vehicles in outdoor environments, to walls, furniture, and people in indoor environments, reflect, refract, diffract, or attenuate the propagated signal. The result is that the propagated signal is scattered out in different directions and multiple independent copies of the original transmitted signal arrive at the receiver at different times. The receiver thus observes multiple delayed versions of the transmitted signal which may add up destructively leading to erroneous detection. This phenomenon is referred to as 'multi-path fading', and it severely hampers the quality of service that can be provided by wireless technologies.

One of the most promising methods to combat multi-path fading is to employ 'diversity' techniques. Diversity techniques employ a concept whereby multiple independent copies of the transmitted signal are deliberately propagated over multiple channels with different

characteristics. The concept is based on the fact that it is unlikely that different channels will experience identical fading events. Thus the probability that all the multiple independent signals will be corrupted by fading is considerably low. There are several types of diversity techniques that have been popularly employed to combat fading in wireless networks. These include temporal diversity, frequency diversity, and spatial diversity. While temporal diversity techniques transmit multiple copies of the transmitted signal at different time instants, frequency diversity techniques spread the transmitted signal across different frequency channels or across multiple frequency carriers in a wide spectrum. Spatial diversity techniques on the other hand have received the widest attention compared to other popular diversity techniques. Spatial diversity is achieved by propagating independent versions of the transmitted signal over multiple transmit antennas, or employing multiple receive antennas to recover the transmitted signal. When multiple antennas are used at the transmitter it is referred to as transmit diversity. Conversely, when multiple receive antennas are employed at the receiver it is referred to as receive diversity. Spatial diversity techniques have been well exploited by multiple-input multiple-output (MIMO) systems. MIMO systems, also, referred to as multiple-antenna systems, improve the robustness and reliability of communication by employing multiple transmit and/or multiple receive antennas, and utilizing spatial diversity techniques. In order to reap the benefits of spatial diversity, the multiple antennas need to be spaced sufficiently far apart, usually antenna separation of at least a few wavelengths is required to guarantee spatial diversity.

1.1.1 Cooperative Diversity

As wireless technologies like cellular networks, multi-hop adhoc networks and wireless sensor networks continue to gain significant attraction in the wireless communications industry, it has become necessary to extend the benefits of spatial diversity to these

technologies. In order to extend these benefits, it is intuitive that the nodes or devices that constitute these networks have size restrictions and are able to incorporate only a limited level of complexity on the wireless terminal, in line with their associated power supply limitations. Thus, it is impractical to incorporate multiple antennas on the nodes that make up such networks [1]. The effects of multi-path fading is however critical in cellular, adhoc and sensor network scenarios because the physical deployment of nodes makes them more susceptible to interference from the environment. Thus, it is imperative to adopt a mechanism to achieve spatial diversity. Since the broadcast nature of the wireless medium makes it easy for communicating nodes to hear each other, it is possible for them to cooperate and share their physical resources specifically their single antennas, thereby creating a virtual multiple-antenna array. In other words, instead of traditionally relaying independent signals to the destination, nodes listen to each other and jointly communicate. Thus, several single antenna nodes cooperate to achieve spatial diversity by forming a distributed multiple antenna system. This concept is termed 'cooperative diversity'.

Cooperative diversity techniques have been increasingly used to exploit the benefits of spatial diversity in networks where space limitations preclude the use of multiple antennas. The different intermediate nodes or users that make up the network cooperatively use their single antennas to emulate multiple-antenna systems thereby increasing the reliability and capacity of transmission. Wireless networks that employ the concept of cooperative diversity are referred to as cooperative networks.

1.1.2 Cooperative Diversity Protocols

Since the works of Laneman et al [2] and Sendonaris et al [3] [4] that introduced the concept of cooperative diversity, several protocols have been investigated in [5] to initiate their implementation. From these, two major cooperative diversity protocols have emerged,

namely: the amplify-and-forward (AF) and decode-and-forward (DF) protocols. These models are inspired by the observation [6] and cooperation [7] schemes respectively. In order to explain the concept of the AF and DF models, consider a classic multi-hop wireless network with; a source node, one relay node, and a destination as illustrated in Fig.1.1. This analysis can easily be extended to a network with multiple relay nodes. The complexity of the network model is intentionally limited for ease of potential explanation. For a particular transmission interval between the source node and the destination, the intermediate relay node does not have any data symbol of its own to transmit; it is only used to enhance the quality of communication between the source node and the destination via cooperation. Let f denote the channel between the source node and the relay node and g the channel between the relay node and the destination. The channels are assumed to capture the effects of multipath fading and remain coherent throughout the transmission interval.

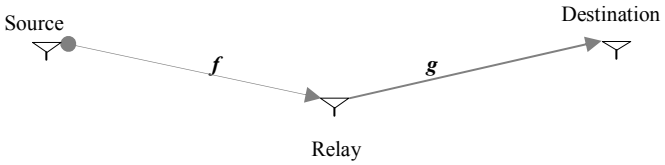

Fig.1.1 Multi-hop wireless network

In the AF model, the relay node receives the information signal transmitted by the source node, amplifies it, and forwards it to the destination, without any additional signal processing. Then the destination receives and makes a final decision on the transmitted information signal. If the source node sends information signal s_i at the i_{th} transmission interval, the signal received at relay node is given by:

$$r_i = f s_i + n_i \tag{1.1}$$

where n_i captures the effect of the relay noise. As the relay node receives r_i, it applies amplification co-efficient α, such that it transmits αr_i. Thus the signal transmitted by the relay node is:

$$t_i = \alpha(fs_i + n_i) \tag{1.2}$$

In practice the amplification co-efficient is carefully set such that it does not cause saturation at the amplifier of the relay when f is very large. The systematic selection of α to achieve optimum power allocation among relays is discussed in [8]. From (1.2) we note that the noise at the relay is also amplified, this is a major challenge of the AF scheme as it induces additional noise at the destination. Nevertheless, the model is simple to implement and since t_i in (1.2) contains the information signal s_i, the protocol can be effectively used to achieve cooperative diversity.

The DF model allows the relay node to decode the received signal from the source node, re-encode it and forward the resulting signal to the destination, without having to amplify it as in the AF case. In the DF model, while the relay node receives r_i as in (1.1), it transmits $\tilde{s}_i$ which denotes the decoded version of s_i. The fundamental difference between the AF and DF model is based on the fact that in the latter a re-encoded signal is sent from the relay node which precludes the amplified noise at the relay. However the ability of the DF model to fully exploit the benefits of cooperative diversity depends on whether the relay node can correctly decode the received information signal. In other words, incorrect detection may lead to error propagation at the relay node, especially when the source-relay link is weak. To mitigate this, error detection coding can be applied such that $\tilde{s}_i$ tends to s_i as much as possible. In [9] cyclic redundancy check (CRC) codes are used to alleviate erroneous decoding at the relay. The authors in [10] apply a signal-to-noise ratio (SNR) threshold at the relay such that

cooperation only takes place when the received SNR is larger than the threshold. Generally, depending on the design, the DF model is likely to exhibit slightly better error performance than the AF model, however, added error detection coding at the relay may increase system complexity. On the other hand the AF model has the low complexity advantage and it has been shown in [11] that the performance of the AF model approaches the DF model as far as diversity is concerned.

1.1.3 Diversity Coding Schemes

In addition to the AF and DF protocols discussed in the previous section, other algorithms have been integrated with cooperative systems to enhance diversity performance. Unlike un-coded cooperative systems where signals are directly relayed to the destination using either the AF or DF protocol, other cooperative scenarios exist where diversity coding schemes are integrated with cooperative signaling. Several types of diversity coding schemes have been investigated for cooperative networks, and the results show that they can yield significant performance gains. Amongst the different diversity coding schemes, channel coding schemes [12] [13], network coding schemes [14] [15], repetition-based coding schemes [5] [16] [17], and distributed space time block codes [18] have been popularly investigated in the literature.

The idea of integrating channel coding schemes with cooperative communication was first introduced by Hunter et al [12] and Stefanov et al [13]. These works base their concept on the fact that cooperative systems employ the block fading channel model, thus channel codes that have been popularly used for block fading channels in non-cooperative systems, can be integrated with cooperative communication. Since then different types of channel codes have been used in cooperative networks. The rate-compatible punctured codes were used in [12] and [19], turbo codes have also been popularly used with cooperative signaling in [20]. When channel coding is integrated with cooperative communication, the cooperating nodes operate

using a time sharing approach such that nodes transmit and receive on different channels. Generally, orthogonal channels are used, such that the signals transmitted by the cooperating nodes experience independent fading. The use of orthogonal channels however results in loss of bandwidth which is a major drawback.

The idea of integrating network coding [21] with cooperative signaling has also been well investigated. The fundamental idea is to implement simple coding capability at relay nodes in order to enhance network capacity gain. The results in [15] show that for cooperative systems, network coding yields additional diversity performance especially when there is a large number of cooperating nodes. It is also possible to incorporate existing channel codes on top of a network coding scheme.

Laneman in [22] derived an upper-bound for the diversity gain achievable in a cooperative network by comparing the AF and DF models. In his work, 'repetition-based coding' is adopted where the source node is allocated a first time slot to transmit its information signal, and the relay node is allocated a second time slot to convey this signal to the destination. The results show that the network achieves a diversity order d when there are d cooperating relay nodes in the network. The simplicity of the strategy and its ability to achieve full diversity order has spanned research into repetition-based coding in cooperative networks [5] [16] [17] [23]. In order to continue with our discussion, we define the 'data rate' of a cooperative network as the average number of symbols transmitted by the relay nodes per transmission interval. This implies that the data rate of the repetition-based cooperative network is $1/d$, and $1/(1+d)$ when the source node is involved in cooperation [8], clearly this implies a loss in terms of data rate and bandwidth efficiency. To alleviate the loss of bandwidth characterized by the aforementioned diversity coding schemes, researchers are now looking into techniques to improve bandwidth efficiency.

A new approach to ensure cooperative diversity in multi-hop networks while evading the bandwidth penalty emerges from the idea of space time block codes (STBC) in multiple antenna systems [24]-[26]. This idea aims at applying STBC in a distributed fashion among cooperating nodes giving rise to the concept of 'distributed space time block codes' (DSTBC). DSTBC was first proposed in [27] where the cooperating nodes distribute the codeword matrix amongst themselves in such a fashion that the structure of the coding matrix is retained at the destination. The architecture of cellular, multi-hop Adhoc and sensor networks makes them particularly amenable to DSTBC. DSTBC has been shown in [28] to exhibit improved bandwidth efficiency when compared to repetition-based coding, thus the work in this thesis focuses on the design of practical DSTBC for cooperative networks.

1.2 Motivation

In order to improve the performance of MIMO systems, many works have focused on the design of STBC which exploits the available spatial and temporal diversity in fading channels. The reliability and performance improvements offered by STBC has instigated the wide popularity and focus in the research area. Following these developments, it has become necessary to extend the benefits of STBC to cooperative multi-hop networks. DSTBC schemes in cooperative multi-hop networks can be considered as the counterpart of STBC schemes in MIMO systems. Thus, in this work, the focus is to develop DSTBC schemes for cooperative networks. The work concentrates on the design of several DSTBC schemes for cooperative networks with different configurations, operating in different scenarios. The principal objective of this work is to improve the achievable diversity gain and enhance system performance.

In most of the works that have designed DSTBC for cooperative networks, the source node is not involved in cooperation. Thus there is no direct link between the source node and the destination. However considering that additional benefits can be exploited in terms of diversity and error performance when the source node is actively involved in cooperation, we propose a DSTBC scheme for cooperative networks where the source node is involved in the cooperative process. This strategy, which is discussed in Chapter 2 of this thesis, is able to improve the diversity performance of cooperative networks.

In order to exploit the benefits of cooperative diversity, cooperative networks utilizing DSTBC require full channel state information (CSI) at the destination. In practice, some scenarios exist where CSI is unavailable or cannot be acquired. To mitigate this problem in MIMO systems, STBC were incorporated with differential schemes and differential STBC became popular. Compared to MIMO systems, the problem of channel estimation is even more critical in single-antenna multi-hop networks with large number of nodes such as adhoc or wireless sensor networks. Also, because of the power constraints of this sort of networks, a viable solution is to incorporate differential strategies with DSTBC schemes to tackle the problem of CSI acquisition. Thus, in Chapter 3 of this thesis, the focus is on designing differential DSTBC schemes for cooperative networks. Specifically, a co-efficient vector-based differential DSTBC scheme is proposed and the performance in cooperative networks is investigated.

In order to meet high data rate requirements in MIMO systems, full code-rate STBC schemes are of the essence. Orthogonal STBC schemes are capable of achieving full code-rate for multiple-antenna systems with a maximum of two transmit antennas. When orthogonal STBC schemes are utilized in MIMO systems with more than two transmit antennas, code-rate deficiency is experienced. Similarly, cooperative networks with more than two relay nodes

experience code-rate deficiency when orthogonal DSTBC schemes are utilized. To counter the code-rate deficiency problem, quasi-orthogonal STBC were proposed for multiple-antenna systems. Thus in this work, predominantly in Chapter 4, the focus is on developing quasi-orthogonal designs for cooperative networks. In order to achieve full code-rate designs for cooperative networks operating in environments where CSI acquisition is impractical, differential strategies are integrated with quasi-orthogonal DSTBC and the performance is investigated.

Some works in the literature now investigate DSTBC schemes for cooperative broadband multi-hop networks transmitting across frequency selective channels. This paradigm has led to the realization of DSTBC orthogonal frequency division multiplexing (DSTBC-OFDM) schemes and distributed space-frequency coding (DSFC) schemes. In DSTBC-OFDM, elements of the space-time (ST) code matrix transmitted by cooperating relay nodes are applied at individual sub-carriers over multiple OFDM blocks. Such schemes are able to exhibit maximum spatial and temporal gain at the expense of frequency diversity and inherent processing delay. To exploit the achievable frequency diversity and counteract the processing delay, DSFC transmits elements of the ST code matrix across multiple sub-carriers within a single OFDM block. Further comparative analysis of these schemes indicates that while DSTC-OFDM is insensitive to high delay spread, it is highly susceptible to Doppler frequency. This limits the application of the scheme to slow fading channels. On the other hand, DSFC is more robust to fast fading channels such that the scheme exhibits maximum frequency and spatial proficiency when utilized in fast fading environments. The outlined benefit of DSFC over DSTC-OFDM has instigated us to focus on design of DSFC for cooperative broadband multi-hop networks in Chapter 5 of this thesis.

The final aspect of this thesis identifies that additional temporal diversity advantage can be achieved by extending the space-time-frequency (STF) designs that are now popular in multiple-antenna systems, to cooperative networks. STF schemes have been implemented for multiple antenna broadband networks, and authors show that such schemes can exploit temporal diversity by coding over multiple OFDM blocks. Thus, in Chapter 6 of this thesis, we propose distributed STF schemes for use in cooperative broadband networks.

1.3 Thesis Contribution

The major contributions of this thesis are summarized as follows:

- A source-assisting (SA) strategy is proposed for distributed orthogonal and quasi-orthogonal space-time block coded cooperative multi-hop networks. Numerical and simulation results show that the SA strategy exhibits improved diversity performance compared to the conventional distributed orthogonal and quasi-orthogonal designs, at the expense of slightly increased complexity of the maximum likelihood (ML) detector. An explanation on the modified structure of the ML detector is provided.

- Co-efficient vector based differential orthogonal DSTBC is proposed for cooperative networks utilizing the DF protocol. We present the generalized mapping scheme and differential recipe for utilizing co-efficient vectors in cooperative networks with any number of relay nodes. Using simulation results, we compare and contrast the unitary matrices and co-efficient vector designs in terms of computational complexity and bit error rate (BER) performance.

- Differential distributed quasi-orthogonal STBC (DQSTBC) is proposed for cooperative networks. The work extends non-unitary full code-rate quasi-orthogonal codes utilized in multiple-antenna systems to differential cooperative networks where channel information is unavailable. We show how non-unitary matrices are constructed from a proper choice of constellation sets. We then present the full differential encoding and decoding procedure for non-unitary full code-rate quasi-orthogonal codes in cooperative networks with 4 relay nodes. Next, we identify that significant benefits can be realized in terms of SNR performance when a direct source-destination link exists. From this, we propose a multi-differential scheme for cooperative networks. The overall objective of our new scheme is to improve the quality of the detected signal at the destination with negligible increase in the computational complexity of the detector.

- We extend full rate quasi-orthogonal codes to differential cooperative broadband networks where channel information is unavailable. From this, we propose a generalized differential distributed quasi-orthogonal space-frequency coding (DQSFC) scheme for cooperative broadband networks. Our proposed scheme is able to achieve full rate and full spatial and frequency diversity in cooperative networks with any number of relays. Through pairwise error probability analysis we show that the diversity gain of our scheme can be improved by appropriate code construction and sub-carrier allocation. Based on this, we derive sufficient conditions for the proposed code structure at the source node and relay nodes to achieve full spatial and frequency diversity. Considering that significant benefits in terms of SNR

performance can be realized when a direct link exists between the source node and the destination, we propose a multi-differential DQSFC scheme.

- We propose a differential distributed quasi-orthogonal space-time-frequency coding (DQSTFC) scheme to cater for high data rate transmission and improve the performance of non-coherent cooperative broadband networks operating in highly mobile environments. Our approach is to integrate the concept of distributed space-time-frequency coding (DSTFC) with differential modulation, and employ rotated constellation quasi-orthogonal codes. From this, we design a scheme which is able to address the problem of performance degradation in highly selective fading environments while guaranteeing non-coherent signal recovery and full code rate in cooperative broadband networks. The coding scheme employed in our work relaxes the assumption of constant channel variation in the temporal and frequency dimensions over long symbol periods, thus performance degradation is reduced in frequency-selective and time-selective fading environments. Simulation results illustrate the performance of our proposed differential DQSTFC scheme in different channel conditions.

1.4 Organization

In Chapter 2, we design and analyze the performance of distributed orthogonal and quasi-orthogonal STBC in multi-hop networks incorporating single and multiple antennas at the destination. The rest of Chapter 2 is organized as follows: In Section 2.2, the properties of different wireless channel models are discussed and the cooperative system architecture is presented. In Section 2.3 we design distributed orthogonal and quasi-orthogonal STBC using our proposed SA strategy, and present the detection schemes used for signal recovery. We conclude Section 2.3 by showing how a reduced constellation order in the first time slot further improves the BER performance of the proposed scheme. In Section 2.4, distributed orthogonal and quasi-orthogonal STBC is extended to cooperative networks incorporating multiple receive-antennas at the destination terminal. We show how our SA strategy can be implemented in such networks. The improved diversity performance offered by our SA strategy is analyzed via numerical and simulation results in Section 2.5. In addition, we show how the use of multiple antennas at the destination improves the diversity performance.

In Chapter 3, we present differential DSTBC schemes for cooperative multi-hop networks. The rest of Chapter 3 is organized as follows: In Section 3.2, we present the concept of differential modulation, and review differential encoding and decoding in non-cooperative networks. We then show how the 'differential decode-and-forward' and 'differential amplify-and-forward' cooperative diversity protocols are implemented in cooperative networks. We present the full differential encoding and decoding procedure using two main differential concepts in Section 3.3 and Section 3.4, namely; 'co-efficient vectors' and 'unitary matrices' respectively. In Section 3.3 we propose differential orthogonal designs for cooperative networks based on co-efficient vectors. We present the generalized mapping scheme and

differential recipe for utilizing co-efficient vectors in cooperative networks with any number of relay nodes. In Section 3.4 we show how differential orthogonal designs can be implemented in cooperative networks using unitary matrices.The differential concept is generalized in Section 3.5 to cooperative networks with three, four, and eight relay nodes using square real-orthogonal codes. In Section 3.6 we analyse via simulation the performance of all the aforementioned differential schemes.

In Chapter 4, we design differential and multi-differential DQSTBC for cooperative networks. The rest of Chapter 4 is organized as follows. Section 4.2 details the differential encoding and decoding procedure for DQSTBC in cooperative networks. In Section 4.3 we introduce our multi-differential protocol while Section 4.4 presents some simulation results.

In Chapter 5, quasi-orthogonal space-frequency codes are designed for cooperative broadband networks operating in environments where CSI acquisition is impractical. The rest of Chapter 5 is organized as follows: In Section 5.2 we present the quasi-orthogonal space frequency (QSF) system model and discuss how the SF codes are designed at the source node and the relay nodes, we also present the structure of the quasi-orthogonal codes used in our scheme. Section 5.3 covers differential encoding and decoding using quasi-orthogonal space-frequency codes. Section 5.4 contains the pairwise error probability (PEP) analysis and discussions on diversity improvement. In Section 5.5 we introduce our multi-differential protocol, and Section 5.6 presents some simulation results.

In Chapter 6, the concepts of; differential modulation, STF mapping, and quasi-orthogonal coding are combined to cater for cooperative networks operating in highly selective fading environments.The rest of the Chapter 6 is organized as follows: Section 6.2discusses STF mapping, while the encoding and decoding procedure for differential DQSTFC is covered in

Section 6.3. Section 6.4 presents some simulation results and Section 6.5 contains the conclusion.

Finally, Chapter 7 concludes the thesis and gives directions for further research.

2. Distributed Space Time Block Codes

2.1 Introduction

As STBC designed for multiple antenna systems become readily extendable to the distributed nature of multi-hop networks, many researchers exploit this idea by extending the STBC designs to single antenna multi-hop networks. In this strategy, the cooperating nodes distribute the codeword matrix amongst themselves in such a fashion that the structure of the coding matrix is retained at the destination. Cooperative networks utilizing DSTBC adopt a two-stage 'transmit-and-cooperate' strategy using either the AF or DF relaying protocol. In the 'transmit' stage, the source node sends information signals to the relay nodes. In the 'cooperate' stage, the relay nodes jointly transmit linear representations of their received signals to the destination. If the DF protocol is utilized, the relay nodes decode the information signal received from the source node before retransmission. On the other hand if the AF protocol is utilized, the relay nodes simply amplify the received signal before retransmission. Based on this, DSTBC schemes have been extensively employed in cooperative networks. The Alamouti code has been used for cooperative networks in [29], real and complex orthogonal codes have been used in [30], quasi-orthogonal codes were used in [31], while the authors in [32] employed both orthogonal and quasi-orthogonal codes. Simulation results show improved performance and beneficial results compared to un-coded cooperative signaling.

In this chapter we design and analyze the performance of distributed orthogonal and quasi-orthogonal STBC in multi-hop networks incorporating single and multiple antennas at the destination. We focus on multi-hop cooperative networks where the source node participates in cooperation. We present the scenario where the source node is actively involved in

cooperation and propose a source-assisting (SA) strategy for our distributed orthogonal and quasi-orthogonal STBC. We then introduce cooperative networks with multiple receive-antennas at the destination. We show that by employing multiple receive-antennas, the diversity performance of the network is further improved at the expense of slight increase in the complexity of the detection scheme.

The rest of Chapter 2 is organized as follows: In Section 2.2, the properties of different wireless channel models are discussed and the cooperative system architecture is presented. In Section 2.3 we design distributed orthogonal and quasi-orthogonal STBC using our proposed SA strategy, and present the detection schemes used for signal recovery. We conclude Section 2.3 by showing how a reduced constellation order in the first time slot further improves the BER performance of the proposed scheme. In Section 2.4, distributed orthogonal and quasi-orthogonal STBC is extended to cooperative networks incorporating multiple receive-antennas at the destination terminal. We show how our SA strategy can be implemented in such networks. The improved diversity performance offered by our SA strategy is analyzed via numerical and simulation results in Section 2.5. In addition, we show how the use of multiple antennas at the destination improves the diversity performance.

2.2 Channel Models and System Model

As discussed, the transmitted signal is propagated across multiple independent paths. Consequently, the signal arrives at the receiver at different trajectories. Fig. 2.1 illustrates a typical scenario where a transmitted signal is propagated in different ways en route the receiver. Multipath components of the transmitted signal arrive at the receiver because of the random nature with which the signal is propagated across the wireless environment. Based on this, researchers [33-35] have examined the fading effects of the wireless channel from the

perspective of two independent phenomena; the 'multipath time delay' and the 'Doppler spread'.

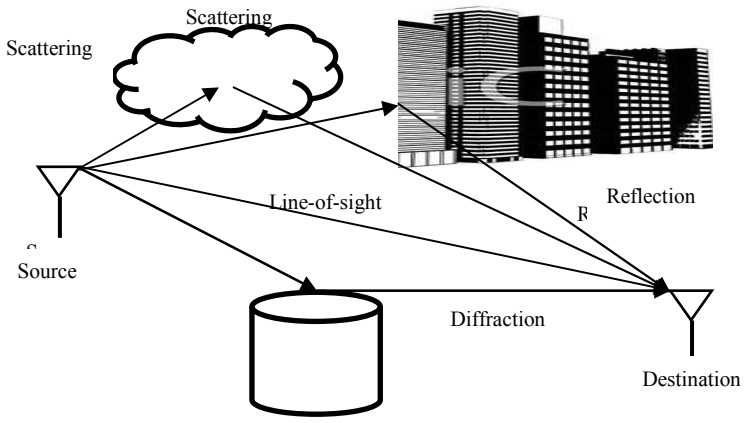

Fig.2.1 Signal propagation in a wireless channel

2.2.1 Multipath Time Delay in Wireless Channels

Multipath time delay occurs because the different multipath components of the transmitted signal arrive at the receiver at different time intervals. Since the multipath components are spatially dispersed by the objects in the wireless environment, individual versions experience separate fading events, specifically path loss and phase fluctuations. This lengthens the time required to receive the different versions of the baseband signal at the destination. This occurrence has been popularly termed 'signal time spreading' by Sklar et al [36]. The multipath channel is modeled as a linear time-varying channel in [35] and is depicted in Fig.2.2.

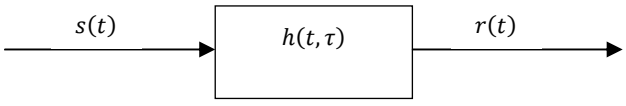

Fig.2.2 Linear time-varying impulse response of a multipath channel

If the multipath channel exhibits linear phase response and constant channel gain over a bandwidth that exceeds the bandwidth of the transmitted signal, the channel is referred to as a narrowband channel. In this case, the transmitted signal is said to have experienced 'flat fading' or 'frequency non-selective fading'. The impulse response of a flat fading channel is modeled mathematically as:

$$h(t,\tau) = \alpha(t)\delta(\tau) \tag{2.1}$$

where δ denotes the Dirac delta function. For frequency non-selective fading, the impulse response is only approximated by one delta function at $\tau = 0$ while the amplitude α may vary with time. When comparing the signal bandwidth with the channel bandwidth, the channel bandwidth is better explained by the delay spread D_s. Consider a multipath channel with L paths or L channel taps, the delay spread D_s can be computed as [35]:

$$D_s = \sqrt{\overline{\tau^2} - \bar{\tau}^2} \tag{2.2}$$

where $\bar{\tau}$ is the weighted average delay given by:

$$\bar{\tau} = \frac{\sum_{l=1}^{L} \alpha_l \tau_l}{\sum_{l=1}^{L} \alpha_l}, \text{and}$$

$$\overline{\tau^2} = \frac{\sum_{l=1}^{L} \alpha_l \tau_l^2}{\sum_{l=1}^{L} \alpha_l} \tag{2.3}$$

The amplitude and delay of the l_{th} path are α_l and τ_l respectively. The channel coherence bandwidth B_c is then computed from the multipath delay spread as follows:

$$B_c = \frac{1}{5D_s} \tag{2.4}$$

Thus, for a flat or frequency non-selective fading channel, the channel coherence bandwidth B_c is greater than the signal bandwidth B_s as illustrated in Fig. 2.3. In contrast, if the multipath channel exhibits linear phase response and constant channel gain over a bandwidth that is less than the bandwidth of the transmitted signal, the channel is referred to as a wideband channel and the transmitted signal is said to have experienced 'frequency selective fading'. The impulse response of a frequency selective fading channel is modeled mathematically as:

$$h(t,\tau) = \sum_{j=1}^{J} \alpha_j(t)\delta(\tau - \tau_j) \tag{2.5}$$

From (2.5) we can observe that, for frequency selective fading, the impulse response is approximated by a number of delta functions $\tau_j, j = 1, \ldots, J$ and each delta function has amplitude $\alpha_j(t)$ that varies independently with time. Similarly, for frequency selective fading, the channel coherence bandwidth B_c is smaller than the signal bandwidth B_s as illustrated in Fig. 2.4. Apart from the delay spread, other factors like transmission rate of the signal can also influence frequency selectivity [35]. However, based on the multipath time delay, the fading channel is either frequency selective or frequency non-selective.

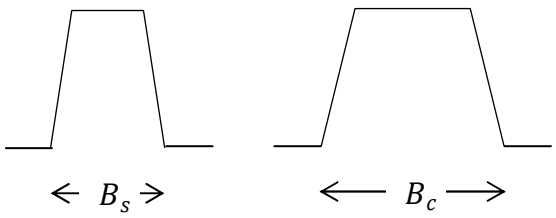

Fig.2.3 Frequency non-selective channel

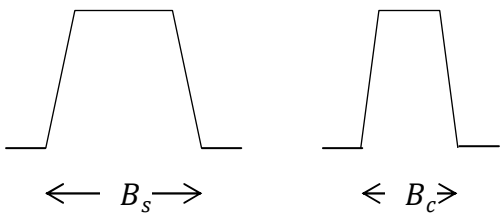

Fig.2.4 Frequency selective channel

2.2.2 Doppler Spread in Wireless Channels

The relative motion of the transmitter, receiver, or the surrounding objects in the wireless environment causes a shift in the frequency of the received signal. This shift in frequency which is relative to the speed of motion is referred to as 'Doppler shift'. The Doppler shift of the received signal is given as [34]:

$$f_d = \frac{v f_c}{c} \cos\theta \tag{2.6}$$

where v is the velocity of the mobile unit, c is the speed of light, f_c is the frequency of the transmitted signal arriving at the receiver at an incident angle θ. The various multipath components of the transmitted signal experience different Doppler shifts because they are propagated at different random angles θ. In addition, if the velocity of motion of the surrounding objects exceeds that of the mobile unit, the various multipath components experience time-varying Doppler shifts [35]. The accumulated multipath versions of the transmitted signal are thus received at the destination over a range of frequencies $f_c \pm f_s$ where f_s is the maximum Doppler shift given as $f_s = v f_c / c$. This results in spectral widening or frequency dispersion [34] of the channel, this range of frequencies over which the spectrum of the received signal in non-zero is popularly called 'Doppler spread'. If the bandwidth of the transmitted signal exceeds the Doppler spread of the channel, then the Doppler spread of the channel has little or no effect on the transmitted signal, in such case the channel is a 'slow fading' channel. In other words, the channel impulse response does not change significantly within the symbol period. Conversely, if the channel impulse response fluctuates significantly within the symbol period, Doppler spread affects the transmitted signal, and the channel is a 'fast fading channel'.

2.2.3 Wireless Channel Models

Due to the random nature of the multipath effects and the random nature of the objects in the wireless environment, it has become necessary to use statistical techniques to model the wireless channel. Rayleigh fading models [37] and Rician fading models [38] have been popularly used to describe the behavior of narrowband multipath channels. If the transmitted signal has a large number of multipath components without a dominant line-of-sight signal component, the envelope of the transmitted signal at any time instant is said to undergo a Rayleigh probability distribution. When a dominant line-of-sight signal component exists, the envelope of the transmitted signal is described by a Rician probability distribution. For wideband channels, frequency selective fading models [34] have been popular used to describe the behavior of the channel.

2.2.4 System Model

In general, the construction method for DSTBC originates from the construction of STBC where each of the cooperating nodes in a multi-hop network transmits a column of the STBC code matrix. In our design of DSTBC we consider the DF protocol such that at each t_{th} transmission interval, the cooperating relay nodes transmit an estimate $\tilde{s}_t$ of the source signal and use this to collectively construct the STBC in a distributed fashion. Consider a cooperative multi-hop network with a source node S, P intermediate relay nodes, and destination node D as shown in Fig.2.5. All nodes in the network are each assumed to have a single antenna. DSTBC can be seen as a mapping of T information symbols onto a $P \times T$ space-time codeword matrix $\boldsymbol{S}$, where P is the number of cooperating relay nodes.

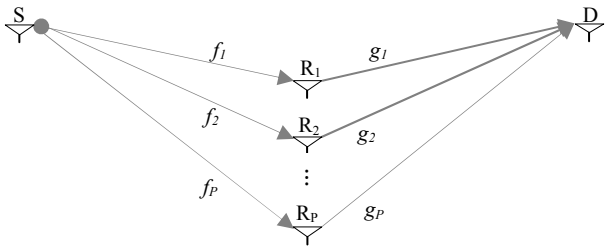

Fig.2.5 Cooperative network model

The Rayleigh flat fading channel vector between the source node and the p_{th} relay node is denoted by $\boldsymbol{f}_p$ while $\boldsymbol{g}_p$ denotes the Rayleigh flat fading channel vector between the p_{th} relay node and the destination. The coherence time of $\boldsymbol{f}_p$ and $\boldsymbol{g}_p$ is assumed to be larger than T. Let $\boldsymbol{s} = [s_1, \dots, s_T]$ denote the symbol vector transmitted from the source node at the t_{th} transmission interval. The signal vector received at p_{th} relay node is given as:

$$\boldsymbol{r}_p = \boldsymbol{f}_p \odot \boldsymbol{s} + \boldsymbol{n}_p \tag{2.7}$$

where $\boldsymbol{n}_p = \left[n_{p,1}, \dots, n_{p,T}\right]$ is the additive white Gaussian noise and $\odot$ represents entry-wise operation. With due cognizance of the DF model, the p_{th} relay node provides estimates $\tilde{\boldsymbol{s}}_p = \left[\tilde{s}_{p,1}, \dots, \tilde{s}_{p,T}\right]$, such that matrix $\boldsymbol{S}$ is formed by arranging the transmitted symbols from each relay node in a predefined array as follows:

$$\boldsymbol{S} = \begin{bmatrix} \tilde{s}_{1,1} & \tilde{s}_{1,2} & \cdots & \tilde{s}_{1,T} \\ \tilde{s}_{2,1} & \tilde{s}_{2,2} & \cdots & \tilde{s}_{2,T} \\ \vdots & \vdots & \ddots & \vdots \\ \tilde{s}_{P,1} & \tilde{s}_{P,2} & \cdots & \tilde{s}_{P,T} \end{bmatrix} \tag{2.8}$$

where the i_{th} row of $\boldsymbol{S}$, given as $\boldsymbol{S}_i = \left[\tilde{s}_{p,1}, \dots, \tilde{s}_{p,T}\right]$ contains the T information symbols transmitted by the p_{th} relay node, and the j_{th} column of $\boldsymbol{S}$, given as $\boldsymbol{S}_j = \left[\tilde{s}_{1,t}, \dots, \tilde{s}_{P,t}\right]^T$ contains the space-time symbols transmitted across all cooperating relay nodes at the t_{th}

transmission interval, $[\cdot]^T$ denotes transpose. This scheme achieves optimization in terms of unitary code-rate because from (2.8) it is clear that the P relay nodes transmit T information symbols in T transmission intervals.

2.3 Source Assisting Distributed Space Time Block Codes

In our discussion on DSTBC in Section 2.2.4 and in most of the works in the literature, for example [31] [39-41], the source node is not involved in cooperation, thus there is no direct link between the source node and the destination. However, considering that additional benefits can be exploited in terms of diversity and error performance when the source node is actively involved in cooperation, we propose a SA strategy for DF cooperative networks by employing orthogonal and quasi-orthogonal STBC originally designed for multiple antenna systems. From this, we model the source-assisting distributed orthogonal STBC (SA-DOSTBC) and the source-assisting distributed quasi-orthogonal STBC (SA-DQSTBC) in Section 2.3.1 and 2.3.3 respectively. Our approach allows us to directly apply the SA strategy on existing STBC used in [24] and [42] originally developed for multiple antenna systems. We first show how the SA strategy is applied on a single relay cooperative network. We then implement the SA strategy for cooperative networks with $P = 3$ relay nodes. For both cases, we adopt a time sharing approach where we allocate separate time slots for inter-node transmission, the time slot approach is clarified subsequently. We then present the additional benefits that can be achieved when the source node is actively involved in cooperation.

Our proposed SA strategy can be implemented in sensor networks or mesh networks where the nodes are is close proximity, and all the nodes are within communication range of the destination. In such scenarios it is expected that a direct path exists between the source and destination. Thus, the source can join the relays and participate in cooperation to enhance

BER and diversity performance at the destination. This performance improvement is illustrated in the simulation results. The SA strategy can also be implemented in cellular networks to enhance cell edge performance.

2.3.1 Source Assisting Distributed Orthogonal Space Time Block Codes

Distributed orthogonal space-time block codes (DOSTBC) are an important class of DSTBC because they achieve a diversity order equal to the number of cooperating nodes. The orthogonal structure of the coding matrix also enables low complexity decoding at the destination. In this section, we show how our SA strategy can be implemented using DOSTBC for a single relay cooperative network. In our work we use the Alamouti code of [24] designed for multiple-antenna systems.

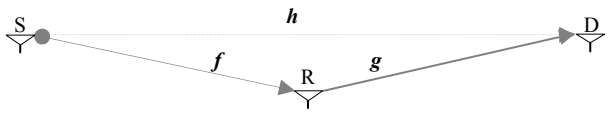

Fig.2.6 SA-DOSTBC Cooperative network model

Consider the SA cooperative multi-hop network with a source node S, single relay node R, and destination node D as shown in Fig.2.6. We apply the half duplex constraint such that the nodes cannot transmit and receive simultaneously. The model adopts a time sharing approach such that the transmission interval between the source node and the destination is sub-divided into time slots t_1 and t_2. In the first time slot t_1, the source node transmits $T = 2$ information symbols to the relay node. In the second time slot t_2, the source node and relay node simultaneously transmit information signals to the destination. Let $\boldsymbol{s} = [s_1, s_2]$ denote the symbol vector transmitted from the source node at t_1, we model the source-relay, relay-destination, and source-destination channels $\boldsymbol{f}$, $\boldsymbol{g}$ and $\boldsymbol{h}$ respectively as Rayleigh flat fading

channels where the channel coherence time is larger than T. Then the received signal vector at the relay node assuming perfect CSI with the DF model implemented is given as:

$$\boldsymbol{r} = \boldsymbol{f} \odot \boldsymbol{s} + \boldsymbol{n} \tag{2.9}$$

where $\boldsymbol{n} = [n_1, n_2]$ is the additive white Gaussian noise. To preserve the relay simplicity, we enable symbol-by-symbol detection using the DF protocol such that the relay node decodes the information signal $\boldsymbol{s}$ and provides estimates $\tilde{\boldsymbol{s}} = [\tilde{s}_1, \tilde{s}_2]$. Obviously what is implemented at t_1 is a direct transmission where the system behaves like a classic single-input-single-output (SISO) system while the transmission at t_2 can be seen as a classic cooperative multiple-input-single-output (MISO) scheme the only limiting factor being $\tilde{s}_t \neq s_t$. The Alamouti DOSTBC is implemented only at t_2 such that the source node now transmits:

$$\boldsymbol{s}_{(S)} = [s_1, -s_2{}^*] \tag{2.10}$$

and the relay node transmits:

$$\boldsymbol{s}_{(R)} = [\tilde{s}_2, \tilde{s}_1{}^*] \tag{2.11}$$

Assuming that perfect CSI is available at the destination, the signal vector received at the destination at t_2 becomes:

$$\boldsymbol{y} = [y_1, y_2]$$

$$y_1 = h_2 s_1 + g\tilde{s}_2 + z_1$$

$$y_2 = -h_2 s_2{}^* + g\tilde{s}_1{}^* + z_2 \tag{2.12}$$

where z_t is the additive white Gaussian noise assumed to be made up of iid random variables. We denote h_2 as the channel between the source node and the destination at t_2, and g as the

channel between the relay node and the destination. From (2.12) above it is obvious that the conjugates of the transmitted symbols are only received in the second transmission interval, thus, the coding matrix constructed at the destination by the source node and relay node is of the form: $\begin{bmatrix} s_1 & \tilde{s}_2 \\ -s_2^* & \tilde{s}_1^* \end{bmatrix}$ which meets the defined structure for complex orthogonal designs even when the source node is actively involved in cooperation. Thus we are able to demonstrate that a diversity order of $d = 2$ can be achieved when the relay node correctly decodes its received information symbols at t_1. Also, depending on the design of the code matrix, the proposed SA strategy can achieve improved diversity and low complexity symbol-wise ML decoding, this aspect is discussed next.

2.3.2 Symbol-wise Maximum-Likelihood Detection

We now provide an explanation on the structure of the signal detector at the destination for the SA-DOSTBC described in Section 2.3.1. Conjugating the received signal y_2 in (2.12), the received signal at the destination at t_2 becomes:

$$\boldsymbol{y} = [y_1, y_2^*]$$

$$y_1 = h_2 s_1 + g\tilde{s}_2 + z_1$$

$$y_2^* = -h_2^* s_2 + g^* \tilde{s}_1 + z_2^* \quad (2.13)$$

Assuming the destination is switched to receiving mode at t_1 such that the source node broadcasts the signal vector $\boldsymbol{s} = [s_1, s_2]$ to the relay node and the destination simultaneously. While the relay node receives the signals in (2.9), the signal vector received by the destination from the source node is given by:

$$\boldsymbol{y}_{SD} = [y_3, y_4]$$

$$y_3 = h_1 s_1 + z_3$$

$$y_4 = h_1 s_2 + z_4 \tag{2.14}$$

where h_1 is the channel between the source node and the destination at t_1. The equivalent signal received at the destination with the SA strategy implemented is obtained by combining (2.13) and (2.14), and is given in short notation as:

$$\boldsymbol{y}_{eq} = [\boldsymbol{y}_{SD}, \boldsymbol{y}] = \boldsymbol{H}\boldsymbol{s} + \boldsymbol{z}_{eq} \tag{2.15}$$

where $\boldsymbol{H}$ denotes the equivalent channel matrix between the source node and relay node, and the destination, and is given as:

$$\boldsymbol{H} = \begin{bmatrix} h_1 & 0 \\ 0 & h_1 \\ h_2 & g \\ g^* & -h_2^* \end{bmatrix} \tag{2.16}$$

If the ML detector can perfectly estimate the channel co-efficients h_1, h_2, and g, they can be used as CSI. Let $s = \{\bar{s_1}, \bar{s_2}\}$ denote the set of all possible transmitted vectors estimated by the ML detector which minimizes the Euclidean distance J from a signal constellation M with equal probabilities, thus:

$$J = \left|\boldsymbol{y}_{eq} - \boldsymbol{H}\boldsymbol{s}\right|^2 \tag{2.17}$$

where $\boldsymbol{y}_{eq} = [y_1, y_2, y_3, y_4]$ and $\boldsymbol{s} = [s_1, s_2]^T$, substituting for y_1 and y_2 in (2.13) and y_3 and y_4 in (2.14) we have:

$$J = |y_1 - h_2\bar{s_1} - g\bar{s_2}|^2 + |y_2 + h_2\bar{s_2}^* - g\bar{s_1}^*|^2 + |y_3 - h_1\bar{s_1}|^2 + |y_4 - h_1\bar{s_2}|^2 \tag{2.18}$$

In order to recover estimates $\hat{s}_1$ and $\hat{s}_2$ of the transmitted information signal, the combiner combines y_1, y_2, y_3 and y_4 such that:

$$\hat{s}_1 = {h_1}^{-1} y_3 + {h_2}^{*} y_1 + g{y_2}^{*} = (1 + |h_2|^2 + |g|^2)s_1 + {h_1}^{-1} z_3 + {h_2}^{*} z_1 + g{z_2}^{*}$$

$$\hat{s}_2 = {h_1}^{-1} y_4 + g^{*} y_1 - h_2 {y_2}^{*} = (1 + |h_2|^2 + |g|^2)s_2 + {h_1}^{-1} z_4 + g^{*} z_1 - h_2 {z_2}^{*} \qquad (2.19)$$

From (2.19) above we can see that the two information symbols can be recovered separately indicating low-complexity decoding. Also, by switching the destination to receiving mode at t_1, the model exhibits improved diversity performance at the cost of slightly increased complexity of the ML detector, notably, the additional power gain $+1$ and the noise term scaled by a factor ${h_1}^{-1}$ in (2.19). This improved diversity performance is shown in the simulation results in Section 2.5. It is obvious that in our explanation of the structure of the ML detector we relax the limiting factor $\tilde{s}_t \neq s_t$ such that there is no confusion, in other words we assume that the relay node correctly decodes the information symbols received from the source node at t_1.

2.3.3 Source-assisting Distributed Quasi-orthogonal Space-time Block Codes

The main disadvantage of DOSTBC is that when complex valued symbols are used, full code rate can only be achieved for a maximum of two cooperating nodes. Several types of DOSTBC schemes proposed in the literature, namely, Alamouti code [24], square-real orthogonal codes and complex-valued orthogonal codes [34] [35] are unable to achieve full code rate when there are more than two cooperating nodes. The only DOSTBC scheme which is capable of achieving full code rate when two cooperating nodes are utilized is the Alamouti code which was discussed in the previous section. To alleviate this problem, Jafarkhani et al in [42] introduced a class of codes called quasi-orthogonal codes for multiple-antenna

systems, these codes achieve full code rate for MIMO systems with more than two transmit antennas. Quasi-orthogonal designs are attractive because they achieve higher code-rate than orthogonal designs and lower decoding complexity than non-orthogonal designs [43]. In contrast with orthogonal designs where single symbols can be recovered separately by the detector, quasi-orthogonal designs rely on recovering symbols in pairs, referred to as pairwise detection [35]. Following the design of quasi-orthogonal codes for multiple-antenna systems, distributed quasi-orthogonal space-time block codes (DQSTBC) was proposed in [31] to extend the benefits of full code rate to cooperative networks with more than two cooperating nodes.

We now extend our SA strategy to cooperative networks utilizing DQSTBC, which we refer to as SA-DQSTBC. For our SA-DQSTBC scheme, we extend our analysis to a cooperative network with a source node S, $P = 3$ relay nodes and destination D as shown in Fig. 2.7.

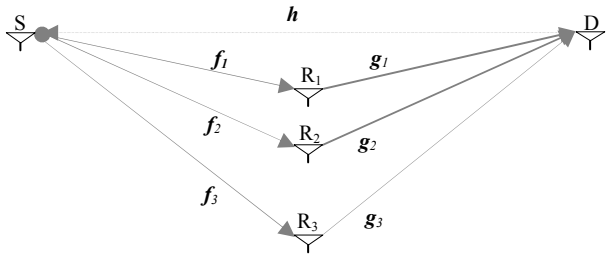

Fig.2.7. SA-DQSTBC Cooperative network model

In the first time slot t_1, we adopt the SISO transmission process as in previous sections such that the source node transmits to the P relay nodes. The only difference in this case is that we increase the symbol length of the information signal such that $\boldsymbol{s} = [s_1, s_2, s_3, s_4]$. In the second time slot t_2, we employ the quasi-orthogonal codes proposed in [42] by Jafarkhani. We design our SA strategy such that the codewords are optimally distributed between the source node and the P relay nodes, and the source node and P relay nodes transmit

simultaneously. We implement the SA-DQSTBC design only at t_2 such that the source node now transmits:

$$\boldsymbol{s}_{(S)} = [s_1, -s_2^*, -s_3^*, s_4] \tag{2.20}$$

and the $P = 3$ relay nodes transmit:

$$\boldsymbol{s}_{(1)} = [\tilde{s}_2, \tilde{s}_1^*, -\tilde{s}_4^*, -\tilde{s}_3]$$

$$\boldsymbol{s}_{(2)} = [\tilde{s}_3, -\tilde{s}_4^*, \tilde{s}_1^*, -\tilde{s}_2]$$

$$\boldsymbol{s}_{(3)} = [\tilde{s}_4, \tilde{s}_3^*, \tilde{s}_2^*, \tilde{s}_1] \tag{2.21}$$

From (2.20) and (2.21) above we can see that the complex conjugates of the information symbols are jointly transmitted in the second and third time instants. Thus the received signal matrix at the destination will only contain conjugates on entire columns, which ensures quasi-orthogonality. The signal received at the destination at t_2 is given as:

$$\boldsymbol{y} = [y_1, y_2, y_3, y_4]$$

$$y_1 = h_2 s_1 + g_1 \tilde{s}_2 + g_2 \tilde{s}_3 + g_3 \tilde{s}_4 + z_1$$

$$y_2 = -h_2 s_2^* + g_1 \tilde{s}_1^* - g_2 \tilde{s}_4^* + g_3 \tilde{s}_3^* + z_2$$

$$y_3 = -h_2 s_3^* - g_1 \tilde{s}_4^* - g_2 \tilde{s}_1^* + g_3 \tilde{s}_2^* + z_3$$

$$y_4 = h_2 s_4 - g_1 \tilde{s}_3 - g_2 \tilde{s}_2 + g_3 \tilde{s}_1 + z_4 \tag{2.22}$$

where h_2 is the channel co-efficient between the source node and the destination at t_2, and g_p is the channel between the p_{th} relay node and the destination.

Thus signal matrix at the receiver is of the form $\begin{bmatrix} s_1 & \tilde{s}_2 & \tilde{s}_3 & \tilde{s}_4 \\ -s_2^* & \tilde{s}_1^* & -\tilde{s}_4^* & \tilde{s}_3^* \\ -s_3^* & -\tilde{s}_4^* & \tilde{s}_1^* & \tilde{s}_2^* \\ s_4 & -\tilde{s}_3 & -\tilde{s}_2 & \tilde{s}_1 \end{bmatrix}$ which meets the defined structure for quasi-orthogonal designs even when the source is actively involved in cooperation. It is also obvious that the scheme achieves full code rate as $T = 4$ complex-valued symbols are received in $T = 4$ transmission intervals.

2.3.4 Pairwise Signal Detection

Next, to discuss the improved diversity performance offered by the SA-DQSTBC, we provide an explanation on the structure of the pairwise signal detector at the destination. Conjugating the received signal y_2 and y_3 in (2.22), the received signal at the destination at t_2 becomes:

$$\boldsymbol{y} = [y_1, y_2^*, y_3^*, y_4]$$

$$y_1 = h_2 s_1 + g_1 \tilde{s}_2 + g_2 \tilde{s}_3 + g_3 \tilde{s}_4 + z_1$$

$$y_2^* = -h_2^* s_2 + g_1^* \tilde{s}_1 - g_2^* \tilde{s}_4 + g_3^* \tilde{s}_3 + z_2^*$$

$$y_3^* = -h_2^* s_3 - g_1^* \tilde{s}_4 + g_2^* \tilde{s}_1 + g_3^* \tilde{s}_2 + z_3^*$$

$$y_4 = h_2 s_4 - g_1 \tilde{s}_3 - g_2 \tilde{s}_2 + g_3 \tilde{s}_1 + z_4 \qquad (2.23)$$

Assuming the destination is switched to receiving mode at t_1, we introduce the vector $\boldsymbol{y}_{SD} = [y_5, y_6, y_7, y_8]$ as the information symbols received at the destination from the source node at t_1 if $\boldsymbol{s} = [s_1, s_2, s_3, s_4]$ was transmitted. Thus the information signals received at the destination from the source node at t_1 is given by:

$$y_5 = h_1 s_1 + z_5$$

$$y_6 = h_1 s_2 + z_6$$

$$y_7 = h_1 s_3 + z_7$$

$$y_8 = h_1 s_4 + z_8 \tag{2.24}$$

The equivalent signal received at the destination with the SA strategy implemented is obtained by combining (2.23) and (2.24), and is given in short notation as:

$$\boldsymbol{y}_{eq} = [\boldsymbol{y}_{SD}, \boldsymbol{y}] = \boldsymbol{H}\boldsymbol{s} + \boldsymbol{z}_{eq}$$

where $\boldsymbol{H}$ denotes the equivalent channel matrix between the source node and relay nodes, and the destination. In order to recover the transmitted information signals, the combiner obtains a new decision vector $\boldsymbol{v} = [v_1, v_2, v_3, v_4]$ given by:

$$\boldsymbol{v} = \boldsymbol{H}^H \boldsymbol{y}_{eq} = \boldsymbol{H}^H \boldsymbol{H}\boldsymbol{s} + \boldsymbol{H}^H \boldsymbol{z}_{\boldsymbol{eq}} \tag{2.25}$$

$$\boldsymbol{v} = \boldsymbol{M}\boldsymbol{s} + \boldsymbol{H}^H \boldsymbol{z}_{\boldsymbol{eq}} \tag{2.26}$$

where $\boldsymbol{M}$ is the Gramian matrix which dictates the complexity of the decoding algorithm and is given as:

$$\boldsymbol{M} = \boldsymbol{H}^{\mathrm{H}}\boldsymbol{H} = \boldsymbol{H}\boldsymbol{H}^{\mathrm{H}} = \alpha^2 \begin{bmatrix} 1 & 0 & 0 & \beta \\ 0 & 1 & -\beta & 0 \\ 0 & -\beta & 1 & 0 \\ \beta & 0 & 0 & 1 \end{bmatrix} \tag{2.27}$$

where $\alpha^2 = (|h_1|^2 + |h_2|^2 + |g_1|^2 + |g_2|^2 + |g_3|^2)$ is the power gain on the main diagonal and $\beta = \left(2Re(h_2 g_3{}^* - g_1 g_2{}^*)\right)/\alpha^2$ is an additional interfering element at off-diagonal positions. The pairwise ML detector is now applied to $\boldsymbol{v}$ for all pair of symbols $\{\overline{s_1}, \overline{s_4}\}$ and $\{\overline{s_2}, \overline{s_3}\}$ which minimize the Euclidean distance J.

$$J_{(s_1,s_4)} = \frac{1}{1-\beta^2}\left(|v_1 - \alpha^2(\bar{s_1} + \beta\bar{s_4})|^2 + |v_4 - \alpha^2(\bar{s_4} + \beta\bar{s_1})|^2\right)$$

$$-2\beta Re([v_1 - \alpha^2(\bar{s_1} + \beta\bar{s_4})][{v_4}^* - \alpha^2({\bar{s_4}}^* + \beta{\bar{s_1}}^*)])$$

$$J_{(s_2,s_3)} = \frac{1}{1-\beta^2}\left(|v_2 - \alpha^2(\bar{s_2} + \beta\bar{s_3})|^2 + |v_3 - \alpha^2(\bar{s_3} + \beta\bar{s_2})|^2\right)$$

$$-2\beta Re([v_2 - \alpha^2(\bar{s_2} + \beta\bar{s_3})][{v_3}^* - \alpha^2({\bar{s_3}}^* + \beta{\bar{s_2}}^*)]) \quad (2.28)$$

The combiner now jointly recovers the estimates of the information signals $\hat{s}_1$ and $\hat{s}_4$, and $\hat{s}_2$ and $\hat{s}_3$ in pairs by combining (2.23) and (2.24) as follows:

$$\hat{s}_1 + \hat{s}_4 = \left({h_1}^{-1}y_5 + {h_2}^*y_1 + g_1{y_2}^* + g_2{y_3}^* + {g_3}^*y_4\right)$$

$$+\left({h_1}^{-1}y_8 + {h_2}^*y_4 - g_1{y_3}^* - g_2{y_2}^* + {g_3}^*y_1\right)$$

$$= (s_1 + s_4)\left(\bar{\alpha}^2 + \bar{\beta}\right) + Z_{1,4}$$

$$\hat{s}_2 + \hat{s}_3 = \left({h_1}^{-1}y_6 - h_2{y_2}^* + {g_1}^*y_1 + {g_2}^*y_4 + g_3{y_3}^*\right)$$

$$+\left({h_1}^{-1}y_7 - h_2{y_3}^* - {g_1}^*y_4 + {g_2}^*y_1 + g_3{y_2}^*\right)$$

$$= (s_2 + s_3)\left(\bar{\alpha}^2 + \bar{\beta}\right) + Z_{2,3} \quad (2.29)$$

where $\bar{\alpha}^2 = (1 + |h_2|^2 + |g_1|^2 + |g_2|^2 + |g_3|^2)$, $\bar{\beta} = 2Re(h_2{g_3}^* - g_1{g_2}^*)$ and Z_n captures all the noise terms. We notice that switching the destination to receiving mode at t_1 only slightly incurs an additional power gain on $\bar{\alpha}^2$ notably $+1$, however, it does not increase the magnitude of the interfering element $\bar{\beta}$, while still offering improved diversity performance. The diversity performance is illustrated in the simulation results.

2.3.5 Improved BER Performance Based on Selective Modulation Order

In order to discuss the other achievable benefits when the source node is actively involved in cooperation, we define the bit rate of a cooperative network as the average number of information bits that can be correctly decoded at the destination per signal transmission interval. Clearly, because the matrix $\boldsymbol{S}$ contains T information bearing symbols which are sent in T transmission intervals, it is easy to see that the bit rate of $\boldsymbol{S}$ is upper-bounded by $(T/T) = 1$ at t_2 alone. We identify that the use of two time slots due to cooperation introduces a level of redundancy, such that the bit rate of the cooperative network becomes upper bounded by $(T/2T)$, where the additional term in the denominator is induced by the transmission interval at t_1. Thus, if we increase the amount of bits in the $m = log_2 M$ signal constellation transmitted at t_2 relative to that transmitted at t_1 the overall diversity performance of the system improves relatively. Selective modulation order is useful for scenarios where the cooperating nodes employ the DF relaying protocol. In this case, the use of a low constellation order for source-relay transmission will lead to less erroneous decoding at the relay and subsequent improved BER performance at the destination. It is noteworthy that the use of a higher constellation order for relay-destination transmission will introduce a considerable level of delay. This issue can be addressed by the use of redundancy bits at the relays. To demonstrate this benefit we increase the value of m at t_2 such that the constellation order at t_2 is higher than that at t_1. The improved BER performance achieved is shown in the simulation results.

2.4 Distributed Space Time Block Codes with Multiple Antennas

Distributed space-time coding can be extended to a cooperative multi-hop network where some of the communicating nodes are equipped with multiple co-located antennas. For a

multi-hop network with P relay nodes, and multiple antennas M_t and N_t at the source node and destination respectively, it is shown in [44] that provided the coherence time is long enough, the network can achieve a diversity order of $min\{M_t, N_t\}P$ when $M_t \neq N_t$. Also, DSTBC is shown in [45] to be optimal for multi-hop networks with $M_t \neq N_t$ because the diversity order of the first hop is upper-bounded by M_tP and the second-hop is upper-bounded by N_tP, therefore with DSTBC, cooperative multi-hop networks incorporating multiple antennas can achieve the same diversity order as multiple antenna systems.

The SNR at the destination can be optimized by coherent combination of information signals received by multiple antennas incorporated at its terminal. In this case, the increase in SNR is proportional to the number of receive antennas [46]. This concept is referred to as 'receive diversity' where the information signals arriving at the destination further experience independent fades along their paths. In this section, we extend the design of orthogonal and quasi-orthogonal codes to cooperative multi-hop networks with multiple antennas at the destination. Practically, this is an appropriate model for any wireless sensor network or cellular network scenario where the access point or base station respectively can be equipped with multiple antennas. Considering the fact that the information signals in a cooperative multi-hop network will more or less originate from independent communicating nodes, the configuration of our network can be viewed as a combined transmit and receive diversity system, this is shown in [47] to be valid only when the transmission paths exhibit iid characteristics. Thus the network can offer a diversity order C_nN_t, where C_n is the number of cooperating nodes in the network. Such that N_t becomes a design parameter for the space-time code matrix $\boldsymbol{S}$ at the destination, and it dictates the structure of the ML detector.

Consider a DF cooperative multi-hop network model with a single relay node and multiple receive antennas N_t at the destination as shown in Fig 2.8. The transmission and space-time

coding scheme for this configuration is identical to the scenario where the destination is equipped with a single antenna the only difference is that the information signals received at each t_{th} transmission interval in the single antenna case is received by different antennas in the multiple antenna case.

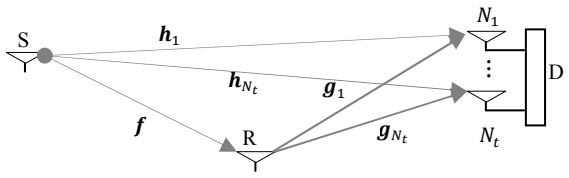

Fig.2.8. Cooperative network model with multiple receive antennas

Let $y_{n,t}$ denote the information signal received at the n_{th} receive antenna at the t_{th} time interval for $n = 1,2, \dots, N_t$ and $t = 1,2, \dots, T$.

$$y_{n,t} = h_n s_1 + g_n s_2 + z_{n,t} \tag{2.30}$$

where $z_{n,t}$ is the additive white Gaussian noise at the n_{th} receive antenna assumed to be iid random variables, h_n and g_n are the Rayleigh flat fading channel co-efficients between the source node and relay node respectively to the n_{th} receive antenna thus the channel experienced by each receive antenna is iid.

2.4.1 Orthogonal Designs with Multiple Receive Antennas

We first show the implementation of the DOSTBC design on a single relay network with multiple receive antennas $N_t = 2$ at the destination, the Alamouti code is applied to suit the requirements of matrix $\boldsymbol{S}$ at each receive antenna. We implement the DOSTBC design only at t_2 as in previous sections such that the source node transmits:

$$\boldsymbol{s}_{(S)} = [s_1, -s_2^*] \tag{2.31}$$

and the relay node transmits:

$$\boldsymbol{s}_{(R)} = [\tilde{s}_2, \tilde{s}_1{}^*] \tag{2.32}$$

Assuming perfect CSI is available as in previous sections such that $\boldsymbol{y}_1 = [y_{1,1}, y_{1,2}]$ is the signal vector received at the first receive antenna and $\boldsymbol{y}_2 = [y_{2,1}, y_{2,2}]$ is the signal vector at the second receive antenna, the combined signal received at the destination at t_2 from both receive antennas is given as:

$$\boldsymbol{y} = [\boldsymbol{y}_1, \boldsymbol{y}_2]$$

$$y_{1,1} = h_1 s_1 + g_1 \tilde{s}_2 + z_{1,1}$$

$$y_{1,2} = -h_1 s_2{}^* + g_1 \tilde{s}_1{}^* + z_{1,2}$$

$$y_{2,1} = h_2 s_1 + g_2 \tilde{s}_2 + z_{2,1}$$

$$y_{2,2} = -h_2 s_2{}^* + g_2 \tilde{s}_1{}^* + z_{2,2} \tag{2.33}$$

The matrix $\boldsymbol{S}$ at the destination is of the form: $\begin{bmatrix} s_1 & \tilde{s}_2 \\ -s_2^* & \tilde{s}_1^* \end{bmatrix}$ at each receive antenna, In order to recover the transmitted information signals, the ML detector obtains estimates $\hat{s}_1$ and $\hat{s}_2$ of the transmitted information signal on each receive antenna, and linearly combines the corresponding signals from the antennas as follows:

$$\hat{s}_1 = y_{1,1} h_1{}^* + y_{1,2}{}^* g_1 + y_{2,1} h_2{}^* + y_{2,2}{}^* g_2$$

$$= \sum_{n=1}^{N_t} \left[(|h_n|^2 + |g_n|^2) s_1 + z_{n,1} h_n{}^* + z_{n,2}{}^* g_n \right]$$

$$\hat{s}_2 = y_{1,1} g_1{}^* - y_{1,2}{}^* h_2 + y_{2,1} g_2{}^* - y_{2,2}{}^* h_2$$

$$= \sum_{n=1}^{N_t}\left[(|h_n|^2 + |g_n|^2)s_2 + z_{n,1}g_n{}^* - z_{n,2}{}^* h_n\right] \quad (2.34)$$

where $N_t = 2$.

2.4.2 Source-assisting Strategy with Multiple Receive Antennas

Consider the scenario where the destination is switched to receiving mode at t_1 as in Section 2.3. The information signals transmitted from the source node to the two receive antennas can be implemented as a two-branch linear combining scheme [34] where the output signal is a linear combination of the replicas of all the received signals, this technique is shown in the simulation results to achieve optimization in terms of SNR. The network can now be viewed as a hybrid combination of the two-branch linear combiner at t_1, and the two-by-two Alamouti scheme at t_2. We denote the vector $\boldsymbol{y}_{SD} = [\boldsymbol{y}_{SD1}, \boldsymbol{y}_{SD2}]$ as the information signals received at the destination at t_1, such that $\boldsymbol{y}_{SD1} = [y_{SD1,1}, y_{SD1,2}]$ and $\boldsymbol{y}_{SD2} = [y_{SD2,1}, y_{SD2,2}]$ are received on the first and second antennas respectively. The resulting signals at the destination are:

$$y_{SD1,1} = h_{SD1}s_1 + z_{SD1,1}$$

$$y_{SD2,1} = h_{SD2}s_1 + z_{SD2,1}$$

$$y_{SD1,2} = h_{SD1}s_2 + z_{SD1,2}$$

$$y_{SD2,2} = h_{SD2}s_2 + z_{SD2,2} \quad (2.35)$$

and the combined signals are:

$$\hat{s}_1 = y_{SD1,1}h_{SD1}{}^* + y_{SD2,1}h_{SD2}{}^*$$

$$= (|h_{SD1}|^2 + |h_{SD2}|^2)s_1 + z_{SD1,1}h_{SD1}{}^* + z_{SD2,1}h_{SD2}{}^*$$

$$\hat{s}_2 = y_{SD1,2}h_{SD1}{}^{*} + y_{SD2,2}h_{SD2}{}^{*}$$

$$= (|h_{SD1}|^2 + |h_{SD2}|^2)s_2 + z_{SD1,2}h_{SD1}{}^{*} + z_{SD2,2}h_{SD2}{}^{*} \quad (2.36)$$

The ML detector obtains estimates $\hat{s}_1$ and $\hat{s}_2$ of the entire transmitted information signals at t_1 and t_2 on each n_{th} receive antenna and linearly obtains the combined signals from the antennas as follows:

$$\hat{s}_1 = \sum_{n=1}^{N_t+1}[(|h_{SDn}|^2 + |g_n|^2)s_1 + Z_1]$$

$$\hat{s}_2 = \sum_{n=1}^{N_t+1}[(|h_{SDn}|^2 + |g_n|^2)s_2 + Z_2] \quad (2.37)$$

where Z_t captures all the noise terms. It is noteworthy that, due to the SA strategy, the achievable diversity order has increased from N_t in (2.34) to $N_t + 1$ in (2.37). The ML decoding rules for the information signals $s = \{\bar{s}_1, \bar{s}_2\}$ are given by:

$$\hat{s}_1 = \underset{\bar{s}_1 \in \boldsymbol{S}}{\operatorname{argmin}}\left[\sum_{n=1}^{N_t}\left((|h_{SDn}|^2 + |g_n|^2) - 1\right)|\bar{s}_1|^2 + d^2(\hat{s}_1, \bar{s}_1)\right]$$

$$\hat{s}_2 = \underset{\bar{s}_2 \in \boldsymbol{S}}{\operatorname{argmin}}\left[\sum_{n=1}^{N_t}\left((|h_{SDn}|^2 + |g_n|^2) - 1\right)|\bar{s}_2|^2 + d^2(\hat{s}_2, \bar{s}_2)\right] \quad (2.38)$$

where $d^2(\hat{s}_t, \bar{s}_t)$ denotes the square of the Euclidean distance between $\hat{s}_t$ and $\bar{s}_t$.

2.4.3 Quasi-orthogonal Designs with Multiple Receive Antennas

It is noted in [48] that by increasing the number of receive antennas, the rate one quasi-orthogonal STBC (QSTBC) provides a higher diversity equal to $M_t N_t$. In this part, we extend the DQSTBC design of Section 2.3.3 to a network with multiple receive-antennas N_t at the destination. The Jafarkhani code [42] is applied to suit the requirements of matrix $\boldsymbol{S}$ at each receive antenna. The implementation of the DQSTBC design on a cooperative network with $P = 3$ relay nodes and N_t multiple receive antennas is shown in Fig.2.9.

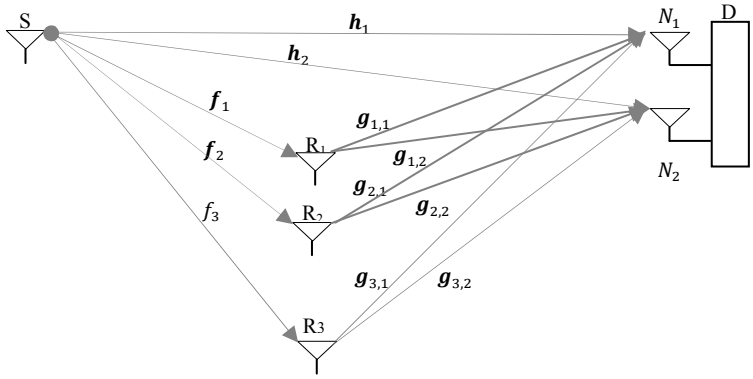

Fig.2.9. Quasi-orthogonal network model with multiple receive antennas

The signal received at the first receive antenna N_1 is $\boldsymbol{y}_1 = [y_{1,1}, y_{1,2}, y_{1,3}, y_{1,4}]$ and the signal received at the second receive antenna N_2 is $\boldsymbol{y}_2 = [y_{2,1}, y_{2,2}, y_{2,3}, y_{2,4}]$. In order to recover the transmitted information signals the receiver combines all signals received at the destination at t_2 from both receive-antennas and obtains the estimate:

$$\hat{s}_t = \sum_{t=1}^{T} \sum_{n=1}^{N_t} y_{n,t} \left(h_n + g_{1,n} + g_{2,n} + g_{3,n}\right), t = 1,2,..,4 \tag{2.39}$$

Unlike the DQSTBC design with a single receive antenna at the destination discussed in Section 2.3.3, the multiple receive antenna case yields a diagonal matrix with elements:

$$\alpha^2 = \sum_{n=1}^{N_t} \left(|\, h_n|^2 + \left|g_{1,n}\right|^2 + \left|g_{2,n}\right|^2 + \left|g_{3,n}\right|^2 \right) \tag{2.40}$$

where N_t which represents the number of receive-antennas, improves the diversity performance of the network. The improved diversity offered by DQSTBC with two-receive antennas is shown in the simulation results.

2.5 Simulation Results

In this section, we show the simulated BER performance of SA-DOSTBC and SA-DQSTBC and compare with the conventional DOSTBC and DQSTBC. The transmitted information

signals encounter Rayleigh flat fading channels where the amplitudes of fading between communicating nodes are mutually uncorrelated. It is further assumed that all the relay nodes and destination acquire perfect CSI. All curves are plotted against the SNR at the destination alone. First, the performance of the SA-DOSTBC using BPSK and 16QAM modulation schemes with Gray coding is considered. The model is a DF cooperative network with a single relay node, where $T = C_n = 2$, the Alamouti code is used. The symbols are recovered at the destination using ML decoding. The results in Fig.2.10 show that with BPSK the SA-DOSTBC achieves improved diversity performance of 2dB at BER $= 10^{-2}$ in contrast with the performance of the conventional DOSTBC (see results in [49] for comparison). A similar behaviour can be observed for the BER performance with 16QAM, again we can see that the proposed scheme is about 2dB better than the conventional scheme. This implies that the theoretical result in (2.19) is consistent with the simulation result, thus we can conclude that the additional information signal received by switching the destination to receiving mode at t_1 improves the BER gain and slightly enhances the diversity gain of the network with negligible performance penalty. We assume that the total power consumed by the network is unchanged when the SA strategy is used. In other words, the source node and relay nodes consume the same amount of power for both the SA schemes and the conventional schemes.

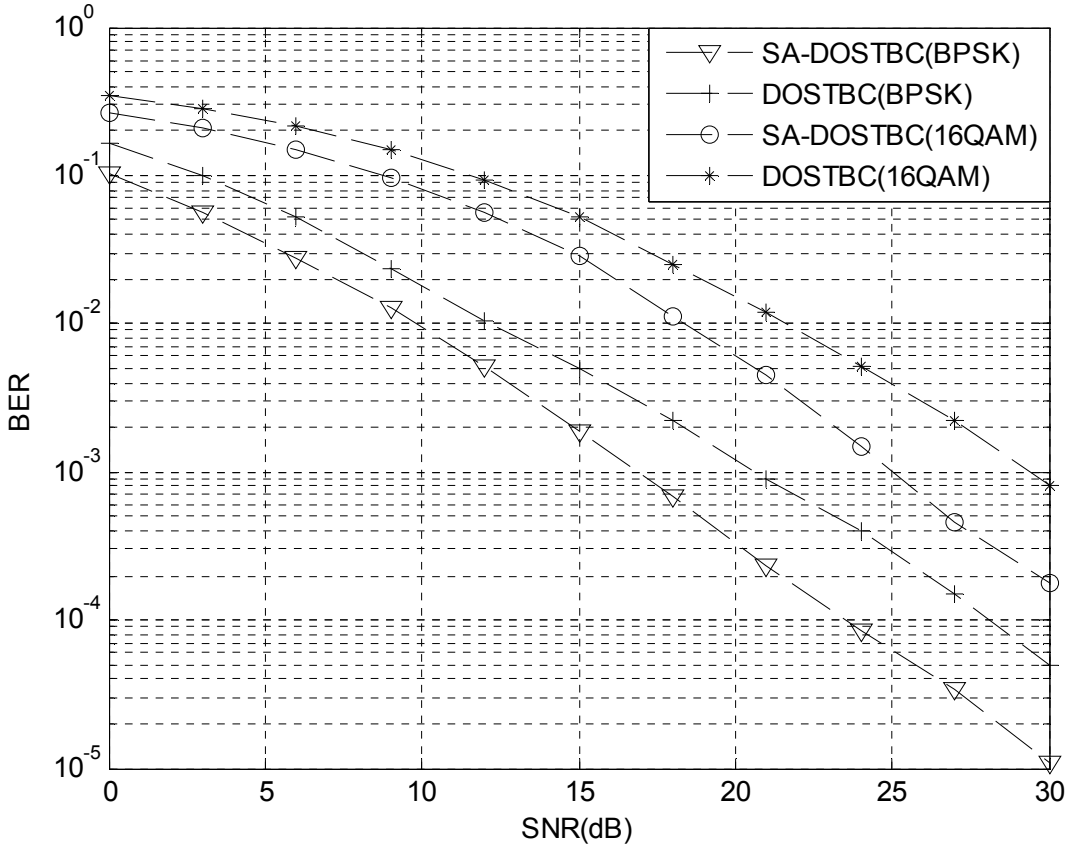

Fig.2.10 Performance comparison of SA-DOSTBC and DOSTBC

Next, in Fig.2.11 we compare the SA-DQSTBC with conventional DQSTBC using BPSK and QPSK modulation for a cooperative network with $P = 3$ relay nodes, thus $T = C_n = 4$. Pairwise decoding is used for symbol recovery. Similarly from the results we can conclude that the SA-DQSTBC outperforms the conventional DQSTBC, for example at BER $= 10^{-2}$, the proposed scheme with QPSK modulation has about 1dB improvement. It is also clear that the SA strategy offers more BER improvement for the orthogonal design compared to the quasi-orthogonal design. This is because the implementation of the SA strategy incurs much lower decoding complexity for the orthogonal design.

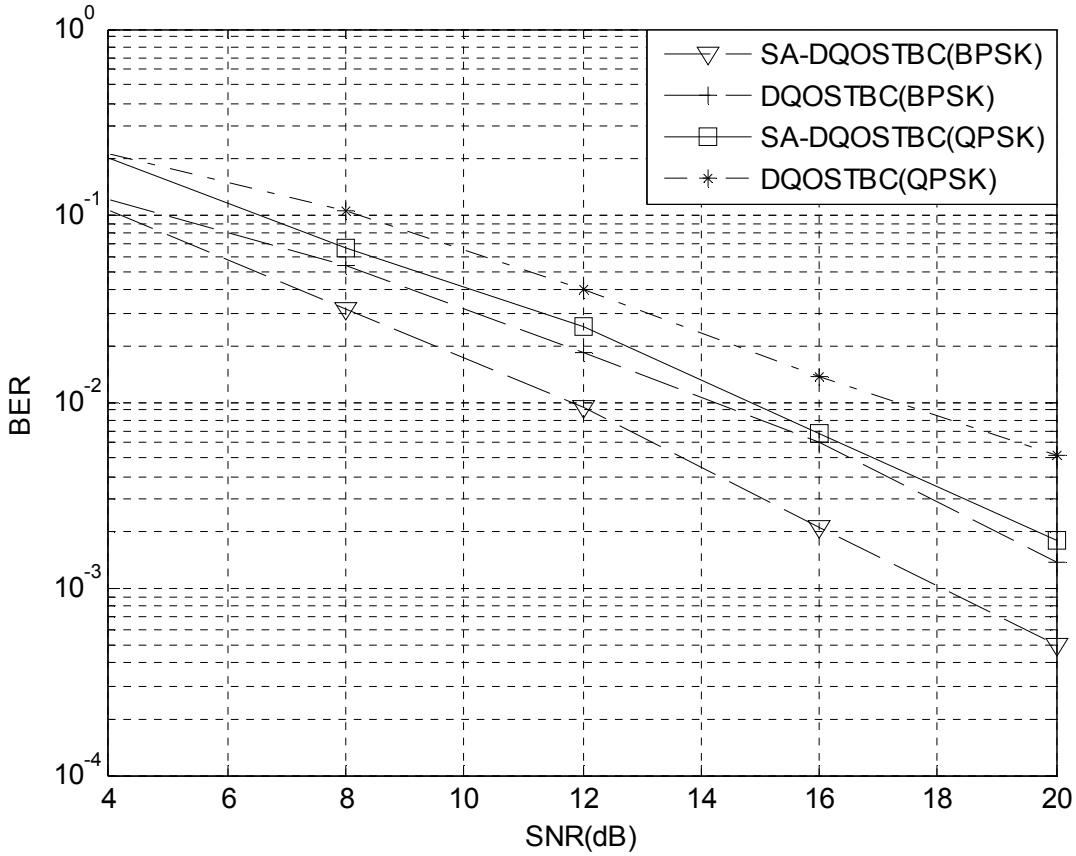

Fig.2.11. Performance comparison of SA-DQOSTBC and DQOSTBC

Next, we keep the modulation order of transmissions on the source-relay link unchanged, while we increase the modulation order of transmissions on the relay-destination link. Fig.2.12 shows the improvement due to the increased constellation order used on the relay-destination link for SA-DOSTBC. First we design the model such that both source-relay and relay-destination links use BPSK, we can see that increasing the constellation order of the relay-destination link alone from BPSK to QPSK improves the BER performance, however further increase in constellation order from 16QAM shows negligible improvement. This can be attributed to the higher BER at the destination due to erroneous decoding at the relay nodes.

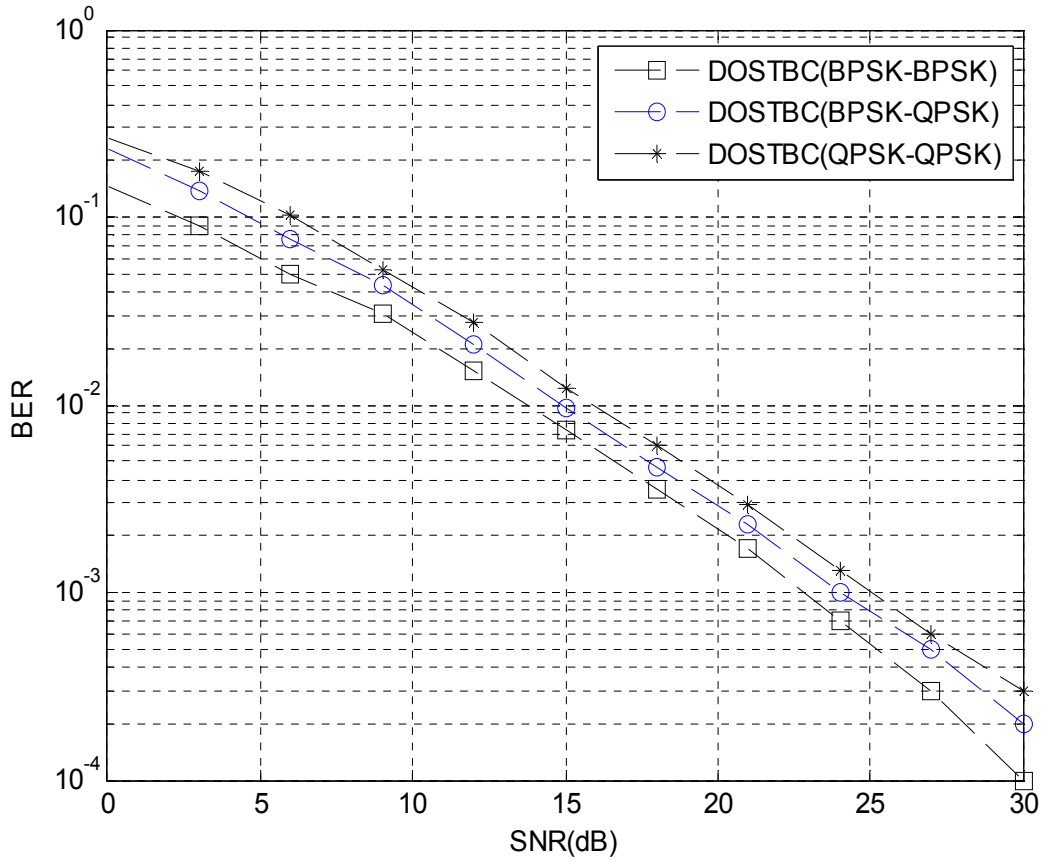

Fig.2.12. Performance improvement due to increased constellation order

We now proceed to evaluate the performance of the DOSTBC and SA-DOSTBC with multiple antennas at the destination over Rayleigh flat fading channels. In the simulation, it is assumed that the amplitudes of the fading channels from each cooperating node to each of the receive antennas at the destination are mutually independent with perfect estimation of CSI. Fig. 2.13 shows the BER performance of the DOSTBC and SA-DOSTBC schemes compared with those of the multiple-antenna configuration using 16QAM modulation. The simulation results show that DOSTBC with two receive antennas performs better than the conventional DOSTBC where a single antenna is used at the destination. Also, the two-receive-antenna SA-DOSTBC shows better performance over all of the other curves because the diversity order d in this case is upper bounded by $(C_n + 1)N_t$ as opposed to the two-receive-antenna

DOSTBC with diversity order upper bounded by $C_n N_t$. The simulation results thus show that by increasing the number of receive-antennas at the destination, the network provides a significant improvement in diversity performance.

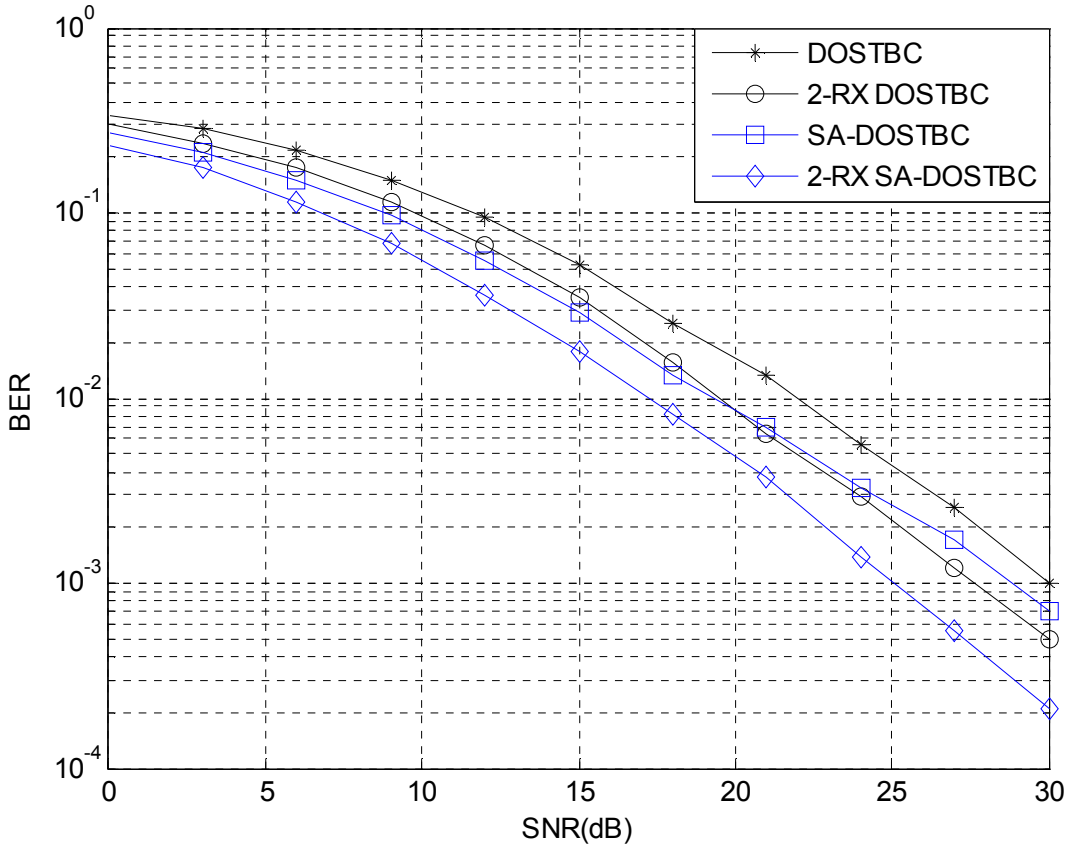

Fig.2.13. Performance of DOSTBC with multiple receive antennas

The BER performance of DQSTBC is compared with that for the multiple-antenna configuration in Fig.2.14 using BPSK modulation. The simulation results show that DQSTBC with two receive-antennas provides about 1dB improvement in SNR. Thus in general, the diversity performance of multi-hop networks can be further improved by incorporating multiple antennas at the destination terminal.

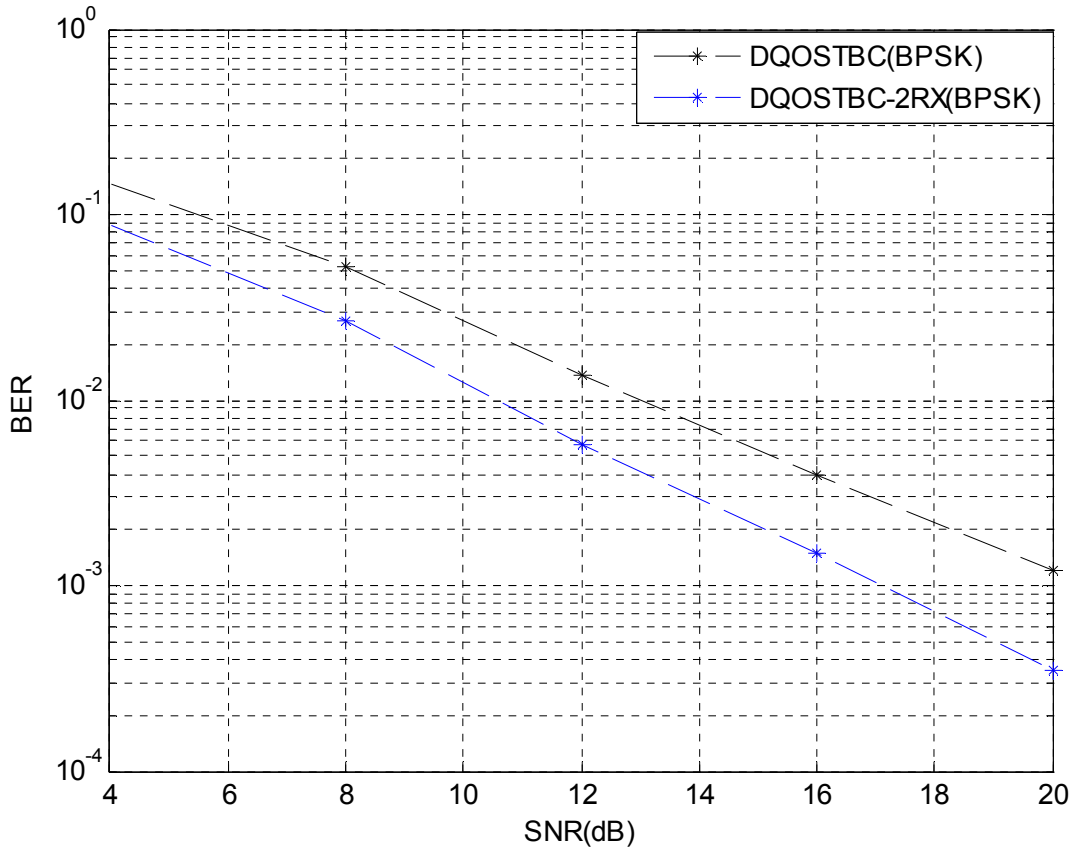

Fig.2.14. Performance of DQOSTBC with multiple receive antennas

2.6 Summary

The design of the SA strategy is considered for orthogonal and quasi-orthogonal DSTBC using DF cooperative multi-hop networks. We identify that most works on DSTBC assume there is no direct source-destination link and thus ignore the benefits that can be extracted when the source node is actively involved in cooperation. In this Chapter, a two time-slot protocol is adopted and the SA design is implemented such that the destination takes advantage of the information signals transmitted from the source node in both time-slots. This approach improves the diversity performance of the network at the expense of slightly increased complexity of the signal detector. The DSTBC design is shown for generalized rate one orthogonal and quasi-orthogonal codes, we then provide an explanation on the modified

structure of the signal detector and the improved diversity performance achieved by our proposed strategy.

3. Differential Distributed Space Time Block Codes

3.1 Introduction

Traditionally, when DSTBC schemes are used in cooperative networks, the communicating nodes are required to have full CSI to decode the signals. CSI acquisition is possible when the channel conditions fluctuate slowly compared to the information symbol rate. In this case, the source node can send training symbols or pilot symbols to enable the destination estimate the CSI accurately. However in reality, some scenarios exist where the acquisition of CSI is impractical. In fact, channel estimation is a costly and challenging task in time-selective fading environments or in environments where the channel conditions fluctuate rapidly. In multiple-antenna systems, the use of training symbols becomes impractical in fast fading channels [30]. Compared to multiple-antenna systems, the difficulty is more pronounced in networks with large number of nodes like adhoc or wireless sensor networks. This is because in such networks the amount of training or convergence time increases with the number of hops. In some situations, it may also be beneficial to forego channel estimation in order to reduce the cost and complexity of the cooperating nodes.

Channel estimation may also be difficult in high mobility environments like that experienced by vehicular sensor networks or 3G and 4G cellular systems designed to provide data access for highly mobile users. This issue is more pertinent with technologies utilizing frequency hopping techniques where fading conditions may fluctuate significantly from one hop to the next. It is thus imperative to incorporate differential strategies with cooperative multi-hop networks utilizing DSTBC schemes.

Differential strategies can recover transmitted information signals without the use of CSI [34]. The idea of differential DSTBC spans from the use of differential schemes in multiple-antenna systems [50] [51], the authors in [52] show that existing differential STBC designed for multiple-antenna systems are favorable choices for single-antenna multi-hop networks. Jing et al in [30] show that orthogonal codes maintain their linear decoding complexity when used differentially in AF cooperative networks. In [53] differential DSTBC is investigated using the AF model for cooperative networks.

In this Chapter, we present differential DSTBC schemes for cooperative multi-hop networks. The rest of the Chapter 3 is organized as follows: In Section 3.2, we present the concept of differential modulation, and review differential encoding and decoding in non-cooperative networks. We then show how the 'differential decode-and-forward' and 'differential amplify-and-forward' cooperative diversity protocols are implemented in cooperative networks. We present the full differential encoding and decoding procedure using two main differential concepts in Section 3.3 and Section 3.4, namely; 'co-efficient vectors' and 'unitary matrices' respectively. In Section 3.3 we propose differential orthogonal designs for cooperative networks based on co-efficient vectors. We present the generalized mapping scheme and differential recipe for utilizing co-efficient vectors in cooperative networks with any number of relay nodes. In Section 3.4 we show how differential orthogonal designs can be implemented in cooperative networks using unitary matrices. The differential concept is generalized in Section 3.5 to cooperative networks with three, four, and eight relay nodes using square real-orthogonal codes. In Section 3.6 we analyze via simulation the performance of all the aforementioned differential schemes.

3.2 Differential Modulation in Cooperative Networks

Differential modulation is useful for channels in which the amplitude and phase fluctuate over time. Such scenarios exist in wireless mobile environments or in situations where there is a residual carrier frequency offset after carrier synchronization. Differential schemes encode the transmitted information into phase differences between two consecutive symbols. The transmitter first provides a set of information symbols which contain no valid data, these information symbols are only used as reference symbols for differential encoding. These reference symbols are then used to generate consecutive phase-shifted signals. The information signals are recovered at the destination by comparing the phase differences between consecutively received symbols. To illustrate the fundamental idea behind the application of differential modulation for non-coherent detection schemes, consider a PSK modulated symbol sequence $s(t)$ transmitted at the t_{th} time interval. Under ideal Nyquist signaling conditions the received samples can be represented by:

$$r(t) = s(t)h(t) + z(t) \tag{3.1}$$

where $h(t)$ represents the path gain at the t_{th} time intervaland $z(t)$ denotes the corresponding noise. If the phase of $h(t)$ fluctuates rapidly and randomly with respect to t, it is impractical to estimate the channel from transitions in the carrier phase. However, if $h(t)$ fluctuates slowly enough with minimal degree of randomness such that it can be estimated over at least two consecutive symbol intervals. Then phase transitions can be used to estimate the channel and thus recover the information symbols. Differential detection schemes originate from schemes like differential phase shift keying (DPSK) that neither require CSI nor employ training symbols. These differential detection schemes have been popularly used in the digital cellular system IEEE IS-54 standards [54] they are also widely used with phase

shift keying (PSK) and quadrature amplitude modulation (QAM) constellations in satellite and radio-relay communication systems.

3.2.1 Differential Modulation in Non-cooperative Networks

Before presenting differential schemes in cooperative networks, we first review the concept of differential encoding and decoding in a classic non-cooperative single-relay network.

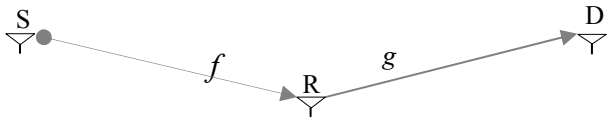

Fig.3.1 Single-relay differential non-cooperative network

Consider a single-relay network made up of a source node S, relay node R, and destination node D as illustrated in Fig.3.1. In this discussion we assume that there is no direct link between the source node and the destination. This sort of analysis is useful in scenarios where the source node cannot reach the destination directly due to power limitations. The source node transmits an arbitrary symbol s^k at the first time instant which we refer to as block k, note that s^k is only used as a reference symbol and carries no valid data. In order to generate s^k, the source node selects a symbol x^k based on m input bits from $m = log_2$M MPSK signal constellation. At the second time instant referred to as block $k+1$, the source node transmits s^{k+1} which is generated using the transmitted signal in the k_{th} block as follows:

$$s^{k+1} = s^k x^{k+1} \tag{3.2}$$

where x^{k+1} refers to the symbols generated from the input bits at the encoder in the $(k+1)_{th}$ block. Note that s^{k+1} maintains the constellation spacing of s^k, also, for a unit energy

MPSK constellation, $|s^{k+1}|$ is always unitary. Assuming that the relay node differentially decodes the information signals correctly, the information signals received at the destination in both blocks is given by:

$$y^k = s^k g + z^k \tag{3.3}$$

$$y^{k+1} = s^{k+1} g + z^{k+1} \tag{3.4}$$

where g represents the path gain between the relay node and the destination, and z^K, $K \in \{k, k+1\}$ denotes the corresponding noise at the destination. In order to recover the transmitted signal in the $(k+1)_{th}$ block, the destination first computes $y^{k+1}y^{k*}$, and then it finds the closest symbol on the MPSK constellation to $y^{k+1}y^{k*}$ as the estimate of the transmitted signal, $(\cdot)^*$ denotes conjugate. Let

$$y^{k+1}y^{k*} = (s^{k+1}g + z^{k+1})(s^k g + z^k)^*$$

$$= |g|^2 s^{k+1}s^{k^*} + s^{k+1}gz^{k^*} + s^{k^*}g^* z^{k+1} + z^{k+1}z^{k^*} \tag{3.5}$$

Substituting for s^{k+1} in (3.2), and assuming $z^{k+1} \cong z^k$ such that the term $z^{k+1}z^{k^*}$ in (3.5) can be disregarded, we can reach:

$$y^{k+1}y^{k*} = |g|^2 s^k x^{k+1} s^{k^*} + s^k x^{k+1} g z^{k^*} + s^{k^*} g^* z^{k+1}$$

$$= |g|^2 x^{k+1} + Z \tag{3.6}$$

where Z captures all the noise terms, the channel between the relay node and the destination g is assumed to remain constant for two consecutive transmission blocks. Therefore the optimal estimation of x^{k+1} is obtained by:

$$\tilde{x}^{k+1} = \arg min |y^{k+1}y^{k*} - |g|^2 x^{k+1}|^2 \tag{3.7}$$

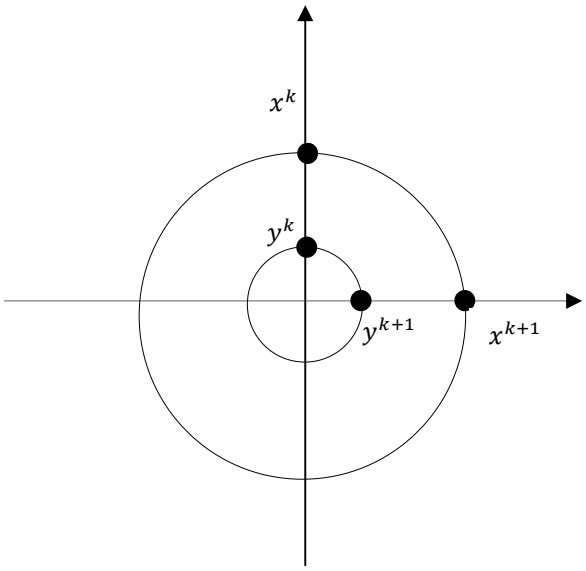

Fig.3.2. Phase and amplitude transition in differential schemes

Consider the two consecutive received signals y^k and y^{k+1}, assuming the noise terms are ignored we can observe that $x^{k+1}x^{k*}$ and $y^{k+1}y^{k*}$ will have the same phase transition. So even if the channel fluctuates rapidly and randomly, provided the phase shift is approximately constant over the two consecutive transmission blocks, the phase difference can be retained. The constellation diagram in Fig.3.2 shows that although the phase shift remains constant, the amplitude of $x^{k+1}x^{k*}$ differs from that of $y^{k+1}y^{k*}$. As discussed in [55], some form of explicit amplitude estimation may be required especially for QAM constellations. In the case of MPSK however, since all the received symbols are uniformly scaled by a factor $|g|^2$, the scaling factor will not alter the detection regions of the MPSK constellation. Therefore (3.7) can be equivalently optimized to:

$$\tilde{x}^{k+1} = \arg min|y^{k+1}y^{k*} - x^{k+1}|^2 \tag{3.8}$$

The optimized detection scheme in (3.8) guarantees that the information symbols can be recovered without CSI. The downside however is that the doubling effect of the channel

power and noise power results in a performance penalty in Rayleigh fading channels, this issue is verified in the simulation results subsequently.

3.2.2 Differential Cooperative Diversity Protocols

In the previous discussion, differential modulation was described in a classic non-cooperative single-relay network, where the source-destination link is non-existent. We now consider differential modulation in cooperative networks using either the AF or DF protocol. Consider a cooperative network scenario where both the source node and the relay node can transmit to the destination as shown in Fig.3.3. To avoid interference, the transmission is divided into two distinct stages, the 'transmit' stage, and the 'cooperate' stage. In the 'transmit' stage, the source node transmits, while relay node and destination listen, in the 'cooperate' stage, the relay node forwards its received signal to the destination using either the AF or DF protocol. The transmission in each stage is made up of two blocks, namely the k_{th} block and the $(k+1)_{th}$ block.

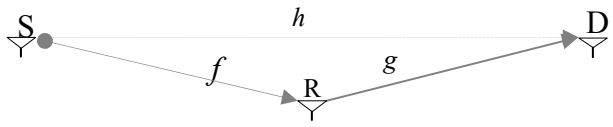

Fig.3.3. Single-relay differential cooperative network

3.2.3 Differential Amplify-and-Forward Cooperative Protocol

We first implement the differential AF (DAF) protocol at the relay node such that it can be integrated with differential modulation. A sequence of symbols $x_{(n)}^{k+1}$ arrive at the encoder of the source node at the $(k+1)_{th}$ block, these symbols are differentially encoded as:

$$s_{(n)}^{k+1} = s_{(n)}^{k} x_{(n)}^{k+1},\ n = 1,2,\dots,N \tag{3.9}$$

where N is the number of symbols within the frame and $s_{(n)}^{k}$ is the information signal transmitted by the source node in the k_{th} block. The received signals at the relay node and destination respectively are given by:

$$r^{k+1} = s_{(n)}^{k+1} f + n^{k+1} \tag{3.10}$$

$$y_{(1)}^{k+1} = s_{(n)}^{k+1} h + z_{(1)}^{k+1} \tag{3.11}$$

The source-relay and source-destination channels are denoted by f and h respectively. The channels are assumed to be Rayleigh fading made up of complex Gaussian random variables with mean μ and variance σ^2. The corresponding noise-samples n^{k+1} and $z_{(1)}^{k+1}$ have zero mean and variance No. For the transmission in the second stage, the relay node applies the amplification co-efficient proposed in [56] to implement the AF protocol given as:

$$\acute{r}^{k+1} = r^{k+1} / var(r^{k+1})^{\frac{1}{2}} \tag{3.12}$$

Note that this amplification co-efficient is amenable to differential modulation because unlike the one in [5] it does not require the channel information $|f|$, instead the values in the denominator of (3.12) can be estimated by time averaging over the frame of consecutive received signals. Now the relay node transmits the amplified signal $\acute{r}^{k+1}$ such that the signal received at the destination in the second stage is:

$$y_{(2)}^{k+1} = \acute{r}^{k+1} g + z_{(2)}^{k+1} \tag{3.13}$$

where g denotes the relay-destination channel. Substituting (3.10) and (3.12) into (3.13)

$$y_{(2)}^{k+1} = s_{(n)}^{k+1} h_{EQ} + z_{EQ}^{k+1} \tag{3.14}$$

where h_{EQ} is the equivalent channel of the combined source-relay and relay-destination links given as $h_{EQ} = gf\, s_{(n)}^{k+1} / var(r^{k+1})^{\frac{1}{2}}$ and z_{EQ}^{k+1} is the equivalent noise given as $z_{EQ}^{k+1} =$

$g\, n^{k+1}/var(r^{k+1})^{\frac{1}{2}} + z_{(2)}^{k+1}$. So far, only signals transmitted via the source-relay-destination link have been considered. In order to achieve additional diversity we implement cooperative communication such that the direct source-destination link is considered. In other words, differential demodulation is achieved for the cooperative set-up by combining the signals received over both links. A simple differential combiner can be obtained by averaging over the received symbols in (3.11) and (3.13) to recover the transmitted information:

$$\tilde{x}^{k+1} = \arg min \left| \left(y_{(2)}^{k+1} y_{(2)}^{k\ *} var(r^{k+1})^{\frac{1}{2}} + y_{(1)}^{k+1} y_{(1)}^{k\ *}/2 \right) - x^{k+1} \right|^2 \tag{3.15}$$

3.2.4 Differential Decode-and-Forward Cooperative Protocol

In this section, differential modulation is considered for cooperative networks utilizing the DF protocol, referred to as differential DF (DDF). Assuming the channel h between the source node and the destination remains unchanged during the transmissions in the k_{th} block and the $(k+1)_{th}$ block, the signal received at the destination via the source-destination link can be written as:

$$y_{(1)}^{k+1} = y_{(1)}^{k} x_{(n)}^{k+1} + \tilde{z}_{(1)}^{k+1} \tag{3.16}$$

where $\tilde{z}_{(1)}^{k+1} \triangleq z_{(1)}^{k+1} - z_{(1)}^{k} x_{(n)}^{k+1}$, in other words the signal received at the destination in the $(k+1)_{th}$ block is conditioned on the received signal in the k_{th} block and the information symbol $x_{(n)}^{k+1}$. Similarly, if we consider the signals received at the relay node via the source-relay link, the received signals can be written as:

$$r^{k+1} = r^{k} x_{(n)}^{k+1} + \tilde{n}^{k+1} \tag{3.17}$$

where $\tilde{n}^{k+1} \triangleq n^{k+1} - n^k x_{(n)}^{k+1}$. At the relay node, the received signal is first differentially decoded as in (3.8) to obtain $\tilde{x}_{(n)}^{k+1}$, next the recovered bits are differentially re-encoded as follows:

$$s_{(n)}^{k+1} = s_{(n)}^{k} \tilde{x}_{(n)}^{k+1}, \; n = 1,2, \dots, N \tag{3.18}$$

In the second stage, the relay node transmits the differentially encoded signals in (3.18), such that the destination receives:

$$y_{(2)}^{k+1} = s_{(n)}^{k+1} g + z_{(2)}^{k+1} \tag{3.19}$$

Substituting (3.18) into (3.19) as in (3.17), we can reach:

$$y_{(2)}^{k+1} = y_{(2)}^{k} \tilde{x}_{(n)}^{k+1} + \tilde{z}_{(2)}^{k+1} \tag{3.20}$$

where $\tilde{z}_{(2)}^{k+1} \triangleq z_{(2)}^{k+1} - z_{(2)}^{k} \tilde{x}_{(n)}^{k+1}$. The independent source-destination and source-relay-destination links thus provide the signals in (3.16) and (3.20) respectively. These signals can then be combined cooperatively for differential demodulation as in (3.15) with the amplification coefficient $var(r^{k+1})^{\frac{1}{2}}$ ignored.

3.3 Differential Schemes using Co-efficient Vectors

Differential DOSTBC can be implemented in cooperative networks by using the differential unitary matrices design as adopted by the authors in [30] [57-60]. Different from the existing works in the literature, differential DOSTBC can also be implemented in cooperative networks by using the differential co-efficient vector design. It is evident from [30] [57-60] that differential DOSTBC schemes adopting the unitary matrices design are amenable to the AF protocol. This is because, when the AF protocol is used, the relay nodes can forego CSI

acquisition such that differential decoding is only performed at the destination. In contrast, for practical scenarios where specific requirements compel the relay nodes to differentially decode and re-transmit information signals from the source node, the co-efficient vector design is better suited. The co-efficient vector design is particularly useful for applications like adhoc and sensor networks where the intermediate nodes are required to recover and retransmit information signals. Some differential DOSTBC schemes based on the DF protocol in [52] [61] also adopt the unitary matrices design. It is important to note that co-efficient vectors have been used for differential modulation in multiple antenna systems, see [50] [62] for example. However, to the best of our knowledge this is the first work to investigate the applicability of co-efficient vectors to cooperative networks utilizing differential DOSTBC. From this, we propose differential DOSTBC designs for cooperative networks based on co-efficient vectors. We present the generalized mapping scheme and differential recipe for utilizing co-efficient vectors in cooperative networks with any number of relay nodes. Using simulation results, we compare and contrast the unitary matrices and co-efficient vector designs in terms of computational complexity and BER performance.

The differential encoding and decoding set-up using co-efficient vectors is generalized to cooperative networks with N relay nodes. Consider the cooperative network with N relay nodes depicted in Fig.3.4. The transmission from the source node to the destination is divided into block k and block $k+1$, and each block is sub-divided into the 'transmit' and 'cooperate' stages. In the 'transmit' stage, the source node sends information signals to the cooperating relay nodes, while in the 'cooperate' stage, the cooperating relay nodes construct the DOSTBC matrix at the destination. For each stage, the nodes are subject to half-duplex constraint such that they cannot transmit and receive simultaneously. We assume symbol level synchronization between the cooperating nodes such that the cooperating nodes transmit

simultaneously. Each stage contains T symbol transmissions meaning that the source node and relay nodes transmit a length T vector of information signals in each block. Our design is valid for networks utilizing square real-orthogonal codes [34] where $N \in \{2,4,8,\dots\}$, we however show that it can easily be extended to networks with any number of relay nodes.

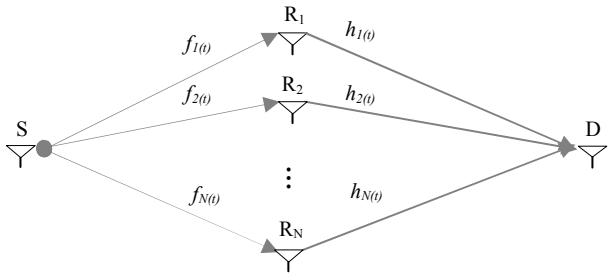

Fig.3.4 Differential cooperative network using co-efficient vectors

Given Nm input bits, the source node constructs a length 2^{Nm} co-efficient vector set given by $V = \left\{\left[v_{1,1}, \dots, v_{N,1}\right]^t, \left[v_{1,2}, \dots, v_{N,2}\right]^t, \dots, \left[v_{1,2^{2m}}, \dots, v_{N,2^{2m}}\right]^t\right\}$, where $[\cdot]^t$ denotes transpose. The co-efficient vector set V is made up of 2^{2m} unit-length distinct vectors $\left[v_{1,j}, \dots, v_{N,j}\right]^t, j \in \{1,2, \dots, 2^{2m}\}$, m is the spectral efficiency. Then a pseudo-random one-to-one mapping scheme $P(.)$ is defined for any $m = log_2 M$ M-PSK signal constellation such that the Nm input bits are mapped onto V. Note that M is the constellation size.

Before commencing differential encoding, we first devise the structure of the square real-orthogonal signal matrix employed in our scheme. Let $\boldsymbol{X}^k$ denote the $T \times N$ square real-orthogonal matrix given by $\boldsymbol{X}^k = \left[\boldsymbol{x}_1^{k\,T}, \dots, \boldsymbol{x}_N^{k\,T}\right]$, where $\boldsymbol{x}_n^k$ is the n_{th} column of $\boldsymbol{X}^k$. The source node commences differential encoding in the k_{th} block by transmitting the reference information signal $\boldsymbol{x}_1^k = \left[x_{1(1)}^k, \dots, x_{1(T)}^k\right]$ to the n_{th} relay node, where $\boldsymbol{x}_n^k$ denotes the n_{th} column of $\boldsymbol{X}^k$. The elements of $\boldsymbol{X}^k$ are normalized such that $E\left\{tr\left(\boldsymbol{X}^{k\,H}\boldsymbol{X}^k\right)\right\} = N$, in other words $\boldsymbol{x}_n^k \in \boldsymbol{X}^k/\sqrt{N}$.

In the transmit stage of the k_{th} block, the source node transmits $\boldsymbol{x}_1^k = \left[x_{1(1)}^k, \ldots, x_{1(T)}^k\right]$, the n_{th} relay node receives

$$\boldsymbol{r}_n^k = \boldsymbol{x}_1^k \odot \boldsymbol{f}_n^k + \boldsymbol{n}_n^k \tag{3.21}$$

where $\boldsymbol{f}_n^k = \left[f_{n(1)}^k, \ldots, f_{n(T)}^k\right]$ is the Rayleigh fading channel model between the source node and the n_{th} relay node assumed to be made up of iid zero mean and unit-variance complex random variables. The corresponding noise $\boldsymbol{n}_n^k = \left[n_{n(1)}^k, \ldots, n_{n(T)}^k\right]$ is made up of independent samples of a zero mean complex Gaussian random variable.

3.3.1 Differential Encoding Using Co-efficient Vectors

The data vector $\boldsymbol{x}_1^{k+1} = \left[x_{n(1)}^{k+1}, \ldots, x_{n(T)}^{k+1}\right]$ transmitted by the source node in the $(k+1)_{th}$ block is generated from the data vector $\boldsymbol{x}_1^k = \left[x_{1(1)}^k, \ldots, x_{1(T)}^k\right]$ transmitted by the source node in the k_{th} block. We first discuss how the data vector in the $(k+1)_{th}$ block is generated using the co-efficient vector set and the information signals in the k_{th} block as shown in Fig.3.5

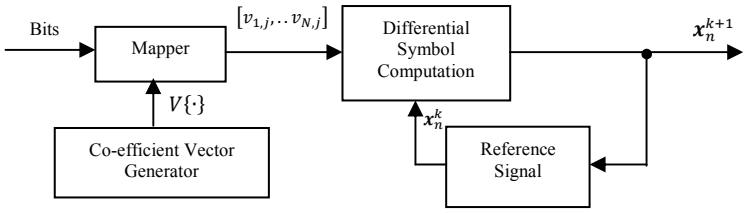

Fig.3.5 Co-efficient vector-based differential encoder

The Nm input bits arriving at the encoder in the $(k+1)_{th}$ block are used to select the corresponding vectors from the co-efficient vector set V. The selected corresponding vectors $\left[v_{1,j}, \ldots, v_{N,j}\right]^t, j \in \{1,2, \ldots, 2^{2m}\}$ are dependent on the Nm input bits and the pseudo-random

one-to-one mapping scheme $P(.)$. The source node then computes the information signals for the $(k+1)_{th}$ block using the transmitted information signals in the k_{th} block and the selected co-efficient vector as follows:

$$\boldsymbol{x}_1^{k+1} = \boldsymbol{X}^k\left[v_{1,j}, \dots, v_{N,j}\right]^t, j \in \{1,2, \dots, 2^{2m}\}, N = \{2,4,8, \dots\} \quad (3.22)$$

where $\boldsymbol{x}_n^{k+1}$ denotes the n_{th} column of the $T \times N$ square real-orthogonal matrix $\boldsymbol{X}^{k+1}$, that is $\boldsymbol{X}^{k+1} = \left[\boldsymbol{x}_1^{k+1^t}, \dots, \boldsymbol{x}_N^{k+1^t}\right]$. The elements of $\boldsymbol{X}^k$ and $\boldsymbol{X}^{k+1}$ form an orthonormal basis for an N-dimensional real signal space, this implies that $\boldsymbol{X}^{k^H}\boldsymbol{X}^k = \boldsymbol{I}_N$ and $\boldsymbol{X}^{k+1^H}\boldsymbol{X}^{k+1} = \boldsymbol{I}_N$. Thus if we take the conjugate-transpose of both sides of (3.22), we can obtain:

$$\left[v_{1,j}, \dots, v_{N,j}\right] = \boldsymbol{x}_1^{k+1}\boldsymbol{X}^{k^H} \quad (3.23)$$

The selected coefficient vector can be represented using (3.23), such that given all the possible outcomes of $\boldsymbol{x}^{k+1}$, there exists 2^{Nm} corresponding coefficient vectors. In other words, there is a one-to-one mapping between the coefficient vectors and the input bits. Note that there is no difference between the differentially encoded symbols generated by our co-efficient vector design in (3.22) and those generated by the unitary matrices design, for example in [30] and [63].

Assuming the cooperating relay nodes can differentially recover the original information bits transmitted by the source node. The relay nodes can then differentially re-encode their signals as implemented by the source node in (3.22). In reality, provided the differential scheme is designed such that all nodes in the network have prior knowledge of the co-efficient vector set and the mapping scheme, there is no requirement for the relay nodes to recover the original information bits. In essence, the relay nodes can simply recover the elements of the co-efficient vector set using (3.24), and then use (3.22) for differential encoding.

$$\left[\tilde{v}_{1,j}, \dots, \tilde{v}_{N,j}\right] = \arg min \left| \boldsymbol{r}_n^{k+1} \boldsymbol{r}_n^k - |\boldsymbol{f}_n^k|^2 \left[v_{1,j}, \dots, v_{N,j}\right] \right|^2 \quad (3.24)$$

where $\boldsymbol{r}_n^{k+1} = \boldsymbol{x}_1^{k+1} \odot \boldsymbol{f}_n^{k+1} + \boldsymbol{n}_n^{k+1}$ is the signal received at the n_{th} relay node in the $(k+1)_{th}$ block. The differential decoding protocol employed by our scheme relies on the assumption that the channel co-efficients remain unchanged for transmissions in consecutive blocks, in other words $\boldsymbol{f}_n^k \cong \boldsymbol{f}_n^{k+1}$.

If our scheme is configured such that the relay nodes only recover the elements of the co-efficient vector set as implemented in (3.24), without recovering the original information bits, the computational complexity of the encoder is reduced because the relay nodes avoid the mapper block and co-efficient vector generator block in Fig 3.5. To be precise, the number of comparisons c at each relay node is reduced by $1 \leq c \leq 2^{Nm}$.

We continue our discussion on differential encoding at the relay nodes by illustrating how the co-efficient vector design is implemented with M-PSK constellations for N relays. Note that we assume that the relay nodes can perfectly compute the elements of the coefficient vector set. Consider an M-PSK modulation scheme with spectral efficiency m, the encoder at each relay node generates N modulated signals from Nm information bits. Denote the set of recovered information bits at the encoder as $b_l, l = 1,2, \dots, 2^{2m}$. Following the design in [50] for multiple antenna systems, the co-efficient vector set is computed as

$V = \left\{ \left[v_{1,1}, \dots, v_{N,1}\right]^t, \left[v_{1,2}, \dots, v_{N,2}\right]^t, \dots, \left[v_{1,2^{2m}}, \dots, v_{N,2^{2m}}\right]^t \right\}$. Thus the mapping scheme $P(.)$ for each set of information bits to a co-efficient vector set is defined by:

$$P\{(b_1), (b_2), \dots, (b_{2^{2m}})\} = \left\{ \left[v_{1,1}, \dots, v_{N,1}\right]^t, \left[v_{1,2}, \dots, v_{N,2}\right]^t, \dots, \left[v_{1,2^{2m}}, \dots, v_{N,2^{2m}}\right]^t \right\} \quad (3.25)$$

Let the information signals recovered at the relay nodes in the k_{th} block be denoted by $\tilde{\boldsymbol{x}}_1^k = \left[\tilde{x}_{1(1)}^k, \ldots, \tilde{x}_{1(T)}^k\right]$, this implies that each relay node can construct $\tilde{\boldsymbol{x}}_n^k, n = 1,2,..,N$. In other words, the N relay nodes can jointly construct $\tilde{\boldsymbol{X}}^k = \left[\tilde{\boldsymbol{x}}_1^{k\,t}, \ldots, \tilde{\boldsymbol{x}}_N^{k\,t}\right]$. Note that the signals generated by the relay nodes in the k_{th} block are only required as reference, thus, they can be exclusively independent of the signals generated by the source node in the k_{th} block. The next step is to discuss how the relay nodes differentially compute information signals for the $(k+1)_{th}$ block and how they forward these signals to the destination such that the orthogonal structure of the coding matrix is retained. In the k_{th} block, if as example, the differentially recovered information bits at each relay is (b_1) using (3.25) $P(b_1) = \left[v_{1,1}, \ldots, v_{N,1}\right]^t$. Each relay node first constructs the T length data vector $\boldsymbol{x}_1^{k+1}$ using (3.26) then the n_{th} relay node transmits the T length data vector $\boldsymbol{x}_n^{k+1}$ in (3.27)

$$\boldsymbol{x}_1^{k+1} = \tilde{\boldsymbol{X}}^k \left[v_{1,1}, \ldots, v_{N,1}\right]^t \tag{3.26}$$

$$\boldsymbol{x}_n^{k+1} = \boldsymbol{G}_n \left(\tilde{\boldsymbol{X}}^k \left[v_{1,1}, \ldots, v_{N,1}\right]^t\right) = \boldsymbol{G}_n\, \boldsymbol{x}_1^{k+1} \tag{3.27}$$

where $\boldsymbol{G}_n$ is the relay matrix at the n_{th} relay node designed to maintain the orthogonal structure of $\boldsymbol{X}^{k+1}$ at the destination. In essence each relay transmits a single column of the orthogonal matrix $\boldsymbol{X}^{k+1}$. The signals to be transmitted in the $(k+1)_{th}$ block are represented in terms of a linear combination of the signals in the k_{th} block and the co-efficient vector. The co-efficient vector $\left[v_{1,1}, \ldots, v_{N,1}\right]^t$ is determined by the recovered information bits (b_1).

3.3.2 Differential Decoding Using Co-efficient Vectors

If one receive antenna is used at the destination, the received signal matrix in the k_{th} block is given by:

$$\boldsymbol{Y}^{k} = \left[\boldsymbol{y}_{(1)}^{k\ t}, \boldsymbol{y}_{(2)}^{k\ t}, \dots, \boldsymbol{y}_{(T)}^{k\ t}\right]^{t} = \widetilde{\boldsymbol{X}}^{k}\boldsymbol{H}^{k} + \boldsymbol{Z}^{k} \tag{3.28}$$

where $\boldsymbol{y}_{(t)}^{k} = \left[y_{(t),1}^{k}, \dots, y_{(t),T}^{k}\right]$ denotes the t_{th} column of the $T \times T$ received signal matrix $\boldsymbol{Y}^{k}$, $\boldsymbol{H}^{k} = \left[\boldsymbol{h}_{(1)}^{k\ t}, \boldsymbol{h}_{(2)}^{k\ t}, \dots, \boldsymbol{h}_{(T)}^{k\ t}\right]^{t}$ is the $N \times T$ channel matrix between the relay nodes and the destination, where $\boldsymbol{h}_{(t)}^{k} = \left[h_{(t),1}^{k}, \dots, h_{(t),N}^{k}\right]$, and $\boldsymbol{Z}^{k} = \left[\boldsymbol{z}_{(1)}^{k\ t}, \boldsymbol{z}_{(2)}^{k\ t}, \dots, \boldsymbol{z}_{(T)}^{k\ t}\right]^{t}$ denotes the corresponding noise samples. Similarly the received signal matrix in the$(k + 1)_{th}$ block is given by:

$$\boldsymbol{Y}^{k+1} = \left[\boldsymbol{y}_{(1)}^{k+1^{t}}, \boldsymbol{y}_{(2)}^{k+1^{t}}, \dots, \boldsymbol{y}_{(T)}^{k+1^{t}}\right]^{t} = \boldsymbol{X}^{k+1}\boldsymbol{H}^{k+1} + \boldsymbol{Z}^{k+1} \tag{3.29}$$

where $\boldsymbol{y}_{(t)}^{k+1} = \left[y_{(t),1}^{k+1}, \dots, y_{(t),T}^{k+1}\right]$ denotes the t_{th} column of the $T \times T$ received signal matrix $\boldsymbol{Y}^{k+1}$, $\boldsymbol{H}^{k+1} = \left[\boldsymbol{h}_{(1)}^{k+1^{t}}, \boldsymbol{h}_{(2)}^{k+1^{t}}, \dots, \boldsymbol{h}_{(T)}^{k+1^{t}}\right]^{t}$ is the $N \times T$ channel matrix between the relay nodes and the destination, where $\boldsymbol{h}_{(t)}^{k+1} = \left[h_{(t),1}^{k}, \dots, h_{(t),N}^{k}\right]$, and the corresponding noise samples is denoted by $\boldsymbol{Z}^{k+1} = \left[\boldsymbol{z}_{(1)}^{k+1^{t}}, \boldsymbol{z}_{(2)}^{k+1^{t}}, \dots, \boldsymbol{z}_{(T)}^{k+1^{t}}\right]^{t}$.

Assuming that the fading conditions remain unchanged during consecutive transmissions in both blocks, i.e. $\boldsymbol{H}^{k} \cong \boldsymbol{H}^{k+1}$, the estimate of the elements of the co-efficient vector can be computed at the destination as the entry-wise product of the received signals in both blocks (3.28) and (3.29) as:

$$\left[\tilde{v}_{1,j}, \tilde{v}_{2,j}, \dots, \tilde{v}_{N,j}\right] = \boldsymbol{y}_{(1)}^{k+1} \odot \boldsymbol{Y}^{k}$$

$$= \left(\boldsymbol{X}^{k+1}\boldsymbol{h}_{(1)}^{k+1} + \boldsymbol{z}_{(1)}^{k+1}\right)\left(\widetilde{\boldsymbol{X}}^{k}\boldsymbol{H}^{k} + \boldsymbol{Z}^{k}\right)^{H}$$

$$= \left(\boldsymbol{x}_{1}^{k+1}\boldsymbol{H}^{k+1} + \boldsymbol{z}_{(1)}^{k+1}\right)\left(\widetilde{\boldsymbol{X}}^{k}\boldsymbol{H}^{k} + \boldsymbol{Z}^{k}\right)^{H}$$

$$= \sum_{n=1}^{N} \left|h_{(t),n}^{k}\right|^{2} \boldsymbol{x}_{n}^{k+1} \widetilde{\boldsymbol{X}}^{k^{H}} + \boldsymbol{z}^{k} \tag{3.30}$$

where the equivalent noise $\boldsymbol{z}^{k} = \boldsymbol{z}_{(1)}^{k+1} \widetilde{\boldsymbol{X}}^{k^{H}} \boldsymbol{H}^{k^{H}} + \boldsymbol{x}_{1}^{k+1} \boldsymbol{H}^{k+1} \boldsymbol{Z}^{k^{H}} + \boldsymbol{z}_{(1)}^{k+1} \boldsymbol{Z}^{k^{H}}$. Provided the information signals are perfectly recovered by the relay nodes, substituting $\boldsymbol{x}_{1}^{k+1} = \left[v_{1,1}, \ldots, v_{N,1}\right] \widetilde{\boldsymbol{X}}^{k}$ into (3.30) and using $\boldsymbol{X}^{k^{H}} \boldsymbol{X}^{k} = I_N$ we can reach:

$$\left[\tilde{v}_{1,j}, \tilde{v}_{2,j}, \ldots, \tilde{v}_{N,j}\right] = \sum_{n=1}^{N} \left|h_{(t),n}^{k}\right|^{2} \left[v_{1,j}, v_{2,j}, \ldots, v_{N,j}\right] + \boldsymbol{z}^{k} \tag{3.31}$$

Thus the estimates of the co-efficient vectors are only a function of the differential co-efficient vectors. Since all the elements of the co-efficient vector set V have equal lengths, the destination selects the closest co-efficient vector to $\left[\tilde{v}_{1,j}, \tilde{v}_{2,j}, \ldots, \tilde{v}_{N,j}\right]$ from V as the detector output. Since all the received symbols are uniformly scaled by a factor $\left|h_{(t),n}^{k}\right|^{2}$, the scaling factor will not alter the detection regions of the MPSK constellation. Then inverse mapping is applied to recover the information bits. From (3.31) it is clear that the differential square real-orthogonal design in an N-relay cooperative network is able to achieve an N-level transmit diversity.

The square real-orthogonal design in cooperative networks described so far for $N = \{2,4,8, \ldots\}$ can be used for any cooperative network with p relay nodes $(2 \leq p \leq N)$. The only difference in design is in the structure of the channel matrix $\boldsymbol{H}^{k}$ and $\boldsymbol{H}^{k+1}$, in this case, the path gain $h_{(t),n}^{k},\ n > p$ between the n_{th} relay node and the destination is set to zero.

3.4 Differential Schemes Using Unitary Matrices

The differential encoding scheme discussed in the previous section requires the use of a unit-length co-efficient vector set and inverse mapping at the destination to recover the original information, this causes additional design complexity. In this section, we discuss a

differential scheme that does not require the computation of a co-efficient vector set. This approach uses ML decoding at the destination to recover the information signals. Consider the cooperative set-up with N relay nodes depicted in Fig.3.4. The transmission from the source node to the destination is divided into block k and block $k+1$, and each block is sub-divided into the 'transmit' and 'cooperate' stages. Each stage contains T symbol transmissions meaning that the information signals are in groups of T symbols. In this set-up we include the power allocation strategy at the source node and the cooperating nodes, and assume that the cooperating nodes simply amplify their received signals and forward to the destination without decoding.

3.4.1 Differential Encoding using Unitary Matrices

Similar to the co-efficient vector design, let $\boldsymbol{X}^k$ denote the $T \times N$ 'reference' orthogonal matrix given by $\boldsymbol{X}^k = \left[\boldsymbol{x}_1^{k\,t}, \ldots, \boldsymbol{x}_N^{k\,t}\right]$ where $\boldsymbol{x}_n^k$ is the n_{th} column of $\boldsymbol{X}^k$. The source node commences differential encoding in the k_{th} block by transmitting the reference information signal $\boldsymbol{x}_1^k = \left[x_{1(1)}^k, \ldots, x_{1(T)}^k\right]$ to the n_{th} relay node, where $\boldsymbol{x}_n^k$ denotes the n_{th} column of $\boldsymbol{X}^k$. The elements of $\boldsymbol{X}^k$ are normalized such that $E\left\{tr\left(\boldsymbol{X}^{k\,H}\boldsymbol{X}^k\right)\right\} = N$, in other words $\boldsymbol{x}_n^k \in \boldsymbol{X}^k/\sqrt{N}$. Specifically, in the 'transmit' stage of the k_{th} block, the source node sends $\sqrt{P_S T}\,\boldsymbol{x}_1^k$ where $P_S T$ is the average transmit power allocated to the source node. The received signal at the n_{th} relay node is:

$$\boldsymbol{r}_n^k = \sqrt{P_S T}\,\boldsymbol{x}_1^k \odot \boldsymbol{f}_n^k + \boldsymbol{n}_n^k \tag{3.32}$$

where $\boldsymbol{f}_n^k = \left[f_{n(1)}^k, \ldots, f_{n(T)}^k\right]$ is the Rayleigh fading channel model between the source node and the n_{th} relay node assumed to be made up of iid zero mean and unit-variance complex

random variables. The corresponding noise $\boldsymbol{n}_n^k = \left[n_{n(1)}^k, \ldots, n_{n(T)}^k\right]$ is made up of independent samples of a zero mean complex Gaussian random variable. The n_{th} relay node linearly processes the received signal $\boldsymbol{r}_n^k = \left[r_{n(1)}^k, \ldots, r_{n(T)}^k\right]$ and transmits a $1 \times T$ data vector $\boldsymbol{t}_n^k = \left[t_{n(1)}^k, \ldots, t_{n(T)}^k\right]$ given by:

$$\boldsymbol{t}_n^k = \sqrt{\frac{P_C}{P_S+1}}\boldsymbol{M}_n\boldsymbol{r}_n^k \tag{3.33}$$

where $\boldsymbol{M}_n$ is the relay matrix at the n_{th} relay node, the matrix $\boldsymbol{M}_n$ is designed as in Section II of [64] per block such that the N relay nodes can generate an orthogonal codeword at the destination. The power allocated to each relay node is denoted by P_C, this implies that an amplification co-efficient $\mu = \sqrt{P_C/(P_S+1)}$ is applied at each relay node. Replicating the power allocation strategy in [65], we set $P_S = P_C N = P/2$, where P denotes the total power available in the network. In other words, the source node and the relay nodes share the available power in the network.

Assuming the relay nodes are synchronized at symbol level such that the nodes transmit simultaneously. The signal received at the destination in the k_{th} block is given by:

$$\boldsymbol{y}_{k,t} = \sum_{n=1}^{N} \boldsymbol{t}_n^k \odot \boldsymbol{g}_n^k + \boldsymbol{z}_{k,t},\ t = 1,2,..,T \tag{3.34}$$

where $\boldsymbol{g}_n^k = \left[g_{n(1)}^k, \ldots, g_{n(T)}^k\right]$ is the Rayleigh fading channel model between the n_{th} relay node and the destination, and $\boldsymbol{z}_{k,t}$ is the corresponding noise. Substituting for $\boldsymbol{t}_n^k$ and then $\boldsymbol{r}_n^k$ in (3.33) and (3.32) respectively (3.34) becomes:

$$\boldsymbol{y}_{k,t} = \sum_{n=1}^{N} \sqrt{\frac{P_C P_S T}{P_S+1}}\boldsymbol{M}_n\boldsymbol{x}_1^k \odot \boldsymbol{f}_n^k \odot \boldsymbol{g}_n^k + \tilde{\boldsymbol{z}}_{k,t} \tag{3.35}$$

where $\tilde{\boldsymbol{z}}_{k,t} = \sum_{n=1}^{N} \mu \boldsymbol{M}_n \boldsymbol{g}_n^k \boldsymbol{n}_n^k + \boldsymbol{z}_{k,t}$ is the equivalent noise. The signal received at the destination in the k_{th}block can be written in compact form as:

$$\boldsymbol{Y}_k = \sqrt{\rho}\boldsymbol{X}^k\boldsymbol{H}^k + \boldsymbol{Z}_k \tag{3.36}$$

where $\boldsymbol{Y}_k = \left[\boldsymbol{y}_{k,1}{}^T, \dots, \boldsymbol{y}_{k,T}{}^T\right]^T \in \mathbb{C}^{T\times T}$, $\boldsymbol{y}_{k,t} = \left[y_{k,t(1)}, \dots, y_{k,t(T)}\right]$, $\rho = \frac{P_C P_S T}{P_S+1}$, $\boldsymbol{X}^k = \left[\boldsymbol{M}_1\boldsymbol{x}_1^{k\,T}, \dots, \boldsymbol{M}_N\boldsymbol{x}_1^{k\,T}\right] \in \mathbb{C}^{T\times N}$, $\boldsymbol{H}^k = \left[\boldsymbol{h}_{k,1}{}^T, \dots, \boldsymbol{h}_{k,T}{}^T\right]^T \in \mathbb{C}^{N\times T}$, $\boldsymbol{h}_{k,t} = \left[h_{k,t(1)}, \dots, h_{k,t(N)}\right]$ and $\boldsymbol{Z}_k = \left[\tilde{\boldsymbol{z}}_{k,1}{}^T, \dots, \tilde{\boldsymbol{z}}_{k,T}{}^T\right]^T \in \mathbb{C}^{T\times T}$

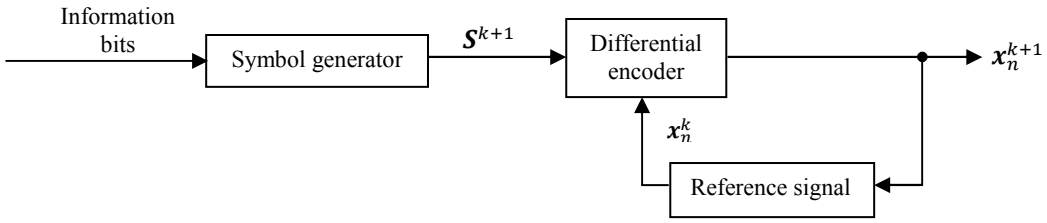

Fig.3.6 Differential encoder using unitary matrices

In the previous section, for differential encoding to take place, the input information bits in the $(k+1)_{th}$ block are used to select corresponding elements of the co-efficient vector set. As depicted in Fig.3.6, the co-efficient vector set is not required for this approach. The input information bits are only used to pick symbols from a normalized constellation set. So instead of using the input bits to select elements from the co-efficient vector set as discussed in the previous section, the input bits are used to select input symbols $\boldsymbol{s}_1^{k+1} = \left[s_{1(1)}^{k+1}, \dots, s_{1(T)}^{k+1}\right]$ from an MPSK or MQAM constellation. The encoder then constructs the input orthogonal matrix $\boldsymbol{S}^{k+1} = \left[\boldsymbol{s}_1^{k+1\,t}, \dots, \boldsymbol{s}_N^{k+1\,t}\right]$ where $\boldsymbol{s}_n^{k+1}$ is the n_{th} column of $\boldsymbol{S}^{k+1}$. For example, for a cooperative network with $N = 2$ relay nodes, the encoder

constructs $\boldsymbol{S}^{k+1} = \begin{bmatrix} s_{1(1)}^{k+1} & s_{1(2)}^{k+1} \\ -s_{1(2)}^{k+1^*} & s_{1(1)}^{k+1^*} \end{bmatrix}$. The information signals $\boldsymbol{x}_1^{k+1} = \left[x_{1(1)}^{k+1}, \dots, x_{1(T)}^{k+1}\right]$ to be transmitted by the source node in the $(k+1)_{th}$ block is obtained by:

$$\boldsymbol{x}_1^{k+1} = \boldsymbol{x}_1^k \boldsymbol{S}^{k+1} \tag{3.37}$$

where $\boldsymbol{x}_n^{k+1}$ is the n_{th} column the $T \times N$ orthogonal signal matrix given by $\boldsymbol{X}^{k+1} = \left[\boldsymbol{x}_1^{k+1^t}, \dots, \boldsymbol{x}_N^{k+1^t}\right]$. The codeword matrix $\boldsymbol{S}^{k+1}$ also has an orthogonal structure such that if all the symbols are normalized, the matrix is unitary, that means $\boldsymbol{S}^{k+1^H}\boldsymbol{S}^{k+1} = I_N$. Due to the orthogonality of the codewords, the resultant orthogonal data matrix $\boldsymbol{X}^{k+1}$ is also unitary, in other words $\boldsymbol{X}^{k+1^H}\boldsymbol{X}^{k+1} = I_N$. Note that the outputs of the two differential encoding approaches in (3.26) and (3.37) are the same.

3.4.2 Differential Decoding using Unitary Matrices

Repeating the transmit-and-cooperate procedure as in the k_{th} block, the signal received at the destination from the cooperating relay nodes in the $(k+1)_{th}$ block can be written in vector form as:

$$\boldsymbol{Y}_{k+1} = \sqrt{\rho}\boldsymbol{X}^{k+1}\boldsymbol{H}^{k+1} + \boldsymbol{Z}_{k+1} \tag{3.38}$$

where $\boldsymbol{Y}_{k+1} = \left[\boldsymbol{y}_{k+1,1}{}^T, \dots, \boldsymbol{y}_{k+1,T}{}^T\right]^T \in \mathbb{C}^{T\times T}$, $\boldsymbol{y}_{k+1,t} = \left[y_{k+1,t(1)}, \dots, y_{k+1,t(T)}\right]$,$\rho = \frac{P_C P_S T}{P_S+1}$, $\boldsymbol{X}^{k+1} = \left[\boldsymbol{M}_1\boldsymbol{x}_1^{k+1^T}, \dots, \boldsymbol{M}_N\boldsymbol{x}_1^{k+1^T}\right] \in \mathbb{C}^{T\times N}$, $\boldsymbol{H}^{k+1} = \left[\boldsymbol{h}_{k+1,1}{}^T, \dots, \boldsymbol{h}_{k+1,T}{}^T\right]^T \in \mathbb{C}^{N\times T}$, $\boldsymbol{h}_{k+1,t} = \left[h_{k+1,t(1)}, \dots, h_{k+1,t(N)}\right]$ and $\boldsymbol{Z}_{k+1} = \left[\tilde{\boldsymbol{z}}_{k+1,1}{}^T, \dots, \tilde{\boldsymbol{z}}_{k+1,T}{}^T\right]^T \in \mathbb{C}^{T\times T}$

We can ignore the power term $\sqrt{\rho}$ and rewrite the received signal at the destinationin the $(k+1)_{th}$ block as:

$$\boldsymbol{y}_{k+1,t} = \boldsymbol{X}^{k+1}\boldsymbol{h}_{k+1,t} + \tilde{\boldsymbol{z}}_{k+1,t} = \boldsymbol{x}_n^{k+1}\,\boldsymbol{H}^{k+1} + \tilde{\boldsymbol{z}}_{k+1,t},\ t = 1,2,\dots,T\ \ n = 1,2,\dots,N \qquad (3.39)$$

If the channel statistics remain unchanged during the transmissions in both blocks, meaning $\boldsymbol{H}^k \cong \boldsymbol{H}^{k+1}$ we can reach:

$$\boldsymbol{y}_{k+1,1} = \boldsymbol{x}_1^{k+1}\,\boldsymbol{H}^k + \tilde{\boldsymbol{z}}_{k+1,1} \qquad (3.40)$$

Substituting for $\boldsymbol{x}_1^{k+1}$in (3.37), the equality in (3.40) becomes:

$$\boldsymbol{y}_{k+1,1} = \boldsymbol{x}_1^{k}\boldsymbol{S}^{k+1}\,\boldsymbol{H}^k + \tilde{\boldsymbol{z}}_{k+1,1}$$

$$\boldsymbol{y}_{k+1,1} = \boldsymbol{S}^{k+1}\left(\boldsymbol{y}_{k,1} - \tilde{\boldsymbol{z}}_{k,1}\right) + \tilde{\boldsymbol{z}}_{k+1,1}$$

$$= \boldsymbol{S}^{k+1}\boldsymbol{y}_{k,1} + \acute{\boldsymbol{z}}_{k+1,1} \qquad (3.41)$$

where $\acute{\boldsymbol{z}}_{k+1,1} = \tilde{\boldsymbol{z}}_{k+1,1} - \tilde{\boldsymbol{z}}_{k,1}\boldsymbol{S}^{k+1}$. Since the noise components are all made up of iid Gaussian vectors with zero mean, we can induce that $\acute{\boldsymbol{z}}_{k+1,1} \approx \tilde{\boldsymbol{z}}_{k+1,1}$. Thus, the input codeword $\boldsymbol{S}^{k+1}$ which contains the original information symbols $s_{1(1)}^{k+1},\dots,s_{1(T)}^{k+1}$ can be linearly recovered using ML decoding. For example for a cooperative network with $N = 2$ relay nodes and $T = 2$, the information symbols $s_{1(1)}^{k+1}$ and $s_{1(2)}^{k+1}$ can be recovered using ML decoding as follows:

$$\tilde{\boldsymbol{S}}^{k+1} = \underbrace{\arg\min}_{\boldsymbol{S}^{k+1}} \left\|\boldsymbol{y}_{k+1,1} - \boldsymbol{S}^{k+1}\boldsymbol{y}_{k,1}\right\|_F^2 \qquad (3.42)$$

where $\|A\|_F$ is the Frobenius norm. Replacing the Frobenius norm with the trace function $tr(A^H A)$, (3.42) becomes:

$$\tilde{\boldsymbol{S}}^{k+1} = \underbrace{\arg\min}_{\boldsymbol{S}^{k+1}}\ tr\left[\left(\boldsymbol{y}_{k+1,1} - \boldsymbol{S}^{k+1}\boldsymbol{y}_{k,1}\right)^H\left(\boldsymbol{y}_{k+1,1} - \boldsymbol{S}^{k+1}\boldsymbol{y}_{k,1}\right)\right] \qquad (3.43)$$

Expanding the terms in (3.43) and ignoring the identity matrix results in:

$$\tilde{\boldsymbol{S}}^{k+1} = \underbrace{\arg min}_{\boldsymbol{S}^{k+1}} \; tr\left[-\boldsymbol{S}^{k+1}\boldsymbol{y}_{k,1}\boldsymbol{y}_{k+1,1}{}^{H} - \boldsymbol{S}^{k+1}{}^{H}\boldsymbol{y}_{k,1}{}^{H}\boldsymbol{y}_{k+1,1}\right]$$

$$= \underbrace{\arg max}_{\boldsymbol{S}^{k+1}} \; tr\left[\Re\left\{\boldsymbol{y}_{k+1,1}{}^{H}\boldsymbol{S}^{k+1}\boldsymbol{y}_{k,1}\right\}\right] \tag{3.44}$$

Decoupling the input codeword $\boldsymbol{S}^{k+1}$ into the real and imaginary parts of the input symbols, $\Re\{s_{1(t)}^{k+1}\}$ and $\Im\{s_{1(t)}^{k+1}\}$ respectively, we can reach:

$$\boldsymbol{S}^{k+1} = \Re\{s_{1(1)}^{k+1}\}\begin{bmatrix}1 & 0\\ 0 & 1\end{bmatrix} + \Re\{s_{1(2)}^{k+1}\}\begin{bmatrix}0 & 1\\ -1 & 0\end{bmatrix} + j\Im\{s_{1(1)}^{k+1}\}\begin{bmatrix}1 & 0\\ 0 & -1\end{bmatrix} + j\Im\{s_{1(2)}^{k+1}\}\begin{bmatrix}0 & 1\\ 1 & 0\end{bmatrix} \tag{3.45}$$

By substituting (3.45) into (3.44), the ML decoder can independently recover the input symbols using the received signals in both blocks as follows:

$$\tilde{s}_{1(1)}^{k+1} =$$

$$\underbrace{\arg max}_{s_{1(1)}^{k+1}}\left[\Re\left\{tr\left[\boldsymbol{y}_{k+1,1}{}^{H}\begin{bmatrix}1 & 0\\ 0 & 1\end{bmatrix}\boldsymbol{y}_{k,1}\right]\right\}\Re\{s_{1(1)}^{k+1}\} + \Re\left\{tr\left[\boldsymbol{y}_{k+1,1}{}^{H}j\begin{bmatrix}1 & 0\\ 0 & -1\end{bmatrix}r_{d(i)}^{k}\right]\right\}\Im\{s_{1(1)}^{k+1}\}\right]$$

$$\tilde{s}_{1(2)}^{k+1} =$$

$$\underbrace{\arg max}_{s_{1(2)}^{k+1}}\left[\Re\left\{tr\left[\boldsymbol{y}_{k+1,1}{}^{H}\begin{bmatrix}0 & 1\\ -1 & 0\end{bmatrix}\boldsymbol{y}_{k,1}\right]\right\}\Re\{s_{1(2)}^{k+1}\} + \Re\left\{tr\left[\boldsymbol{y}_{k+1,1}{}^{H}j\begin{bmatrix}0 & 1\\ 1 & 0\end{bmatrix}\boldsymbol{y}_{k,1}\right]\right\}\Im\{s_{1(2)}^{k+1}\}\right] \tag{3.46}$$

Expanding (3.46) results in:

$$\tilde{s}_{1(1)}^{k+1} = \underbrace{\arg max}_{s_{1(1)}^{k+1}}\left[\Re\{y_{k+1,1(1)}{}^{H}y_{k,1(1)} + y_{k+1,1(2)}{}^{H}y_{k,1(2)}\}\Re\{s_{1(1)}^{k+1}\}\right.$$

$$\left. + \Re\{j\left[y_{k+1,1(1)}{}^{H}y_{k,1(1)} - y_{k+1,1(2)}{}^{H}y_{k,1(2)}\right]\}\Im\{s_{1(1)}^{k+1}\}\right]$$

$$\tilde{s}_{1(2)}^{k+1} =$$

$$\underbrace{\arg max}_{s_{1(2)}^{k+1}} \left[\Re\{-{y_{k+1,1(2)}}^{H} y_{k,1(1)} + {y_{k+1,1(1)}}^{H} y_{k,1(2)}\}\Re\{s_{1(2)}^{k+1}\} + \Re\{j[{y_{k+1,1(2)}}^{H} y_{k,1(1)} + {y_{k+1,1(1)}}^{H} y_{k,1(2)}]\}\Im\{s_{1(2)}^{k+1}\}\right] \quad (3.47)$$

3.5 Differential Square Real Orthogonal Designs in Cooperative Networks

The differential orthogonal scheme can be extended to cooperative networks with $N > 2$ relay nodes using square real-orthogonal codes. Differential square real orthogonal codes were first proposed in [62] for multiple antenna systems, and are shown in [34] [35] [66] to achieve full diversity, full rate and linear decoding in multiple antenna systems with four and eight transmit antennas. Differential square real-orthogonal designs were introduced to cooperative networks with four and eight relay nodes in [30]. There the authors discuss the generalized structure of the operating matrix at the relay nodes and present a generalized differential encoding and decoding scheme. In this section we show how differential encoding and decoding of square real-orthogonal codes can be implemented in cooperative networks using co-efficient vectors as utilized in Section 3.2, we also present differential encoding and decoding using unitary matrices based on the design for multiple antenna systems in [35]. We first consider differential square real-orthogonal designs for 4-relay networks, we then discuss for networks with three and eight relay nodes.

3.5.1 Differential Square Real-orthogonal Designs using Co-efficient Vectors

Consider a 4-relay cooperative network with a source node S, $N = 4$ relay nodes and destination D as illustrated in Fig.3.7. The transmission from S to D is divided into block k

and block $k+1$, and each block is sub-divided into the 'transmit' and 'cooperate' stages. Each stage contains T symbol transmissions meaning that the information signals are in groups of T symbols $s_i^K, i = (1, \dots, T),\ K \in \{k, k+1\}$.

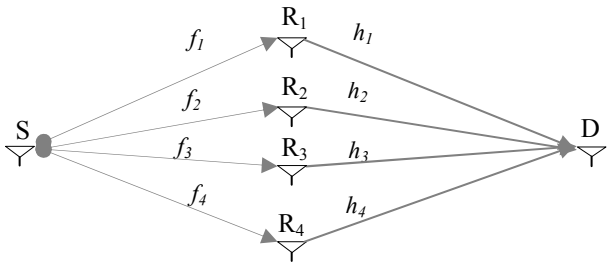

Fig.3.7 Four-relay cooperative network

In this set-up, emphasis is on how differential encoding and decoding takes place at the source node and destination respectively. Similar to the co-efficient vector design in Section 3.2, let $\boldsymbol{X}^k$ denote the $T \times N$ 'reference' orthogonal matrix given by $\boldsymbol{X}^k = \left[\boldsymbol{x}_1^{k\,t}, \dots, \boldsymbol{x}_N^{k\,t}\right]$ where $\boldsymbol{x}_n^k$ is the n_{th} column of $\boldsymbol{X}^k$. The source node transmits $\boldsymbol{x}_1^k = \left[x_{1(1)}^k, x_{1(2)}^k, x_{1(3)}^k, x_{1(4)}^k\right]$ to the $N = 4$ cooperating nodes, in essence in the k_{th} block; the source node transmits a column vector of $\boldsymbol{X}^k$. The N cooperating relay nodes then construct codewords using their relay matrices to generate the $N \times T$ square real-orthogonal matrix $\boldsymbol{X}^k$ at the destination. In the $(k+1)_{th}$ block, a set of Nm information bits from $m = log_2 M$ MPSK constellation is generated at the source node by the encoder. Note that for real orthogonal designs, the resultant symbols must be real.

The source node constructs a length 2^{Nm} co-efficient vector set given by $V = \left\{\left[v_{1,1}, \dots, v_{N,1}\right]^t, \left[v_{1,2}, \dots, v_{N,2}\right]^t, \dots, \left[v_{1,2^{2m}}, \dots, v_{N,2^{2m}}\right]^t\right\}$. Then based on the input information bits, the encoder selects the corresponding N-length co-efficient vector $\left[v_{1,j}, \dots, v_{N,j}\right]^t, j \in \{1,2, \dots, 2^{2m}\}$ from V. The source node then computes the information

signals for the $(k+1)_{th}$ block using the information signals in the k_{th} block and the selected co-efficient vector as follows:

$$\boldsymbol{x}_1^{k+1} = \boldsymbol{X}^k \left[v_{1,j}, \ldots, v_{N,j}\right]^t \tag{3.48}$$

where $\boldsymbol{x}_n^{k+1}$ denotes the n_{th} column of the $N \times T$ square real-orthogonal matrix $\boldsymbol{X}^{k+1}$. The elements of $\boldsymbol{X}^k$ form an orthonormal basis for a four-dimensional real signal space, this implies that $\boldsymbol{X}^{k^H}\boldsymbol{X}^k = I_4$ thus if we take the conjugate-transpose of both sides of (3.48), we can obtain:

$$\left[v_{1,j}, \ldots, v_{N,j}\right]^t = \boldsymbol{X}^k \boldsymbol{x}_1^{k+1^H} \tag{3.49}$$

The selected coefficient vector can be represented using (3.49), such that given all the possible outcomes of $\boldsymbol{x}_1^{k+1}$, there exists 2^{Nm} corresponding coefficient vectors. In other words, there is a one-to-one mapping between the coefficient vectors and the input information signals.

Assuming that the relay nodes can compute the coefficient vector set such that they can differentially decode and re-encode their received signals as in Section 3.2, if one receive antenna is used at the destination, the received signal in the k_{th} block is given by:

$$\boldsymbol{Y}^k = \left[\boldsymbol{y}_{(1)}^k, \boldsymbol{y}_{(2)}^k, \boldsymbol{y}_{(3)}^k, \boldsymbol{y}_{(4)}^k\right]^t = \widetilde{\boldsymbol{X}}^k \boldsymbol{H}^k + \left[\boldsymbol{z}_{(1)}^k, \boldsymbol{z}_{(2)}^k, \boldsymbol{z}_{(3)}^k, \boldsymbol{z}_{(4)}^k\right]^t \tag{3.50}$$

where $\boldsymbol{y}_{(t)}^k = \left[y_{t(1)}^k, y_{t(2)}^k, y_{t(3)}^k, y_{t(4)}^k\right]^t$, $\boldsymbol{H}^k$ is the $N \times T$ channel matrix between the relay nodes and the destination given by

$$\boldsymbol{H}^k = \begin{bmatrix} h_1 & h_2 & h_3 & h_4 \\ h_2 & -h_1 & h_4 & h_3 \\ h_3 & h_4 & -h_1 & -h_2 \\ h_4 & -h_3 & h_2 & -h_1 \end{bmatrix} \tag{3.51}$$

where h_n is the channel co-efficient between the n_{th} relay node and the destination, and $\boldsymbol{z}_{(t)}^{k} = \left[z_{t(1)}^{k}, z_{t(2)}^{k}, z_{t(3)}^{k}, z_{t(4)}^{k}\right]^{t}$ denotes the corresponding noise samples. Similarly the received signal in the first transmission interval of the $(k+1)_{th}$ block is given by:

$$\boldsymbol{y}_{(1)}^{k+1} = \tilde{\boldsymbol{x}}_{1}^{k+1}\boldsymbol{H}^{k+1} + \boldsymbol{z}_{(1)}^{k+1} \tag{3.52}$$

Assuming that the fading conditions remain unchanged during the transmission in both blocks, i.e. $\boldsymbol{H}^{k} \cong \boldsymbol{H}^{k+1}$, the estimate of elements of the co-efficient vector can be computed as the entry-wise product of the received signals in both blocks (4.3) and (4.5) as:

$$\begin{aligned}\left[\tilde{v}_{1,j}, \tilde{v}_{2,j}, \tilde{v}_{3,j}, \tilde{v}_{4,j}\right] &= \boldsymbol{y}_{(1)}^{k+1} \odot \boldsymbol{Y}^{k} \\ &= \left(\tilde{\boldsymbol{x}}_{1}^{k+1}\boldsymbol{H}^{k+1} + \boldsymbol{z}_{(1)}^{k+1}\right)\left(\tilde{\boldsymbol{X}}^{k}\boldsymbol{H}^{k} + \boldsymbol{Z}^{k}\right)^{H} \\ &= \sum_{n=1}^{4}\left|h_{R_nD}\right|^{2}\tilde{\boldsymbol{x}}_{1}^{k+1}{\tilde{\boldsymbol{X}}^{k}}^{H} + \tilde{\boldsymbol{z}}^{k}\end{aligned} \tag{3.53}$$

where the equivalent noise $\tilde{\boldsymbol{z}}^{k} = {\boldsymbol{Z}^{k}}^{H}\tilde{\boldsymbol{x}}_{1}^{k+1}\boldsymbol{H}^{k+1} + \boldsymbol{z}_{(1)}^{k+1}{\tilde{\boldsymbol{X}}^{k}}^{H}{\boldsymbol{H}^{k}}^{H} + {\boldsymbol{Z}^{k}}^{H}\boldsymbol{z}_{(1)}^{k+1}$. Provided the information signals are perfectly recovered by the relay nodes, substituting (3.49) into (3.53) we can reach:

$$\left[\tilde{v}_{1,j}, \tilde{v}_{2,j}, \tilde{v}_{3,j}, \tilde{v}_{4,j}\right] = \sum_{n=1}^{4}\left|h_{R_nD}\right|^{2}\left[v_{1,j}, v_{2,j}, v_{3,j}, v_{4,j}\right] + \tilde{\boldsymbol{z}}^{k} \tag{3.54}$$

Thus the estimates of the co-efficient vectors are only a function of the differential co-efficient vectors. Since all the elements of the co-efficient vector set V have equal lengths, the destination selects the closest co-efficient vector to $\left[\tilde{v}_{1,j}, \tilde{v}_{2,j}, \tilde{v}_{3,j}, \tilde{v}_{4,j}\right]$ from V as the detector output. Then inverse mapping is applied to recover the information bits. From (3.54) it is clear that the differential real-orthogonal design in a 4-relay cooperative set-up is able to achieve a four-level transmit diversity.

3.5.2 Differential Square Real-orthogonal Designs using Unitary Matrices

For differential square-real-orthogonal designs utilizing unitary matrices, the differential encoding and decoding procedure is identical to the case of differential orthogonal designs in 2-relay cooperative networks utilizing unitary matrices discussed in Section 3.4. Consider the same cooperative set-up with $N = 4$ relay nodes depicted in Fig.3.7, in the k_{th} block the source node generates $T = 4$ information symbols selected from normalized signal points of an MPSK constellation. Reiterating the transmit-and-cooperate procedure as in the design for the 2-relay cooperative network, in the k_{th} block, the relay nodes receive the signal from the source node and cooperatively construct the $N \times T$ square real-orthogonal matrix at the destination. Hence, the received signal in the k_{th} block is given in compact form as:

$$\boldsymbol{Y}_k = \sqrt{\rho}\boldsymbol{X}^k\boldsymbol{H}^k + \boldsymbol{Z}_k \tag{3.55}$$

where $\boldsymbol{Y}_k = \left[\boldsymbol{y}_{k,1}{}^t, \dots, \boldsymbol{y}_{k,T}{}^t\right]^t \in \mathbb{C}^{T\times T}$, $\boldsymbol{y}_{k,t} = \left[y_{k,t(1)}, \dots, y_{k,t(T)}\right]$, $\rho = \frac{P_C P_S T}{P_S+1}$, $\boldsymbol{X}^k = \left[\boldsymbol{M}_1\boldsymbol{x}_1^{k\,t}, \boldsymbol{M}_2\boldsymbol{x}_1^{k\,t}, \boldsymbol{M}_3\boldsymbol{x}_1^{k\,t}, \boldsymbol{M}_4\boldsymbol{x}_1^{k\,t}\right] \in \mathbb{C}^{T\times N}$, $\boldsymbol{H}^k = \left[\boldsymbol{h}_{k,1}{}^t, \dots, \boldsymbol{h}_{k,T}{}^t\right]^t \in \mathbb{C}^{N\times T}$, $\boldsymbol{h}_{k,t} = \left[h_{k,t(1)}, \dots, h_{k,t(N)}\right]$ and $\boldsymbol{Z}_k = \left[\tilde{\boldsymbol{z}}_{k,1}{}^t, \dots, \tilde{\boldsymbol{z}}_{k,T}{}^t\right]^t \in \mathbb{C}^{T\times T}$

$\boldsymbol{M}_n$ is the relay matrix at the n_{th} relay node and the elements are given by:

$$\boldsymbol{M}_1 = \boldsymbol{I}_4,\quad \boldsymbol{M}_2 = \begin{bmatrix} 0 & 1 & 0 & 0 \\ -1 & 0 & 0 & 0 \\ 0 & 0 & 0 & -1 \\ 0 & 0 & 1 & 0 \end{bmatrix},\ \boldsymbol{M}_3 = \begin{bmatrix} 0 & 0 & 1 & 0 \\ 0 & 0 & 0 & 1 \\ -1 & 0 & 0 & 0 \\ 0 & -1 & 0 & 0 \end{bmatrix},\ \boldsymbol{M}_4 = \begin{bmatrix} 0 & 0 & 0 & 1 \\ 0 & 0 & -1 & 0 \\ 0 & 1 & 0 & 0 \\ -1 & 0 & 0 & 0 \end{bmatrix}$$

Provided the information symbols are selected from normalized constellation points, the only difference between (3.55) and (3.36) is the structure of the signal matrix $\boldsymbol{X}^k$ and the channel

matrix $\boldsymbol{H}^k$. Similarly the information signal $\boldsymbol{x}_1^{k+1}$ to be transmitted by the source in the $(k+1)_{th}$ block is obtained as in (3.37) by:

$$\boldsymbol{x}_1^{k+1} = \boldsymbol{x}_1^k \boldsymbol{S}^{k+1} \tag{3.56}$$

Here, $\boldsymbol{x}_n^{k+1}$ and $\boldsymbol{x}_n^k$ are $1 \times N$ signal matrices which denote the n_{th} column of their corresponding $N \times T$ square real-orthogonal signal matrix, and $\boldsymbol{S}^{k+1}$ is the $N \times T$ input unitary codeword whose elements represent the information symbols from the encoder in the $(k+1)_{th}$ block, $\boldsymbol{S}^{k+1}$ is of the form [34]:

$$\boldsymbol{S}^{k+1} = \begin{bmatrix} s_1^{k+1} & s_2^{k+1} & s_3^{k+1} & s_4^{k+1} \\ -s_2^{k+1} & s_1^{k+1} & -s_4^{k+1} & s_3^{k+1} \\ -s_3^{k+1} & s_4^{k+1} & s_1^{k+1} & -s_2^{k+1} \\ -s_4^{k+1} & -s_3^{k+1} & s_2^{k+1} & s_1^{k+1} \end{bmatrix} \tag{3.57}$$

The codeword matrix $\boldsymbol{S}^{k+1}$ is an orthogonal design such that if all the symbols are normalized, the codewords are unitary, that means $\boldsymbol{S}^{k+1^H}\boldsymbol{S}^{k+1} = \boldsymbol{I}_4$. Due to the orthogonality of the codewords, the resultant orthogonal data matrix $\boldsymbol{X}^{k+1}$ is also unitary. In other words, $\boldsymbol{X}^{k+1^H}\boldsymbol{X}^{k+1} = \boldsymbol{X}^{k^H}\boldsymbol{X}^k = \boldsymbol{I}_4$. Repeating the transmit-and-cooperate stages for the $(k+1)_{th}$ block as in Section 3.3, the signal received at the destination is given in compact form as:

$$\boldsymbol{y}_{(t)}^{k+1} = \sqrt{\rho}\boldsymbol{x}_1^{k+1}\boldsymbol{H}^{k+1} + \boldsymbol{z}_{(t)}^{k+1} \tag{3.58}$$

Substituting for $\boldsymbol{x}_1^{k+1}$ in (3.56) into (3.58) we have:

$$\boldsymbol{y}_{(t)}^{k+1} = \sqrt{\rho}\boldsymbol{x}_1^k\boldsymbol{S}^{k+1}\boldsymbol{H}^{k+1} + \boldsymbol{z}_{(t)}^{k+1} \tag{3.59}$$

If the channel statistics remain unchanged during the transmissions in both blocks, meaning $\boldsymbol{H}^k = \boldsymbol{H}^{k+1}$ we can reach:

$$\boldsymbol{y}_{(t)}^{k+1} = \boldsymbol{S}^{k+1}\left(\boldsymbol{y}_{(t)}^{k} - \boldsymbol{z}_{(t)}^{k}\right) + \boldsymbol{z}_{(t)}^{k+1}$$

$$= \boldsymbol{S}^{k+1}\boldsymbol{y}_{(t)}^{k} + \acute{\boldsymbol{z}}_{(t)}^{k+1} \tag{3.60}$$

where $\acute{\boldsymbol{z}}_{(t)}^{k+1} = \boldsymbol{z}_{(t)}^{k+1} - \boldsymbol{S}^{k+1}\boldsymbol{z}_{(t)}^{k}$. Since the noise components are all made up of iid Gaussian vectors with zero mean, we can induce that $\boldsymbol{z}_{(t)}^{k+1} \approx \acute{\boldsymbol{z}}_{(t)}^{k+1}$. Thus, the input codeword $\boldsymbol{S}^{k+1}$ which contains the original information signals $s_t^{k+1}, t \in \{1,2, \dots 4\}$ can be linearly recovered using ML decoding:

$$\tilde{\boldsymbol{S}}^{k+1} = \underbrace{\arg min}_{S^{k+1}} \left\| \boldsymbol{y}_{(t)}^{k+1} - \boldsymbol{S}^{k+1}\boldsymbol{y}_{(t)}^{k} \right\|_F^2 \tag{3.61}$$

$$\tilde{\boldsymbol{S}}^{k+1} = \underbrace{\arg min}_{S^{k+1}} \; tr\left[\left(\boldsymbol{y}_{(t)}^{k+1} - \boldsymbol{S}^{k+1}\boldsymbol{y}_{(t)}^{k}\right)^H \left(\boldsymbol{y}_{(t)}^{k+1} - \boldsymbol{S}^{k+1}\boldsymbol{y}_{(t)}^{k}\right)\right] \tag{3.62}$$

Expanding the terms in (3.62) and ignoring the identity matrix results in:

$$\tilde{\boldsymbol{S}}^{k+1} = \underbrace{\arg min}_{S^{k+1}} \; tr\left[-\boldsymbol{S}^{k+1}\boldsymbol{y}_{(t)}^{k}\boldsymbol{y}_{(t)}^{k+1^H} - \boldsymbol{S}^{k+1^H}\boldsymbol{y}_{(t)}^{k\;H}\boldsymbol{y}_{(t)}^{k+1}\right]$$

$$= \underbrace{\arg max}_{S^{k+1}} \; tr\left[\Re\left\{\boldsymbol{y}_{(t)}^{k+1^H}\boldsymbol{S}^{k+1}\boldsymbol{y}_{(t)}^{k}\right\}\right] \tag{3.63}$$

Decoupling the input codeword $\boldsymbol{S}^{k+1}$ in (3.57) into its constituent real and imaginary parts, $\Re\{s_t^{k+1}\}$ and $\Im\{s_t^{k+1}\}$, we can reach:

$$\boldsymbol{S}^{k+1} = \sum_{t=1}^{T} \Re\{s_t^{k+1}\}\boldsymbol{M}_n + j\Im\{s_t^{k+1}\}\boldsymbol{M}_n\,,\; n = i \tag{3.64}$$

By substituting (3.64) into (3.63), the ML decoder can independently recover the input symbols using the received signals in both blocks as follows:

$$\tilde{s}_1^{k+1} = \underbrace{\arg max}_{s_1^{k+1}} \left[\Re\left\{tr\left[\boldsymbol{y}_{(t)}^{k+1^H}\boldsymbol{M}_1\boldsymbol{y}_{(t)}^{k}\right]\right\}\Re\{s_1^{k+1}\} + \Re\left\{tr\left[\boldsymbol{y}_{(t)}^{k+1^H} j\boldsymbol{M}_1\boldsymbol{y}_{(t)}^{k}\right]\right\}\Im\{s_1^{k+1}\}\right]$$

$$\tilde{s}_2^{k+1} = \underbrace{\arg max}_{s_2^{k+1}} \left[\Re\left\{ tr\left[\boldsymbol{y}_{(t)}^{k+1^H} \boldsymbol{M}_2 \boldsymbol{y}_{(t)}^k \right] \right\} \Re\{s_2^{k+1}\} + \Re\left\{ tr\left[\boldsymbol{y}_{(t)}^{k+1^H} j\boldsymbol{M}_2 \boldsymbol{y}_{(t)}^k \right] \right\} \Im\{s_2^{k+1}\} \right]$$

$$\tilde{s}_3^{k+1} = \underbrace{\arg max}_{s_3^{k+1}} \left[\Re\left\{ tr\left[\boldsymbol{y}_{(t)}^{k+1^H} \boldsymbol{M}_3 \boldsymbol{y}_{(t)}^k \right] \right\} \Re\{s_3^{k+1}\} + \Re\left\{ tr\left[\boldsymbol{y}_{(t)}^{k+1^H} jM_3 \boldsymbol{y}_{(t)}^k \right] \right\} \Im\{s_3^{k+1}\} \right]$$

$$\tilde{s}_4^{k+1} = \underbrace{\arg max}_{s_4^{k+1}} \left[\Re\left\{ tr\left[\boldsymbol{y}_{(t)}^{k+1^H} \boldsymbol{M}_4 \boldsymbol{y}_{(t)}^k \right] \right\} \Re\{s_4^{k+1}\} + \Re\left\{ tr\left[\boldsymbol{y}_{(t)}^{k+1^H} j\boldsymbol{M}_4 \boldsymbol{y}_{(t)}^k \right] \right\} \Im\{s_4^{k+1}\} \right] \quad (3.65)$$

3.5.3 Differential Square Real-orthogonal Designs in Three and Eight Relay Networks

We now discuss differential square real-orthogonal schemes implemented in cooperative networks with three and eight relay nodes. For square real-orthogonal designs in 3-relay networks, the achievable code-rate is the same as the case of 4-relay networks discussed in Section 3.4.1 and 3.4.2. Hence, the differential encoding and decoding procedure is the same. The only difference in design is in the structure of the channel matrix $\boldsymbol{H}^k$ and $\boldsymbol{H}^{k+1}$, in this case, the path gain h_{R_4D} between the fourth relay node and the destination in (3.51) is set to zero, hence, the channel matrix becomes:

$$\boldsymbol{H}^k \cong \boldsymbol{H}^{k+1} = \begin{bmatrix} h_1 & h_2 & h_3 & 0 \\ h_2 & -h_1 & 0 & h_3 \\ h_3 & 0 & -h_1 & -h_2 \\ 0 & -h_3 & h_2 & -h_1 \end{bmatrix} \quad (3.66)$$

The decision statistics to recover the transmitted information bits is obtained as in (3.54) by:

$$\left[\tilde{v}_{1,j}, \tilde{v}_{2,j}, \tilde{v}_{3,j}, \tilde{v}_{4,j}\right] = \sum_{n=1}^{3} \left|h_{R_nD}\right|^2 \left[v_{1,j}, v_{2,j}, v_{3,j}, v_{4,j}\right] + \tilde{\boldsymbol{Z}}^k \quad (3.67)$$

This implies that the design is able to achieve full three-level diversity for 3-relay cooperative networks.

The differential encoding and decoding set-up using co-efficient vectors or unitary codes can be generalized to cooperative networks with $N = 8$ relay nodes. For these designs, the encoding and decoding procedure is also similar to that used in 4-relay cooperative networks. The information signal $\boldsymbol{x}_1^{k+1}$ to be transmitted by the source in the $(k+1)_{th}$ block is obtained as in (3.56) by:

$$\boldsymbol{x}_1^{k+1} = \boldsymbol{x}_1^{k}\boldsymbol{S}^{k+1} \tag{3.68}$$

The only difference between this setup and the setup in Section 3.4.1 is that, in the former,$\boldsymbol{x}_n^k$ and $\boldsymbol{x}_n^{k+1}$ are $1 \times N$ signal matrices where $N = T = 8$, and S^{k+1} is of the form of [26] for 8-relay networks:

$$\boldsymbol{S}^{k+1} = \begin{bmatrix} s_1^{k+1} & -s_2^{k+1} & -s_3^{k+1} & -s_4^{k+1} & -s_5^{k+1} & -s_6^{k+1} & -s_7^{k+1} & -s_8^{k+1} \\ s_2^{k+1} & s_1^{k+1} & -s_4^{k+1} & s_3^{k+1} & -s_6^{k+1} & s_5^{k+1} & s_8^{k+1} & -s_7^{k+1} \\ s_3^{k+1} & s_4^{k+1} & s_1^{k+1} & -s_2^{k+1} & -s_7^{k+1} & -s_8^{k+1} & s_5^{k+1} & s_6^{k+1} \\ s_4^{k+1} & -s_3^{k+1} & s_2^{k+1} & s_1^{k+1} & -s_8^{k+1} & s_7^{k+1} & -s_6^{k+1} & s_5^{k+1} \\ s_5^{k+1} & s_6^{k+1} & s_7^{k+1} & s_8^{k+1} & s_1^{k+1} & -s_2^{k+1} & -s_3^{k+1} & -s_4^{k+1} \\ s_6^{k+1} & -s_5^{k+1} & s_8^{k+1} & -s_7^{k+1} & s_2^{k+1} & s_1^{k+1} & s_4^{k+1} & -s_3^{k+1} \\ s_7^{k+1} & -s_8^{k+1} & -s_5^{k+1} & s_6^{k+1} & s_3^{k+1} & -s_4^{k+1} & s_1^{k+1} & s_2^{k+1} \\ s_8^{k+1} & s_7^{k+1} & -s_6^{k+1} & -s_5^{k+1} & s_4^{k+1} & s_3^{k+1} & -s_2^{k+1} & s_1^{k+1} \end{bmatrix} \tag{3.69}$$

The structure of the operating matrix $\boldsymbol{M}_n$ at the n_{th} relay nodes is also different from that given in Section 3.4.1, the structure of $\boldsymbol{M}_n$ is obtained by decoupling $\boldsymbol{S}^{k+1}$in (3.69). Similar to the differential set-up for 3-relay cooperative networks where the codes are designed from the set-up for 4-relay cooperative networks, the design for cooperative networks with five, six and seven relay nodes can be designed from the set-up for 8-relay cooperative networks. This

is achieved by simply setting the corresponding element of the channel matrix to zero as implemented in (3.66).

In general, for the differential square real-orthogonal designs to be valid, the data matrices must be unitary, i.e. $\boldsymbol{X}^{k+1^H}\boldsymbol{X}^{k+1} = \boldsymbol{X}^{k+1^H}\boldsymbol{X}^{k} = \boldsymbol{I}_N$, and the information symbols must be selected from real constellations such that the information symbols can be recovered independently at the destination. The designs are also reliant on the assumption that the fading conditions remain unchanged in two consecutive blocks.

3.6 Simulation Results

First, the diversity performance of the DAF and DDF schemes are investigated via simulation. For this analysis, an un-coded scheme is assumed for transmission across all communicating nodes. Fig.3.8 shows the performance of the DAF and DDF schemes compared to the classic non-cooperative scheme discussed in Section 3.2. For this analysis, the source node and the relay nodes transmit in BPSK configuration and the communicating nodes are assumed to lack CSI. For the DAF and DDF schemes, in the first transmission interval, the source node sends to the relay node while in the second transmission interval, the source node and the relay node jointly send to the destination.

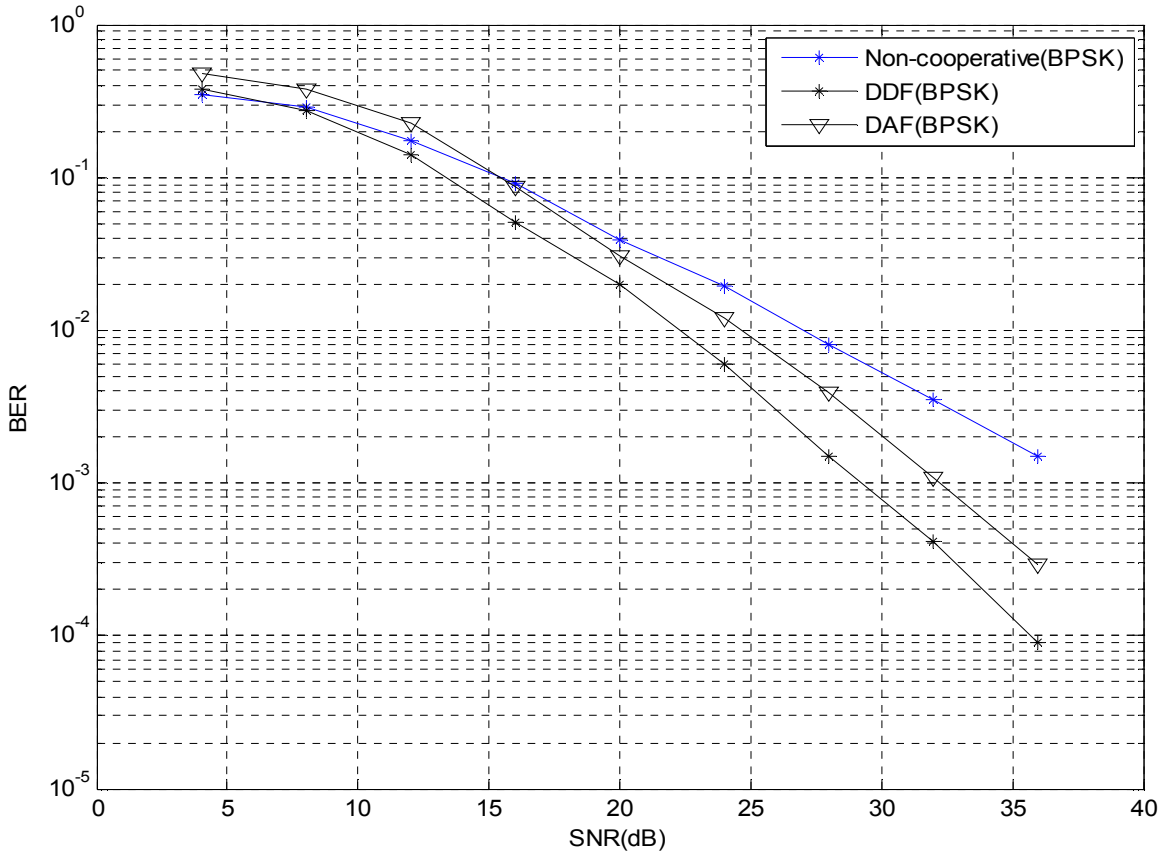

Fig.3.8. Performance comparison of differential modulation in single-relay cooperative and non-cooperative networks

The results show that the DAF and DDF schemes achieve cooperative diversity and outperform the classic non-cooperative scheme. It is also observed that the DDF scheme shows improved diversity performance over the DAF scheme, for example, at 10^{-2} BER, an SNR penalty of about 2.5dB is incurred. This is mainly attributed to the amplification of the noise at the relay by the AF protocol. Another reason is the low bit rate utilized for symbol transmission and the un-coded transmission of information signals. In other words, at low un-coded bit rates, due to the hard-decoding performed by the DDF protocol the likelihood of erroneous decoding is low at the relay node. To further investigate this issue, in Fig.3.9, we plot DDF and DAF schemes utilizing QPSK configuration. The results attest that the performance of the DAF scheme tends towards that of the DDF scheme when a higher order

modulation scheme is used. For example, at 10^{-2} BER, the SNR penalty incurred by the DAF scheme over the DDF scheme is reduced by about 1.5dB, compared to that incurred in BPSK configuration. For comparison, we also include the performance of the DF and AF protocols for a single-relay cooperative network that is able to acquire perfect CSI at the relay and the destination.

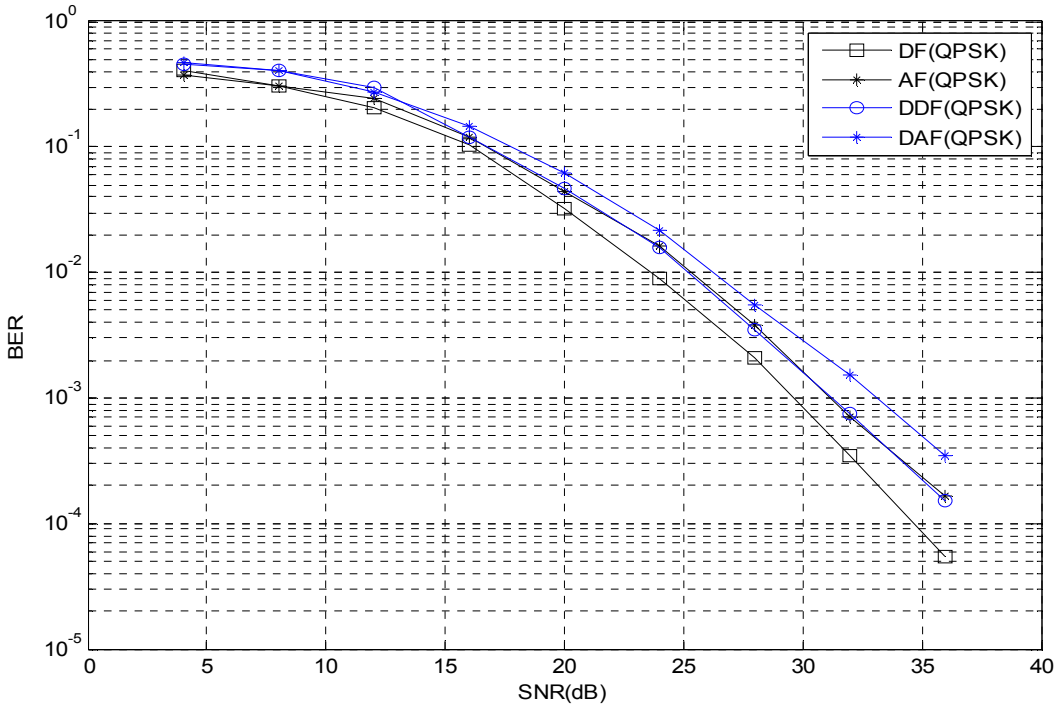

Fig.3.9 Performance comparison of differential modulation in coherent and non-coherent networks

It is observed that both the DAF and DDF schemes incur performance penalties compared to the coherent AF and DF protocols especially in the higher SNR region. This is because differential detection at the relay and destination doubles the effect of the channel and noise power on the received symbols.

In the second part of the simulation results, the performance of the differential square-real orthogonal scheme with cooperating relay nodes over flat fading Rayleigh channels is

evaluated via simulation. The fading is assumed to remain unchanged for at least two consecutive information blocks. We assume that the cooperating nodes and the destination are unable to acquire CSI thus they recover the transmitted bits from consecutively received signals. We first set $N = 2$ and $m = 1$ to form the basis for comparing the BER performance of our co-efficient vector design with that of the unitary matrices design of [30] and [61], where the AF and DF protocols are employed respectively. A similar scheme is also independently simulated for $N = 2$ cooperating nodes in coherent networks that can acquire perfect CSI. The results for BPSK are presented in Fig.3.10.

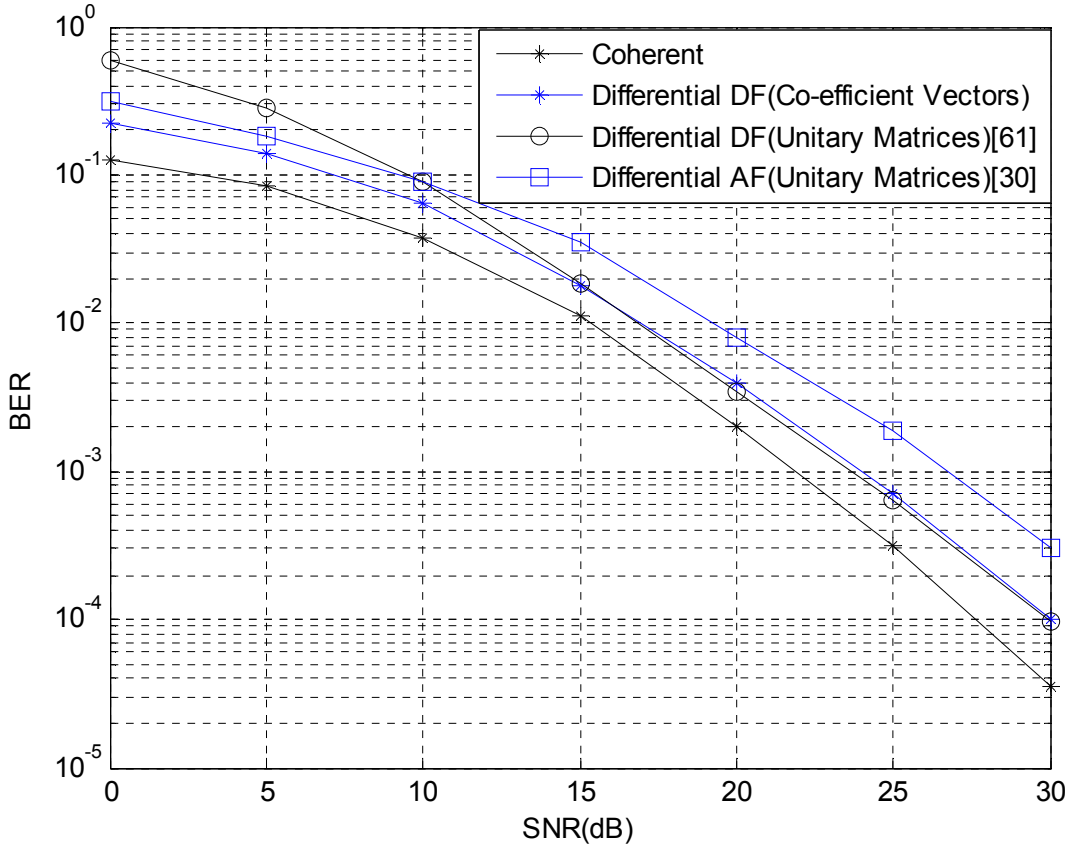

Fig.3.10 Performance comparison of unitary matrices and co-efficient vector designs usingBPSK configuration

From the results it is evident that, compared to the AF protocol of [30], the performance of the differential scheme using co-efficient vectors is slightly better than that obtained using

unitary matrices in the low SNR region, while the performance improves significantly in the high SNR region. For example, at 10^{-3} BER, the performance gain is about 2dB. On the other hand, compared to the DF protocol of [61], the proposed co-efficient vector design achieves notable performance gain at SNR values below 15dB. For higher SNR values, we observe no significant difference in performance gain. The performance curve of our differential scheme using co-efficient vectors also starts from a better point on the BER axis compared to that of [30] and [61]. A notable difference between the designs is however observed in terms of the computation complexity of the decoder at the relay nodes and the destination. For designs utilizing unitary matrices, a simple ML decoder recovers the information bits at the relays and the destination by conducting $c = 2^m$ comparisons, m is the number of bits. In contrast, designs utilizing co-efficient vectors rely on a search over all possible elements of the co-efficient vector. This equates to $c = 2^{2m}$ comparisons to recover the elements of the co-efficient vector set, with a further $1 \leq c \leq 2^{2m}$ comparisons required for mapping and inverse mapping at the encoder and decoder respectively. It is thus clear that, the decoding complexity limitation of the co-efficient vector based design is due to the constellation size. To counter this, suitable optimum detection schemes like those proposed in [67] which are independent of constellation size can be utilized. Customary with differential schemes, differential orthogonal schemes incur a performance penalty compared to that for coherent orthogonal schemes.

In Fig.3.11 we show the performance of co-efficient vector based differential square real-orthogonal designs in cooperative networks with three, four and eight relay nodes. The relay nodes distribute real orthogonal codes amongst themselves in order to construct the

differential DSTBC matrix at the destination; BPSK configuration is used to select the information symbols.

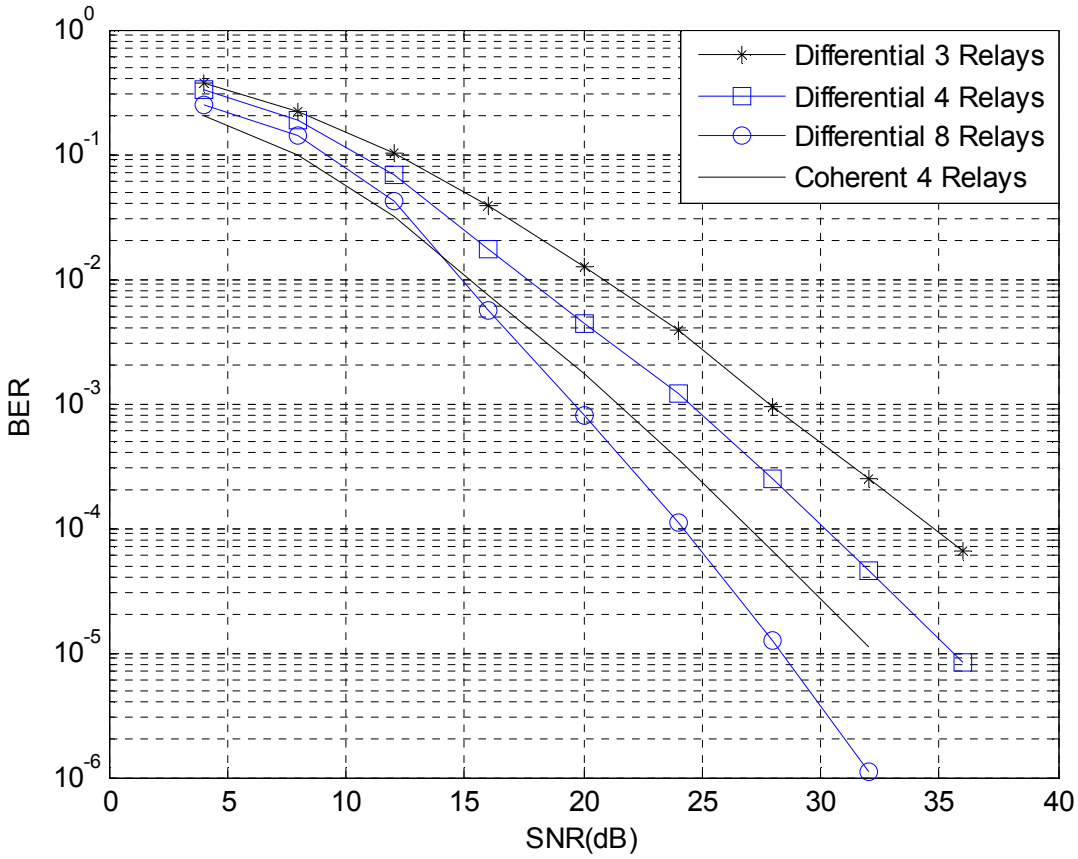

Fig.3.11 Performance comparison of differential Schemes with Three, Four and Eight Relay Nodes using BPSK

From Fig.3.11, we can see that the performance curve of the differential scheme with three cooperating relay nodes is parallel to those with four and eight relay nodes. This indicates that the co-efficient vector based differential DSTBC like the unitary matrices design is able to achieve full diversity, and the diversity performance increases with the number of cooperating nodes. Similar to the results obtained for differential schemes in 2-relay networks, differential schemes with three, four and eight relays also incur performance penalty when compared to their coherent counterparts. Using four relay nodes for example, differential square real-orthogonal codes in four-relay networks incur about 3dB SNR degradation in comparison with coherent networks with four relays.

3.7 Summary

Compared to traditional unitary matrices based differential DSTBC designs amenable to the AF cooperative protocol. In this chapter, differential DSTBC designs based on co-efficient vectors is proposed for DF cooperative networks where the relay nodes are required to differentially decode and re-transmit information signals. We present the generalized mapping scheme and differential recipe for utilizing co-efficient vectors in cooperative networks with any number of relays. Using simulation results, we compare and contrast the unitary matrices and co-efficient vector designs in terms of computational complexity and BER performance. In addition we generalize the co-efficient vector design to cooperative networks with three, four and eight relays utilizing square-real orthogonal codes.

4 Differential and Multi-differential Quasi-orthogonal Space Time Block Codes

4.1 Introduction

So far, we have discussed full code-rate and full diversity differential schemes using complex orthogonal codes in 2-relay cooperative networks, and square real-orthogonal codes in $N > 2$ relay nodes. For networks utilizing $N > 2$ relay nodes, full-rate complex orthogonal codes are non-existent in the literature. Full diversity complex orthogonal codes have been reported for coherent networks with three and four relay nodes in [30] each achieving 0.5 and 0.75 code-rate respectively, this rate deficiency also extends to their counterparts in non-coherent networks.

In order to meet high data rate requirements, high code-rate differential distributed quasi-orthogonal space-time block codes (DQSTBC) for cooperative networks was first presented in [30]. Here, the authors discuss the generalized structure of the so called symplectic matrices Sp(2) codes which have a high code rate and emulate the quasi-orthogonal codes of [42]. The Sp(2) codes in [30] however achieve less than full code rate when utilized in 4-relay cooperative networks. So far, the differential encoding and decoding setup presented in [30] [57] and [68] for cooperative multi-hop networks only utilize codewords from unitary matrices aimed to reduce encoding and decoding complexities. This means that the code design criterion is restricted to only unitary matrices and unitary codewords that can commute. These schemes thus sacrifice full code-rate for encoding and decoding complexity benefits. The first non-unitary quasi-orthogonal codeword constructed for 4-relay networks was illustrated in [63]. Here, the authors present the conditions under which the codewords

are non-unitary, referred to as scaled-unitary. They also present important insights for constructing scaled-unitary codewords. However, their work does not cover the differential encoding and decoding procedure. The work in [69] provides the differential encoding and decoding setup for some unitary codewords. The authors also summarize the design criteria for a dimension-four quasi-orthogonal scaled-unitary codeword. However, different from conventional one-way wireless cooperative networks, their design is restricted to two-way wireless cooperative networks. Therefore, to the best of our knowledge, there has not been any work on the full differential encoding and decoding procedure for non-unitary full code-rate quasi-orthogonal codes in 4-relay cooperative networks. Thus, we propose differential distributed quasi-orthogonal space time block codes (DQSTBC) for cooperative networks. Our work presents the differential encoding and decoding procedure for 4-relay cooperative networks based on the full code-rate quasi-orthogonal codes of [70] originally designed for multiple antenna systems. Our differential DQSTBC scheme utilizes codewords from non-unitary matrices, based on this we show how the transmitted information symbols are constructed from a special choice of signal sets such that full code-rate signals are obtained.

In all the aforementioned related works on differential designs for cooperative multi-hop networks, the assumption is that a direct link between the source node and the destination does not exist. We identify that additional benefits can be extracted in terms of SNR performance when the source node is actively involved in cooperation. We have considered a similar cooperative scheme in [32] and in Chapter 2 for non-differential designs. In this Chapter, we propose a new multi-differential quasi-orthogonal design for cooperative networks. Our proposed strategy uses a multi-differential decoding procedure, whereby, differential decoding occurs multiple times at the destination. The overall objective of this

scheme is to reduce the redundancy of the source node and destination while improving the quality of the detected signal at the destination.

The rest of Chapter 4 is organized as follows. Section 4.2 details the differential encoding and decoding procedure for DQSTBC in cooperative networks. In Section 4.3 we introduce our multi-differential protocol, Section 4.4 presents some simulation results and Section 4.5 contains the summary.

4.2 Differential Encoding and Decoding of Quasi-orthogonal Codes

4.2.1 System Model

The cooperative network consists of a source node, a destination node and N relay nodes as shown in Fig.4.1. Each node is equipped with a single antenna which is used for both transmission and reception. The nodes are subject to half duplex constraint such that they cannot transmit and receive simultaneously. First, we focus on differential DQSTBC where the antennas of the cooperating nodes constructively generate the quasi-orthogonal codewords at the destination, thus, the direct source-destination link is not considered in this section. We address the problem of differential encoding and decoding where neither the relays nor the destination can acquire CSI.

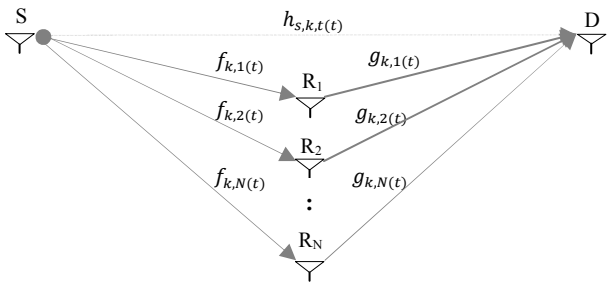

Fig.4.1 N-relay cooperative network utilizing quasi-orthogonal codes

The design in this work adopts a two-block two-stage 'transmit-and-cooperate' protocol. This implies that the protocol is made up of two blocks and each block is divided into two stages namely, the 'transmit' stage and the 'cooperate' stage. In the 'transmit' stage, the source node sends information to the relay nodes, while in the 'cooperate' stage, the source keeps silent and the cooperating relay nodes simply forward the information signals to the destination without decoding. The transmission in each stage has duration of T time instants, such that the transmission in each block lasts for $2T$ time instants.

In order to recover one set of valid information symbols at the destination without CSI, the scheme relies on two consecutive signal matrices $\boldsymbol{S}_k$ and $\boldsymbol{S}_{k+1}$ generated in the k_{th} block and $(k+1)_{th}$ block respectively. The first signal matrix $\boldsymbol{S}_k$ is termed the 'reference' matrix because it is only required for differential decoding and thus contains no valid data, while the subsequent signal matrix $\boldsymbol{S}_{k+1}$ conveys the valid data. We first devise the structure of the reference quasi-orthogonal signal matrix employed in our scheme. Let $\boldsymbol{S}_k$ denote the $T \times N$ reference quasi-orthogonal matrix given by $\boldsymbol{S}_k = \left[{\boldsymbol{s}_{k,1}}^T, \dots, {\boldsymbol{s}_{k,N}}^T\right] \in \mathbb{C}^{T \times N}, \boldsymbol{s}_{k,n} = \left[s_{k,n(1)}, \dots, s_{k,n(T)}\right]$. This implies that $\boldsymbol{s}_{k,n}$ is the n_{th} column vector of $\boldsymbol{S}_k$, the matrix $\boldsymbol{S}_k$ is constructed such that ${\boldsymbol{S}_k}^H \boldsymbol{S}_k \neq \boldsymbol{I}_T$. Thus the reference codeword matrix employed in our scheme is non-unitary unlike the schemes in [30] [57] and [68].

Next, we show how the source node and N relay nodes construct $\boldsymbol{S}_k$ at the destination. In the 'transmit' stage of the k_{th} block, the source node generates a time sequence signal $\boldsymbol{s}_{k,1} = \left[s_{k,1(1)}, \dots, s_{k,1(T)}\right]$ of duration T symbols. Let $s_{k,1(t)}, t = 1,2, \dots, T$ be the t_{th} information symbol transmitted by the source node to the relay nodes in the k_{th} block. The transmitted signal is normalized such that $E\left(\boldsymbol{s}_{k,1}{\boldsymbol{s}_{k,1}}^H\right) = 1$. Assuming the data vector transmitted by the

source node is of the form $\sqrt{P_S T}\boldsymbol{s}_{k,1}$ where $P_S T$ is the average transmit power. The received signal at the n_{th} relay node is

$$\boldsymbol{r}_{k,n} = \sqrt{P_S T}\boldsymbol{s}_{k,1} \odot \boldsymbol{f}_{k,n} + \boldsymbol{n}_{k,n} \tag{4.1}$$

where $\odot$ denotes entry-wise operation, $\boldsymbol{f}_{k,n} = \left[f_{k,n(1)}, \ldots, f_{k,n(T)}\right]$ is the Rayleigh fading channel model between the source node and the n_{th} relay node assumed to be made up of iid zero mean and unit-variance complex random variables. The corresponding noise $\boldsymbol{n}_{k,n} = \left[n_{k,n(1)}, \ldots, n_{k,n(T)}\right]$ is made up of independent samples of a zero mean complex Gaussian random variable. The n_{th} relay node linearly processes the received signal $\boldsymbol{r}_{k,n} = \left[r_{k,n(1)}, \ldots, r_{k,n(T)}\right]$ and transmits a $1 \times T$ data vector $\boldsymbol{t}_{k,n} = \left[t_{k,n(1)}, \ldots, t_{k,n(T)}\right]$ given by:

$$\boldsymbol{t}_{k,n} = \sqrt{\frac{P_C}{P_S+1}}\boldsymbol{r}_{k,n}\boldsymbol{M}_n \tag{4.2}$$

In our DQSTBC scheme, the N relay nodes are designed to construct $T \times N$ quasi-orthogonal signal matrices at the destination. In order to achieve this, each n_{th} relay node is equipped with a $T \times T$ unitary matrix $\boldsymbol{M}_n$ referred to as the 'relay matrix'. The relay matrix is a matrix of 1s and 0s which enables the relay nodes to generate codewords with a quasi-orthogonal structure at the destination. The structure of the relay matrix is given in Section II of [64] for cooperative networks with different number of relay nodes. Due to space limitations however, the structure of the relay matrix is not illustrated in our work, we just borrow the design of [64]. The power allocated to each relay node is denoted by P_C, this implies that an amplification co-efficient $\mu = \sqrt{P_C/(P_S+1)}$ is applied at each relay node. Replicating the power allocation strategy in [65], we set $P_S = P_C N = P/2$, where P denotes

the total power available in the network. In other words, the source node and the relay nodes share the available power in the network.

Assuming the relay nodes are synchronized at symbol level such that the nodes transmit simultaneously. The signal received at the destination in the k_{th} block is given by:

$$\boldsymbol{y}_{k,t} = \sum_{n=1}^{N} \boldsymbol{t}_{k,n} \odot \boldsymbol{g}_{k,n} + \boldsymbol{z}_{k,t},\ t = 1,2,..,T \tag{4.3}$$

where $\boldsymbol{g}_{k,n} = \left[g_{k,n(1)}, \dots, g_{k,n(T)}\right]$ is the Rayleigh fading channel model between the n_{th} relay node and the destination, and $\boldsymbol{z}_{k,t}$ is the corresponding noise. Substituting for $\boldsymbol{t}_{k,n}$ and then $\boldsymbol{r}_{k,n}$ in (4.2) and (4.1) respectively (4.3) becomes:

$$\boldsymbol{y}_{k,t} = \sum_{n=1}^{N} \sqrt{\frac{P_C P_S T}{P_S+1}}\, \boldsymbol{s}_{k,1} \boldsymbol{M}_n \odot \left(\boldsymbol{f}_{k,n} \odot \boldsymbol{g}_{k,n}\right) + \tilde{\boldsymbol{z}}_{k,t} \tag{4.4}$$

where $\tilde{\boldsymbol{z}}_{k,t} = \sum_{n=1}^{N} \mu\, \boldsymbol{M}_n \boldsymbol{g}_{k,n} \boldsymbol{n}_{k,n} + \boldsymbol{z}_k$ is the equivalent noise. The signal received at the destination in the k_{th}block can be written in compact form as:

$$\boldsymbol{Y}_k = \sqrt{\rho} \boldsymbol{S}_k \boldsymbol{H}_k + \boldsymbol{Z}_k \tag{4.5}$$

where $\boldsymbol{Y}_k = \left[{\boldsymbol{y}_{k,1}}^T, \dots, {\boldsymbol{y}_{k,T}}^T\right]^T \in \mathbb{C}^{T \times T}$, $\boldsymbol{y}_{k,t} = \left[y_{k,t(1)}, \dots, y_{k,t(T)}\right]$, $\rho = \frac{P_C P_S T}{P_S+1}$, $\boldsymbol{S}_k = \left[\boldsymbol{M}_1 {\boldsymbol{s}_{k,1}}^T, \dots, \boldsymbol{M}_N {\boldsymbol{s}_{k,1}}^T\right] \in \mathbb{C}^{T \times N}$, $\boldsymbol{H}_k = \left[{\boldsymbol{h}_{k,1}}^T, \dots, {\boldsymbol{h}_{k,T}}^T\right]^T \in \mathbb{C}^{N \times T}$, $\boldsymbol{h}_{k,t} = \left[h_{k,t(1)}, \dots, h_{k,t(N)}\right]$ and $\boldsymbol{Z}_k = \left[{\tilde{\boldsymbol{z}}_{k,1}}^T, \dots, {\tilde{\boldsymbol{z}}_{k,T}}^T\right]^T \in \mathbb{C}^{T \times T}$, the channel co-efficients $h_{k,t(n)} = f_{k,n(t)} \cdot g_{k,n(t)}$.

The $N \times T$ quasi-orthogonal channel matrix $\boldsymbol{H}_k$ captures the channel co-efficients between the source node, the N relay nodes, and the destination. Here we assume that the channel is constant during the transmission of T symbols, that is, $\boldsymbol{h}_{k,t}$ is constant for $t = 1,2, \dots, T$. Note that the matrix $\boldsymbol{S}_k$ generated at the destination by the N relay nodes is a $T \times N$ quasi-orthogonal signal matrix containing either the original complex information symbols

$\{s_{k,n(1)}, \dots, s_{k,n(T)}\}$ or their conjugates $\{s_{k,n(1)}{}^*, \dots, s_{k,n(T)}{}^*\}$. Thus the quasi-orthogonal signal matrix $\boldsymbol{S}_k$ generated at the destination in (5) has the same structure as the reference quasi-orthogonal signal matrix devised earlier in our discussion. In other words, $\boldsymbol{S}_k = [\boldsymbol{M}_1 \boldsymbol{s}_{k,1}{}^T, \dots, \boldsymbol{M}_N \boldsymbol{s}_{k,1}{}^T] = [\boldsymbol{s}_{k,1}{}^T, \dots, \boldsymbol{s}_{k,N}{}^T] \in \mathbb{C}^{T \times N}, \boldsymbol{s}_{k,n} = [s_{k,n(1)}, \dots, s_{k,n(T)}]$, where $\boldsymbol{s}_{k,n}$ is the n_{th} column of $\boldsymbol{S}_k$. In other words, the n_{th} relay node transmits the n_{th} column vector of $\boldsymbol{S}_k$. This implies that the relay matrices $\{\boldsymbol{M}_1, \dots, \boldsymbol{M}_N\}$ maintain the quasi-orthogonal structure of the transmitted codeword, and the codeword matrix generated at the destination is also non-unitary.

4.2.2 Differential Encoding using Quasi-orthogonal Codes

In this section, we discuss the differential encoding procedure employed in the proposed differential DQSTBC scheme. The architecture is typically composed of a hybrid combination of two functional sub-systems, namely, a constellation mapping sub-system and a differential sub-system. Differential encoding is initiated at the source node. Recalling that $\boldsymbol{s}_{k,1} = [s_{k,1(1)}, \dots, s_{k,1(T)}] \in \mathbb{C}^{1 \times T}$ is the source node data generated in the k_{th} block, the next step is for the source node to generate the data vector $\boldsymbol{s}_{k+1,1}$ for the $(k+1)_{th}$ block. This involves the following processes:

First, the constellation mapping sub-system generates the information symbols $\boldsymbol{v}_{k+1,1} = [v_{k+1,1(1)}, \dots, v_{k+1,1(T)}] \in \mathbb{C}^{1 \times T}$, where $\boldsymbol{v}_{k+1,1}$ represents the valid transmitted information symbols that must be recovered at the destination without CSI. We now show how the elements of $\boldsymbol{v}_{k+1,1}$ are computed at the source node from a proper choice of signal sets such that a full diversity non-unitary quasi-orthogonal codeword is obtained. The elements of $\boldsymbol{v}_{k+1,1}$ are modulated symbols drawn from an $m = log_2$M M-PSK or M-QAM constellation,

m is the spectral efficiency. Let $\Phi = diag\left[1, e^{j\theta_1}, \dots, e^{j\theta_{T/2-1}}\right]$, the information symbols are constructed as $\Phi \cdot \left[v_{k+1,1(1)}, v_{k+1,1(3)}, \dots, v_{k+1,1(T-1)}\right]^T$ and $\Phi \cdot \left[v_{k+1,1(2)}, v_{k+1,1(4)}, \dots, v_{k+1,1(T)}\right]^T$. This implies that, $\left[v_{k+1,1(1)}, v_{k+1,1(2)}, \dots\right]$ are mapped onto a signal constellation $\mathcal{A}$ of size 2^m, while $\left[v_{k+1,1(3)}, v_{k+1,1(4)}, \dots\right]$ are mapped onto a signal constellation $\mathcal{A}_r$ which is a rotated version of $\mathcal{A}$. The mapping of information symbols is illustrated in Fig. 4.2 for QPSK constellation. The rotation angles θ of the information symbols ensure that the codes achieve full diversity, see Chapter 5 of [35] for further explanation on constellation rotation.

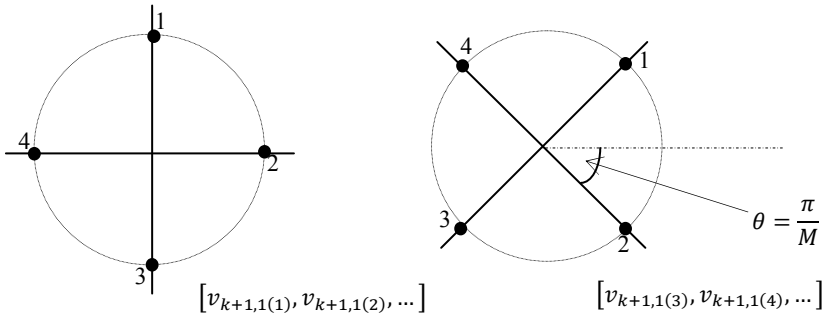

Fig.4.2 Symbol mapping for QPSK constellation

The next step is for the differential encoder to generate the $1 \times T$ data vector $\boldsymbol{s}_{k+1,1}$ for the $(k+1)_{th}$ block. We assume that the source node has prior knowledge of the relay matrices $\{\boldsymbol{M}_1, \dots, \boldsymbol{M}_N\}$, since the source node already knows $\boldsymbol{s}_{k,1}$, it can easily construct $\boldsymbol{S}_k = \left[\boldsymbol{M}_1 \boldsymbol{s}_{k,1}{}^T, \dots, \boldsymbol{M}_N \boldsymbol{s}_{k,1}{}^T\right]$. Thus the data vector generated in the $(k+1)_{th}$ block is of the form:

$$\boldsymbol{s}_{k+1,1} = \boldsymbol{v}_{k+1,1} \boldsymbol{S}_k \tag{4.6}$$

where $\boldsymbol{s}_{k+1,1} \in \mathbb{C}^{1\times T}$, $\boldsymbol{v}_{k+1,1} \in \mathbb{C}^{1\times T}$ and $\boldsymbol{S}_k = \left[\boldsymbol{s}_{k,1}{}^T, \dots, \boldsymbol{s}_{k,N}{}^T\right]^T$ is the reference quasi-orthogonal signal matrix generated by the N relay nodes in the k_{th} block. Let $\boldsymbol{V}_{k+1} = \left[\boldsymbol{v}_{k+1,1}{}^T, \dots, \boldsymbol{v}_{k+1,N}{}^T\right] \in \mathbb{C}^{T\times N}$, $\boldsymbol{v}_{k+1,n} = \left[v_{k+1,n(1)}, \dots, v_{k+1,n(T)}\right]$, this implies that $\boldsymbol{v}_{k+1,n}$ is

the n_{th} column vector of the quasi-orthogonal information symbol matrix $\boldsymbol{V}_{k+1}$, and $\boldsymbol{V}_{k+1}{}^{H}\boldsymbol{V}_{k+1} \neq \boldsymbol{I}_{T}$. Thus our information symbol matrix is non-unitary in contrast with other proposed schemes which force $\boldsymbol{V}_{k+1}{}^{H}\boldsymbol{V}_{k+1} = \boldsymbol{I}_{T}$. Since $\boldsymbol{v}_{k+1,1}$ and $\boldsymbol{S}_{k}$ have a quasi-orthogonal structure, then $\boldsymbol{s}_{k+1,1}$ also has a quasi-orthogonal structure.

In order to construct $\boldsymbol{S}_{k+1}$ at the destination, the source node and N relay nodes follow the same process as in the k_{th} block.The received signal at the n_{th} relay node in the $(k+1)_{th}$block is of the form of (4.1). Similar to the case of the k_{th} block, the relay node data is constructed and transmitted as discussed in Section 4.2.1. The received signal at the destination in the $(k+1)_{th}$ block is similar to (4.5) and can be written in compact form as:

$$\boldsymbol{Y}_{k+1} = \sqrt{\rho}\boldsymbol{S}_{k+1}\boldsymbol{H}_{k+1} + \boldsymbol{Z}_{k+1} \tag{4.7}$$

where $\boldsymbol{Y}_{k+1} = \left[\boldsymbol{y}_{k+1,1}{}^{T}, \dots, \boldsymbol{y}_{k+1,T}{}^{T}\right]^{T} \in \mathbb{C}^{T\times T}$, $\boldsymbol{y}_{k+1,t} = \left[y_{k+1,t(1)}, \dots, y_{k+1,t(T)}\right]$, $\rho = \frac{P_C P_S T}{P_S+1}$, $\boldsymbol{S}_{k+1} = \left[\boldsymbol{M}_1\boldsymbol{s}_{k+1,1}{}^{T}, \dots, \boldsymbol{M}_N\boldsymbol{s}_{k+1,1}{}^{T}\right] \in \mathbb{C}^{T\times N}$,$\boldsymbol{H}_{k+1} = \left[\boldsymbol{h}_{k+1,1}{}^{T}, \dots, \boldsymbol{h}_{k+1,T}{}^{T}\right]^{T} \in \mathbb{C}^{N\times T}$, $\boldsymbol{h}_{k+1,t} = \left[h_{k+1,t(1)}, \dots, h_{k+1,t(N)}\right]$ and $\boldsymbol{Z}_{k+1} = \left[\tilde{\boldsymbol{z}}_{k+1,1}{}^{T}, \dots, \tilde{\boldsymbol{z}}_{k+1,T}{}^{T}\right]^{T} \in \mathbb{C}^{T\times T}$, the channel coefficients $h_{k+1,t(n)} = f_{k+1,n(t)} \cdot g_{k+1,n(t)}$.We assume that the channels $\boldsymbol{f}_{k,n}$, $\boldsymbol{g}_{k,n}$, $\boldsymbol{f}_{k+1,n}$ and $\boldsymbol{g}_{k+1,n}$ which are made up of iid zero mean and unit variance complex random variables, have a Rayleigh flat fading model. Our differential decoding technique relies on a multi-block channel fading model where the channel is assumed to be identical for two consecutive blocks of $2T$ transmissions, in other words $\boldsymbol{H}_{k} \cong \boldsymbol{H}_{k+1}$.

4.2.3 Differential Decoding using Quasi-orthogonal Codes

As far as the destination is concerned, consecutive blocks of codewords have been received across N relay nodes. So far, consecutive $T \times N$ quasi-orthogonal signal matrices $\boldsymbol{S}_{k}$ and

$\boldsymbol{S}_{k+1}$ have been generated at the destination based on (4.5) and (4.7). We can rewrite the received signals at the destination as

$$\boldsymbol{y}_{k,t} = \boldsymbol{s}_{k,n}\boldsymbol{H}_k + \tilde{\boldsymbol{z}}_{k,n} = \left[\boldsymbol{S}_k {\boldsymbol{h}_{k,t}}^T + {\tilde{\boldsymbol{z}}_{k,n}}^T\right]^T,\ t = 1,2,\dots,T\ \ n = 1,2,\dots,N \tag{4.8}$$

$$\boldsymbol{y}_{k+1,t} = \boldsymbol{s}_{k+1,n}\boldsymbol{H}_{k+1} + \tilde{\boldsymbol{z}}_{k+1,n} = \left[\boldsymbol{S}_{k+1} {\boldsymbol{h}_{k+1,t}}^T + {\tilde{\boldsymbol{z}}_{k+1,n}}^T\right]^T,\ t = 1,2,\dots,T\ \ n = 1,2,\dots,N \tag{4.9}$$

Note that we intentionally omit the power term $\sqrt{\rho}$ for ease of explanation. Using the signals received in (4.8) and (4.9) in the k_{th} block and $(k+1)_{th}$ block respectively, the valid information symbols $\boldsymbol{v}_{k+1,1} = \left[v_{k+1,1(1)}, \dots, v_{k+1,1(T)}\right]$ can be recovered pairwisely at the destination without CSI. For example, for a cooperative network with $N = 4$ relay nodes and $T = 4$, in order to recover $\boldsymbol{v}_{k+1,1}$, we first obtain the quasi-orthogonal signal and channel matrices for two consecutive transmission blocks as follows:

$$\boldsymbol{S}_j = \begin{bmatrix} s_{j,1(1)} & s_{j,2(2)} & s_{j,3(3)} & s_{j,4(4)} \\ -s_{j,1(2)}^* & s_{j,2(1)}^* & -s_{j,3(4)}^* & s_{j,4(3)}^* \\ -s_{j,1(3)}^* & -s_{j,2(4)}^* & s_{j,3(1)}^* & s_{j,4(2)}^* \\ s_{j,1(4)} & -s_{j,2(3)} & -s_{j,3(2)} & s_{j,4(1)} \end{bmatrix}$$

$$\boldsymbol{H}_j = \begin{bmatrix} h_{j,1(1)} & h_{j,2(2)}^* & h_{j,3(3)}^* & h_{j,4(4)} \\ h_{j,1(2)} & -h_{j,2(1)}^* & h_{j,3(4)}^* & -h_{j,4(3)} \\ h_{j,1(3)} & h_{j,2(4)}^* & -h_{j,3(1)}^* & -h_{j,4(2)} \\ h_{j,1(4)} & -h_{j,2(3)} & -h_{j,3(2)}^* & h_{j,4(1)} \end{bmatrix}$$

where $\boldsymbol{S}_j \in \mathbb{C}^{T\times N}$ and $\boldsymbol{H}_j \in \mathbb{C}^{N\times T}$, $j \in \{k, k+1\}$ are quasi-orthogonal signal and channel matrices respectively. The t_{th} information signal transmitted by the source node, through the n_{th} relay node is denoted by $s_{j,n(t)}$, and $h_{j,t(n)}$ captures the channel co-efficient between the source node, the n_{th} relay node, and the destination, in the t_{th} transmission interval. Since we assume that the channel is constant during the transmission of T symbols, $h_{j,t(n)}$ is

constant for $t = 1,2,\dots,T$, similarly, $s_{j,n(t)}$ is constant for $n = 1,2,\dots,N$ since all the cooperating relay nodes transmit the same information signals. Thus we can imply that $h_{j,1(n)} =, \dots, = h_{j,4(n)} = h_{j(n)}$ and $s_{j,1(t)} =, \dots, = s_{j,4(t)} = s_{j(t)}$. Based on this, we can compute

$$\boldsymbol{S}_j \boldsymbol{S}_j{}^H = \begin{bmatrix} S_1 & 0 & 0 & S_2 \\ 0 & S_1 & -S_2 & 0 \\ 0 & -S_2 & S_1 & 0 \\ S_2 & 0 & 0 & S_1 \end{bmatrix}$$

$$\boldsymbol{H}_j \boldsymbol{H}_j{}^H = \begin{bmatrix} H_1 & 0 & 0 & H_2 \\ 0 & H_1 & -H_2 & 0 \\ 0 & -H_2 & H_1 & 0 \\ H_2 & 0 & 0 & H_1 \end{bmatrix}$$

$S_1 = \sum_{t=1}^{4} \left|s_{j(t)}\right|^2$ is the signal power and $S_2 = 2Re\left(s_{j(1)} s_{j(4)}{}^* - s_{j(2)} s_{j(3)}{}^*\right)$ is a self-interference parameter. Similarly, $H_1 = \sum_{n=1}^{4} \left|h_{j(n)}\right|^2$ is the channel power and $H_2 = 2Re\left\{h_{j(1)} h_{j(4)}{}^* - h_{j(2)} h_{j(3)}{}^*\right\}$ is a self-interference parameter. The elements of $\boldsymbol{v}_{k+1,1}$ are then recovered as follows:

$$\begin{aligned} \boldsymbol{y}_{k+1,1} \boldsymbol{y}_{k,1}{}^H &= \boldsymbol{s}_{k+1,1} \boldsymbol{S}_k{}^H \boldsymbol{H}_{k+1} \boldsymbol{h}_{k,1}{}^H + Z_1 \\ &= \boldsymbol{v}_{k+1,1} \boldsymbol{S}_k \boldsymbol{S}_k{}^H \boldsymbol{H}_{k+1} \boldsymbol{h}_{k,1}{}^H + Z_1 \\ &= v_{k+1,1(1)}(S_1 H_1 + S_2 H_2) + v_{k+1,1(4)}(S_1 H_2 + S_2 H_1) + Z_1 \\ &= v_{k+1,1(1)} A + v_{k+1,1(4)} B + Z_1 \end{aligned} \quad (4.10)$$

Similarly,

$$\boldsymbol{y}_{k+1,1} \boldsymbol{y}_{k,2}{}^H = \boldsymbol{s}_{k+1,1} \boldsymbol{S}_k{}^H \boldsymbol{H}_{k+1} \boldsymbol{h}_{k,2}{}^H + Z_2$$

$$= \boldsymbol{v}_{k+1,1}\boldsymbol{S}_k{\boldsymbol{S}_k}^H\boldsymbol{H}_{k+1}{\boldsymbol{h}_{k,2}}^H + Z_2$$

$$= v_{k+1,1(2)}A - v_{k+1,1(3)}B + Z_2 \tag{4.11}$$

$$\boldsymbol{y}_{k+1,1}{\boldsymbol{y}_{k,3}}^H = \boldsymbol{s}_{k+1,1}{\boldsymbol{S}_k}^H\boldsymbol{H}_{k+1}{\boldsymbol{h}_{k,3}}^H + Z_3$$

$$= \boldsymbol{v}_{k+1,1}\boldsymbol{S}_k{\boldsymbol{S}_k}^H\boldsymbol{H}_{k+1}{\boldsymbol{h}_{k,3}}^H + Z_3$$

$$= -v_{k+1,1(2)}B + v_{k+1,1(3)}A + Z_3 \tag{4.12}$$

$$\boldsymbol{y}_{k+1,1}{\boldsymbol{y}_{k,4}}^H = \boldsymbol{s}_{k+1,1}{\boldsymbol{S}_k}^H\boldsymbol{H}_{k+1}{\boldsymbol{h}_{k,4}}^H + Z_4$$

$$= \boldsymbol{v}_{k+1,1}\boldsymbol{S}_k{\boldsymbol{S}_k}^H\boldsymbol{H}_{k+1}{\boldsymbol{h}_{k,4}}^H + Z_4$$

$$= v_{k+1,1(1)}B + v_{k+1,1(4)}A + Z_4 \tag{4.13}$$

where Z_n captures the noise, $A = S_1H_1 + S_2H_2$ and $B = S_1H_2 + S_2H_1$, we refer to A and B as the differential decoding parameters required to recover $\boldsymbol{v}_{k+1,1}$. The differential decoding parameters are computed at the destination as:

$$\boldsymbol{y}_{k,1}{\boldsymbol{y}_{k,4}}^H = \boldsymbol{S}_k{\boldsymbol{S}_k}^H\boldsymbol{h}_{k,1}{\boldsymbol{h}_{k,4}}^H + \tilde{Z}_4 = A + \tilde{Z}_4$$

$$\boldsymbol{y}_{k,1}{\boldsymbol{y}_{k,1}}^H = \boldsymbol{S}_k{\boldsymbol{S}_k}^H\boldsymbol{h}_{k,1}{\boldsymbol{h}_{k,1}}^H + \tilde{Z}_1 = B + \tilde{Z}_1 \tag{4.14}$$

This implies that $\boldsymbol{y}_{k,1}{\boldsymbol{y}_{k,4}}^H \approx A$ and $\boldsymbol{y}_{k,1}{\boldsymbol{y}_{k,1}}^H \approx B$ since$Z_n \approx \tilde{Z}_n$. It is thus obvious from (4.14) that the scheme does not require CSI to recover $\boldsymbol{v}_{k+1,1}$. The non-coherent recovery of $\boldsymbol{v}_{k+1,1}$ rather depends on consecutively received signals in the k_{th} block and $(k+1)_{th}$ block under the constraint that $\boldsymbol{H}_k \cong \boldsymbol{H}_{k+1}$. Once A and B are computed at the destination using (4.14), the information signals in (4.10) to (4.13) can be recovered pairwisely. The system architecture for the differential decoder at the destination is illustrated in Fig. 4.3.

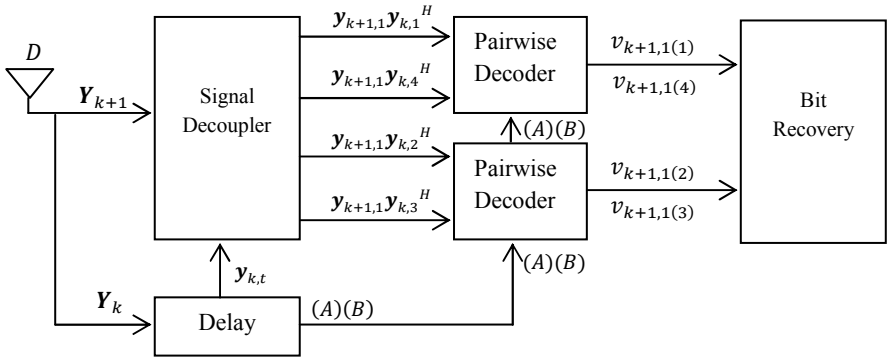

Fig.4.3 Pairwise differential decoder

So far, we can see that in each transmission block a two-stage transmit-and-cooperate differential protocol is adopted. In the transmit stage of each block the destination is idle while in the cooperate stage of each block the source is idle and only the cooperating relay nodes transmit. Next we discuss a scenario where a direct link exists between the source node and the destination, such that the source node transmits in all stages and the destination receives in all stages.

4.3 Multi-differential Encoding and Decoding of Quasi-orthogonal Codes

4.3.1 Multi-differential Encoding Using Quasi-orthogonal Codes

The diversity performance of our differential DQSTBC scheme can be improved by exploiting the additional diversity path provided by the source-destination link. If a direct link is available between the source node and the destination, the destination can differentially recover information symbols using the signals from the source node and the signals from the relay nodes. In the previous section, the source node is idle at certain transmission intervals, specifically when the relay nodes are transmitting to the destination. Our multi-differential scheme is designed such that the source node can use these idle transmission intervals to

generate quasi-orthogonal matrices at the destination. If the structure of the quasi-orthogonal matrices generated at the destination by the source node is identical to the structure of the quasi-orthogonal matrices generated at the destination by the relay nodes in Section 4.2, then the destination can use the same decoding metric to jointly recover the two sets of information symbols without incurring additional decoding complexity. Thus the principal objective of our multi-differential scheme is to improve the SNR gain at the destination with negligible decoding complexity penalties.

We observe from Section 4.2.2 that the source node has prior knowledge of the relay matrices $\{\boldsymbol{M}_1, \dots, \boldsymbol{M}_N\}$, since $\boldsymbol{S}_k = \left[\boldsymbol{M}_1 \boldsymbol{s}_{k,1}{}^T, \dots, \boldsymbol{M}_N \boldsymbol{s}_{k,1}{}^T\right] = \left[\boldsymbol{s}_{k,1}{}^T, \dots, \boldsymbol{s}_{k,N}{}^T\right]$ then the source node can construct $\boldsymbol{s}_{k,n}$ for any $n = 1,2, \dots, N$. The source-destination channel matrix is denoted as $\boldsymbol{H}_{s,k} \in \mathbb{C}^{T \times T}$ and given by $\boldsymbol{H}_{s,k} = \left[\boldsymbol{h}_{s,k,1}, \dots, \boldsymbol{h}_{s,k,T}\right]$, $\boldsymbol{h}_{s,k,t} = \left[h_{s,k,t(1)}, \dots, h_{s,k,t(T)}\right]^T$, this implies that $\boldsymbol{h}_{s,k,t}$, $t = 1,2, \dots, T$ is the t_{th} column of $\boldsymbol{H}_{s,k}$ and $h_{s,k,t(t)}$ denotes the channel co-efficient between the source node and the destination at the t_{th} transmission interval. If the channel co-efficients remain unchanged during all the source-destination transmission cycles, then we can imply that $\boldsymbol{h}_{s,k,1} =, \dots, = \boldsymbol{h}_{s,k,4}$.

The data vector transmitted by the source node in the 'transmit' stage of the k_{th} block is $\boldsymbol{s}_{k,1} = \left[s_{k,1(1)}, \dots, s_{k,1(T)}\right]$. While the cooperating relay nodes receive the signals in (4.1) from the source node, the signal received by the destination from the source node is of the form:

$$y_{s,k,1(1)} = \sqrt{\alpha}\boldsymbol{s}_{k,1}\boldsymbol{h}_{s,k,1} + z_{s,k,1(1)} \tag{4.15}$$

where $\boldsymbol{h}_{s,k,1} = \left[h_{s,k,1(1)}, \ldots, h_{s,k,1(T)}\right]^T \in \mathbb{C}^{T\times 1}$ is the Rayleigh fading channel model between the source node and the destination assumed to be made up of iid zero mean and unit-variance complex random variables, the corresponding noise is $z_{s,k,1(1)}$ and α denotes the power term. In the 'cooperate' stage of the k_{th} block, while the destination receives the signals in (4.3) from the relay nodes, the source node transmits $\boldsymbol{s}_{k,2}$ such that the destination receives:

$$y_{s,k,1(2)} = \sqrt{\alpha}\boldsymbol{s}_{k,2}\boldsymbol{h}_{s,k,2} + z_{s,k,1(2)} \tag{4.16}$$

The source node already knows $\boldsymbol{S}_k$ and $\boldsymbol{v}_{k+1,1}$, thus it can construct $\boldsymbol{s}_{k+1,1}$ using (4.6), the source node can also construct $\boldsymbol{S}_{k+1} = \left[{\boldsymbol{s}_{k+1,1}}^T, \ldots, {\boldsymbol{s}_{k+1,N}}^T\right]$ since it knows the relay matrices $\{\boldsymbol{M}_1, \ldots, \boldsymbol{M}_N\}$. Thus, in the 'transmit' stage of the $(k+1)_{th}$ block, while the relay nodes receive differentially modulated signals from the source node, the signal received by the destination from the source node is:

$$\boldsymbol{y}_{s,k+1,1} = \sqrt{\bar{\alpha}}\boldsymbol{S}_{k+1}\boldsymbol{h}_{\boldsymbol{s},k+1,1} + \boldsymbol{z}_{s,k+1,1} \tag{4.17}$$

where $\bar{\alpha}$ is the power term. In the 'cooperate' stage of the $(k+1)_{th}$ block, while the destination receives the signals in (4.7) from the relay nodes, with a slight misuse of notation the source node transmits $\boldsymbol{s}_{k,3}$ such that the destination receives:

$$y_{s,k,1(3)} = \sqrt{\alpha}\boldsymbol{s}_{k,3}\boldsymbol{h}_{\boldsymbol{s},k,3} + z_{s,k,1(3)} \tag{4.18}$$

Finally, the source node transmits $\boldsymbol{s}_{k,4}$ such that the destination receives:

$$y_{s,k,1(4)} = \sqrt{\alpha}\boldsymbol{s}_{k,4}\boldsymbol{h}_{\boldsymbol{s},k,4} + z_{s,k,1(4)} \tag{4.19}$$

At the end of the source-destination transmission cycles, the destination has received $\boldsymbol{y}_{s,k,1} =$

$[y_{s,k,1(1)}, \dots, y_{s,k,1(4)}]$ and $\boldsymbol{y}_{s,k+1,1} = [y_{s,k+1,1(1)}, \dots, y_{s,k+1,1(4)}]$. We can write the received signal matrices in compact form as

$$\boldsymbol{Y}_{s,k} = \boldsymbol{S}_k \boldsymbol{H}_{s,k} + \boldsymbol{Z}_{s,k}$$

$$\boldsymbol{Y}_{s,k+1} = \boldsymbol{S}_{k+1} \boldsymbol{H}_{s,k+1} + \boldsymbol{Z}_{s,k+1} \quad (4.20)$$

where $\boldsymbol{Y}_{s,k} = \left[\boldsymbol{y}_{s,k,1}{}^T, \dots, \boldsymbol{y}_{s,k,T}{}^T\right]^T \in \mathbb{C}^{T \times T}$ and $\boldsymbol{Y}_{s,k+1} = \left[\boldsymbol{y}_{s,k+1,1}{}^T, \dots, \boldsymbol{y}_{s,k+1,T}{}^T\right]^T \in \mathbb{C}^{T \times T}$ and $\boldsymbol{y}_{s,k,t}$ and $\boldsymbol{y}_{s,k+1,t}$ denote the t_{th} column of $\boldsymbol{Y}_{s,k}$ and $\boldsymbol{Y}_{s,k+1}$ respectively.

4.3.2 Multi-differential Decoding Using Quasi-orthogonal Codes

As far as the destination is concerned, consecutive $T \times N$ quasi-orthogonal signal matrices have been received from the source node. So we can rewrite the received signals as

$$\boldsymbol{y}_{s,k,t} = \boldsymbol{S}_k \boldsymbol{h}_{\boldsymbol{s},k,t} + \boldsymbol{z}_{s,k,t} = \left[\boldsymbol{s}_{k,n} \boldsymbol{H}_{s,k} + \tilde{\boldsymbol{z}}_{s,k,t}\right]^T, t = 1,2, \dots, T \;\; n = 1,2, \dots, N \quad (4.21)$$

$$\boldsymbol{y}_{s,k+1,t} = \boldsymbol{S}_{k+1} \boldsymbol{h}_{\boldsymbol{s},k+1,t} + \boldsymbol{z}_{s,k+1,t} = \left[\boldsymbol{s}_{k+1,n} \boldsymbol{H}_{s,k+1} + \tilde{\boldsymbol{z}}_{s,k+1,t}\right]^T, t = 1,2, \dots, T \;\; n = 1,2, \dots, N \quad (4.22)$$

Similar to the case of our differential DQSTBC scheme, using the signals received in (4.21) and (4.22) $\boldsymbol{v}_{k+1,1} = [v_{k+1,1(1)}, \dots, v_{k+1,1(T)}]$ can be recovered pairwisely at the destination without CSI as follows

$$\begin{aligned} \boldsymbol{y}_{s,k+1,1} \boldsymbol{y}_{s,k,1}{}^H &= \boldsymbol{s}_{k+1,1} \boldsymbol{S}_k{}^H \boldsymbol{H}_{s,k+1} \boldsymbol{h}_{s,k,1}{}^H + Z_{s,1} \\ &= \boldsymbol{v}_{k+1,1} \boldsymbol{S}_k \boldsymbol{S}_k{}^H \boldsymbol{H}_{s,k+1} \boldsymbol{h}_{s,k,1}{}^H + Z_{s,1} \\ &= v_{k+1,1(1)} \left(S_1 H_{s,1} + S_2 H_{s,2}\right) + v_{k+1,1(4)} \left(S_1 H_{s,2} + S_2 H_{s,1}\right) + Z_{s,1} \\ &= v_{k+1,1(1)} C + v_{k+1,1(4)} D + Z_{s,1} \end{aligned} \quad (4.23)$$

Similarly,

$$\boldsymbol{y}_{s,k+1,1}\boldsymbol{y}_{s,k,2}{}^{H} = \boldsymbol{s}_{k+1,1}\boldsymbol{S}_k{}^{H}\boldsymbol{H}_{s,k+1}\boldsymbol{h}_{s,k,2}{}^{H} + Z_{s,2}$$

$$= \boldsymbol{v}_{k+1,1}\boldsymbol{S}_k\boldsymbol{S}_k{}^{H}\boldsymbol{H}_{s,k+1}\boldsymbol{h}_{s,k,2}{}^{H} + Z_{s,2}$$

$$= v_{k+1,1(2)}C - v_{k+1,1(3)}D + Z_{s,2} \quad (4.24)$$

$$\boldsymbol{y}_{s,k+1,1}\boldsymbol{y}_{s,k,3}{}^{H} = \boldsymbol{s}_{k+1,1}\boldsymbol{S}_k{}^{H}\boldsymbol{H}_{s,k+1}\boldsymbol{h}_{s,k,3}{}^{H} + Z_{s,3}$$

$$= \boldsymbol{v}_{k+1,1}\boldsymbol{S}_k\boldsymbol{S}_k{}^{H}\boldsymbol{H}_{s,k+1}\boldsymbol{h}_{s,k,3}{}^{H} + Z_{s,3}$$

$$= -v_{k+1,1(2)}D + v_{k+1,1(3)}C + Z_{s,3} \quad (4.25)$$

$$\boldsymbol{y}_{s,k+1,1}\boldsymbol{y}_{s,k,4}{}^{H} = \boldsymbol{s}_{k+1,1}\boldsymbol{S}_k{}^{H}\boldsymbol{H}_{s,k+1}\boldsymbol{h}_{s,k,4}{}^{H} + Z_{s,4}$$

$$= \boldsymbol{v}_{k+1,1}\boldsymbol{S}_k\boldsymbol{S}_k{}^{H}\boldsymbol{H}_{s,k+1}\boldsymbol{h}_{s,k,4}{}^{H} + Z_{s,4}$$

$$= v_{k+1,1(1)}D + v_{k+1,1(4)}C + Z_{s,4} \quad (4.26)$$

where $Z_{s,n}$ captures the noise, $C = S_1H_{s,1} + S_2H_{s,2}$ and $D = S_1H_{s,2} + S_2H_{s,1}$, we refer to C and D as the differential decoding parameters required to recover $\boldsymbol{v}_{k+1,1}$, the channel power is denoted by $H_{s,1} = \sum_{t=1}^{4}\left|h_{s,j(t)}\right|^2$ and $H_{s,2} = 2Re\left\{h_{s,j(1)}h_{s,j(4)}{}^{*} - h_{s,j(2)}h_{s,j(3)}{}^{*}\right\}$ is a self-interference parameter. Similar to the differential decoding scheme in the previous section, if C and D are available at the destination the signals in (4.23) to (4.26) can be recovered pairwisely. The estimated values of the decoding parameters, C and D, can now be obtained by:

$$\boldsymbol{y}_{s,k,1}\boldsymbol{y}_{s,k,4}{}^{H} = \boldsymbol{S}_k\boldsymbol{S}_k{}^{H}\boldsymbol{h}_{s,k,1}\boldsymbol{h}_{s,k,4}{}^{H} + \tilde{Z}_{s,4} = D + \tilde{Z}_{s,4} \quad (4.27)$$

$$\boldsymbol{y}_{s,k,1}\boldsymbol{y}_{s,k,1}{}^{H} = \boldsymbol{S}_k\boldsymbol{S}_k{}^{H}\boldsymbol{h}_{s,k,1}\boldsymbol{h}_{s,k,1}{}^{H} + \tilde{Z}_{s,1} = C + \tilde{Z}_{s,1} \quad (4.28)$$

This implies that $\boldsymbol{y}_{s,k,1}\boldsymbol{y}_{s,k,4}{}^{H} \approx D$ and $\boldsymbol{y}_{s,k,1}\boldsymbol{y}_{s,k,1}{}^{H} \approx C$ since $Z_{s,n} \approx \tilde{Z}_{s,n}$. Now we have obtained all the results required for multi-differential decoding, obviously, all the decision signals are only a function of a pair of input signals which exist with dissimilar constellation angles. This offers the possibility of decoding in pairs. We can decide for each pair of recovered symbols independently using a pairwise least square decoder as follows:

$$\left[\tilde{v}_{k+1,1(1)}, \tilde{v}_{k+1,1(4)}\right] = \arg\min\Big[\left|\boldsymbol{y}_{k+1,1}\boldsymbol{y}_{k,1}{}^{H} - \left(v_{k+1,1(1)}A + v_{k+1,1(4)}B\right)\right|^2 + \left|\boldsymbol{y}_{k+1,1}\boldsymbol{y}_{k,4}{}^{H} - \left(v_{k+1,1(4)}A + v_{k+1,1(1)}B\right)\right|^2 + \left|\boldsymbol{y}_{s,k+1,1}\boldsymbol{y}_{s,k,1}{}^{H} - \left(v_{k+1,1(1)}C + v_{k+1,1(4)}D\right)\right|^2 + \left|\boldsymbol{y}_{s,k+1,1}\boldsymbol{y}_{s,k,4}{}^{H} - \left(v_{k+1,1(4)}C + v_{k+1,1(1)}D\right)\right|^2\Big] \quad (4.29)$$

$$\left[\tilde{v}_{k+1,1(2)}, \tilde{v}_{k+1,1(3)}\right] = \arg\min\Big[\left|\boldsymbol{y}_{k+1,1}\boldsymbol{y}_{k,2}{}^{H} - \left(v_{k+1,1(2)}A - v_{k+1,1(3)}B\right)\right|^2 + \left|\boldsymbol{y}_{k+1,1}\boldsymbol{y}_{k,3}{}^{H} - \left(v_{k+1,1(3)}A - v_{k+1,1(2)}B\right)\right|^2 + \left|\boldsymbol{y}_{s,k+1,1}\boldsymbol{y}_{s,k,2}{}^{H} - \left(v_{k+1,1(2)}C - v_{k+1,1(3)}D\right)\right|^2 + \left|\boldsymbol{y}_{s,k+1,1}\boldsymbol{y}_{s,k,3}{}^{H} - \left(v_{k+1,1(3)}C - v_{k+1,1(2)}D\right)\right|^2\Big] \quad (4.30)$$

The pairwise least square decoder performs an exhaustive search over all possible combination of constellation points to determine the pair of signals that minimize the terms in (4.29) and (4.30). This decoding is based on the pairwise decoding metric of [42], and is equivalent to finding the minimum Euclidean distance between the noisy received signals and the known constellation points. Then finally symbol level demodulation is applied to recover the original bits. The complexity of this process is equivalent to 2^{M+1}since this is the number of constellation points to be examined. Compared to the differential scheme, the additional computational complexity incurred by the multi-differential scheme is negligible since the number of constellation points to be examined is unchanged. Thus, the destination has jointly decoded information signals transmitted across the source-destination link, and the relay-destination links. As stated previously, the multi-differential scheme improves the diversity

order of the differential scheme from N to $(N+1)$ as a result of the additional diversity path provided by the source node, this conclusion is proved in our simulation results. Although we have stated that the principal objective of our multi-differential scheme is to improve the SNR gain at the destination with negligible decoding complexity penalties, we also note that our scheme incurs additional power penalties due to α and $\bar{\alpha}$, and additional signal processing at the source node due to the transmissions in (4.15) to (4.19).

4.4 Simulation Results

In this section we provide simulation results for the performance of our differential and multi-differential DQSTBC schemes, these results are studied in comparison with the corresponding coherent detection scheme of [31]. For further analysis, we have also included the results for the differential4×4 real orthogonal design and Sp(2) codes of [30] whose algorithms and design parameters are independently reproduced in our environment. Simulation results have been obtained assuming a cooperative multi-hop network with single antenna nodes. Fig.4.4 shows the results for BPSK constellation, all the schemes compared in the results transmit the same number of symbols across $N = 4$ relay nodes. Thus the bit rate of each scheme in Fig.4.4 is equal to the code-rate. Specifically, the full code-rate coherent quasi-orthogonal code, 4×4 real orthogonal code, SP (2) code, and our differential DQSTBC have bit rates 1, 0.5, 6.5 and 1 respectively. We analyze the diversity performance of our full code-rate quasi-orthogonal design using optimum rotation angles. The optimum rotation angles are set as $\theta \in \{1, \pi/M\}$, where $M = 2$ is the constellation size. As illustrated, our differential DQSTBC scheme and the 4×4 real orthogonal scheme of [30] offer approximately identical diversity performance. However, our differential DQSTBC scheme provides full code-rate of 1 as opposed to the code-rate of 0.5 for the latter. Similarly, our

differential DQSTBC scheme shows improved diversity performance of about 2dB over the SP(2) scheme which only provide code-rate of 0.65. Compared to the full code-rate coherent scheme, our differential DQSTBC scheme is about 3dB worse which is due to the doubling effect of the noise power in non-coherent detection schemes.

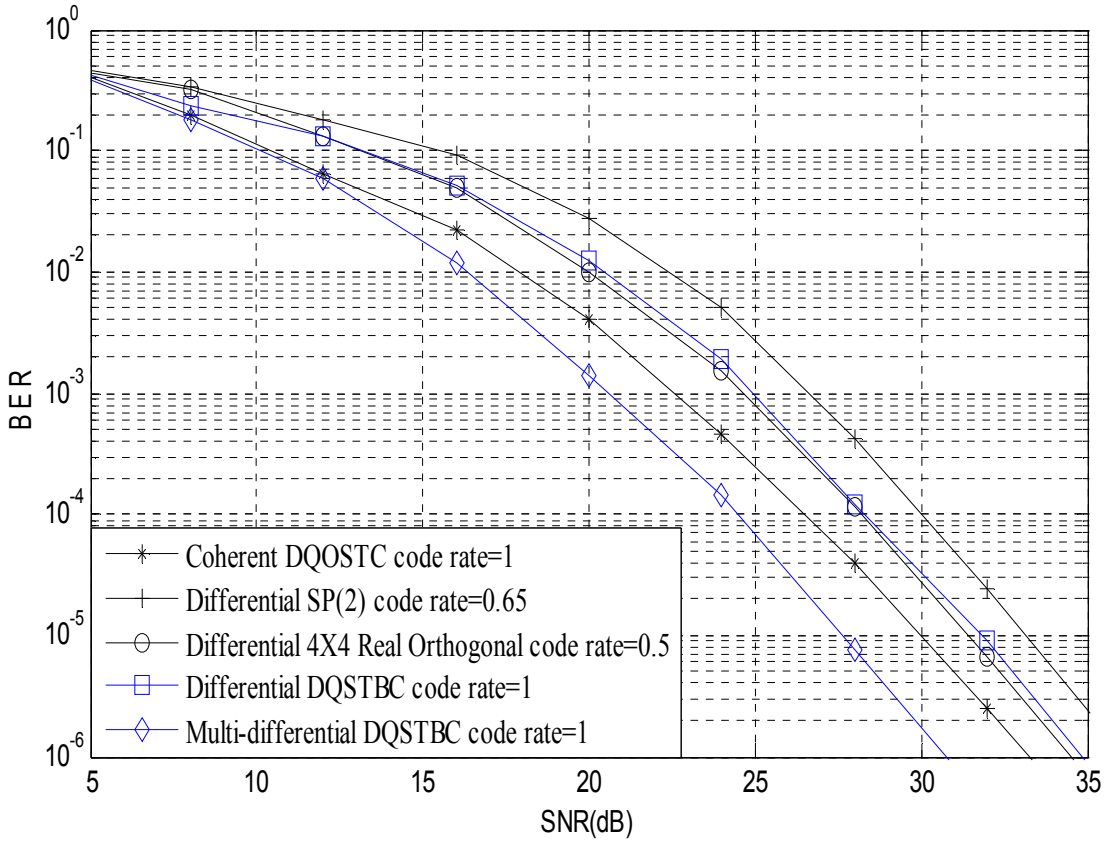

Fig.4.4. Performance comparison of space-time coding schemes in cooperative networks

The performance of our differential and multi-differential DQSTBC schemes for different constellations is illustrated in Fig.4.5. In this part, the signal constellation was set at QPSK, QAM and 16-QAM, with rotation angle $\theta \in \{1, \pi/4, \pi/16\}$. We assume that the total power consumed by the network is fixed for the differential and multi-differential scheme. As shown, the multi-differential DQSTBC scheme out-performs the conventional differential counterpart especially at the higher SNR region. Both schemes have full code-rate and

identical decoding complexity, however, the diversity product of the multi-differential scheme is always larger. This is easily due to the additional diversity path achieved when the destination receives multiple copies of the transmitted signal from the source node and the cooperating relay nodes, and also because the increase in computational complexity of the decoder is negligible.

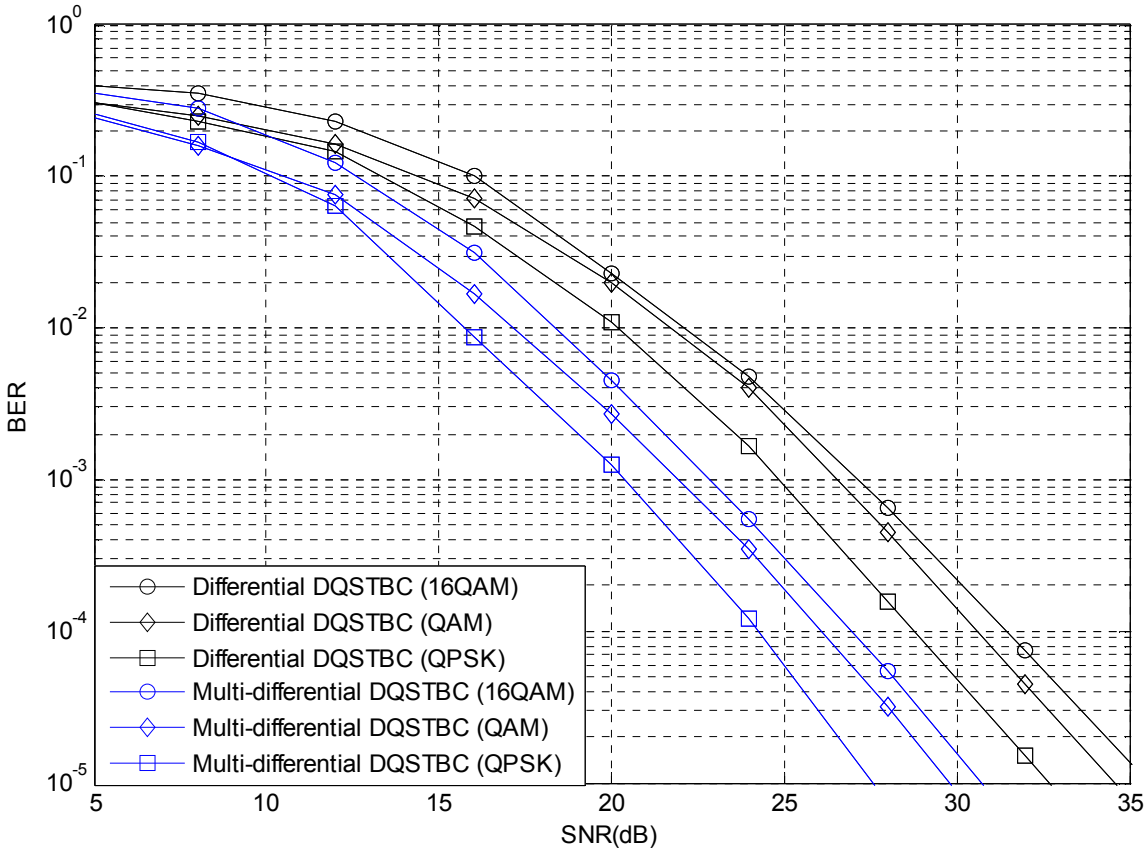

Fig.4.5. Performance comparison of differential and multi-differential schemes using different constellation orders

As discussed earlier, the rotated angles of the information symbols ensure that the codes achieve full diversity. To analyze this issue further, we have included a partial diversity differential DQSTBC design with non-rotated constellation symbols. As shown in Fig.4.6, the diversity product of the non-rotated codes degrades faster than that of rotated codes in the

high SNR region. However, we identify that designs with non-rotated constellation symbols offer low complexity symbol-wise decoding (see Appendix A) as opposed to the pairwise decoding offered by differential and multi-differential schemes.

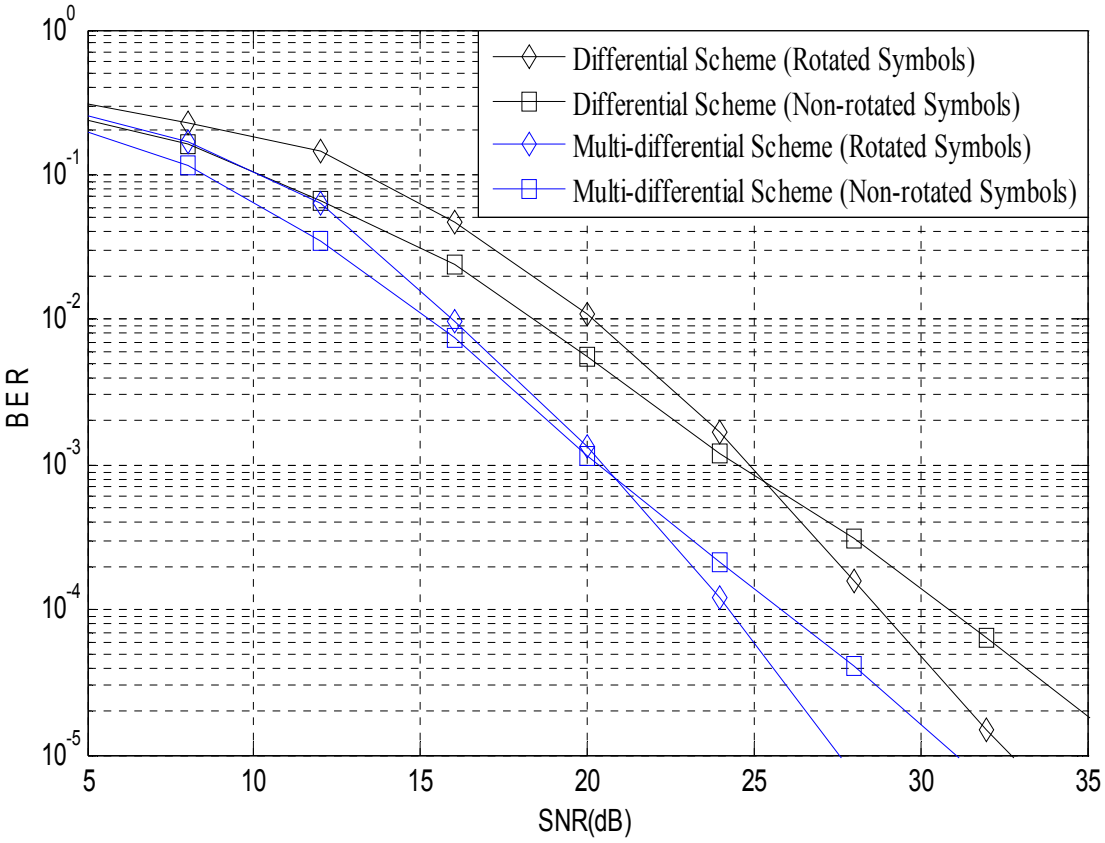

Fig.4.6. Performance comparison of rotated and non-rotated symbols with QAM

4.5 Summary

Compared to recent differential schemes utilizing real and complex valued orthogonal codes, SP(2) codes, and unitary codes all of which transmit below full code-rate for 4-relay cooperative networks. In this work we show that non-unitary full code-rate quasi-orthogonal codes can achieve full diversity performance when used differentially in 4-relay cooperative networks. We have presented the full differential encoding and decoding procedure for DQSTBC in a 4-relay cooperative network. We have also proposed a multi-differential

DQSTBC scheme which exploits the direct source-destination link. Here differential decoder at the destination jointly decodes multiple copies of the transmitted signal such that the quality of the detected signal at the destination is significantly increased with negligible increase in the computational complexity of the detection scheme. Simulation results show that implementation of this scheme in cooperative networks can provide very useful results in the practical SNR range.

5 Differential and Multi-differential Quasi-orthogonal Space-Frequency Coding

5.1 Introduction

DSTBC protocols are now being investigated for cooperative broadband multi-hop networks transmitting across frequency selective channels. This has led to the design of DSTBC orthogonal frequency division multiplexing (DSTBC-OFDM) schemes and distributed space-frequency coding (DSFC) schemes. In DSTBC-OFDM, the information symbols that are transmitted by cooperating relay nodes are applied at individual sub-carriers over multiple OFDM blocks. DSTBC-OFDM schemes are able to exhibit maximum spatial and temporal gain at the expense of frequency diversity and inherent processing delay. To exploit the achievable frequency diversity and counteract the processing delay, DSFC transmits information symbols across multiple sub-carriers within a single OFDM block. Further comparative analysis on these schemes shows that while DSTBC-OFDM is insensitive to high delay spread, it is highly susceptible to Doppler frequency. This limits the application of the scheme to slow fading channels. On the other hand, DSFC is more robust to fast fading channels such that the scheme exhibits maximum frequency and spatial diversity when utilized in fast fading environments. The outlined benefit of DSFC over DSTBC-OFDM has instigated our focus in this work on the former for cooperative broadband multi-hop networks operating in fast fading environments.

As discussed in previous chapters, CSI estimation is a problem in high mobility environments like that experienced by vehicular sensor networks or 3G and 4G cellular systems designed to provide broadband data access for highly mobile users. For example in the recent mobile

broadband wireless communication standard developed by the American Society for Testing and Material (ASTM) E17.51 working group for dedicated short range communication, and the IEEE 802.20 working group for mobile broadband wireless access, the standards use packet-based channel estimation [71]. Packet-based transmission emulates the traditional pilot-based training symbols that are used for channel estimation. Packet-based channel estimation like pilot-based channel estimation will suffer severe performance degradation in time-varying frequency selective fading channels. These limitations have thus made it imperative to incorporate differential strategies with cooperative broadband multi-hop networks utilizing DSFC schemes.

The study of differential space-frequency (SF) coding strategies in frequency selective fading environments has been reported in a few works [72–75] in the context of multiple-antenna systems, and [53] in the context of cooperative broadband multi-hop networks. The aforementioned work in the cooperative context utilizes codeword matrices from orthogonal designs and is thus only capable of providing full rate and full diversity for a maximum of two-relay cooperative networks. We therefore identify the need to design a scheme that realizes full rate transmission for cooperative networks with more than two relay nodes. Here, full rate means that our scheme achieves unitary code rate as well as full symbol rate (one symbol per sub-carrier use) when relay nodes forward information signals to the destination node. The differential coding scheme proposed in [76], and the non-differential coding schemes proposed in [77] and [78] for coherent broadband cooperative networks have been shown to achieve full symbol rate. In contrast however, our scheme employs quasi-orthogonal codes which provide the added advantage of unitary code rate. Based on this, we propose a differential distributed quasi-orthogonal space-frequency coding (DQSFC) protocol which is able to achieve full rate and full spatial and frequency diversity in non-coherent

cooperative networks with any number of relays. We use the class of quasi-orthogonal codes with rotated constellations derived in [79] which are guaranteed to achieve full spatial diversity. We contrast our work with [80] and [81], while these works investigate hybrid combinations of quasi-orthogonal codes with OFDM in coherent multiple-antenna networks. Our work is the first to focus on non-coherent detection in single-antenna cooperative broadband networks where quasi-orthogonal codes are transmitted in the spatial and frequency dimensions. We carefully provide a systematic construction of the code matrix and present the full differential procedure. The PEP analysis shows that the diversity performance of our scheme can be improved through code construction and sub-carrier allocation. Based on this, we devise a code structure which maximizes the diversity performance of our scheme. Using the permutation scheme of [82], we also introduce a sub-carrier allocation strategy which improves the diversity gain.

In addition, we identify that additional benefits can be realized in terms of SNR performance when the source node is actively involved in cooperation. Consequently, we present a scenario where a direct link between the source node and the destination exists. From this set-up which is different from existing ones, we propose a new multi-differential DQSFC scheme for cooperative broadband networks. Our proposed strategy uses a multi-differential decoding procedure, whereby, differential decoding occurs multiple times at the destination. The overall objective of this scheme is to reduce the redundancy of the source node and destination while improving the quality of the detected signal at the destination with negligible decoding complexity.

The rest of Chapter 5 is organized as follows: In Section 5.2 we present the quasi-orthogonal space frequency (QSF) system model and discuss how the SF codes are designed at the source node and the relay nodes, we also present the structure of the quasi-orthogonal codes

used in our scheme. Section 5.3 covers the encoding and decoding procedure for differential DQSFC. Section 5.4 contains the PEP analysis and discussions on diversity improvement. In Section 5.5 we introduce our multi-differential protocol, and Section 5.6 presents some simulation results.

5.2 Quasi-orthogonal Space Frequency Coding

5.2.1 System Model

The cooperative network consists of a source node, a destination node and P relay nodes as shown in Fig.5.1. Each node is equipped with a single antenna which is used for both transmission and reception. The transmission from the source node to the destination is divided into the 'transmit' and 'cooperate' stages. In the 'transmit' stage, the source node sends information signals to the cooperating relay nodes, while in the 'cooperate' stage, the source node keeps silent and the cooperating relay nodes simply forward the information signals to the destination. For each stage, the nodes are subject to half-duplex constraint such that they cannot transmit and receive simultaneously. First, we focus on differential DQSFC where the antennas of the cooperating nodes constructively generate the quasi-orthogonal codewords at the destination, thus, the direct source-destination link is not considered in this section. A scenario where the direct source-destination link is considered is discussed in Section 5.5. We address the problem of differential encoding and decoding where the relay nodes and the destination are unable to acquire CSI.

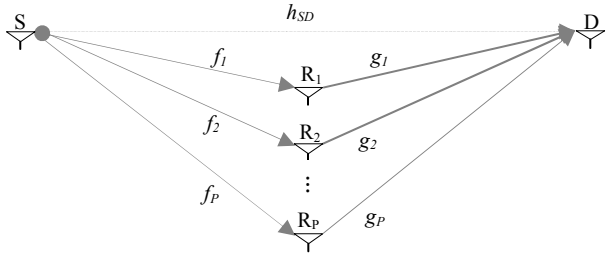

Fig.5.1 P-relay cooperative broadband network

The multipath fading channel between the source node and the p_{th} relay node is modeled as $f_p(t) = \sum_{l=0}^{L_{SR}-1} f_p(l)\delta(t-\alpha_l)$. Similarly, the multipath fading channel between the p_{th} relay node and the destination node is modeled as $g_p(t) = \sum_{l=0}^{L_{RD}-1} g_p(l)\delta(t-\beta_l)$ where the complex amplitudes $f_p(l)$ and $g_p(l)$ are assumed to be independent zero-mean complex Gaussian random variables with variances $E\left(\left|f_p(l)\right|^2\right) = \sigma_{SR}^2(l)$ and $E\left(\left|g_p(l)\right|^2\right) = \sigma_{RD}^2(l)$ respectively. The delay of the l_{th} path is denoted by α_l and β_l, while $\delta(\cdot)$ is the Dirac delta function, L_{SR} and L_{RD} denote the number of independent channel taps on the source-relay $(S-R)$link and relay-destination $(R-D)$link respectively. We assume that the channels are spatially uncorrelated, thus $f_p(l)$ and $g_p(l)$ are independent for different relay nodes.

5.2.2 Source Node Coding

The cooperative system is based on OFDM modulation with N sub-carriers and T OFDM blocks. At the source node, a stream of Nmodulated symbols are generated from an $m = log_2 M$ $MPSK$ constellation, m is the spectral efficiency. Unlike SF coding in multiple-antenna systems, SF coding in cooperative networks must be implemented in two distinct stages, namely; coding at the source node, and coding at the relay nodes. We now describe how the coded data is designed at the source node such that a diversity of order $L =$

$min\{L_{SR}, L_{RD}\}$ is achieved at each relay node. We first define a fixed positive integer $\Gamma \leq L \ll N$, we then partition the Nmodulated symbols into $K = \lfloor N/P\Gamma \rfloor$ blocks of codewords, such that each k_{th} block is of length $P\Gamma$. From this, we obtain the coded source node data

$$\boldsymbol{x} = [x(0), x(1), \ldots, x(N-1)] = [\boldsymbol{x}_1^T, \boldsymbol{x}_2^T, \ldots, \boldsymbol{x}_K^T, \boldsymbol{0}_{N-KP\Gamma}^T]^T \tag{5.1}$$

where $\boldsymbol{x}_k = [x_k(1), \ldots, x_k(P\Gamma)]^T$ is the $P\Gamma \times 1$ source node code transmitted in the k_{th} block, $(N - KP\Gamma)$ zeros are padded into $\boldsymbol{x}$ if N is not an integer multiple of $P\Gamma$. The elements of $\boldsymbol{x}_k$ are stacked in parallel unto $P\Gamma$ adjacent data sub-carriers within a single OFDM block. We assume that the channel remains constant within each OFDM block, and varies independently from block to block. Based on this assumption, differentially modulated symbols will be placed on adjacent groups of $P\Gamma$ sub-carriers within the same OFDM block. Let $\boldsymbol{x}_k = [x_k(1), \ldots, x_k(P\Gamma)]^T$ be the $P\Gamma \times 1$ data vector transmitted in the k_{th} block, where $x_k(n)$ denotes the symbol transmitted on the n_{th} sub-carrier from the source node to the p_{th} relay node in the k_{th} block. The elements of $\boldsymbol{x}$ are normalized such that $E(|\boldsymbol{x}_k|^2) = 1$. Since the source node transmits the data vector $\boldsymbol{x}_k$ to P relay nodes on $P\Gamma$ data sub-carriers, then the source node is capable of achieving a diversity of order $\Gamma \leq L$ at each relay node. The criteria for achieving this diversity order will be clarified later.

If the data vector generated by the source node is of the form $\sqrt{E_S P\Gamma}\boldsymbol{x}_k$ where E_S denotes average transmit-power, the signal received at the p_{th} relay node in the k_{th} block after CP removal and FFT demodulation is given in vector form by:

$$\boldsymbol{r}_{k,p} = \sqrt{E_S N_C}\boldsymbol{x}_k \odot \boldsymbol{f}_{k,p} + \boldsymbol{n}_{k,p} \tag{5.2}$$

where $\odot$ denotes Hadamard product or entry-wise operation, $\boldsymbol{r}_{k,p} = \left[r_{k,p}(1), \ldots, r_{k,p}(P\Gamma)\right]^T$, $\boldsymbol{f}_{k,p} = \left[f_{k,p}(1), \ldots, f_{k,p}(P\Gamma)\right]^T$ and $\boldsymbol{n}_{k,p} = \left[n_{k,p}(1), \ldots, n_{k,p}(P\Gamma)\right]^T$ is the zero-mean complex Gaussian noise term with covariance $N_0 I_{P\Gamma}$. The average signal-to-noise ratio (SNR) of the channel between the source node and the p_{th} relay node is given by $\Upsilon_{SR} = E_S P\Gamma / N_0$. The frequency response of the channel at the n_{th} sub-carrier of the p_{th} relay node in the k_{th} block is denoted by $f_{k,p}(n) = \sum_{l=0}^{L_{SR}-1} f_p(l) e^{-j2\pi ln/N} = \boldsymbol{f}_p \boldsymbol{\omega}$, $\boldsymbol{f}_p = \left[f_p(0), \ldots, f_p(L_{SR}-1)\right]$, $\boldsymbol{\omega} = \left[1, e^{-j2\pi n/N}, \ldots, e^{-j2\pi L-1 n/N}\right]^T$.

5.2.3 Relay Node Coding

We now discuss the how the SF codes are constructed at the relay nodes. Given that the p_{th} relay node receives $\boldsymbol{r}_{k,p}$ in (2) on $P\Gamma$ sub-carriers, it is only allowed to forward the data received on Γ sub-carriers, while the data on the remaining $(P\Gamma - \Gamma)$ sub-carriers is discarded. This means that each relay node must forward its received data only on Γ sub-carriers indexed as $\left[n_{k((p-1)\Gamma+1)}, \ldots, n_{k((p-1)\Gamma+\Gamma)}\right]$, $k = 1,2, \ldots, K$, $p = 1,2, \ldots, P$. Specifically, the p_{th} relay node will forward a subset of $\boldsymbol{r}_{k,p}$ given by $\bar{\boldsymbol{r}}_{k,p} = \left[r_{k,p}(1), \ldots, r_{k,p}(\Gamma)\right]^T \in \mathbb{C}^{\Gamma \times 1}$. Based on this, we can rewrite the received signal at the p_{th} relay node as:

$$\bar{\boldsymbol{r}}_{k,p} = \sqrt{E_S N_C}\, \bar{\boldsymbol{x}}_k \odot \bar{\boldsymbol{f}}_{k,p} + \bar{\boldsymbol{n}}_{k,p} \tag{5.3}$$

where $\bar{\boldsymbol{x}}_k = [x_k(1), \ldots, x_k(\Gamma)]^T$, $\bar{\boldsymbol{f}}_{k,p} = \left[f_{k,p}(1), \ldots, f_{k,p}(\Gamma)\right]^T$ and $\bar{\boldsymbol{n}}_{k,p} = \left[n_{k,p}(1), \ldots, n_{k,p}(\Gamma)\right]^T$.

In our DQSFC scheme, the P relay nodes are designed to construct $\Gamma \times P$ quasi-orthogonal signal matrices at the destination. In order to achieve this, each p_{th} relay node is equipped

with a $\Gamma \times \Gamma$ unitary matrix $\boldsymbol{M}_p$ referred to in [63] as the 'relay matrix'. The relay matrix is a matrix of 1s and 0s which enables the relay nodes to generate codewords with a quasi-orthogonal structure at the destination. The structure of the relay matrix is given in Section III and IV of [30] for cooperative networks with different number of relay nodes. Due to space limitations however, the structure of the relay matrix is not illustrated in our work, we just borrow the design of [30]. Specifically, we assume that J relay nodes are programmed to multiply their relay matrix by the received signal $\left[r_{k,p}(1), \ldots, r_{k,p}(\Gamma)\right]^T$ while the remaining $P - J$ relay nodes are programmed to multiply their relay matrix by the conjugate of the received signal $\left[r_{k,p}(1)^*, \ldots, r_{k,p}(\Gamma)^*\right]^T$. Thus, in the k_{th} block, the p_{th} relay node transmits a $\Gamma \times 1$ vector $\boldsymbol{t}_{k,p}$ given by:

$$\boldsymbol{t}_{k,p} = \sqrt{\frac{E_C}{E_S+1}}\boldsymbol{M}_p\bar{\boldsymbol{r}}_{k,p}, \;\; \bar{\boldsymbol{r}}_{k,p} \in \left\{\left[r_{k,p}(1), \ldots, r_{k,p}(\Gamma)\right]^T, \left[r_{k,p}(1)^*, \ldots, r_{k,p}(\Gamma)^*\right]^T\right\} \tag{5.4}$$

The power allocated to each relay node is denoted by E_C, this implies that an amplification co-efficient $\mu = \sqrt{E_C/E_S + 1}$ is applied at each relay node. Replicating the power allocation strategy in [30], we set $E_S = E_C P = E/2$, where E denotes the total power available in the network. In other words, the source node and the relay nodes share the available power in the network.

Since each p_{th} relay node transmits the data vector $\boldsymbol{t}_{k,p}$ to the destination on Γ sub-carriers, then all the P relay nodes can jointly achieve a diversity of order $P\Gamma$ at the destination. Based on this we define $\boldsymbol{t}_k = \left[t_{k,1}(1), \ldots, t_{k,1}(\Gamma), \ldots, t_{k,P}(1), \ldots, t_{k,P}(\Gamma)\right]$as the symbols transmitted in parallel on $P\Gamma$ sub-carriers by all P relay nodes. Fig. 5.2 gives a diagrammatic illustration of SF coding at the relay nodes for a cooperative network with 4 relay nodes.

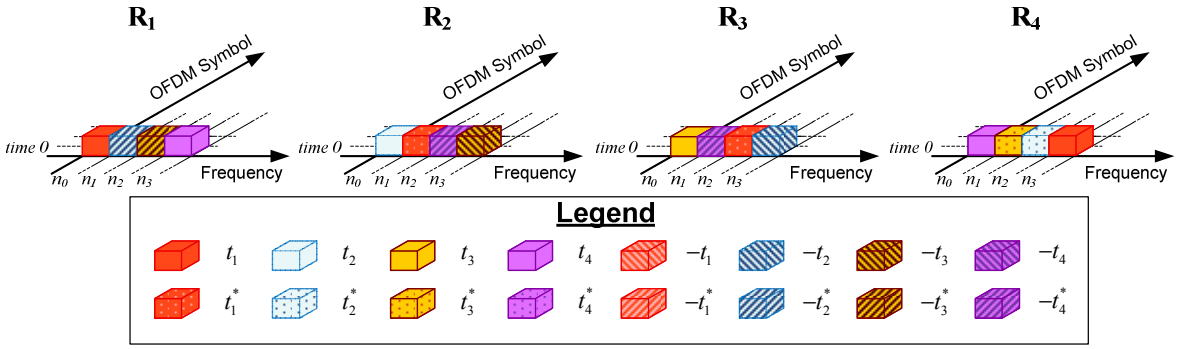

Fig.5.2 Space-frequency coding at the relay nodes

Assuming the relay nodes are synchronized at symbol level such that the nodes can transmit simultaneously, the signal received at the destination in the k_{th} block after cyclic prefix (CP) removal and fast Fourier transform (FFT) demodulation is given by:

$$\boldsymbol{y}_{k,n} = \sum_{p=1}^{P} \boldsymbol{t}_{k,p} \odot \boldsymbol{g}_{k,p} + \boldsymbol{z}_{k,n},\ n = 1,2,\dots,\Gamma \tag{5.5}$$

where $\boldsymbol{y}_{k,n} = \left[y_{k,n}(1),\dots,y_{k,n}(\Gamma)\right]^T$, $\boldsymbol{g}_{k,p} = \left[g_{k,p}(1),\dots,g_{k,p}(\Gamma)\right]^T$ and $\boldsymbol{z}_{k,n} = \left[z_{k,n}(1),\dots,z_{k,n}(\Gamma)\right]^T$ is the zero-mean complex Gaussian noise term with covariance $N_0 I_\Gamma$. The frequency response of the channel at the n_{th} sub-carrier between the p_{th} relay node and the destination in the k_{th} block is denoted by $g_{k,p}(n) = \sum_{l=0}^{L_{RD}-1} g_p(l) e^{-j2\pi ln/N} = \boldsymbol{g}_p \boldsymbol{\omega}$, $\boldsymbol{g}_p = \left[g_p(0),\dots,g_p(L_{SR}-1)\right]$. The average SNR of the channel between the p_{th} relay node and the destination is given by $\Upsilon_{RD} = E_C/N_0$. Substituting for $\bar{\boldsymbol{r}}_{k,p}$ in (5.3) and $\boldsymbol{t}_{k,p}$ in (5.4), (5.5) becomes:

$$\boldsymbol{y}_{k,n} = \sum_{p=1}^{P} \sqrt{\frac{E_C E_S N_C}{E_S+1}}\, \bar{\boldsymbol{x}}_k \boldsymbol{M}_p \left(\bar{\boldsymbol{f}}_{k,p} \odot \boldsymbol{g}_{k,p}\right) + \tilde{\boldsymbol{z}}_{k,n},\ n = 1,2,\dots,\Gamma \tag{5.6}$$

where $\tilde{\boldsymbol{z}}_{k,n} = \sum_{p=1}^{P} \mu\, \boldsymbol{M}_p \boldsymbol{g}_{k,p} \odot \bar{\boldsymbol{n}}_{k,p} + \boldsymbol{z}_{p,k,n}$ is the equivalent noise. The signal received at the destination in the k_{th} block can be written in compact form as:

$$\boldsymbol{Y}_k = \sqrt{\rho}\boldsymbol{X}_k\boldsymbol{H}_k + \boldsymbol{Z}_k \tag{5.7}$$

where $\boldsymbol{Y}_k = \left[\boldsymbol{y}_{k,1}, \dots, \boldsymbol{y}_{k,\Gamma}\right]^T \in \mathbb{C}^{\Gamma\times\Gamma}$,$\boldsymbol{y}_{k,n} = \left[y_{k,n}(1), \dots, y_{k,n}(\Gamma)\right]^T$,$\rho = \frac{E_C E_S N_C}{E_S+1}$, $\boldsymbol{X}_k = \left[\boldsymbol{M}_1\overline{\boldsymbol{x}}_k, \dots, \boldsymbol{M}_J\overline{\boldsymbol{x}}_k, \boldsymbol{M}_{J+1}\overline{\boldsymbol{x}}_k{}^*, \dots, \boldsymbol{M}_P\overline{\boldsymbol{x}}_k{}^*\right] \in \mathbb{C}^{\Gamma\times P}$, $\boldsymbol{H}_k = \left[\boldsymbol{h}_{k,1}, \dots, \boldsymbol{h}_{k,\Gamma}\right] \in \mathbb{C}^{P\times\Gamma}$, $\boldsymbol{h}_{k,n} = [h_k(1), \dots, h_k(P)]^T = (\boldsymbol{I}_P \otimes \boldsymbol{\omega}^T) \odot \boldsymbol{h}$, $\boldsymbol{h} = [h_1(0), \dots, h_1(L-1), .., h_P(0), \dots, h_P(L-1)]^T$and $\boldsymbol{Z}_k = \left[\tilde{\boldsymbol{z}}_{k,1}, \dots, \tilde{\boldsymbol{z}}_{k,\Gamma}\right]^T \in \mathbb{C}^{\Gamma\times\Gamma}$, the channel co-efficients $h_p(l) = f_p(l) \cdot g_p(l)$. The $P \times \Gamma$ quasi-orthogonal channel matrix $\boldsymbol{H}_k$ captures the channel co-efficients between the source node, the P relay nodes, and the destination. Here we assume that the channel is constant during the transmission of Γ symbols, that is, $\boldsymbol{h}_{k,n}$ is constant for $n = 1,2, \dots, \Gamma$.

The matrix $\boldsymbol{X}_k$ generated at the destination by the P relay nodes is a $\Gamma \times P$ quasi-orthogonal signal matrix containing either complex information symbols $\{x_k(1), \dots, x_k(\Gamma)\}$ or their conjugates$\{x_k(1)^*, \dots, x_k(\Gamma)^*\}$. Thus $\boldsymbol{X}_k$ in (5.7) can be rewritten as $\boldsymbol{X}_k = [\overline{\boldsymbol{x}}_k(1)^T, \dots, \overline{\boldsymbol{x}}_k(P)^T] \in \mathbb{C}^{\Gamma\times P}$, $\overline{\boldsymbol{x}}_k(p) = [x_k(1), \dots, x_k(\Gamma)]$, where $\overline{\boldsymbol{x}}_k(p)$ is the p_{th} column of $\boldsymbol{X}_k$. In other words, the p_{th} relay node transmits the p_{th} column vector of $\boldsymbol{X}_k$.

In order to recover information symbols at the destination without CSI, two consecutive quasi-orthogonal signal matrices $\boldsymbol{X}_k$ and $\boldsymbol{X}_{k+1}$must be received at the destination in the k_{th} block and $(k+1)_{th}$ block respectively. The first signal matrix $\boldsymbol{X}_k$ is termed the 'reference' quasi-orthogonal matrix because it is only required for differential decoding and thus contains no valid data, while the subsequent quasi-orthogonal signal matrix $\boldsymbol{X}_{k+1}$ conveys the valid data.

5.2.4 Quasi-orthogonal Space Frequency Code Construction

We now devise the structure of QSF codes that can achieve our targeted diversity of order $P\Gamma$. Since quasi-orthogonal codes will be used to build the SF codewords, it is necessary to employ the class of codes with a block-diagonal structure, for example, the quasi-orthogonal codes designed in [80] for multiple antenna systems. Denote $\boldsymbol{\mathcal{V}}$ as the generalized quasi-orthogonal matrix with a block-diagonal structure, $\boldsymbol{\mathcal{V}}$ can be used to construct codewords for a cooperative network with any $P = 2q$ relay nodes where $q = 2^r$ for a positive integer r.

$$\boldsymbol{\mathcal{V}} = diag[\mathcal{G}(v_1, v_2), \mathcal{G}(v_3, v_4), \dots, \mathcal{G}(v_{P-1}, v_P) \dots], \mathcal{G}(v_i, v_j) = \begin{bmatrix} v_i & v_j \\ -v_i^* & v_j^* \end{bmatrix} \tag{5.8}$$

The entries of $\boldsymbol{\mathcal{V}}$ are made up of combined symbols $v_1 = \mathrm{v}_1 + \tilde{\mathrm{v}}_3$, $v_2 = \mathrm{v}_2 + \tilde{\mathrm{v}}_4$, $v_3 = \mathrm{v}_1 - \tilde{\mathrm{v}}_3$, $v_4 = \mathrm{v}_2 - \tilde{\mathrm{v}}_4$ and so on, where $\tilde{\mathrm{v}}_i$ is the rotated version of v_i. The main challenge is how to construct the source node codeword from $\boldsymbol{\mathcal{V}}$, such that spatial and frequency diversity is exploited, and full rate is guaranteed. For any cooperative network with P relay nodes, the quasi-orthogonal code for any k_{th} block $\boldsymbol{\mathcal{V}}_k$ is constructed from $\boldsymbol{\mathcal{V}}$ as:

$$\boldsymbol{\mathcal{V}}_k = diag[\mathcal{G}(v_1, v_2), \dots, \mathcal{G}(v_{P-1}, v_P)] \tag{5.9}$$

Using (5.9), the source node then constructs a $P \times 1$ codeword from the elements of $\boldsymbol{\mathcal{V}}_k$ as

$$\boldsymbol{v}_k = [v_1, \dots, v_P]^T \tag{5.10}$$

The quasi-orthogonal code in (5.9) has full rate and will achieve full spatial diversity in any cooperative network with P relay nodes in a quasi-static fading channel scenario. The proof of full rate and full spatial diversity for the quasi-orthogonal code of (5.9) is given in [35, Section 5.4]. The code is however sub-optimal for our scheme because it is unable to exploit

frequency diversity. In order to design a SF codeword that guarantees full spatial and frequency diversity of order $P\Gamma$ where $\Gamma \leq L \ll N$, we construct the quasi-orthogonal code from $\boldsymbol{\mathcal{V}}$ as

$$\boldsymbol{\mathcal{V}}_k = diag[\mathcal{G}(v_1, v_2), \dots, \mathcal{G}(v_{P-1}, v_P), \dots, \mathcal{G}(v_{P\Gamma-1}, v_{P\Gamma})] \tag{5.11}$$

Using (5.11), the source node then constructs a $P\Gamma \times 1$codeword from the elements of $\boldsymbol{\mathcal{V}}_k$ as

$$\boldsymbol{v}_k = [v_1, \dots, v_P, \dots, v_{P\Gamma}]^T \tag{5.12}$$

The quasi-orthogonal code in (5.11) exploits full spatial and frequency diversity, and achieves our targeted diversity order, see proof in Appendix B. The code also provides pairwise decoding as will be shown in Section 5.3.2. Note that $v_p,\ p \leq P$ in (5.12) are the original symbols, while $v_p,\ p > P$ are replicas of theoriginal symbols which will be forwarded by the relay nodes.

As an example, for a cooperative network with $P = 4$ relay nodes, if we set $\Gamma = 4$, the $P\Gamma \times 1$ quasi-orthogonal source node data is constructed as

$$\begin{aligned}\boldsymbol{v}_k &= \left[v_{i(1)}, \dots, v_{i(4)}, \dots, v_{i(16)}\right]^T, i \in \{1,2,..,\Gamma\} \\ &= \left[\left(v_{1(1)}, v_{2(2)}, v_{3(3)}, v_{4(4)}\right),\left(v_{1(5)}, v_{2(6)}, v_{3(7)}, v_{4(8)}\right), \left(v_{1(9)}, v_{2(10)}, v_{3(11)}, v_{4(12)}\right),\right. \\ &\left.\left(v_{1(13)}, v_{2(14)}, v_{3(15)}, v_{4(16)}\right)\right]^T \\ &= [(v_1, v_2, v_3, v_4)_1, (-{v_2}^*, {v_1}^*, -{v_4}^*, {v_3}^*)_2, (-{v_3}^*, -{v_4}^*, {v_1}^*, {v_2}^*)_3, (v_4, -v_3, -v_2, v_1)_4]^T\end{aligned} \tag{5.13}$$

where $v_{i(n)}, n \leq 4$ are the original information symbols and $v_{i(n)}, n > 4$ are replicas, $(\cdot)_p$ is the $\Gamma \times 1$ data vector that will eventually be forwarded by the p_{th} relay node during the 'cooperate' stage. Thus the proposed code structure guarantees one symbol per sub-carrier use and unitary code rate when the relay nodes transmit to the destination, which we refer to

here as full rate. Specifically, $v_1, \ldots, v_\Gamma$ complex information symbols are transmitted simultaneously by P relay nodes on Γ sub-carriers. Our quasi-orthogonal code achieves a diversity order of $P\Gamma$ for any $(P+\Gamma) = 2^{r+1}, \forall\, P = \Gamma$ where r is a positive integer. In general, to construct the codeword for$(P+\Gamma) = J, 2^r < J < 2^{r+1}$, the quasi-orthogonal code is first constructed for $(P+\Gamma) = 2^{r+1}$ then $v_P,\ J < p \leq (P+\Gamma)$ is set to zero. For example, to obtain the codeword when $P = 4$ relay nodes and $\Gamma = 2$, that is $(P+\Gamma) = 6$, we first construct the codeword for $(P+\Gamma) = 2^{r+1} = 8$ then we set $\mathcal{G}(v_7, v_8)$ to zero.

5.3 Differential DQSFC Encoding and Decoding Procedure

5.3.1 Differential DQSFC Encoding

In this section, we discuss the differential encoding procedure employed in the proposed differential DQSFC scheme as depicted in Fig.5.3. The architecture is typically composed of a hybrid combination of three functional sub-systems, namely, a constellation mapping sub-system, a differential sub-system and a space-frequency sub-system. Differential encoding is initiated at the source node. Recalling that $\boldsymbol{x}_k$ is the $P\Gamma \times 1$ source node data generated in the k_{th} block, the next step is for the source node to generate the $P\Gamma \times 1$ data $\boldsymbol{x}_{k+1}$ for the $(k+1)_{th}$ block. This involves the following processes:

First, the constellation mapping sub-system generates the information symbols $\overline{\boldsymbol{v}}_{k+1} = [v_{k+1}(1), \ldots, v_{k+1}(\Gamma)]^T$ where $\overline{\boldsymbol{v}}_{k+1}$ represents the valid information symbols that must be recovered at the destination without CSI. We now show how the elements of $\overline{\boldsymbol{v}}_{k+1}$ are computed at the source node. A stream of $m\Gamma$ information bits are mapped into Γ symbols denoted by $\mathrm{v}_i, i = 1,2, \ldots, \Gamma$. The symbols are then combined as $v_1 = \mathrm{v}_1 + \tilde{\mathrm{v}}_3$, $v_2 = \mathrm{v}_2 + \tilde{\mathrm{v}}_4$, $v_3 = \mathrm{v}_1 - \tilde{\mathrm{v}}_3$, $v_4 = \mathrm{v}_2 - \tilde{\mathrm{v}}_4$ and so on. Let $\Phi = \mathrm{D} \cdot diag\left[1, e^{j\theta_1}, \ldots, e^{j\theta_{(\Gamma/2)-1}}\right]$, where D is a

$(\Gamma/2) \times (\Gamma/2)$ Hadamard matrix, the information symbols are then constructed as $[v_{k+1}(1), v_{k+1}(3), \dots, v_{k+1}(\Gamma-1)]^T = \Phi \cdot [v_1, v_3, \dots, v_{\Gamma-1}]^T$ and $[v_{k+1}(2), v_{k+1}(4), \dots, v_{k+1}(\Gamma)]^T = \Phi \cdot [v_2, v_4, \dots, v_\Gamma]^T$. Thus, $[v_{k+1}(1), v_{k+1}(2), \dots]^T$ are mapped onto a signal constellation $\mathcal{A}$ of size 2^m, while $[v_{k+1}(3), v_{k+1}(4), \dots]^T$ are mapped onto a signal constellation $\mathcal{A}_r$ which is a rotated version of $\mathcal{A}$. The rotation angles θ of the information symbols ensure that the codes achieve full diversity as will be shown in Section 5.4.2.

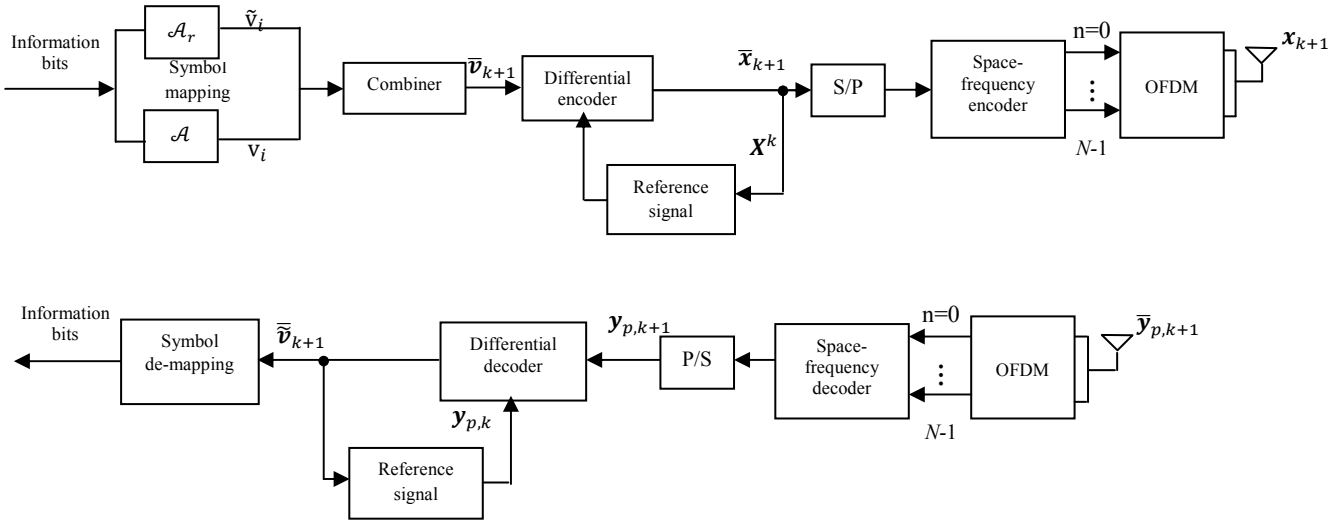

Fig.5.3. Differential DQSFC System Architecture

Next, the differential encoder generates the $\Gamma \times 1$ data vector $\overline{\boldsymbol{x}}_{k+1} = [x_{k+1}(1), \dots, x_{k+1}(\Gamma)]^T$ for the $(k+1)_{th}$ block as follows.

$$\overline{\boldsymbol{x}}_{k+1} = \boldsymbol{X}_k \overline{\boldsymbol{v}}_{k+1} \tag{5.14}$$

where $\overline{\boldsymbol{v}}_{k+1} = [v_{k+1}(1), \dots, v_{k+1}(\Gamma)]^T$ and $\boldsymbol{X}_k$ is the reference quasi-orthogonal signal matrix generated by the P relay nodes in the k_{th} block. We assume that the source node has prior knowledge of the relay matrices $\{\boldsymbol{M}_1, \dots, \boldsymbol{M}_J, \boldsymbol{M}_{J+1}, \dots, \boldsymbol{M}_P\}$, since the source node

knows $\overline{\boldsymbol{x}}_k = [x_k(1), \dots, x_k(\Gamma)]^T$, hence $\boldsymbol{X}_k = \left[\boldsymbol{M}_1\overline{\boldsymbol{x}}_k, \dots, \boldsymbol{M}_J\overline{\boldsymbol{x}}_k, \boldsymbol{M}_{J+1}\overline{\boldsymbol{x}}_k{}^*, \dots, \boldsymbol{M}_P\overline{\boldsymbol{x}}_k{}^*\right]$ can be computed.

Then finally the source node constructs the $P\Gamma \times 1$ data $\boldsymbol{x}_{k+1} = [x_{k+1}(1), \dots, x_{k+1}(P\Gamma)]^T$ from $\overline{\boldsymbol{x}}_{k+1}$ by adding replicas as in (5.13). The quasi-orthogonal structure of $\overline{\boldsymbol{v}}_{k+1} \in \boldsymbol{\mathcal{V}}$ guarantees that $\overline{\boldsymbol{x}}_{k+1}$ is quasi-orthogonal. Differential encoding is performed in the frequency domain, thus the differentially modulated symbols are stacked unto adjacent blocks of sub-carriers within a single OFDM block. We define the blocks of sub-carriers $\boldsymbol{n} = [\boldsymbol{n}_1{}^T, \boldsymbol{n}_2{}^T, \dots, \boldsymbol{n}_K{}^T, \boldsymbol{n}_{N-KP\Gamma}{}^T]^T$, where $\boldsymbol{n}_k$ is of length $P\Gamma$ and $(N - KP\Gamma)$ denotes the number of idle sub-carriers. Our differential encoding process is formulated in (5.14) under the constraint that the sub-channel gain of adjacent blocks of sub-carriers is almost constant. In other words the channel response, $\boldsymbol{h}(\boldsymbol{n}_k) \cong \boldsymbol{h}(\boldsymbol{n}_{k+1}), k = 1,2, \dots, K-1$, this implies that $\boldsymbol{H}_k \cong \boldsymbol{H}_{k+1}$, which is valid when N is very large [72].

The differential encoding process at the source node generates the $P\Gamma \times 1$ complex symbol vector $\boldsymbol{x}_{k+1} = [x_{k+1}(1), \dots, x_{k+1}(P\Gamma)]^T$ which is transmitted on $P\Gamma$ sub-carriers. In order to construct $\boldsymbol{X}_{k+1}$ at the destination, the source node and P relay nodes follow the same process as in the k_{th} block. The received signal at the p_{th} relay node in the $(k+1)_{th}$ block is of the form of (5.2). Similar to the case of the k_{th} block, the relay node data is constructed and transmitted as discussed in Section 5.2.3. The received signal at the destination in the $(k+1)_{th}$ block after FFT demodulation is similar to (5.7) and can be written in compact form as:

$$\boldsymbol{Y}_{k+1} = \sqrt{\rho}\boldsymbol{X}_{k+1}\boldsymbol{H}_{k+1} + \boldsymbol{Z}_{k+1} \tag{5.15}$$

5.3.2 Differential DQSFC Decoding

As far as the destination is concerned, consecutive blocks of information codewords have been received across different sub-carriers. So far, consecutive quasi-orthogonal matrices $\boldsymbol{X}_k$ and $\boldsymbol{X}_{k+1}$ have been generated at the destination by P relay nodes based on (5.7) and (5.15). We can write

$$\boldsymbol{y}_{k,n} = \boldsymbol{X}_k \boldsymbol{h}_{k,n} + \tilde{\boldsymbol{z}}_{k,n} = \left[\overline{\boldsymbol{x}}_k{}^T \boldsymbol{H}_k + \tilde{\boldsymbol{z}}_{k,n}{}^T\right]^T,\ n = 1,2,\dots,\Gamma \tag{5.16}$$

$$\boldsymbol{y}_{k+1,n} = \boldsymbol{X}_{k+1} \boldsymbol{h}_{k+1,n} + \tilde{\boldsymbol{z}}_{k+1,n} = \left[\overline{\boldsymbol{x}}_{k+1}{}^T \boldsymbol{H}_{k+1} + \tilde{\boldsymbol{z}}_{k+1,n}{}^T\right]^T \quad n = 1,2,\dots,\Gamma \tag{5.17}$$

Note that we intentionally omit the power term $\sqrt{\rho}$ for ease of explanation. Using the signals received in (5.16) and (5.17) in the k_{th} block and $(k+1)_{th}$ block respectively, $\overline{\boldsymbol{v}}_{k+1} = [v_{k+1}(1),\dots,v_{k+1}(\Gamma)]^T$ can be recovered pairwisely at the destination without CSI. For example, for a cooperative network with $P = 4$ relay nodes and $\Gamma = 4$, in order to recover $\overline{\boldsymbol{v}}_{k+1}$ we first obtain the quasi-orthogonal signal and channel matrices for two consecutive transmission blocks as follows:

$$\boldsymbol{X}_j = \begin{bmatrix} x_j(1) & x_j(2) & x_j(3) & x_j(4) \\ -x_j(2)^* & x_j(1)^* & -x_j(4)^* & x_j(3)^* \\ -x_j(3)^* & -x_j(4)^* & x_j(1)^* & x_j(2)^* \\ x_j(4) & -x_j(3) & -x_j(2) & x_j(1) \end{bmatrix} \quad \boldsymbol{H}_j = \begin{bmatrix} h_j(1) & h_j(2)^* & h_j(3)^* & h_j(4) \\ h_j(2) & -h_j(1)^* & h_j(4)^* & -h_j(3) \\ h_j(3) & h_j(4)^* & -h_j(1)^* & -h_j(2) \\ h_j(4) & -h_j(3)^* & -h_j(2)^* & h_j(1) \end{bmatrix}$$

where $\boldsymbol{X}_j$ and $\boldsymbol{H}_j$, $j \in \{k, k+1\}$ are quasi-orthogonal signal and channel matrices respectively. The information signal transmitted by the source node, through the p_{th} relay node on the n_{th} subcarrier is denoted by $x_j(n)$, and $h_j(p)$ captures the channel co-efficients between the source node, the p_{th} relay node, and the destination. Based on this, we can compute

$$\boldsymbol{X}_j\boldsymbol{X}_j{}^H = \begin{bmatrix} X_1 & 0 & 0 & X_2 \\ 0 & X_1 & -X_2 & 0 \\ 0 & -X_2 & X_1 & 0 \\ X_2 & 0 & 0 & X_1 \end{bmatrix} \quad \boldsymbol{H}_j\boldsymbol{H}_j{}^H = \begin{bmatrix} H_1 & 0 & 0 & H_2 \\ 0 & H_1 & -H_2 & 0 \\ 0 & -H_2 & H_1 & 0 \\ H_2 & 0 & 0 & H_1 \end{bmatrix}$$

where $X_1 = \sum_{n=1}^{4}\left|x_j(n)\right|^2$ is the signal power and $X_2 = 2Re\left(x_j(1)x_j(4)^* - x_j(2)x_j(3)^*\right)$ is a self-interference parameter. Similarly, $H_1 = \sum_{p=1}^{4}\left|h_j(p)\right|^2$ is the channel power and $H_2 = 2Re\left\{h_j(1)h_j(4)^* - h_j(2)h_j(3)^*\right\}$ is a self-interference parameter.The elements of $\overline{\boldsymbol{v}}_{k+1}$ are then recovered as follows:

$$\begin{aligned} \boldsymbol{y}_{k+1,1}\,\boldsymbol{y}_{k,1}{}^H &= \overline{\boldsymbol{x}}_{k+1}\boldsymbol{X}_k{}^H\boldsymbol{H}_{k+1}\boldsymbol{h}_{k,1}{}^H + Z_1 \\ &= \overline{\boldsymbol{v}}_{k+1}\boldsymbol{X}_k\boldsymbol{X}_k{}^H\boldsymbol{H}_{k+1}\boldsymbol{h}_{k,1}{}^H + Z_1 \\ &= v_{k+1}(1)(X_1H_1 + X_2H_2) + v_{k+1}(4)(X_1H_2 + X_2H_1) + Z_1 \\ &= v_{k+1}(1)A + v_{k+1}(4)B + Z_1 \end{aligned} \tag{5.18}$$

Similarly,

$$\begin{aligned} \boldsymbol{y}_{k+1,1}\,\boldsymbol{y}_{k,2}{}^H &= \overline{\boldsymbol{x}}_{k+1}\boldsymbol{X}_k{}^H\boldsymbol{H}_{k+1}\boldsymbol{h}_{k,2}{}^H + Z_2 \\ &= v_{k+1}(2)A - v_{k+1}(3)B + Z_2 \end{aligned} \tag{5.19}$$

$$\begin{aligned} \boldsymbol{y}_{k+1,1}\,\boldsymbol{y}_{k,3}{}^H &= \overline{\boldsymbol{x}}_{k+1}\boldsymbol{X}_k{}^H\boldsymbol{H}_{k+1}\boldsymbol{h}_{k,3}{}^H + Z_3 \\ &= -v_{k+1}(2)B + v_{k+1}(3)A + Z_3 \end{aligned} \tag{5.20}$$

$$\begin{aligned} \boldsymbol{y}_{k+1,1}\,\boldsymbol{y}_{k,4}{}^H &= \overline{\boldsymbol{x}}_{k+1}\boldsymbol{X}_k{}^H\boldsymbol{H}_{k+1}\boldsymbol{h}_{k,4}{}^H + Z_4 \\ &= v_{k+1}(1)B + v_{k+1}(4)A + Z_4 \end{aligned} \tag{5.21}$$

where Z_n captures the noise, $A = X_1H_1 + X_2H_2$ and $B = X_1H_2 + X_2H_1$, we refer to A and B as the differential decoding parameters required to recover $\overline{\boldsymbol{v}}_{k+1}$. The differential decoding parameters are computed at the destination as:

$$\boldsymbol{y}_{k,1}\,\boldsymbol{y}_{k,4}{}^{H} = \boldsymbol{X}_k\boldsymbol{h}_{k,1}\boldsymbol{X}_k{}^{H}\boldsymbol{h}_{k,4}{}^{H} + \tilde{Z}_4 = A + \tilde{Z}_4$$

$$\boldsymbol{y}_{k,1}\,\boldsymbol{y}_{k,1}{}^{H} = \boldsymbol{X}_k\boldsymbol{h}_{k,1}\boldsymbol{X}_k{}^{H}\boldsymbol{h}_{k,1}{}^{H} + \tilde{Z}_1 = B + \tilde{Z}_1 \qquad (5.22)$$

This implies that $\boldsymbol{y}_{k,1}\,\boldsymbol{y}_{k,4}{}^{H} \approx A$ and $\boldsymbol{y}_{k,1}\,\boldsymbol{y}_{k,1}{}^{H} \approx B$ since$Z_n \approx \tilde{Z}_n$. It is thus obvious from (5.22) that the scheme does not require CSI to recover $\overline{\boldsymbol{v}}_{k+1}$. The non-coherent recovery of $\overline{\boldsymbol{v}}_{k+1}$ rather depends on consecutively received signals in the k_{th} block and $(k+1)_{th}$ block under the constraint that $\boldsymbol{H}_k \cong \boldsymbol{H}_{k+1}$. Once A and B are computed at the destination using (5.22), the information signals in (5.18) to (5.21) can be recovered pairwisely. The decoding complexity of our SF codeword is exponential in Γ. It is thus necessary to set Γ such that a trade-off is reached between decoding complexity and frequency diversity. If we choose $1 \leq \Gamma \leq L$, then our scheme provides enough flexibility such that the necessary trade-off is achieved for any design preference.

So far, we can see that in each transmission block a two-stage transmit-and-cooperate differential protocol is adopted. In the 'transmit' stage of each block the destination is idle, while in the 'cooperate' stage of each block the source keeps silent and only the cooperating relay nodes transmit. In Section 5.5 we discuss a scenario where a direct link exists between the source and the destination, such that the source transmits in all stages and the destination receives in all stages.

5.4 Pairwise Error Probability Analysis and Diversity Improvement

5.4.1 Pairwise Error Probability Analysis

We now proceed to develop sufficient design criteria, based on the PEP analysis, for our code to achieve full diversity of order $P\Gamma$ while the coding gain is maximized as much as possible. Since each of the K blocks contains arbitrary symbols which are independently distributed across the relay nodes, we only require a single block k for our PEP analysis, which is valid for any $k = 1,2,\dots,K$. The frequency response vector between the source node and the relay nodes is denoted by $\boldsymbol{f}_k = [f_k(1),\dots,f_k(P\Gamma)]^T$, and similarly, the frequency response vector between the relay nodes and the destination is $\boldsymbol{g}_k = \left[g_{k,1}(1),\dots,g_{k,1}(\Gamma),\dots,g_{k,P}(1),\dots,g_{k,P}(\Gamma)\right]^T$. The correlation matrix of the channel frequency response can be found as $\boldsymbol{R} = E\{\boldsymbol{h}_k{\boldsymbol{h}_k}^H\} = E\{(\boldsymbol{f}_k \odot \boldsymbol{g}_k)(\boldsymbol{f}_k \odot \boldsymbol{g}_k)^H\}$. Unlike the case of multiple antenna systems, the cooperative network has the 'transmit' and 'cooperate' stages, thus $\boldsymbol{R}$ can be decomposed as $\boldsymbol{R} = \boldsymbol{R}_1 \odot \boldsymbol{R}_2$. We can easily show that $\boldsymbol{R}$, $\boldsymbol{R}_1$and $\boldsymbol{R}_2$ are full rank based on the following:

$$\boldsymbol{R}_1 = E\{\boldsymbol{f}_k{\boldsymbol{f}_k}^H\} = \boldsymbol{W}_1 E\{\boldsymbol{f}_p{\boldsymbol{f}_p}^H\}{\boldsymbol{W}_1}^H$$
$$= \boldsymbol{W}_1 diag({\sigma_{SR}}^2(0),\dots,{\sigma_{SR}}^2(L_{SR}-1)){\boldsymbol{W}_1}^H \quad (5.23)$$

$$\boldsymbol{R}_2 = E\{\boldsymbol{g}_k{\boldsymbol{g}_k}^H\} = \boldsymbol{W}_2 E\{\boldsymbol{g}_p{\boldsymbol{g}_p}^H\}{\boldsymbol{W}_2}^H$$
$$= \boldsymbol{W}_2 diag({\sigma_{RD}}^2(0),\dots,{\sigma_{RD}}^2(L_{RD}-1)){\boldsymbol{W}_2}^H \quad (5.24)$$

$$\boldsymbol{W}_1 = \left[{\boldsymbol{w}^{\alpha_0}}^T,\dots,{\boldsymbol{w}^{\alpha_{L-1}}}^T\right], \boldsymbol{W}_2 = \left[{\boldsymbol{w}^{\beta_0}}^T,\dots,{\boldsymbol{w}^{\beta_{L-1}}}^T\right], \boldsymbol{w} = \left[1,\omega^1,\dots,\omega^{(P\Gamma-1)}\right], \omega = e^{-j2\pi\Delta f} \quad (5.25)$$

where $\boldsymbol{f}_p = \left[f_p(0),\dots,f_p(L_{SR}-1)\right]^T$ and $\boldsymbol{g}_p = \left[g_p(0),\dots,g_p(L_{RD}-1)\right]^T$ and $\Delta f = 1/T$ is the sub-carrier spacing. From (5.25) if $\boldsymbol{W}_1$and $\boldsymbol{W}_2$ are unitary matrices, (obtainable if all L_{SR}

and L_{RD} fall within the sampling instances of the relay nodes and destination respectively [94]) then $\boldsymbol{W}_1$ and $\boldsymbol{W}_2$ have full rank, $R_{\boldsymbol{W}_1} = \Gamma \leq L$ and $R_{\boldsymbol{W}_2} = \Gamma \leq L$, respectively. We can then verify that $\boldsymbol{R}$, $\boldsymbol{R}_1$ and $\boldsymbol{R}_2$ are positive definite (full rank correlation matrices) based on the theorem in Section 1.2.4 of [83], which states that; if $\boldsymbol{R}_1$ and $\boldsymbol{R}_2$ are positive definite, then $\boldsymbol{R}$ is itself a positive definite (full rank correlation matrix).

Since we have established that $\boldsymbol{R}$ has full rank, we now proceed to discuss the criteria to achieve maximum diversity. We define statistically independent samples of the $S-R$ channel as $\boldsymbol{f} = [f_1(0), \dots, f_1(L_{SR}-1), \dots, f_P(0), \dots, f_P(L_{SR}-1)]$. Similarly, statistically independent samples of the $R-D$ channel are defined as $\boldsymbol{g} = [g_1(0), \dots, g_1(L_{RD}-1), \dots, g_P(0), \dots, g_P(L_{RD}-1)]$. Under the assumption that all $f_p(l)$ and $g_p(l)$ are independent identically distributed complex Gaussian variables, we can imply that $\boldsymbol{h} = [h_1(0), \dots, h_1(L-1), \dots, h_P(0), \dots, h_P(L-1)]$, $h_p(l) = f_p(l) \cdot g_p(l)$. For any k_{th} block, the SF codeword can be viewed as a collection of symbols transmitted across Γ sub-carriers by P relay nodes. Based on this, the consecutively received signals at the destination in the k_{th} block and $(k+1)_{th}$ block can be rewritten as (5.26) under the constraint that the sub-channel gain of adjacent blocks of sub-carriers is almost constant.

$$\boldsymbol{Y}^k = \overline{\boldsymbol{X}}^k \boldsymbol{\Lambda h} + \boldsymbol{Z}^k$$
$$\boldsymbol{Y}^{k+1} = \overline{\boldsymbol{X}}^{k+1} \boldsymbol{\Lambda h} + \boldsymbol{Z}^{k+1} \quad (5.26)$$

where $\boldsymbol{Y}^k = [\boldsymbol{y}_1^k, \dots, \boldsymbol{y}_\Gamma^k]^T$, $\boldsymbol{y}_n^k = [y^k(1), \dots, y^k(\Gamma)]^T$, $\boldsymbol{Y}^{k+1} = [\boldsymbol{y}_1^{k+1}, \dots, \boldsymbol{y}_\Gamma^{k+1}]^T$,

$\boldsymbol{y}_n^{k+1} = \left[y^{k+1}(1), \dots, y^{k+1}(\Gamma)\right]^T$, $\overline{\boldsymbol{X}}^k = diag\left[\boldsymbol{x}_{k,1}, \dots, \boldsymbol{x}_{k,\Gamma}\right]$, $\boldsymbol{x}_{k,n} = \left[x_{k,n}(1), \dots, x_{k,n}(P)\right]$,

$\overline{\boldsymbol{X}}^{k+1} = \left[\boldsymbol{x}_{k+1,1}, \dots, \boldsymbol{x}_{k+1,\Gamma}\right]$, $\boldsymbol{x}_{k+1,n} = diag\left[x_{k+1,n}(1), \dots, x_{k+1,n}(P)\right]$, $\boldsymbol{\Lambda} = [\boldsymbol{\Lambda}(1), \dots, \boldsymbol{\Lambda}(\Gamma)]^T$,

$\boldsymbol{\Lambda}(n) = \boldsymbol{I}_P \otimes \boldsymbol{\omega}^T$, $\boldsymbol{\omega} = \left[1, e^{-j2\pi n/N}, \dots, e^{-j2\pi L-1 n/N}\right]^T$.

Using the following notations:

$\boldsymbol{Y} = \left[\boldsymbol{Y}^{k^T}, \boldsymbol{Y}^{k+1^T}\right]^T, \boldsymbol{V}^{k+1} = diag\left[\boldsymbol{v}_{k+1,1}, \ldots, \boldsymbol{v}_{k+1,\Gamma}\right]$, $\boldsymbol{v}_{k+1,n} = \left[v_{k+1,n}(1), \ldots, v_{k+1,n}(P)\right]$,

$\boldsymbol{X} = \left[\boldsymbol{I}_{P\Gamma}{}^T, \boldsymbol{V}^{k+1^T}\right], \boldsymbol{Z} = \left[\boldsymbol{Z}^{k^T}, \boldsymbol{Z}^{k+1^T}\right]^T$,and the recursion

$\bar{\boldsymbol{X}}^{k+1} = \begin{cases} \boldsymbol{V}^{k+1}\bar{\boldsymbol{X}}^k, & k \geq 1 \\ \boldsymbol{I}_{P\Gamma}, & k = 0 \end{cases}$, we can write:

$$\boldsymbol{Y} = \boldsymbol{X}\boldsymbol{W}\boldsymbol{h} + \boldsymbol{Z} \tag{5.27}$$

The conditional probability density function of the receive signal matrix $\boldsymbol{Y}$ is

$$p(\boldsymbol{Y}|\boldsymbol{V}^{k+1}) = \frac{\exp(-tr\{\boldsymbol{Y}(\boldsymbol{I}_{P\Gamma} + \Upsilon\boldsymbol{X}\boldsymbol{\Lambda}\boldsymbol{R}\boldsymbol{\Lambda}^H\boldsymbol{X}^H)^{-1}\boldsymbol{Y}^H\})}{\pi^{P\Gamma}\det(\boldsymbol{I}_{P\Gamma} + \Upsilon\boldsymbol{X}\boldsymbol{\Lambda}\boldsymbol{R}\boldsymbol{\Lambda}^H\boldsymbol{X}^H)} \tag{5.28}$$

where $\mathbf{C}_{\mathrm{v}} = (\boldsymbol{I}_{P\Gamma} + \Upsilon\boldsymbol{X}\boldsymbol{\Lambda}\boldsymbol{R}\boldsymbol{\Lambda}^H\boldsymbol{X}^H)$ is the covariance matrix of $\boldsymbol{Y}$, tr denotes the trace function and Υ is the average SNR of the received signal given as $\Upsilon = \frac{P\Upsilon_{SR}\Upsilon_{RD}}{1+\Upsilon_{SR}+P\Upsilon_{RD}}$. Thus the non-coherent ML decoder is given by:

$$\widehat{\boldsymbol{V}}^{k+1} = \arg\max_{\boldsymbol{V}^{k+1}\in\boldsymbol{\mathcal{V}}} p(\boldsymbol{Y}|\boldsymbol{V}^{k+1}) \tag{5.29}$$

Substituting $\boldsymbol{Y}^k$ into $\boldsymbol{Y}^{k+1}$ in (5.26) and using $\bar{\boldsymbol{X}}^{k+1} = \boldsymbol{V}^{k+1}\bar{\boldsymbol{X}}^k$ we have $\boldsymbol{Y}^{k+1} = \boldsymbol{V}^{k+1}\boldsymbol{Y}^k + \grave{\boldsymbol{Z}}^{k+1}$ where $\grave{\boldsymbol{Z}}^{k+1} = \boldsymbol{Z}^{k+1} - \boldsymbol{V}^{k+1}\boldsymbol{Z}^k$. The non-coherent ML decoder can thus be simplified as

$$\widehat{\boldsymbol{V}}^{k+1} = \arg\max_{\boldsymbol{V}^{k+1}\in\boldsymbol{\mathcal{V}}} \left\|\boldsymbol{Y}^k + \boldsymbol{V}^{k+1^H}\boldsymbol{Y}^{k+1}\right\| \tag{5.30}$$

where $\|\cdot\|$ is the Frobenius norm. The Chernoff bound on the PEP of mistaking $\boldsymbol{V}^{k+1}$ by $\acute{\boldsymbol{V}}^{k+1}$ can be given as [72] [84].

$$PEP\left(\boldsymbol{V}^{k+1} - \acute{\boldsymbol{V}}^{k+1}\right) = \frac{1}{2}\left\{\frac{\det\left[\lambda(\boldsymbol{I}_{P\Gamma} + \Upsilon\boldsymbol{X}\boldsymbol{\Lambda}\boldsymbol{R}\boldsymbol{\Lambda}^H\boldsymbol{X}^H) + (1-\lambda)\left(\boldsymbol{I}_{P\Gamma} + \Upsilon\acute{\boldsymbol{X}}\boldsymbol{\Lambda}\boldsymbol{R}\boldsymbol{\Lambda}^H\acute{\boldsymbol{X}}^{\boldsymbol{H}}\right)\right]}{\det^{\lambda}(\boldsymbol{I}_{P\Gamma} + \Upsilon\boldsymbol{X}\boldsymbol{\Lambda}\boldsymbol{R}\boldsymbol{\Lambda}^H\boldsymbol{X}^H)\cdot\det^{(1-\lambda)}\left(\boldsymbol{I}_{P\Gamma} + \Upsilon\acute{\boldsymbol{X}}\boldsymbol{\Lambda}\boldsymbol{R}\boldsymbol{\Lambda}^H\acute{\boldsymbol{X}}^{\boldsymbol{H}}\right)}\right\} \quad (5.31)$$

where $\boldsymbol{X}$ and $\acute{\boldsymbol{X}}$ are two distinct codewords, $\acute{\boldsymbol{X}} = \left[\boldsymbol{I}_{P\Gamma}{}^T, \acute{\boldsymbol{V}}^{k+1}{}^T\right]$ and $\lambda = E\left\{\exp\left(\lambda\left[\ln p(\boldsymbol{Y}|\boldsymbol{V}^{k+1}) - p\left(\boldsymbol{Y}\middle|\acute{\boldsymbol{V}}^{k+1}\right)\right]\right)\right\}$ is used to get the tightest bound. By simple algebraic manipulation (5.31) can be simplified as

$$PEP\left(\boldsymbol{V}^{k+1} - \acute{\boldsymbol{V}}^{k+1}\right) = \frac{1}{2}\left\{\frac{\det\left[\boldsymbol{I}_{P\Gamma} + \Upsilon\boldsymbol{\Lambda}\boldsymbol{R}\boldsymbol{\Lambda}^H\left(\boldsymbol{X}\lambda\boldsymbol{X}^{\boldsymbol{H}} + \acute{\boldsymbol{X}}(1-\lambda)\acute{\boldsymbol{X}}^{\boldsymbol{H}}\right)\right]}{\det[\boldsymbol{I}_{P\Gamma} + 2\Upsilon\boldsymbol{\Lambda}\boldsymbol{R}\boldsymbol{\Lambda}^H]}\right\} \quad (5.32)$$

Since the relay nodes in our scheme linearly process their received signals, our achievable diversity order is bounded by $L = min\{L_{SR}, L_{RD}\}$. Thus, targeting maximum diversity order we choose $\Gamma = L$. Other values of Γ may be desirable, for example, when targeting minimum decoding complexity or when high SNR is considered. We can deduce from (5.32) that for all values of k, if $\acute{\boldsymbol{V}}^{k+1} - \boldsymbol{V}^{k+1}$ or similarly if $\acute{\boldsymbol{X}} - \boldsymbol{X}$ has full rank, then our scheme will achieve a diversity order of PL. At high SNR, the term in (5.32) can be further bounded as (5.33) where $\lambda = 1/2$ is selected to get the tightest bound [72] [85].

$$PEP\left(\boldsymbol{V}^{k+1} - \acute{\boldsymbol{V}}^{k+1}\right) \leq \left(\frac{\Upsilon}{8}\left(\det(\boldsymbol{\Lambda}\boldsymbol{R}\boldsymbol{\Lambda}^H)\det\left[\left(\acute{\boldsymbol{V}}^{k+1} - \boldsymbol{V}^{k+1}\right)^H\left(\acute{\boldsymbol{V}}^{k+1} - \boldsymbol{V}^{k+1}\right)\right]\right)^{\frac{1}{PL}}\right)^{-PL} \quad (5.33)$$

We observe from (5.33) that the performance of our code is determined by $\boldsymbol{R}$, $\boldsymbol{\Lambda}^H\boldsymbol{\Lambda}$ and $\left(\acute{\boldsymbol{V}}^{k+1} - \boldsymbol{V}^{k+1}\right)^H\left(\acute{\boldsymbol{V}}^{k+1} - \boldsymbol{V}^{k+1}\right)$. We have already established that $\boldsymbol{R}$ has full rank, thus our scheme will achieve maximum diversity if and only if $\boldsymbol{\Lambda}^H\boldsymbol{\Lambda}$ and $\left(\acute{\boldsymbol{V}}^{k+1} - \boldsymbol{V}^{k+1}\right)^H\left(\acute{\boldsymbol{V}}^{k+1} - \boldsymbol{V}^{k+1}\right)$ have full rank. Since we are interested in achieving maximum diversity while the coding gain is maximized as much as possible, the code must be designed such that $\acute{\boldsymbol{V}}^{k+1} - \boldsymbol{V}^{k+1}$ has full rank PL over all possible pairwise errors. When

maximum diversity is achieved, that is when $\acute{\boldsymbol{V}}^{k+1} - \boldsymbol{V}^{k+1}$ has full rank, the coding gain is only determined by $\det(\boldsymbol{\Lambda}^H\boldsymbol{\Lambda})$ and $\det\left[\left(\acute{\boldsymbol{V}}^{k+1} - \boldsymbol{V}^{k+1}\right)^H\left(\acute{\boldsymbol{V}}^{k+1} - \boldsymbol{V}^{k+1}\right)\right]$. In order to maximize the coding gain, the first step is to provide PL uncorrelated channels such that $\det(\boldsymbol{\Lambda}^H\boldsymbol{\Lambda})$ is maximized. For the second step, we consider the diversity product ζ_c which measures the quality of the code given as $\zeta_c = \frac{1}{2}\min_{\acute{\boldsymbol{V}}^{k+1}\neq\boldsymbol{V}^{k+1}\forall\boldsymbol{\mathcal{V}}}\left|\det\left(\acute{\boldsymbol{V}}^{k+1} - \boldsymbol{V}^{k+1}\right)\right|^{\frac{1}{PL}}$ where $\zeta_c > 0$ achieves maximum diversity. Thus the coding gain is maximized when we maximize ζ_c under the constraint that: $0 \leq \zeta_c \leq 1$ and$\left(\acute{\boldsymbol{V}}^{k+1} - \boldsymbol{V}^{k+1}\right), \forall\, \acute{\boldsymbol{V}}^{k+1} \neq \boldsymbol{V}^{k+1}$. Next we discuss the measures taken to maximize ζ_c based on code construction and to maximize $\det(\boldsymbol{\Lambda}^H\boldsymbol{\Lambda})$ based on sub-carrier grouping.

5.4.2 Diversity Improvement Based on Code Design

We now discuss the criteria for our block-diagonal quasi-orthogonal code $\boldsymbol{\mathcal{V}}_k, k = 1,2,\ldots,K$ of (5.11) to achieve full diversity. When SNR is high and when the relay nodes and destination are unable to acquire CSI, we have identified that the performance of our code is determined by the diversity product ζ_c which is given in the previous section. Hence our focus is to build constellations that maximize ζ_c as much as possible. Given two distinct pair of codewords $\boldsymbol{\mathcal{V}}_k = diag[\mathcal{G}(v_1, v_2), \ldots, \mathcal{G}(v_{P\Gamma-1}, v_{P\Gamma})]$ and $\acute{\boldsymbol{\mathcal{V}}}_k = diag[\mathcal{G}(\acute{v_1}, \acute{v_2}), \ldots, \mathcal{G}(v_{P\acute{\Gamma}-1}, \acute{v_{P\Gamma}})]$, the coding gain difference (CGD) is given by [35, Section 5.2].

$$det\left[\left(\boldsymbol{\mathcal{V}}_k - \acute{\boldsymbol{\mathcal{V}}}_k\right)^H\left(\boldsymbol{\mathcal{V}}_k - \acute{\boldsymbol{\mathcal{V}}}_k\right)\right] = P\Gamma det\left[\left(\mathcal{G}(v_1, v_2) - \mathcal{G}(\acute{v_1}, \acute{v_2})\right)\right]det\left[\left(\mathcal{G}(v_3, v_4) - \mathcal{G}(\acute{v_3}, \acute{v_4})\right)\right]\ldots det\left[\left(\mathcal{G}(v_{P\Gamma-1}, v_{P\Gamma}) - \mathcal{G}(v_{P\acute{\Gamma}-1}, \acute{v_{P\Gamma}})\right)\right] \quad (5.34)$$

$$= (|v_1 - \acute{v_1}|^2 + |v_2 - \acute{v_2}|^2)^2(|v_3 - \acute{v_3}|^2 + |v_4 - \acute{v_4}|^2)^2 \ldots (|v_{P\Gamma-1} - v_{P\acute{\Gamma}-1}|^2 + |v_{P\Gamma} - \acute{v_{P\Gamma}}|^2)^2 \quad (5.35)$$

where $\acute{v}_1 = \acute{\mathrm{v}}_1 + \tilde{\acute{\mathrm{v}}}_3, \acute{v}_2 = \acute{\mathrm{v}}_2 + \tilde{\acute{\mathrm{v}}}_4, \acute{v}_3 = \acute{\mathrm{v}}_1 - \tilde{\acute{\mathrm{v}}}_3,\ \acute{v}_4 = \acute{\mathrm{v}}_2 - \tilde{\acute{\mathrm{v}}}_4$ and so on. The bit label $\tilde{\acute{\mathrm{v}}}_\iota$ is the rotated version of $\acute{\mathrm{v}}_\iota$ by θ. In order to guarantee that the code achieves full diversity, the rotation angles $\{\theta_1, \theta_2, \dots, \theta_{P\Gamma}\}$corresponding to $\{\mathrm{v}_1, \mathrm{v}_2, \dots, \mathrm{v}_{P\Gamma}\}$ and $\{\acute{\mathrm{v}}_1, \acute{\mathrm{v}}_2, \dots, \acute{\mathrm{v}}_{P\Gamma}\}$are selected such that$det\left[\left(\mathcal{G}(v_i, v_j) - \mathcal{G}(\acute{v}_\iota, \acute{v}_j)\right)\right] \neq 0, \forall\, i, j \in \{1,2, \dots, P\Gamma\}$. This equivalently means that$(\mathrm{v}_i - \acute{\mathrm{v}}_\iota) + (\mathrm{v}_j - \acute{\mathrm{v}}_J) \neq 0, \forall\, i, j \in \{1,2, \dots, P\Gamma\}$. Therefore we can deduce from (5.35) that $\prod_{p=1}^{P\Gamma}\left|v_p - \acute{v}_p\right|^2 \neq 0$. Thus, our code satisfies the full diversity criterion for space-frequency codes given in Theorem 3.1 of [82]. Our generalized quasi-orthogonal code thus has the same properties as the quasi-orthogonal code of [70] and [80] designed for multiple-antenna systems. We can calculate the overall diversity product

$$\zeta_{eq} = \frac{1}{2}\min_{\forall \acute{\boldsymbol{v}}_k \neq \boldsymbol{v}_k \in \boldsymbol{\mathcal{V}}} \left| det\left(\left[\left(\boldsymbol{\mathcal{V}}_k - \acute{\boldsymbol{\mathcal{V}}}_k\right)^H \left(\boldsymbol{\mathcal{V}}_k - \acute{\boldsymbol{\mathcal{V}}}_k\right)\right] \odot \boldsymbol{R}\right)\right|^{\frac{1}{2P\Gamma}}$$

$$= \frac{1}{2}\min_{\forall \acute{\boldsymbol{v}}_k \neq \boldsymbol{v}_k \in \boldsymbol{\mathcal{V}}} \prod_{p=1}^{P\Gamma} \left|v_p - \acute{v}_p\right|^{\frac{1}{P\Gamma}} |\det(\boldsymbol{R})|^{\frac{1}{2\Gamma}}$$

$$= \frac{1}{2}\min\nolimits_{\forall \acute{\boldsymbol{V}}^{k+1} \neq \boldsymbol{V}^{k+1} \in \boldsymbol{\mathcal{V}}} \left|\det\left(\acute{\boldsymbol{V}}^{k+1} - \boldsymbol{V}^{k+1}\right)\right|^{\frac{1}{P\Gamma}} |\det(\boldsymbol{R})|^{\frac{1}{2\Gamma}} = \zeta_c . |\det(\boldsymbol{R})|^{\frac{1}{2\Gamma}} \qquad (5.36)$$

From (5.36) we can observe that if our code is constructed such that $\prod_{p=1}^{P\Gamma}\left|v_p - \acute{v}_p\right|^2 \neq 0$, then ζ_{eq} is non-zero and our scheme achieves diversity order of $P\Gamma, \Gamma \leq L$. Thus $|\det(\boldsymbol{R})|^{\frac{1}{2L}}$ which is determined by the power profile of the channel,$\sigma(l) = \sigma_{SR}(l) \cdot \sigma_{RD}(l)$, is independent of the code structure. Likewise ζ_c which is independent of the power profile, is only dependent on the constellation design and code structure which are optimized for maximum ζ_c.

The coding gain can be further maximized when optimum rotation angles θ_i are selected for the block diagonal codes. The symbols contained in $\boldsymbol{\mathcal{V}}_k$, that is, $\mathrm{v}_i, i = 1, \dots, 2^{m\Gamma}$ can be designed such that optimum values Φ_{op} of θ_i are selected for each v_i as

$\Phi_{\mathrm{op}} = diag\left(e^{j\theta_1(\mathrm{v}_1)}, \ldots, e^{j\theta_F(\mathrm{v}_F)}\right)$

where $F = 2^{m\Gamma}$. Since we have established that our DQSFC has the same properties as the quasi-orthogonal codes of [70] and [80], we can utilize the optimum rotation angles obtained via computer search as follows [80]:

$m = 1, \quad P = 4, \quad \theta_i \in \{1, \pi/M\}$

$m = 2, \quad P = 4, \quad \theta_i \in \{1, \pi/M\}$

$m = 1, \quad P = 6, \quad \theta_i \in \{1, \pi/2M\, , 3\pi/2M\}$

$m = 2, \quad P = 6, \quad \theta_i \in \{1, 0.4638, 0.9275\}$

$m = 1, \quad P = 8, \quad \theta_i \in \{1, \pi/M\, , \pi/2M, 3\pi/2M\}$

$m = 2, \quad P = 8, \quad \theta_i \in \{1, \pi/M\, , \pi/2M\, , 3\pi/2M\}$

5.4.3 Diversity Improvement Based on Sub-carrier Interleaving

In order to improve the diversity product, an appropriate sub-carrier allocation method which maximizes $\det(\boldsymbol{\Lambda}^H\boldsymbol{\Lambda})$ must be selected. The distribution of K codewords across $N_C = P\Gamma$ equally spaced blocks of sub-carriers as implemented in our system model has been shown to maximize $\det(\boldsymbol{\Lambda}^H\boldsymbol{\Lambda})$ in [72]. This is subject to the assumption that $\boldsymbol{\Lambda}$ is unitary. To further improve the coding gain of the DQSFC scheme we introduce a sub-carrier allocation method based on the permutation scheme of [82] which requires prior knowledge of the channel. However, if the source node and the relay nodes lack prior knowledge of the power delay profile (${\sigma_{SR}}^2$, ${\sigma_{RD}}^2$, α_l and β_l) of the channels, a randomized interleaving scheme can be utilized [82].

The elements of the quasi-orthogonal codeword $\boldsymbol{v}_k = [v_1, \ldots, v_P, \ldots, v_{P\Gamma}]^T, k = 1,2, \ldots, K$ of (5.12) are re-allocated to a new set of sub-carriers such that we obtain the interleaved version of $\boldsymbol{v}_k$which is given by $\varrho(\boldsymbol{v}_k)$. Given the difference operation $(\boldsymbol{v}_k - \acute{\boldsymbol{v}}_k), \forall \acute{\boldsymbol{v}}_k \neq \boldsymbol{v}_k$, we can

equivalently write $(v_p - \acute{v}_p), \forall \acute{v}_p \neq v_p$, where $p = 1,2,\dots,P\Gamma$. Based on the sub-carrier allocation method, $(v_p - \acute{v}_p)$ is now set as the $n_p th$ entry of $\varrho\{(\boldsymbol{v} - \acute{\boldsymbol{v}})\}$, or in simpler terms, v_p which was initially transmitted on the n_{th} sub-carrier is now transmitted on the $n_p th$ $(0 \leq n_p \leq N-1)$ sub-carrier. Specifically, for any k_{th} block all the $\left(n_{(p-1)\Gamma+\mathrm{i}}, n_{(p-1)\Gamma+\mathrm{j}}\right)_{th}$ entries of $\varrho[(\boldsymbol{v} - \acute{\boldsymbol{v}})]\varrho[(\boldsymbol{v} - \acute{\boldsymbol{v}})]^H$ are non-zero, where $p = 1,2,\dots,P$ and $1 \leq i,j \leq \Gamma$. Thus all the $\left(n_{(p-1)\Gamma+\mathrm{i}}, n_{(p-1)\Gamma+\mathrm{j}}\right)_{th}$entries of $(\varrho[(\boldsymbol{v} - \acute{\boldsymbol{v}})]\varrho[(\boldsymbol{v} - \acute{\boldsymbol{v}})]^H) \odot \boldsymbol{R}$ are non-zero. We define $\boldsymbol{T}_p, p = 1,2,\dots,P$ as the $\Gamma \times \Gamma$ matrix which determines the entries of $(\varrho[(\boldsymbol{v} - \acute{\boldsymbol{v}})]\varrho[(\boldsymbol{v} - \acute{\boldsymbol{v}})]^H) \odot \boldsymbol{R}$. In other words, the $(i,j)_{th}$ entries of $\boldsymbol{T}_p$ (where $1 \leq i,j \leq \Gamma$) is the $\left(n_{(p-1)\Gamma+\mathrm{i}}, n_{(p-1)\Gamma+\mathrm{j}}\right)_{th}$ entry of $(\varrho[(\boldsymbol{v} - \acute{\boldsymbol{v}})]\varrho[(\boldsymbol{v} - \acute{\boldsymbol{v}})]^H) \odot \boldsymbol{R}$.

Given that the correlation matrix $\boldsymbol{R} = \boldsymbol{R}_1 \odot \boldsymbol{R}_2$, and $\boldsymbol{R}$, $\boldsymbol{R}_1$ and $\boldsymbol{R}_2$ have the structure of a Toeplitz matrix, the correlation co-efficient between the $(i,j)_{th}(0 \leq i,j \leq N-1)$ entries of $\boldsymbol{R}_1$ and $\boldsymbol{R}_2$ are given respectively as $R_{1i,j} = \sum_{l=0}^{L_{SR}-1} {\sigma_{SR}}_l^2 \, \omega^{(i-j)\alpha_l}$ and $R_{2i,j} = \sum_{l=0}^{L_{RD}-1} {\sigma_{RD}}_l^2 \, \omega^{(i-j)\beta_l}$. From this we obtain the correlation co-efficient between the $(i,j)_{th}(0 \leq i,j \leq N-1)$entries of $\boldsymbol{R}$ as

$$R_{i,j} = \sum_{l=0}^{L-1} \sigma_l^2 \, \omega^{(i-j)\tau_l} \tag{5.37}$$

where $\sigma_l^2 = {\sigma_{SR}}_l^2 \cdot {\sigma_{RD}}_l^2$ and $\tau_l = min(\alpha_l, \beta_l)$. Thus the correlation co-efficient between the $(i,j)_{th}(1 \leq i,j \leq \Gamma)$ entries of $\boldsymbol{T}_p$ can be given by

$$T_{pi,j} = \Delta \sum_{l=0}^{L-1} \sigma_l^2 \, \omega^{\left(n_{(p-1)\Gamma+\mathrm{i}}, n_{(p-1)\Gamma+\mathrm{j}}\right)\tau_l} \tag{5.38}$$

where $\Delta = P.[(v_c - \acute{v}_c)(v_d - \acute{v}_d)^*]$, $c = (p-1)\Gamma + i$, and $d = (p-1)\Gamma + j$. The $\Gamma \times \Gamma$ matrix $\boldsymbol{T}_p, p = 1,\dots,P$ can be represented by

$$\boldsymbol{T}_p = \bar{\Delta}\boldsymbol{W}_p diag\left(\sigma^2_{(0)}, \dots, \sigma^2_{(L-1)}\right)\boldsymbol{W}_p^H \bar{\Delta}^H \tag{5.39}$$

where $\bar{\Delta} = \sqrt{P}.[(v_c - \acute{v}_c)(v_d - \acute{v}_d)^*]$ and $\boldsymbol{W}_p = \left[\boldsymbol{w}^{0^T}, \dots, \boldsymbol{w}^{(L-1)^T}\right]^T$,

$\boldsymbol{w} = \left[1, \omega^1, \dots, \omega^{(PL-1)}\right]$

We can calculate the determinant of $\boldsymbol{T}_p$ as

$$det\left(\boldsymbol{T}_p\right) = P^{\Gamma}\prod_{i=1}^{\Gamma}|(v_c - \acute{v}_c)|^2\, det\left(\boldsymbol{W}_p diag\left(\sigma^2_{(0)}, \dots, \sigma^2_{(L-1)}\right)\boldsymbol{W}_p^H\right) \tag{5.40}$$

Thus the overall diversity product after interleaving is

$$\zeta_{eq} = \frac{1}{2}\min_{\acute{\boldsymbol{v}}_k \neq \boldsymbol{v}_k \forall \boldsymbol{v}}\left(\prod_{p=1}^{\mathrm{P}\Gamma}|(v_c - \acute{v}_c)|\right)^{\frac{1}{\mathrm{P}\Gamma}}\left(\prod_{p=1}^{\mathrm{P}}\left|det\left(\boldsymbol{W}_p diag\left(\sigma^2_{(0)}, \dots, \sigma^2_{(L-1)}\right)\boldsymbol{W}_p^H\right)\right|\right)^{\frac{1}{2\mathrm{P}\Gamma}}$$

$$= \frac{1}{2}\min_{\acute{\mathbf{V}}_{k+1} \neq \mathbf{V}_{k+1} \forall \boldsymbol{v}}\left|\det\left(\acute{\boldsymbol{V}}^{k+1} - \boldsymbol{V}^{k+1}\right)\right|^{\frac{1}{\mathrm{P}\Gamma}}.\left(\prod_{p=1}^{\mathrm{P}}\left|det\left(\boldsymbol{W}_p diag\left(\sigma^2_{(0)}, \dots, \sigma^2_{(L-1)}\right)\boldsymbol{W}_p^H\right)\right|\right)^{\frac{1}{2\mathrm{P}\Gamma}}$$

$$= \zeta_c.\zeta_s \tag{5.41}$$

We observe from (5.41) above that ζ_s is only determined by the power delay profile and thus the interleaving approach can independently maximize ζ_s. On the other hand, ζ_c which was defined earlier is only dependent on the constellation design and code structure.

Another approach to maximize $\det(\boldsymbol{R})$ is to minimize the correlation between adjacent sub-carriers. As we can observe from (5.37), the correlation co-efficient $R_{i,j}$ is only determined by the difference between the $(i,j)_{th}(1 \leq i,j \leq \Gamma)$ entries, which we denote as $d = j - i$, $(d \in \{0, \pm 1, \dots, \pm N - 1\})$. If the value of d is large, then the value of $R_{i,j}$ is reduced and $\det(\boldsymbol{R})$ is maximized. In other words, if we can increase the sub-carrier spacing between every adjacent Γ sub-carriers of each relay node, then consequently, the correlation co-efficient is minimized and $\det(\boldsymbol{R})$ is maximized. The sub-carrier spacing in the k_{th} block of the p_{th} relay node can be given as

$d_{k(p)} = \{\boldsymbol{n}_{k(p)}\}_j - \{\boldsymbol{n}_{k(p)}\}_i, \qquad (1 \leq i,j \leq \Gamma)$

$\det(\boldsymbol{R})$ is maximized if we make $d_{k(p)}$ as large as possible under the assumption that the number of idle sub-carriers $\boldsymbol{n}_{idle} = N - KP\Gamma$ is very small, that is $N \gg \boldsymbol{n}_{idle}$.

5.5 Multi-differential DQSFC Encoding and Decoding

The diversity performance of our differential DQSFC scheme can be improved by exploiting the additional channel taps provided by the source-destination $(S-D)$ link. If a direct link is available between the source node and the destination, the destination can differentially recover information symbols using the signals from the source node and the signals from the relay nodes. In Section 5.3, the source node is idle at certain transmission intervals, specifically when the relay nodes are transmitting to the destination. Our multi-differential scheme is designed such that the source node can use these idle transmission intervals to generate quasi-orthogonal matrices at the destination. If the structure of the quasi-orthogonal matrices generated at the destination by the source node is identical to the structure of the quasi-orthogonal matrices generated at the destination by the relay nodes in Section 5.3, then the destination can use the same decoding metric to jointly recover the two sets of information symbols without incurring additional decoding complexity. Thus the principal objective of our multi-differential scheme is to improve the SNR gain at the destination with negligible decoding complexity penalties.

The multipath fading channel between the source node and the destination node is modeled as

$$h_{SD}(t) = \sum_{l=0}^{L_{SD}-1} h_{SD}(l)\delta(t-\kappa_l) \tag{5.42}$$

where $h_{SD}(l)$ is the complex amplitude of the l_{th} path and the $h_{SD}(l)$'s are assumed to be independent zero-mean complex Gaussian random variables with variance $\sigma_{SD}^2(l)$. The delay

of the l_{th} path is denoted by κ_l, while L_{SD} denotes the number of independent channel taps on the $S-D$ link, and the independent channel taps are described by the discrete-time impulse response vector $\boldsymbol{h}_{SD} = [h_{SD}(0), \dots, h_{SD}(L_{SD}-1)]$. Since there are L_{SD} channel taps on the $S-D$ link, the coding at the source node is designed to achieve a diversity of order $\Gamma \leq L_{SD}$ at the destination.

The source node has prior knowledge of the relay matrices $\{\boldsymbol{M}_1, \dots, \boldsymbol{M}_J, \boldsymbol{M}_{J+1}, \dots, \boldsymbol{M}_P\}$, and $\boldsymbol{X}_k = \left[\boldsymbol{M}_1\overline{\boldsymbol{x}}_k, \dots, \boldsymbol{M}_J\overline{\boldsymbol{x}}_k, \boldsymbol{M}_{J+1}\overline{\boldsymbol{x}}_k{}^*, \dots, \boldsymbol{M}_P\overline{\boldsymbol{x}}_k{}^*\right] = \left[\overline{\boldsymbol{x}}_{k,1}{}^T, \dots, \overline{\boldsymbol{x}}_{k,P}{}^T\right] \in \mathbb{C}^{\Gamma\times P}, \overline{\boldsymbol{x}}_{k,p} = [x_k(1), \dots, x_k(\Gamma)]$, where $\overline{\boldsymbol{x}}_{k,p}$ is the p_{th} column of $\boldsymbol{X}_k$. Thus the source node can construct $\overline{\boldsymbol{x}}_{k,p} = [x_k(1), \dots, x_k(\Gamma)]$ for any $p = 1,2, \dots, P$. The source-destination channel matrix is denoted as $\boldsymbol{H}_{SD,k} \in \mathbb{C}^{\Gamma\times\Gamma}$ and given by $\boldsymbol{H}_{SD,k} = \left[\boldsymbol{h}_{SD,k}(1), \dots, \boldsymbol{h}_{SD,k}(\Gamma)\right]$, $\boldsymbol{h}_{SD,k}(n) = \left[h_{SD,k}(1), \dots, h_{SD,k}(\Gamma)\right]^T$, this implies that $\boldsymbol{h}_{SD,k}(n), n = 1,2, \dots, \Gamma$ is the n_{th} column of $\boldsymbol{H}_{SD,k}$ and $h_{SD,k}(n)$ denotes the channel co-efficient between the source node and the destination on the n_{th} subcarrier given by $h_{SD,k}(n) = \sum_{l=0}^{L_{SD}-1} h_{SD}(l)e^{-j2\pi ln/N} = \boldsymbol{h}_{SD}{}^T\boldsymbol{\omega}(n)$. If the channel co-efficients remain unchanged during all the source-destination transmission cycles, then we can imply that $\boldsymbol{h}_{SD,k}(1) =, \dots, = \boldsymbol{h}_{SD,k}(\Gamma)$.

The signal received by the destination from the source node in the k_{th} block can be written in compact form as

$$\boldsymbol{Y}^{S,k} = \boldsymbol{X}_k\boldsymbol{H}_{SD,k} + \boldsymbol{Z}^{S,k} \tag{5.43}$$

where $\boldsymbol{Y}^{S,k} = [\boldsymbol{y}^{S,k}(1)^T, \dots, \boldsymbol{y}^{S,k}(\Gamma)^T]^T$, $\boldsymbol{y}^{S,k}(\mathrm{n}) = diag\left(\overline{\boldsymbol{x}}_{k(n)}\right)\boldsymbol{h}_{SD,k}(n) + \boldsymbol{z}^{S,k}(\mathrm{n}),\ n = 1, \dots, \Gamma$

We observe that the source already knows $\overline{\boldsymbol{v}}_{k+1}$ and $\boldsymbol{X}_k$, thus it can differentially compute $\overline{\boldsymbol{x}}_{k+1}$ using (5.14). The source node can also construct $\boldsymbol{X}_{k+1}$ using the relay

matrices$\{\boldsymbol{M}_1, \dots, \boldsymbol{M}_J, \boldsymbol{M}_{J+1}, \dots, \boldsymbol{M}_P\}$. The signal received by the destination from the source node in the $(k+1)_{th}$ block can be written in compact form as

$$\boldsymbol{Y}^{S,k+1} = \boldsymbol{X}_{k+1}\boldsymbol{H}_{SD,k+1} + \boldsymbol{Z}^{S,k+1} \tag{5.44}$$

The signals in (5.43) and (5.44) have the same structure and properties as the signals in (5.16) and (5.17), thus similar to Section 5.3.2, using the signals received in (5.43) and (5.44) and the differential encoding equation in (5.14), the elements of $\overline{\boldsymbol{v}}_{k+1} = [v_{k+1}(1), \dots, v_{k+1}(\Gamma)]$ can be recovered pairwisely at the destination without CSI. Since the $S-D$ link has L_{SD} independent channel taps and the coding at the source node is designed to achieve a diversity of order $\Gamma \leq L_{SD}$, the multi-differential protocol improves the diversity performance of our differential DQSFC scheme from $P\Gamma$ to $(P+1)\Gamma$. Thisis as a result of the additional diversity path provided by the source node, and is evident from our simulation results.

5.6 Simulation Results

In this section, we present simulation results to demonstrate the performance of our proposed differential and multi-differential DQSFC schemes. The settings for our cooperative broadband network are based on the specifications described in the IEEE802.16e Mobile WiMax standard. The number of sub-carriers used is $N = 200$ with a channel bandwidth of 3.5MHz. We assume that neither the relay nodes nor destination can acquire CSI. The frequency selective channels of the source-relay and relay-destination links remain approximately constant within two consecutive blocks, which is required for differential decoding as explained earlier. We illustrate the frequency diversity performance of our proposed differential DQSFC protocol using BPSK modulation for the case of:

$L_{SR_1} = \cdots = L_{SR_p},\ L_{RD_1} = \cdots = L_{RD_p},\ L_{SR} = \{1, \dots, 4 \dots\}, L_{RD} = \{1, \dots, 4 \dots\}$

$\alpha_l = \beta_l \in \{0\mu s, 0.5\mu s, 1.5\mu s, 5\mu s\}$, $\sigma_{SR(1)} = \cdots = \sigma_{SR(L_{SR})} = 1$, $\sigma_{RD(1)} = \cdots = \sigma_{RD(L_{SR})} = 1$

For frequency diversity analysis, we consider two main scenarios: the symmetric case where $L_{SR} = L_{RD}$, and the asymmetric case where $L_{SR} \neq L_{RD}$. We consider the symmetric case in Fig.5.4, for $P = 4$ relay nodes, we first set $L = L_{SR} = L_{RD} = 2$ to form the basis for comparing our differential DQSFC scheme with the non-differential DSFC scheme of [77] where $L = 2$ and $P = 4$. We consider SER performance to enable fair comparison with the scheme of [77]. From the results, we observe that the SER performance of our scheme slightly surpasses that of [77] despite the 3dB loss incurred by our scheme due to differential decoding. Our curve denoted 'Differential DQSFC $L = 2$ $P = 4$' also has a similar slope to that of [77]. This indicates that, like coherent designs, our non-coherent design exploits the maximum spatial and frequency diversity available in frequency selective channels even in scenarios where CSI cannot be acquired. In addition, while the scheme in [77] has full symbol rate, our scheme has the additional advantage of full code rate for $P \geq 2$ relays. We also observe that our scheme shows corresponding performance improvement when the number of channel taps increases from $L = 1$ (corresponding to a flat fading channel) to $L = 3$.

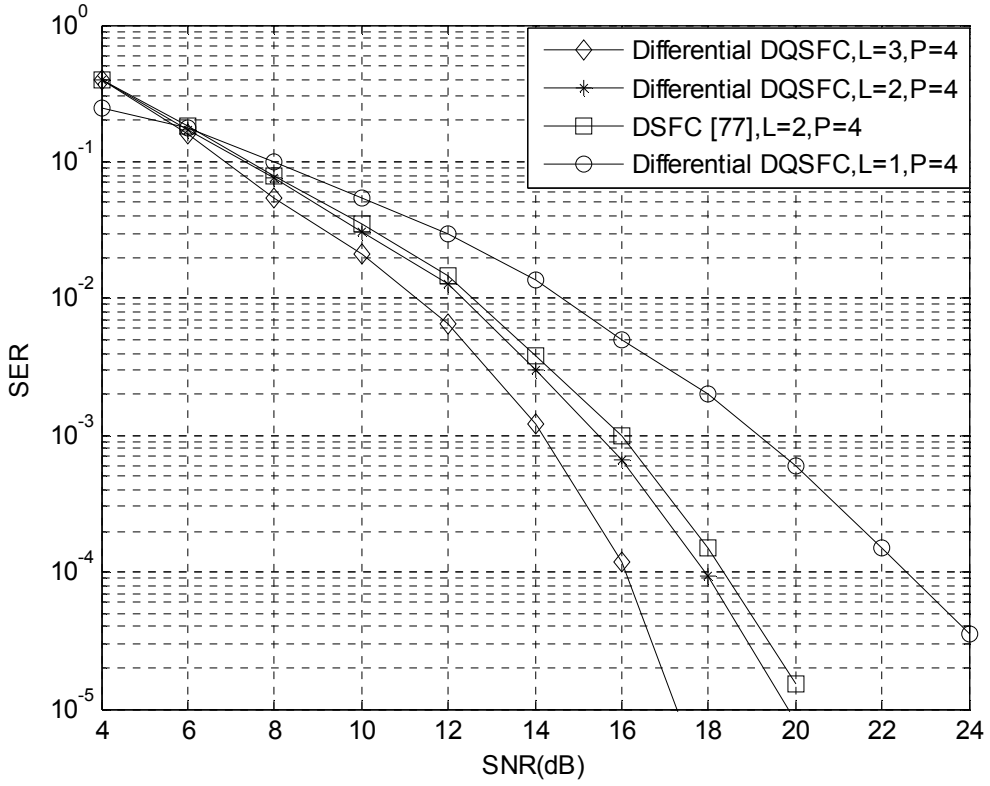

Fig.5.4 Frequency diversity performance of differential DQSFC scheme for the symmetric case

In Fig.5.5 we include the results for scenarios where $L_{SR} \neq L_{RD}$ to verify the achievable diversity gain based on our PEP analysis. From the results, we observe that the SER curve of our differential DQSFC scheme when $L_{SR} = 2$ and $L_{RD} = 3$ has the same slope as that of $L_{SR} = 3$ and $L_{RD} = 2$ which signifies that for cases where $L_{SR} \neq L_{RD}$ the diversity performance is bounded by $PL = P(min\{L_{SR}, L_{RD}\})$ which is consistent with the achievable diversity order based on our PEP analysis. Thus maximal diversity order is achieved when the coding at the source node and relay nodes are designed using $L = min\{L_{SR}, L_{RD}\}$. We also observe that a gain of about 1dB is achieved when L_{SR} exceeds L_{RD}. This implies that the extra channel taps on the source-relay link provides stronger diversity advantage in

comparison with the case when L_{RD} exceeds L_{SR}. This is owed to the fact that when L_{SR} exceeds L_{RD}, the relay nodes deliver less erroneous symbols to the destination. We then vary the number of channel taps using $L = 1$ and $L = 2$ for different number of relay nodes $P = 2$ and $P = 4$. We can observe from Fig.5.5 that for different cases, a diversity order of PL is achieved. For example, the differential DQSFC curve with $L = 1$ and $P = 4$ has an identical slope to that of $L = 2$ and $P = 2$. This verifies that our scheme exploits the achievable spatial and frequency diversity when quasi-orthogonal codes are utilized in scenarios where CSI is unavailable. In terms of SER performance, we can also deduce that the spatial diversity advantage (due to number of relays) slightly supersedes the multipath diversity advantage (due to number of channel taps).

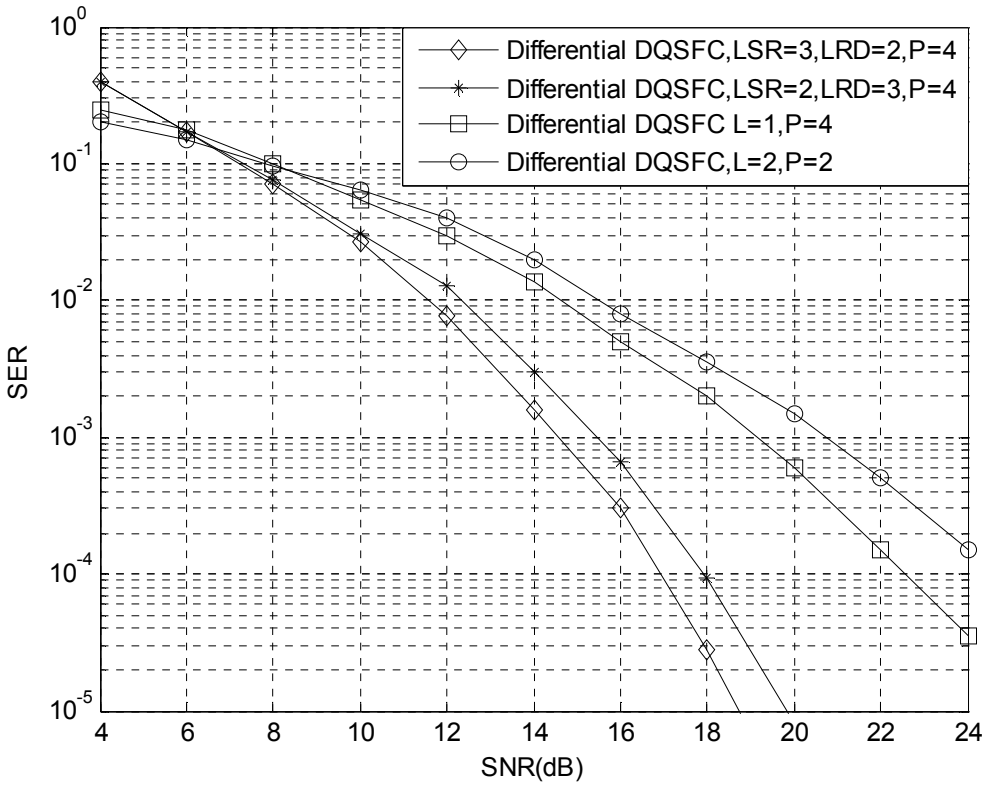

Fig.5.5 Frequency diversity performance of differential DQSFC scheme for the asymmetric case

In Fig.5.6 we analyse the diversity performance of our full rate quasi-orthogonal design using optimum rotation angles and sub-carrier interleaving, where $P = 4, L = 2$. For our quasi-orthogonal codes, the optimum rotation angles are set as$\{1, \pi/M\}$, where $M = 2$ is the constellation size. To illustrate the diversity gain due to constellation rotation, we include the BER curve of non-rotated differential DQSFC schemes. We observe from Fig.5.6 that compared to our differential DQSFC scheme with optimum rotation angles, non-rotated differential DQSFC schemes exhibit similar performance at SNR values below 15dB. At higher SNR values, our differential DQSFC scheme with optimum rotation angles exhibits better performance. Simulation results also show that when interleaving is applied, there is a 1-2.5dB improvement compared to the case where interleaving is not applied.

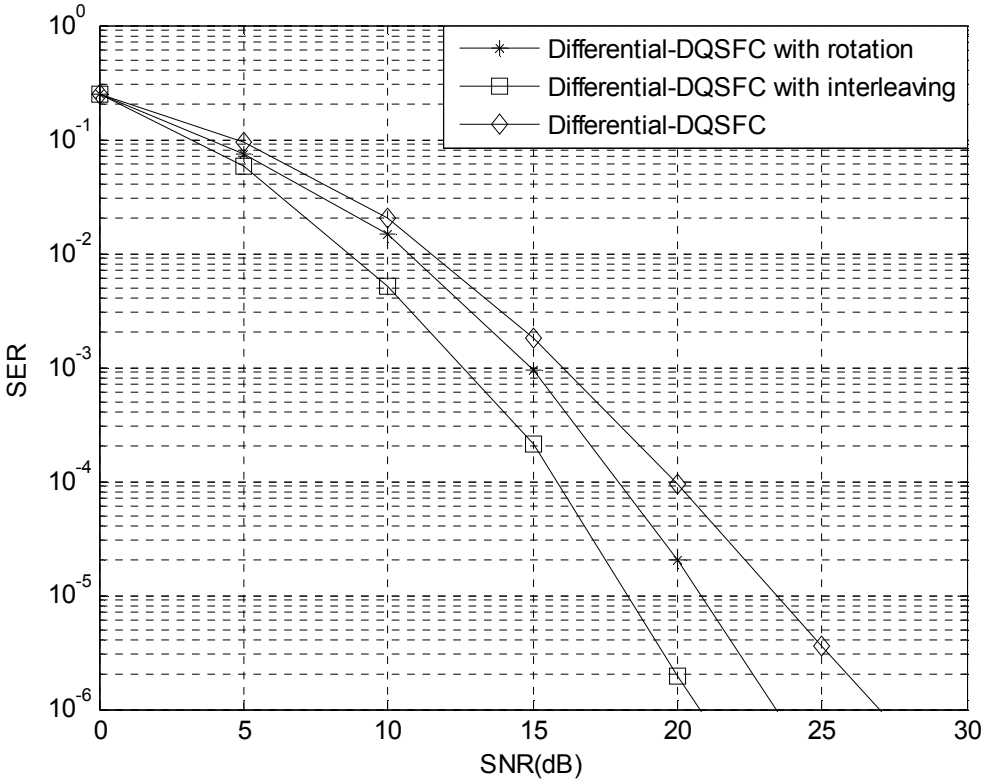

Fig.5.6 Diversity performance of differential DQSFC scheme with optimum constellation rotation and interleaving

Fig.5.7 shows the performance of our multi-differential DQSFC scheme using BPSK modulation for static communication, and at different Doppler frequencies f_D of 50Hz and 200Hz corresponding to approximate mobile speeds of 20km/h and 90km/h respectively. The results indicate that the multi-differential protocol demonstrates significant performance gains over the differential protocol especially in the higher SNR region. For example at $f_D =$ 200Hz and 10^{-4} BER, the multi-differential scheme achieves about 4dB performance gain over the differential scheme. This is easily due to the additional diversity path provided by the $S - D$ link. Thus, this confirms that multi-differential protocol improves the diversity performance of our differential DQSFC scheme from $P\Gamma$ to$(P + 1)\Gamma$. The multi-differential scheme also incurs negligible increase in decoding complexity compared to its differential DQSFC counterpart because the amount of search $2^{m\Gamma+1}$ remains unchanged. It is also clear from the results that loss in diversity performance occurs when node speed increases.

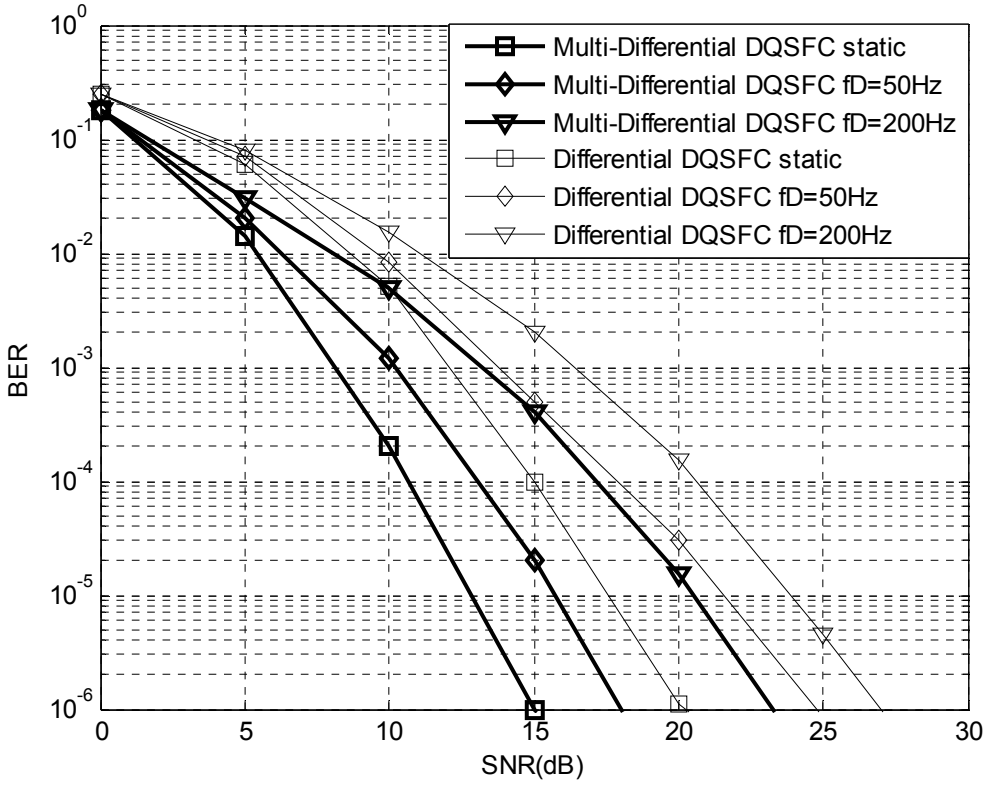

Fig.5.7 Diversity performance of proposed multi-differential DQSFC scheme

5.7 Summary

Existing DSFC protocols from orthogonal designs are capable of achieving maximum spatial and frequency diversity over frequency selective channels. However, CSI acquisition is impractical in cooperative broadband networks where the frequency selective channels have many taps or when communicating nodes are mobile. Moreover, an attempt to increase the data rate of such networks results in less than full code rate. To combat the problem of CSI acquisition and code rate in cooperative broadband networks, we integrate differential modulation and full rate quasi-orthogonal designs with DSFC protocols. From this we propose a differential DQSFC protocol which is capable of achieving full rate, as well as exploiting the maximum spatial and frequency diversity in non-coherent cooperative broadband networks. Through PEP analysis, we show that the diversity performance of our scheme can be improved by appropriate code construction and sub-carrier allocation. Based on this, we devise a code structure and sub-carrier allocation method to maximize the diversity performance of our scheme. In addition we propose a multi-differential protocol which exploits the additional diversity path provided by the $S-D$ link, simulations results illustrate the improved BER performance achieved by our multi-differential protocol.

6 Differential Distributed Quasi-Orthogonal Space Time Frequency Coding

6.1 Introduction

In order to maximize the achievable capacity gain, DSTBC are now being utilized in cooperative networks to achieve diversity in multiple dimensions. In addition to spatial diversity, DSTBC-OFDM schemes and DSFC schemes are capable of exploiting diversity in the temporal and frequency dimensions respectively. In DSTBC-OFDM, elements of the codeword matrix, transmitted by cooperating relay nodes, are applied at individual sub-carriers over multiple OFDM time slots, thus space-time (ST) diversity is achieved. On the other hand, DSFC transmits elements of the codeword matrix across multiple sub-carriers within a single OFDM time slot thereby achieving space-frequency (SF) diversity. The performance of DSTBC-OFDM schemes however depreciates in severe time-selective fading environments, especially during the transmission of signals with long symbol period. This is because the conditions for constant channel gain across multiple OFDM time slots cannot be satisfied. Similarly, DSFC schemes show performance degradation in severe frequency-selective environments because the requirements for constant channel gain across multiple frequency sub-carriers cannot be satisfied. Thus when signals with long symbol period are transmitted, or similarly when the number of cooperating nodes is large, severe time selectivity and frequency selectivity will cause inter-symbol interference.

Effort is now directed towards designing a protocol which concatenates the DSTBC-OFDM and DSFC schemes such that their combined benefits can be realized, while their shortcomings are alleviated. The fundamental idea behind this concept is to provide a scheme

which concurrently exploits coding in the spatial, temporal and frequency dimensions. This paradigm has led to the design of distributed space-time-frequency coding (DSTFC) schemes. In DSTFC schemes, elements of the codeword matrix are simultaneously transmitted from spaced cooperating nodes across multiple OFDM time slots and frequency sub-carriers. The principal objective is to design a coding scheme that mitigates the performance degradation experienced by DSTC-OFDM and DSFC schemes in severe time-selective and frequency-selective fading channels. In the DSTBC-OFDM schemes of [53] [64] and the DSFC schemes of [86] [77] for example, the channel gain on adjacent OFDM time slots and frequency sub-carriers respectively is assumed to remain quasi-static to facilitate signal recovery at the destination. This assumption is impractical when signals with long symbol duration are transmitted, or when the number of cooperating nodes is large. DSTFC schemes can be designed to mitigate this problem by simultaneously transmitting across OFDM time-slots and frequency sub-carriers, such that the requirement for constant channel gain in the temporal and frequency dimensions is more relaxed.

The study of STF coding schemes in frequency-selective and time-selective fading environments has been reported in a few works [87-89] for multiple antenna systems. For cooperative networks, DSTFC schemes have recently been investigated in [90] and [91], where the authors study the performance of the DSTFC coding in frequency-selective fading channels. All these schemes assume coherent signal recovery, thus CSI acquisition is practical. In the case of non-coherent cooperative networks operating in environments where CSI acquisition is impractical, the differential DSTFC strategy has only been investigated in [92]. However, the authors in [92] focus mainly on the security issues affecting the cooperative system.

We thus deem it pertinent to study the performance of DSTFC schemes in highly selective fading environments where the nodes in the cooperative network are unable to acquire CSI. Thus in our work, we incorporate differential strategies with DSTFC schemes. These aforementioned works utilize codeword matrices from orthogonal designs and are thus only capable of providing full code-rate for a maximum of two-relay cooperative networks. In contrast, in the context of multiple antenna systems, the STF coding scheme in [80] achieves full code-rate for any number of antennas by utilizing quasi-orthogonal codes. Similarly, the work in [78], in the context of cooperative multi-hop networks, achieves full code-rate for any number of relays. However, these schemes require CSI to recover the transmitted information. In order to cater for high data rate cooperative broadband multi-hop networks operating in scenarios where CSI cannot be acquired, we propose a differential distributed quasi-orthogonal space-time-frequency coding (DQSTFC) protocol. Our proposed scheme is able to achieve full code-rate for any number of relay nodes in high data rate cooperative broadband networks. We use the class of quasi-orthogonal codes with rotated constellations derived in [93] guaranteed to achieve full code-rate. Here, full code-rate means that our scheme achieves unitary code-rate as well as full symbol rate (one symbol per sub-carrier/time-slot use) when relay nodes forward information signals to the destination node.

In the proposed design, elements of the transmitted code matrix are simultaneously distributed in the temporal and frequency dimensions. This is to relax the assumption that the channel is quasi-static in the time and frequency domains for long symbol periods especially for networks with a large number of nodes. Our work is the first to focus on STF coding in non-coherent cooperative broadband networks utilizing quasi-orthogonal designs. We carefully provide a systematic construction of the code matrix and present the full differential procedure.The objectives of our new scheme are thus summarized as follows:

(1) Reduce performance degradation in highly selective channels by relaxing the quasi-static channel assumption.

(2) Optimize transmit code rate for cooperative networks with more than two relays by employing the rotated constellation quasi-orthogonal codes.

(3) Incorporate differential modulation to enable non-coherent signal recovery at the destination.

We first present our STF mapping scheme, we then show how the quasi-orthogonal codewords are constructed from a special choice of signal sets such that full code-rate signals are obtained. We then present the full differential encoding and decoding recipe for our differential DQSTFC scheme in cooperative networks with four relay nodes. Using simulation results, we study the performance of our proposed scheme under different fading conditions.

The rest of the chapter is organized as follows: Section 6.2 discusses STF mapping, while the encoding and decoding procedure for differential DQSTFC is covered in Section 6.3. Section 6.4 presents some simulation results and Section 6.5 contains the conclusion.

6.2 Differential STF Mapping

6.2.1 System Model

The cooperative network consists of a source node, a destination node and P relay nodes as shown in Fig.6.1. Each node is equipped with a single antenna which is used for both transmission and reception. The nodes are subject to half duplex constraint such that they cannot transmit and receive simultaneously. First, we show how the STF mapping scheme is implemented, we then focus on our differential DQSTFC scheme where the antennas of the

cooperating nodes constructively generate the quasi-orthogonal codewords at the destination. We address the problem of differential encoding and decoding where neither the relay nodes nor the destination can acquire CSI. The design in this work adopts a two-block two-stage 'transmit-and-cooperate' protocol. This implies that the protocol is made up of two blocks and each block is divided into two stages namely, the 'transmit' stage and the 'cooperate' stage. In the 'transmit' stage, the source node sends information to the relay nodes, while in the 'cooperate' stage, the source node keeps silent and the cooperating relay nodes simply forward the information signals to the destination without decoding.

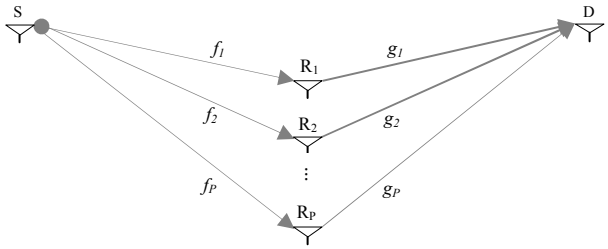

Fig.6.1 P-relay cooperative network

A STF codeword contains $P \times T \times N$ complex-valued information symbols. This implies that the source node and P relay nodes are assigned N frequency sub-carriers and T OFDM time slots. At the source node, a sequence of input information bits is used to generate a stream of symbols from an $MPSK$ constellation, M is the constellation size. The input symbols are simultaneously distributed across $t = 0,1, \dots, T-1$ OFDM time slots and $n = 0,1, \dots, N-1$ frequency sub-carriers. In the temporal dimension, the T OFDM time slots are grouped into $K = \lfloor T/T_C \rfloor$ blocks of ST codewords. Similarly, in the frequency dimension, the N sub-carriers are grouped into $K = \lfloor N/N_C \rfloor$ blocks of SF codewords. Such that each k_{th} block, $k = 1,2, \dots, K$ is made up of $\Gamma = T_C N_C$ elements, where T_C and N_C denote the number of time slots and frequency sub-carriers respectively per block. We now define the time-slot index vector as $\boldsymbol{t} = \left[\boldsymbol{t}_0{}^T, \boldsymbol{t}_1{}^T, \dots, \boldsymbol{t}_K{}^T, \boldsymbol{0}_{T-KT_C}\right]^T$, $\boldsymbol{t}_k = \left[t_0, \dots, t_{T_C-1}\right]$ where $T - KT_C$ zeros are

padded into T if T is not an integer multiple of T_C. Similarly, we define the sub-carrier index vector as $\boldsymbol{n} = \left[\boldsymbol{n}_0{}^T, \boldsymbol{n}_1{}^T, \dots, \boldsymbol{n}_K{}^T, \boldsymbol{0}_{N-KN_C}\right]^T$, $\boldsymbol{n}_k = \left[n_0, \dots, n_{T_C-1}\right]$ where $N - KN_C$ zeros are padded into N if N is not an integer multiple of N_C.

The channel at the t_{th} OFDM time slot between the source node and the p_{th} relay node is described by the impulse response vector $\boldsymbol{f}_{p,t} = \left[f_{p,t}(0), \dots, f_{p,t}(L_{SR} - 1)\right]^T$. Similarly, the channel at the t_{th} OFDM time slot between the p_{th} relay node and the destination is described by the impulse response vector $\boldsymbol{g}_{p,t} = \left[g_{p,t}(0), \dots, g_{p,t}(L_{RD} - 1)\right]^T$, where L_{SR} and L_{RD} denote the number of independent channel taps on the source-relay link and relay-destination link respectively. In order to achieve a diversity of order $P\Gamma$ we set $\Gamma \leq L\tau \ll NT$ where $L = min\{L_{SR}, L_{RD}\}$, and $\tau = min\{\tau_{SR}, \tau_{RD}\}$, τ_{SR} and τ_{RD} denote the coherence time of the channel on the source-relay and relay-destination links respectively, this is equivalent to setting $\Gamma \leq T_C N_C \ll NT$.

6.2.2 STF Mapping

The data vector generated by the source node in the k_{th} block is designed to achieve a diversity of order Γ at each relay node. In order to implement the STF mapping scheme, in the k_{th} block, the input symbols are transmitted in the temporal dimension across T_C adjacent time slots and in the frequency dimension across N_C adjacent sub-carriers. From this we obtain the source node data

$$\boldsymbol{x} = [\boldsymbol{x}_1^T, \boldsymbol{x}_2^T, \dots, \boldsymbol{x}_K^T, \boldsymbol{0}_{TN-K\Gamma}^T]^T \tag{6.1}$$

where $\boldsymbol{x}_k = [xm(0)_k, \dots, xm(\Gamma)_k]^T \in \mathbb{C}^{\Gamma \times 1}$, $xm(i)_k$ denotes the m_{th} symbol transmitted in the i_{th} slot during the k_{th} block, $(TN - K\Gamma)$ zeros are padded into $\boldsymbol{x}$ if TN is not an integer multiple of Γ. The source node coded data can be viewed as a concatenation of information

symbols in the temporal and frequency dimensions. Assuming the system is perfectly synchronized in the time and frequency domains, the ST and SF codewords are combined such that at the n_{th} sub-carrier of the k_{th} block within the t_{th} OFDM time-slot a STF data vector:

$$\boldsymbol{x}_{k,1} = [x1(t_0, n_0)_k, x2(t_1, n_0)_k, x3(t_0, n_1)_k, x4(t_1, n_1)_k]^T$$

$$= [xm(0)_k, \dots, xm(\Gamma)_k]^T \quad (6.2)$$

where $xm(t, n)_k$ is the m_{th} symbol transmitted at the n_{th} sub-carrier of the k_{th} block within the t_{th} OFDM time-slot. For a cooperative network with $P = 4, \Gamma = 4$ we observe that $m = 1,2, \dots ,4$ information symbols are applied over two successive time-slots and two successive frequency sub-carriers. Thus, in contrast with the schemes of [53][64][77][86] where the quasi-static channel assumption is adopted for the entire length of the information symbols, our scheme relaxes the quasi-static channel assumption to only two adjacent time-slots and frequency sub-carriers.

In order to recover information symbols at the destination without CSI, two consecutive quasi-orthogonal signal matrices $\boldsymbol{X}_k$ and $\boldsymbol{X}_{k+1}$ must be received at the destination in the k_{th} block and $(k+1)_{th}$ block respectively. The first signal matrix $\boldsymbol{X}_k$ is termed the 'reference' quasi-orthogonal matrix because it is only required for differential decoding and thus contains no valid data, while the subsequent quasi-orthogonal signal matrix $\boldsymbol{X}_{k+1}$ conveys the valid data. Let $\boldsymbol{X}_k$ denote the $\Gamma \times P$ reference quasi-orthogonal matrix given by $\boldsymbol{X}_k = [\boldsymbol{x}_{k,1}, \dots, \boldsymbol{x}_{k,P}] \in \mathbb{C}^{\Gamma \times P}, \boldsymbol{x}_{k,p} = [xm(0)_k, \dots, xm(\Gamma)_k]^T$. This implies that $\boldsymbol{x}_{k,P}$ is the p_{th} column of $\boldsymbol{X}_k$.

Next, we show how the source node and P relay nodes construct $\boldsymbol{X}_k$ at the destination. In the transmit stage of the k_{th} block, the source node transmits $\sqrt{E_S\Gamma}\boldsymbol{x}_{k,1}$ where E_S is the source node transmit power. After CP removal and FFT demodulation, the signal received at the n_{th} sub-carrier of the p_{th} relay in the k_{th} block during the t_{th} OFDM time slot is given by:

$$\boldsymbol{r}_p(i)_k = \sqrt{E_S\Gamma}\boldsymbol{x}_{k,1} \odot \boldsymbol{f}_p(i)_k + \boldsymbol{n}_p(i)_k \tag{6.3}$$

$$\boldsymbol{f}_p(i)_k = \left[f_p(t_0,n_0)_k, f_p(t_1,n_0)_k, f_p(t_0,n_1)_k, f_p(t_1,n_1)_k\right]^T$$

$$= \left[f_p(0)_k, \dots, f_p(\Gamma)_k\right]^T \tag{6.4}$$

where $f_p(t,n)_k$ is the channel gain between the source node and the p_{th} relay node at the n_{th} sub-carrier during the t_{th} time-slot, and $\boldsymbol{n}_p(i)_k$ is the corresponding noise. The multipath fading channel $f_p(t,n)_k$ between the source node and the p_{th} relay node is modelled as $f_p(t,n)_k = \sum_{l=0}^{L_{SR}-1} f_{p,t}(l)e^{-j2\pi ln/N} = \boldsymbol{f}_{p,t}\boldsymbol{\omega}$. The complex amplitudes $f_{p,t}(l)$ are assumed to be independent zero-mean complex Gaussian random variables with variances $E\left(\left|f_{p,t}(l)\right|^2\right) = \sigma_{SR}^2(l)$, and $\boldsymbol{\omega} = \left[1, e^{-j2\pi n/N}, \dots, e^{-j2\pi Ln/N}\right]^T$. The channels are normalized such that $\sum_{l=0}^{L_{SR}-1}\sigma_{SR}^2(l) = 1$. The received signal at the p_{th} relay node can be written in vector form as

$$\boldsymbol{r}_p(i)_k = \left[r_p(t_0,n_0)_k, r_p(t_1,n_0)_k, r_p(t_0,n_1)_k, r_p(t_1,n_1)_k\right]^T$$

$$= \left[r_p(0)_k, \dots, r_p(\Gamma)_k\right]^T \tag{6.5}$$

where $r_p(t,n)_k$ denotes the received signal at the n_{th} sub-carrier during the t_{th} time-slot. The P relay nodes apply the STF mapping scheme as implemented by the source node. Specifically, the P relay nodes map their received symbols across adjacent OFDM time-slots

and frequency sub-carriers. The relay nodes process their signals by applying amplification co-efficient $\mu = \sqrt{E_p/E_S + 1}$, E_p denotes the power allocated to each relay node. The relay nodes also multiply their signals by a 'relay matrix' $\boldsymbol{M}_p$. The 'relay matrix' as explained in Section 5.2.3, ensures that the signal generated at the destination has a quasi-orthogonal structure. An example of the mapping of information symbols to OFDM time-slots and frequency subcarriers for a cooperative network with $P = 4$ relay nodes is illustrated in Fig.6.2. Thus, in the k_{th} block, the p_{th} relay node receives $\boldsymbol{r}_p(i)_k \in \mathbb{C}^{\Gamma \times 1}$ in (6.3) and transmits

$$\boldsymbol{t}_1(i)_k = [t1(t_0, n_0)_k, t2(t_1, n_0)_k, t3(t_0, n_1)_k, t4(t_1, n_1)_k]^T$$

$$\boldsymbol{t}_2(i)_k = [-t2^*(t_0, n_0)_k, t1^*(t_1, n_0)_k, -t4^*(t_0, n_1)_k, t3^*(t_1, n_1)_k]^T$$

$$\boldsymbol{t}_3(i)_k = [-t3^*(t_0, n_0)_k, -t4^*(t_1, n_0)_k, t1^*(t_0, n_1)_k, t2^*(t_1, n_1)_k]^T$$

$$\boldsymbol{t}_4(i)_k = [t4(t_0, n_0)_k, -t3(t_1, n_0)_k, -t2(t_0, n_1)_k, t1(t_1, n_1)_k]^T \quad (6.6)$$

Specifically, the p_{th} relay node transmits

$$\boldsymbol{t}_p(i)_k = \mu \boldsymbol{M}_p \boldsymbol{r}_p(i)_k\,, \quad i = 1,2,\ldots,\Gamma \quad (6.7)$$

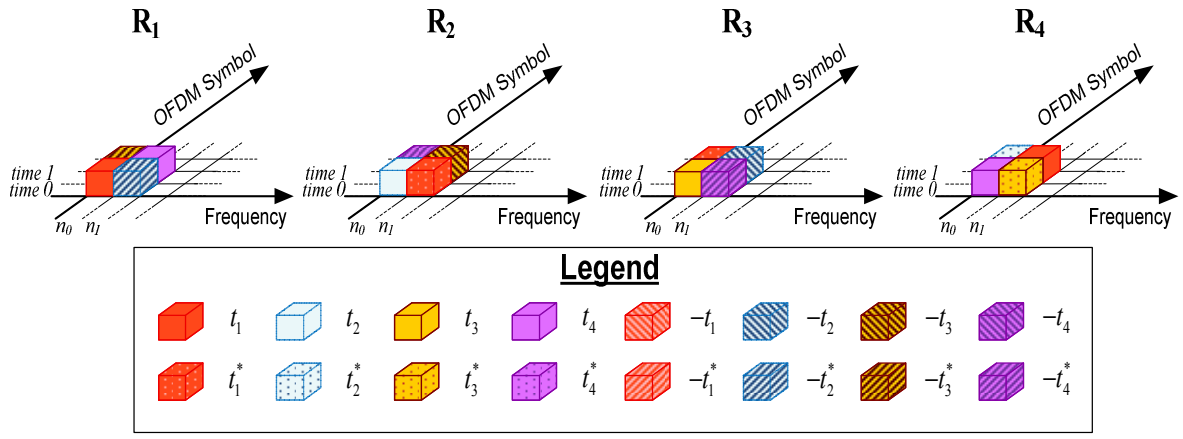

Fig.6.2 STF mapping in four-relay networks

Assuming the relay nodes are synchronized at symbol level such that the nodes can transmit simultaneously, the signal received at the n_{th} sub-carrier of the destination in the k_{th}block during the t_{th} OFDM time slot (after CP removal and FFT demodulation) is given by:

$$\boldsymbol{y}(i)_k = \sum_{p=1}^{P} \boldsymbol{t}_p(i)_k \odot \boldsymbol{g}_p(i)_k + \boldsymbol{z}(i)_k \tag{6.8}$$

$$\boldsymbol{g}_p(i)_k = \left[g_p(t_0, n_0)_k, g_p(t_1, n_0)_k, g_p(t_0, n_1)_k, g_p(t_1, n_1)_k\right]^T$$

$$= \left[g_p(0)_k, \dots, g_p(\Gamma)_k\right]^T \tag{6.9}$$

where $g_p(t,n)_k$ is the channel gain between the p_{th} relay node and the destination at the n_{th} sub-carrier during the t_{th} time-slot, and $\boldsymbol{z}(i)_k$ is the noise. The multipath fading channel $g_p(t,n)_k$ between the p_{th} relay node and the destination is modelled as $g_p(t,n)_k = \sum_{l=0}^{L_{RD}-1} g_{p,t}(l)e^{-j2\pi ln/N} = \boldsymbol{g}_{p,t}\boldsymbol{\omega}$. The complex amplitudes $g_{p,t}(l)$ are assumed to be independent zero-mean complex Gaussian random variables with variances $E\left(\left|g_{p,t}(l)\right|^2\right) = \sigma_{RD}^2(l)$. The channels are normalized such that $\sum_{l=0}^{L_{RD}-1} \sigma_{RD}^2(l) = 1$. Substituting for $\boldsymbol{t}_p(i)_k$ and then $\boldsymbol{r}_p(i)_k$ in (6.7) and (6.3) respectively, (6.8) becomes

$$\boldsymbol{y}(i)_k = \sum_{p=1}^{P} \sqrt{\frac{E_C E_S N_C}{E_S+1}} \boldsymbol{M}_p \boldsymbol{x}_{k,1} \odot \left(\boldsymbol{f}_p(i)_k \odot \boldsymbol{g}_p(i)_k\right) + \tilde{\boldsymbol{z}}(i)_k \tag{6.10}$$

where $\tilde{\boldsymbol{z}}(i)_k = \sum_{p=1}^{P} \mu \boldsymbol{M}_p \boldsymbol{g}_p(i)_k \odot \boldsymbol{n}_p(i)_k + \boldsymbol{z}(i)_k$ is the equivalent noise. The signal received at the destination in the k_{th} block can be written in compact form as:

$$\boldsymbol{Y}_k = \sqrt{\rho}\boldsymbol{X}_k\boldsymbol{H}_k + \boldsymbol{Z}_k \tag{6.11}$$

where $\boldsymbol{Y}_k = [\boldsymbol{y}(1)_k, \dots, \boldsymbol{y}(\Gamma)_k]^T \in \mathbb{C}^{\Gamma\times\Gamma}$, $\boldsymbol{y}(i)_k = [y(1)_k, \dots, y(\Gamma)_k]^T$, $\rho = \frac{E_p E_S \Gamma}{E_S+1}\boldsymbol{X}_k =$

$\left[\boldsymbol{M}_1\boldsymbol{x}_{k,1}, \dots, \boldsymbol{M}_P\boldsymbol{x}_{k,1}\right] \in \mathbb{C}^{\Gamma\times P}$, $\boldsymbol{H}_k = [\boldsymbol{h}(1)_k, \dots, \boldsymbol{h}(\Gamma)_k] \in \mathbb{C}^{P\times\Gamma}$, $\boldsymbol{h}(i)_k = [h_1(i)_k, \dots, h_P(i)_k]^T$

and $\boldsymbol{Z}_k = [\tilde{\boldsymbol{z}}(1)_k, \ldots, \tilde{\boldsymbol{z}}(\Gamma)_k]^T \in \mathbb{C}^{\Gamma \times \Gamma}$, the channel co-efficients $h_p(i)_k = f_p(i)_k \cdot g_p(i)_k$. The $P \times \Gamma$ quasi-orthogonal channel matrix $\boldsymbol{H}_k$ captures the channel co-efficients between the source node, the P relay nodes, and the destination. Here we assume that the channel co-efficient between the source node, the P relay nodes, and the destination remain quasi-static, at least, across T_C adjacent OFDM time slots and N_C adjacent frequency sub-carriers. This equivalently means that the channel is constant during the transmission of Γ symbols, that is, $\boldsymbol{h}(i)_k$ is constant for $i = 1,2, \ldots, \Gamma$.

6.3 Differential DQSTFC Encoding and Decoding

6.3.1 Differential DQSTFC Encoding

In this section, we show how full rate quasi-orthogonal codewords are constructed in the proposed differential DQSTFC scheme. Differential encoding is initiated at the source node. Recalling that $\boldsymbol{x}_{k,1} = [xm(0)_k, \ldots, xm(\Gamma)_k]^T$ is the source node data generated in the k_{th} block, the next step is for the source node to generate thedata vector $\boldsymbol{x}_{k+1,1}$ for the $(k+1)_{th}$ block. This involves the following processes:

First, the constellation mapping sub-system generates the information symbols $\boldsymbol{v}_{k+1,1} = [vm(0)_{k+1}, \ldots, vm(\Gamma)_{k+1}]^T$ where $\boldsymbol{v}_{k+1,1}$ represents the valid transmitted information symbols that must be recovered at the destination without CSI. We now show how the elements of $\boldsymbol{v}_{k+1,1}$ are computed at the source node from a proper choice of signal sets so that a full rate quasi-orthogonal codeword is generated. The elements of $\boldsymbol{v}_{k+1,1}$ are modulated symbols drawn from an $m = log_2 M$ M-PSK constellation, m is the spectral efficiency. Let $\Phi = diag\left[1, e^{j\theta_2}, \ldots, e^{j\theta_{\Gamma/2}}\right]$, the symbols are constructed as $\Phi \cdot [v1(i)_k, v3(i)_k]^T$ and $\Phi \cdot [v2(i)_{k+1}, v4(i)_{k+1}]^T$. This implies that, $[v1(i)_{k+1}, v2(i)_{k+1}]$ are mapped onto a signal

constellation $\mathcal{A}$ of size 2^m, while$[v3(i)_{k+1}, v4(i)_{k+1}]$ are mapped onto a signal constellation $\mathcal{A}_r$ which is a rotated version of $\mathcal{A}$. The rotation angles θ of the information symbols ensure that the codes achieve full diversity.

The next step is for the differential encoder to generate the data vector $\boldsymbol{x}_{k+1,1}$ for the $(k+1)_{th}$ block. We assume that the source node has prior knowledge of the relay matrices $\{\boldsymbol{M}_1, \dots, \boldsymbol{M}_P\}$, since the source node already knows $\boldsymbol{x}_{k,1}$, it can easily construct $\boldsymbol{X}_k = [\boldsymbol{M}_1\boldsymbol{x}_{k,1}, \dots, \boldsymbol{M}_P\boldsymbol{x}_{k,1}]$. Thus the data vector generated in the $(k+1)_{th}$ block is obtained as:

$$\boldsymbol{x}_{k+1,1} = \boldsymbol{X}_k\boldsymbol{v}_{k+1,1} \tag{6.12}$$

where $\boldsymbol{x}_{k+1,1} = [xm(0)_{k+1}, \dots, xm(\Gamma)_k]^T$ and $\boldsymbol{X}_k = [\boldsymbol{x}_{k,1}, \dots, \boldsymbol{x}_{k,P}]$ is the reference quasi-orthogonal signal matrix generated by the P relay nodes in the k_{th} block. The quasi-orthogonal structure of $\boldsymbol{v}_{k+1,1}$ guarantees that $\boldsymbol{x}_{k+1,1}$ is quasi-orthogonal. The source node generates the differentially modulated, STF encoded, cyclically shifted complex symbol vector $\boldsymbol{x}_{k+1,1}$ whose elements are transmitted across the n_{th} sub-carrier in the $(k+1)_{th}$ block during the t_{th} time slot. In order to construct $\boldsymbol{X}_{k+1} = [\boldsymbol{x}_{k+1,1}, \dots, \boldsymbol{x}_{k+1,P}]$ at the destination, the source node and P relay nodes follow the same process as in the k_{th} block. The signal received at the n_{th} sub-carrier of the p_{th} relay node during the t_{th} time slot is of the form of (6.3). Similar to the case of the k_{th} block, the relay node data is constructed and transmitted as discussed in Section II A. The received signal at the destination in the $(k+1)_{th}$ block is similar to (6.11) and can be written in compact form as:

$$\boldsymbol{Y}_{k+1} = \sqrt{\rho}\boldsymbol{X}_{k+1}\boldsymbol{H}_{k+1} + \boldsymbol{Z}_{k+1} \tag{6.13}$$

6.3.2 Differential DQSTFC Decoding

Two consecutive blocks of quasi-orthogonal matrices $\boldsymbol{X}_k$ and $\boldsymbol{X}_{k+1}$ have now been generated at the destination by P relay nodes based on (6.11) and (6.13). We can write

$$\boldsymbol{y}(i)_k = \boldsymbol{X}_k \boldsymbol{h}(i)_k + \tilde{\boldsymbol{z}}(i)_k = \left[\boldsymbol{x}_{k,p}\boldsymbol{H}_k + \tilde{\boldsymbol{z}}(i)_k\right]^T,\ i = 1,2,\dots,\Gamma\ \ p = 1,2,\dots,P \tag{6.14}$$

$$\boldsymbol{y}(i)_{k+1} = \boldsymbol{X}_{k+1} \boldsymbol{h}(i)_{k+1} + \tilde{\boldsymbol{z}}(i)_{k+1} = \left[\boldsymbol{x}_{k+1,p}\boldsymbol{H}_{k+1} + \tilde{\boldsymbol{z}}(i)_{k+1}\right]^T, i = 1,2,\dots,\Gamma\ \ p = 1,2,\dots,P \tag{6.15}$$

Note that we intentionally omit the power term $\sqrt{\rho}$ for ease of explanation. Using the signals received in (6.14) and (6.15) in the k_{th} block and $(k+1)_{th}$ block respectively, $\boldsymbol{v}_{k+1,1} = [vm(0)_{k+1}, \dots, vm(\Gamma)_{k+1}]$ can be recovered pairwisely at the destination without CSI. For example, for a cooperative network with $P = 4$ relay nodes and $\Gamma = 4$, in order to recover $\boldsymbol{v}_{k+1,1}$ we first obtain the quasi-orthogonal signal and channel matrices for two consecutive transmission blocks as follows:

$$\boldsymbol{X}_j = \begin{bmatrix} x1(t_0,n_0)_j & x2(t_0,n_0)_j) & x3(t_0,n_0)_j & x4(t_0,n_0)_j \\ -x2^*(t_1,n_0)_j & x1^*(t_1,n_0)_j & -x4^*(t_1,n_0)_j & x3^*(t_1,n_0)_j \\ -x3^*(t_0,n_1)_j & -x4^*(t_0,n_1)_j & x1^*(t_0,n_1)_j & x2^*(t_0,n_1)_j \\ x4(t_1,n_1)_j & x3(t_1,n_1)_j & -x2(t_1,n_1)_j & x1(t_1,n_1)_j \end{bmatrix}$$

$$\boldsymbol{H}_j = \begin{bmatrix} h_1(t_0,n_0)_j & h_2{}^*(t_1,n_0)_j & h_3{}^*(t_0,n_1)_j & h_4(t_1,n_1)_j \\ h_2(t_0,n_0)_j & -h_1{}^*(t_1,n_0)_j & h_4{}^*(t_0,n_1)_j & -h_3(t_1,n_1)_j \\ h_3(t_0,n_0)_j & h_4{}^*(t_1,n_0)_j & -h_1{}^*(t_0,n_1)_j & -h_2(t_1,n_1)_j \\ h_4(t_0,n_0)_j & -h_3{}^*(t_1,n_0)_j & -h_2{}^*(t_0,n_1)_j & h_1(t_1,n_1)_j \end{bmatrix}$$

where $\boldsymbol{X}_j \in \mathbb{C}^{\Gamma \times P}$ and $\boldsymbol{H}_j \in \mathbb{C}^{P \times \Gamma}$, $j \in \{k, k+1\}$ are quasi-orthogonal signal and channel matrices respectively. The i_{th} information signal transmitted by the source node, through the p_{th} relay node on the n_{th} sub-carrier during the t_{th} OFDM time slot is denoted by $xm(t,n)_j$, and $h_p(t,n)_j$ captures the channel co-efficient between the source node, the

p_{th} relay node, and the destination, on the n_{th} sub-carrier during the t_{th} OFDM time slot. Since we assume that the channel co-efficients remain constant across T_C adjacent OFDM time slots and N_C adjacent frequency sub-carriers, then $h_p(t,n)_j$ is constant for t_0 and t_1, and n_0 and n_1. Similarly, since all the cooperating relay nodes transmit the same information signals in every block then $xm(t,n)_j$ is constant for t_0 and t_1, and n_0 and n_1. Thus we can imply that $h_p(t_0,n_0)_j =, \dots, = h_p(t_1,n_1)_j = h_{p,j}$ and $xm(t_0,n_0)_j =, \dots, = xm(t_1,n_1)_j = xm_j$. Based on this, we can compute

$$\boldsymbol{X}_j\boldsymbol{X}_j{}^H = \begin{bmatrix} X_1 & 0 & 0 & X_2 \\ 0 & X_1 & -X_2 & 0 \\ 0 & -X_2 & X_1 & 0 \\ X_2 & 0 & 0 & X_1 \end{bmatrix} \quad \boldsymbol{H}_j\boldsymbol{H}_j{}^H = \begin{bmatrix} H_1 & 0 & 0 & H_2 \\ 0 & H_1 & -H_2 & 0 \\ 0 & -H_2 & H_1 & 0 \\ H_2 & 0 & 0 & H_1 \end{bmatrix}$$

where $X_1 = \sum_{m=1}^{4}\left|xm_j\right|^2$ is the signal power and $X_2 = 2Re\left(x1_j x4_j{}^* - x2_j x3_j{}^*\right)$ is a self-interference parameter. Similarly, $H_1 = \sum_{p=1}^{4}\left|h_{p,j}\right|^2$ is the channel power and $H_2 = 2Re\left\{h_{1,j}h_{4,j}{}^* - h_{2,j}h_{3,j}{}^*\right\}$ is a self-interference parameter. The elements of $\boldsymbol{v}_{k+1,1}$ are then recovered as follows:

$$\boldsymbol{y}(1)_{k+1}\boldsymbol{y}(1)_k{}^H = \boldsymbol{x}_{k+1,1}\boldsymbol{X}_k{}^H\boldsymbol{H}_{k+1}\boldsymbol{h}(1)_k{}^H + Z_1$$

$$= \boldsymbol{v}_{k+1,1}\boldsymbol{X}_k\boldsymbol{X}_k{}^H\boldsymbol{H}_{k+1}\boldsymbol{h}(1)_k{}^H + Z_1$$

$$= v1(i)_{k+1}(X_1H_1 + X_2H_2) + v4(i)_{k+1}(X_1H_2 + X_2H_1) + Z_1$$

$$= v1(i)_{k+1}A + v4(i)_{k+1}B + Z_1 \qquad (6.16)$$

Similarly,

$$\boldsymbol{y}(1)_{k+1}\boldsymbol{y}(2)_k{}^H = \boldsymbol{x}_{k+1,1}\boldsymbol{X}_k{}^H\boldsymbol{H}_{k+1}\boldsymbol{h}(2)_k{}^H + Z_2$$

$$= \boldsymbol{v}_{k+1,1}\boldsymbol{X}_k\boldsymbol{X}_k{}^H\boldsymbol{H}_{k+1}\boldsymbol{h}(2)_k{}^H + Z_2$$

$$= v2(i)_{k+1}A - v3(i)_{k+1}B + Z_2 \tag{6.17}$$

$$\boldsymbol{y}(1)_{k+1}\boldsymbol{y}(3)_k{}^H = \boldsymbol{x}_{k+1,1}\boldsymbol{X}_k{}^H\boldsymbol{H}_{k+1}\boldsymbol{h}(3)_k{}^H + Z_3$$

$$= \boldsymbol{v}_{k+1,1}\boldsymbol{X}_k\boldsymbol{X}_k{}^H\boldsymbol{H}_{k+1}\boldsymbol{h}(3)_k{}^H + Z_3$$

$$= -v2(i)_{k+1}B + v3(i)_{k+1}A + Z_3 \tag{6.18}$$

$$\boldsymbol{y}(1)_{k+1}\boldsymbol{y}(4)_k{}^H = \boldsymbol{x}_{k+1,1}\boldsymbol{X}_k{}^H\boldsymbol{H}_{k+1}\boldsymbol{h}(4)_k{}^H + Z_4$$

$$= \boldsymbol{v}_{k+1,1}\boldsymbol{X}_k\boldsymbol{X}_k{}^H\boldsymbol{H}_{k+1}\boldsymbol{h}(4)_k{}^H + Z_4$$

$$= v1(i)_{k+1}B + v4(i)_{k+1}A + Z_4 \tag{6.19}$$

where Z_n captures the noise, $A = X_1H_1 + X_2H_2$ and $B = X_1H_2 + X_2H_1$, we refer to A and B as the differential decoding parameters required to recover $\boldsymbol{v}_{k+1,1}$. The differential decoding parameters are computed at the destination as:

$$\boldsymbol{y}(1)_k\boldsymbol{y}(4)_k{}^H = \boldsymbol{X}_k\boldsymbol{X}_k{}^H\boldsymbol{h}(1)_k\boldsymbol{h}(4)_k{}^H + \tilde{Z}_4 = A + \tilde{Z}_4$$

$$\boldsymbol{y}(1)_k\boldsymbol{y}(1)_k{}^H = \boldsymbol{X}_k\boldsymbol{X}_k{}^H\boldsymbol{h}(1)_k\boldsymbol{h}(1)_k{}^H + \tilde{Z}_1 = B + \tilde{Z}_1 \tag{6.20}$$

This implies that $\boldsymbol{y}(1)_k\boldsymbol{y}(4)_k{}^H \approx A$ and $\boldsymbol{y}(1)_k\boldsymbol{y}(1)_k{}^H \approx B$ since $Z_n \approx \tilde{Z}_n$. It is thus obvious from (6.20) that the scheme does not require CSI to recover $\boldsymbol{v}_{k+1,1}$. The non-coherent recovery of $\boldsymbol{v}_{k+1,1}$ rather depends on consecutively received signals in the k_{th} block and $(k+1)_{th}$ block under the constraint that $\boldsymbol{H}_k \cong \boldsymbol{H}_{k+1}$. Once A and B are computed at the destination using (6.20), the information signals in (6.16) to (6.19) can be recovered pairwisely.

Obviously, all the decision signals are only a function of a pair of input signals which exist with dissimilar constellation angles. This offers the possibility of decoding in pairs. We can decide for each pair of recovered symbols independently using a pairwise least square decoder as follows:

$$(\tilde{v}1(i)_{k+1}, \tilde{v}4(i)_{k+1}) = \arg\min \left[\left| \boldsymbol{y}(1)_{k+1} \boldsymbol{y}(1)_k^{\,H} - (v1(i)_{k+1} A + v4(i)_{k+1} B) \right|^2 + \left| \boldsymbol{y}(1)_{k+1} \boldsymbol{y}(4)_k^{\,H} - (v1(i)_{k+1} B + v4(i)_{k+1} A) \right|^2 \right] \quad (6.21)$$

$$(\tilde{v}2(i)_{k+1}, \tilde{v}3(i)_{k+1}) = \arg\min \left[\left| \boldsymbol{y}(1)_{k+1} \boldsymbol{y}(2)_k^{\,H} - (v2(i)_{k+1} A - v3(i)_{k+1} B) \right|^2 + \left| \boldsymbol{y}(1)_{k+1} \boldsymbol{y}(3)_k^{\,H} - (v3(i)_{k+1} A - v2(i)_{k+1} B) \right|^2 \right] \quad (6.22)$$

The pairwise least square decoder performs an exhaustive search over all possible combination of constellation points to determine the pair of signals that minimize the terms in (6.21) and (6.22). This decoding is based on the pairwise least square decision metric of [93], and is equivalent to finding the minimum Euclidean distance between the noisy received signals and the known constellation points.The resultant symbols in (6.21) and (6.22) can be interpreted as noisy versions of the scaled transmitted symbols. The scaling A and B, however have a negligible effect on the geometry of the detection region. The complexity of this process is equivalent to $2^{m\Gamma+1}$ since this is the number of constellation points to be examined.

6.4 Simulation Results

In this section, we present simulation results to demonstrate the BER performance of our proposed differential DQSTFC scheme. The settings for our cooperative broadband network, where $P = 4$ and $\Gamma = 4$, are based on the specifications described in the IEEE802.16e Mobile

WiMax standard, the number of sub-carriers $N = 256$ with a channel bandwidth of 2MHz. The OFDM symbol duration is $T = 128\mu s$ while the length of the CP is $1/4$ of the symbol duration i.e. $32\mu s$. We assume a typical urban macro-cellular mobile radio environment with multi-ray channels where delay spreads are mostly within the range of $100\eta s$ to $10\mu s$. We analyse the performance of our proposed scheme in frequency-selective and time-selective channels. Specifically we set our simulation parameters for different Doppler frequencies f_D ranging from 40Hz to 200Hz and different root mean square delay spreads τ_{rms} between $0.1\mu s$ and $4\mu s$, the Doppler frequencies correspond to mobile speeds between 22km/h and 108km/h. We assume that neither the relay nodes nor destination can acquire CSI, while the channel gain of the source-relay and relay-destination links remain approximately constant within two consecutive blocks. For the quasi-orthogonal codes, the rotation angles are set to θ/M, where M is the constellation size.

For different channel conditions, the performance of our proposed differential DQSTFC scheme is compared with the differential quasi-orthogonal DSTC-OFDM and DSFC schemes (whose parameters are simulated in our environment). We study the effects of Doppler spread and delay spread on the aforementioned coding schemes using different simulation parameters. We first set τ_{rms} to a low value of $0.1\mu s$ such that the effect of delay spread is negligible. To study the influence of Doppler spread, we investigate BER performance at different Doppler frequencies. The SNR is fixed at 12dB, the symbols are chosen from a QPSK constellation, and all the coding schemes have the same transmission rate of 2 bits/s/Hz. From Fig. 6.3 we observe that for values of f_D between 78Hz and 135Hz the BER performance of our proposed differential DQSTFC scheme is better than that of the differential quasi-orthogonal DSTC-OFDM and DSFC schemes. This is because at such values of f_D the coherence time t_c and coherence bandwidth b_c of the channel are large

enough to satisfy the requirements of constant channel gain across adjacent time slots and adjacent subcarriers. The BER performance of DSTC-OFDM is better than that of our proposed scheme only at values of f_D below 78Hz. At such values of f_D the coherence time is large and $t_c \geq \Gamma$ can be satisfied. Thus, DSTC-OFDM schemes which require constant channel gain in the temporal dimension for the entire duration of $\Gamma = 4$ symbols, have the best BER performance. When the Doppler spread increases and f_D is between 78Hz and 135Hz, the coherence time reduces and $t_c \geq \Gamma$ can no longer be satisfied, however the coherence time is still large enough to satisfy $t_c \geq \Gamma/2$ thus the BER performance of DSTC-OFDM degrades beyond that of our proposed scheme. When the Doppler spread is severe and f_D is above 135Hz, coding in the temporal dimension introduces a significant amount of inter-symbol interference, thus, our proposed scheme and the DSTC-OFDM scheme experience performance degradation. However, the BER performance of the DSFC scheme is better in this situation because the delay spread is low and the coherence bandwidth is large enough to satisfy $b_c \geq \Gamma$. Thus, DSFC schemes which require constant channel gain in the frequency dimension for the entire duration of $\Gamma = 4$ symbols, has the best BER performance. In contrast with DSTC-OFDM and DSFC schemes where the requirements for constant channel gain must be satisfied for the entire duration of $\Gamma = 4$ symbols, our scheme only requires constant channel gain during the transmission of $\Gamma = 2$ symbols. Therefore, we can conclude that for cooperative networks operating in environments where CSI cannot be acquired, our proposed scheme is robust against a practical range of Doppler spread.

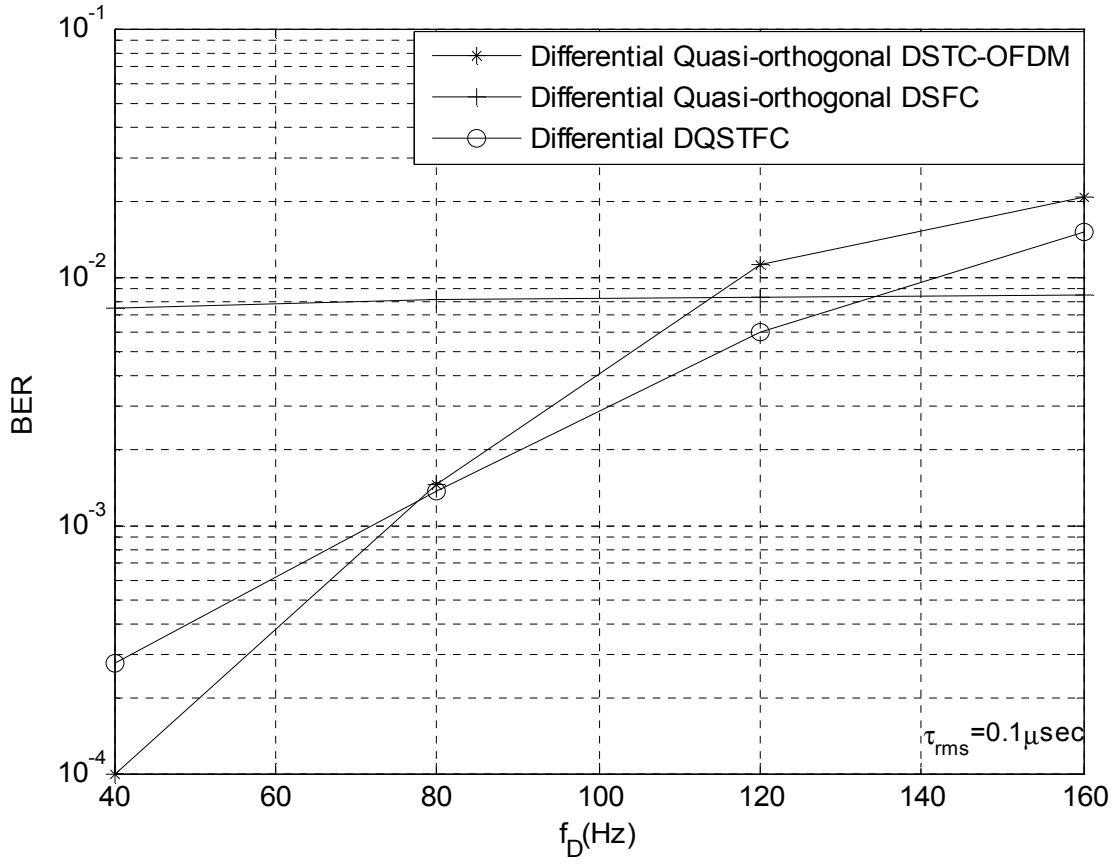

Fig.6.3 BER Performance in Frequency-selective Fading Channels

We then set f_D to a fixed value of 50Hz such that the influence of Doppler spread is low, and compare the performance of all the aforementioned coding schemes at different levels of delay spread. The SNR is fixed at 12dB and all the coding schemes have identical transmission rate of 2 bits/s/Hz. From Fig. 6.4 we observe that our proposed scheme outperforms the other coding schemes when the value of τ_{rms} is between $0.8\mu s$ and $3.2\mu s$. This is because at such values, the coherence time and coherence bandwidth of the channel is large enough to satisfy the requirements of constant channel gain across adjacent time slots and adjacent sub-carriers. When the delay spread is low and τ_{rms} is below $0.8\mu s$ the coherence bandwidth is large and $b_c \geq \Gamma$ can be satisfied. Thus DSFC schemes which require constant channel gain across Γ sub-carriers outperform the other coding schemes.

When the delay spread increases, the coherence bandwidth reduces and $b_c \geq \Gamma$ can no longer be satisfied, however $b_c \geq \Gamma/2$ can still be satisfied. Thus, our proposed scheme exhibits improved BER performance compared to the DSFC scheme. When τ_{rms} is higher than $3.2\mu s$, the coherence bandwidth is very low such that coding in the frequency dimension introduces inter-carrier interference, thus the BER performance of our proposed scheme and the DSFC scheme degrade significantly. In this condition however, DSTC-OFDM outperforms the other schemes.

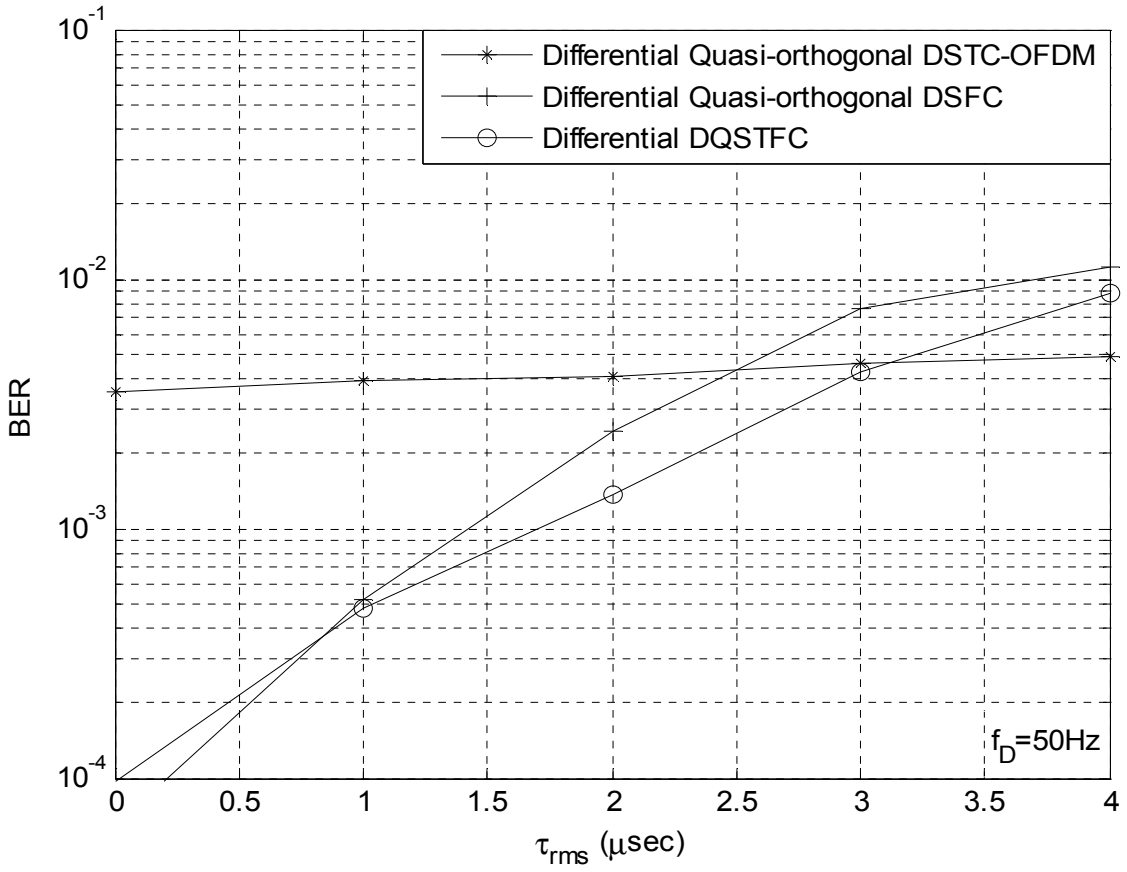

Fig.6.4 BER Performance in Time-selective Fading Channels

In Fig.6.5 we study the performance of our differential DQSTFC scheme at different values of Doppler frequency $f_D = \{80Hz, 100Hz\}$ and compare with the differential quasi-orthogonal DSTC-OFDM scheme. From Fig. 6.5, we observe that our scheme exhibits better

BER performance at each value of f_D. This occurs because at such values of f_D, the magnitude change of the channel becomes more uncorrelated across successive OFDM symbols, in other words, the channel becomes temporally-selective. Thus, under this condition, the requirement of constant channel gain across $\Gamma = 4$ OFDM symbols cannot be satisfied by the differential quasi-orthogonal DSTC-OFDM scheme. However, the requirement of constant channel gain which is relaxed across only $\Gamma = 2$ OFDM symbols for our differential DQSTFC scheme can still be satisfied.

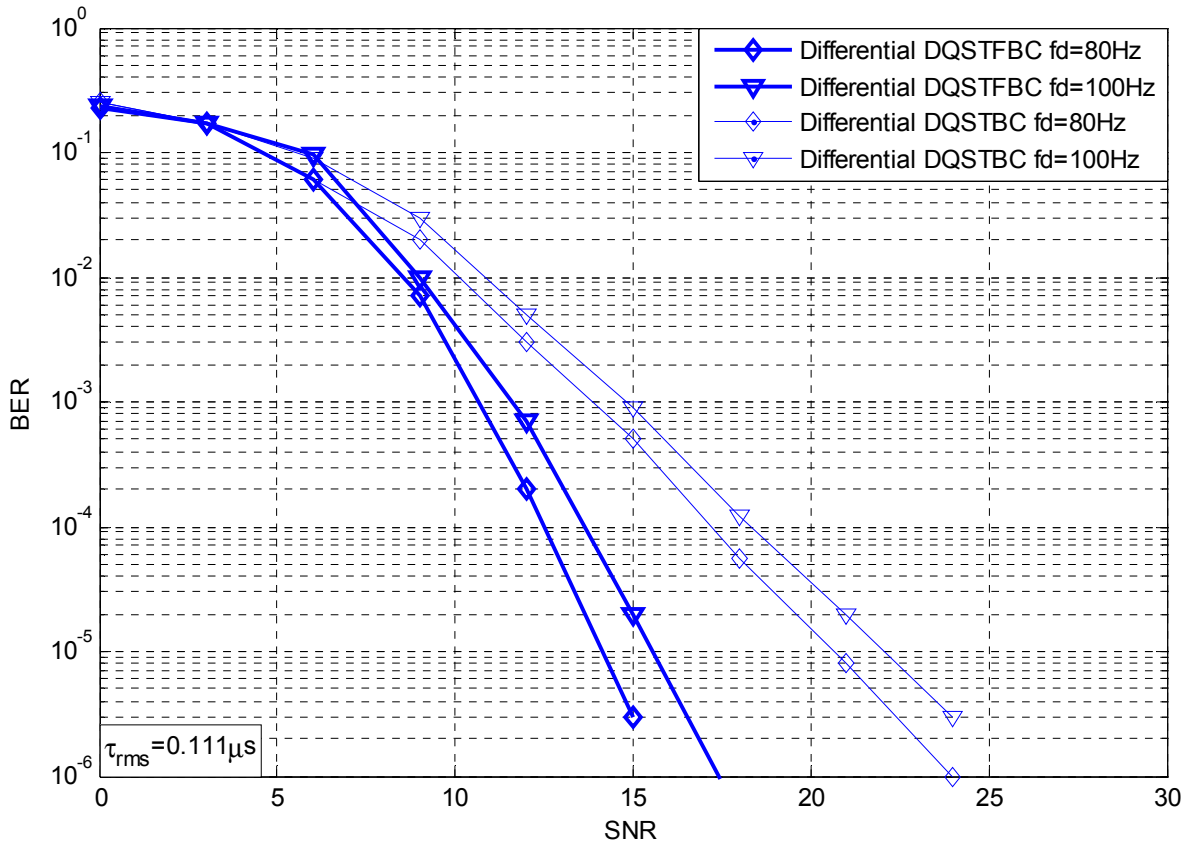

Fig.6.5 Diversity performance of proposed differential DQSTFC and DQSTC schemes

6.5 Summary

It has become necessary to develop a scheme that is capable of exploiting capacity gain in the spatial, temporal and frequency dimensions, while offering full code-rate and non-coherent signal recovery for cooperative broadband networks. In this work, we propose a differential DQSTFC scheme which is essentially a hybrid combination of STF mapping, full code-rate quasi-orthogonal codes, and differential strategies. From this, we obtain a scheme which is robust to frequency-selective fading and time-selective fading, and mitigates the code-rate deficiency exhibited by orthogonal codes in cooperative networks with more than two relay nodes. We introduce our STF mapping strategy, show how the full code-rate quasi-orthogonal codes are devised, and present the full differential encoding and decoding procedure for cooperative networks with four relay nodes. Our scheme relaxes the quasi-static channel assumption to adjacent OFDM time-slots and adjacent frequency sub-carriers. Using simulation results, we study the performance of our proposed scheme under different fading conditions.

7 Conclusion and Future Work

7.1 Conclusion

The recent rapid advancement in research, and design and manufacture of wireless systems has been largely instigated by the massive demand for wireless applications. Users of wireless applications now depend immensely on technologies that provide real-time high-data rate transmission and mobile broadband communication. If wireless technologies are to meet the requirements and expectations of users, then the principal design objective is; 'high quality of service'. One phenomenon that hinders the realization of high quality of service in wireless communications is fading. Fading occurs when the transmitted signal is affected by objects in the wireless environment thereby causing deficiency in the quality of the received signal.

Diversity techniques, namely frequency diversity, temporal diversity, and spatial diversity, have been popularly used to combat the detrimental effects of fading in wireless channels. Of all the diversity techniques, spatial diversity has gained the widest attention because of the simplicity of implementation and the feasibility of deployment. In spatial diversity; multiple antennas are deployed sufficiently far apart at the terminals to produce multiple independent fading paths for the transmitted information signals. Since it is unlikely that the multiple independent paths will experience identical fading events, thus spatial diversity is guaranteed. MIMO communication is a spatial diversity technique that has been successfully used in multiple-antenna systems to improve communication performance. To replicate such strategy in single-antenna systems like cellular networks and wireless sensor networks where size restrictions preclude the use of multiple antennas, cooperative communications was introduced. In cooperative networks, the single-antenna nodes that make up the network

cooperate to emulate MIMO systems. Cooperative diversity is achieved by making the single-antenna nodes form a virtual multiple-antenna system. STBC were introduced to MIMO systems to improve the reliability of data transmission and enhance diversity gain. As a result, research efforts have concentrated on designing DSTBC for cooperative systems as a counterpart of STBC in MIMO systems.

This thesis is devoted to the design and performance analysis of DSTBC schemes in cooperative networks. The concept of cooperative diversity is discussed and cooperative diversity protocols are introduced, the issue of fading in wireless channels is also reviewed. The concept of DSTBC in cooperative networks is then covered in a systematic way. The approach is to extend the design of STBC in MIMO systems to the single antenna nodes of cooperative networks. We first focus of designing unitary rate codes that exhibit improved diversity performance with relatively low complexity decoding, from this, we model DSTBC using orthogonal and quasi-orthogonal designs for cooperative networks. In our work we identify that most works on DSTBC assume that there is no direct link between the source node and the destination. Thus they ignore the benefits that can be extracted when the source node is actively involved in cooperation. To demonstrate these benefits we propose an SA strategy using orthogonal and quasi-orthogonal DSTBC. The SA strategy is shown to improve the diversity performance of the network at the expense of slightly increased complexity of the ML detector.

Orthogonal and Quasi-orthogonal designs are then extended to cooperative networks that incorporate multiple antennas at the destination terminal. This scenario agrees with wireless sensor networks and cellular networks where the access point and base station respectively can be fitted with multiple receive antennas. We show that by incorporating multiple

antennas on the destination terminal, the diversity performance of the network is further improved; we also show the performance of our SA strategy in such networks.

Next, we introduce the concept of differential modulation to cooperative networks where the nodes in the network are unable to acquire perfect CSI. In the practical sense, this scenario occurs in mobile environments where the fast fading nature of channels makes channel estimation difficult. The concept of differential encoding and decoding is first reviewed for non-cooperative networks. The performance of differential modulation in cooperative networks is then analyzed via simulation using the DF and AF protocols. Subsequently, the concatenation of differential strategies with DSTBC is systematically presented. We show how to integrate orthogonal designs like the Alamouti code with differential modulation. We presented the full differential encoding and decoding procedure using two main differential concepts, namely; 'co-efficient vectors' and 'unitary matrices'. These concepts were then generalized to cooperative networks with three, four and eight relay nodes. Differential strategies are then integrated with DQSTBC, based on this, differential and multi-differential DQSTBC is proposed for cooperative networks.

The final part of this thesis deals with the design of DSTBC for cooperative broadband networks. This is motivated by the increasing interest in high data rate services propagated over broadband channels, for example; multimedia, mobile computing, and video conferencing. Specifically, the concatenation of OFDM with DSTBC schemes is considered for non-coherent cooperative networks, from this differential DQSFC and differential DQSTFC which exploit space-frequency diversity gain and space-time-frequency diversity gain respectively are proposed. The proposed schemes are also able to achieve full code rate based on the use of quasi-orthogonal codes.

7.2 Future Work

The DSTBC schemes designed in this thesis can be combined with other transmission schemes to improve the performance of the cooperative network. This can be achieved in many different interesting ways:

7.2.1 DSTBC Schemes with Adaptive Signalling using Limited Feedback

The cooperative signalling concept used throughout this thesis adopts one-way communication where the source node forwards information signals to the destination via relay nodes. Thus there is no available feedback channel between the communicating nodes. The performance of cooperative systems can be improved if limited feedback is available. For example, the feedback channel can be used to adjust certain transmission schemes in the network. Specifically, DSTBC can be combined with adaptive relay selection, in this case, the feedback channel is used to optimally select only the best relays based on certain selection criteria, like channel conditions or SNR. In the same context, the feedback channel can be used to adjust the transmission time of the relay nodes such that synchronized DSTBC can be achieved.

7.2.2 Adaptive DSTBC Selection

The performance of cooperative networks can be further improved if CSI obtained from the destination is fed back to the source node or relay nodes. The destination can return one or two feedback bits in each fading block such that the cooperating nodes can switch between certain predefined DSTBC schemes to optimize performance. For example, in the case of DQSTBC where linear decoding is only possible for pairs of symbols (due to the off-diagonal interfering elements in the Gramian matrix), feedback bits can be returned from the

destination to suppress the interfering elements thereby facilitating simple ML decoding for DQSTBC.

7.2.3 Adaptive Cooperative Diversity Protocols

The availability of a feedback channel can also be used to optimize the performance of the AF and DF cooperative diversity protocols. For example, in the case of adaptive AF schemes, the amplification factor used by the relay nodes can be systematically selected based on feedback information (e.g. CSI) obtained from the destination. Similarly, adaptive DF schemes can use feedback information to systematically select the modulation scheme employed by the relay nodes.

All of the aforementioned techniques can significantly improve the performance of DSTBC in cooperative networks. However, such extensions of DSTBC may also introduce additional signalling overhead, which subsequently increases system complexity. Thus it is vital to obtain a good trade-off between system complexity and signalling overhead.

Appendices

Appendix A

We now present the necessary conditions for our quasi-orthogonal codeword to achieve full diversity in a network with $N = 4$ and $T = 4$. Given a pair of codewords $\boldsymbol{x}_{k,1} = \left[x_{k,1(1)}, x_{k,1(2)}, \tilde{x}_{k,1(3)}, \tilde{x}_{k,1(4)}\right]$ and $\boldsymbol{x}'_{k,1} = \left[\acute{x}_{k,1(1)}, \acute{x}_{k,1(2)}, \acute{\tilde{x}}_{k,1(3)}, \acute{\tilde{x}}_{k,1(4)}\right]$, where $\tilde{x}_{k,1(t)}$ represents the rotated version of $x_{k,1(t)}$, and $\boldsymbol{x}'_{k,1}$ represents the received noisy version of $\boldsymbol{x}_{k,1}$. The coding gain difference between the pair is arrived at by the determinant equality in Chapter 5 of [35] as follows:

$$det\left(\boldsymbol{S}_k{}^H \boldsymbol{S}_k\right) = \left(S_1{}^2 - S_2{}^2\right)\left(S_1{}^2 - S_2{}^2\right) \tag{A.1}$$

where $\boldsymbol{S}_k$ is a non-unitary quasi-orthogonal matrix with structure $\boldsymbol{S}_k = \left[\boldsymbol{s}_{k,1}{}^T, \ldots, \boldsymbol{s}_{k,N}{}^T\right]$, $\boldsymbol{s}_{k,1} = \left[s_{k,1(1)}, \ldots, s_{k,1(T)}\right]$, $S_1 = \sum_{t=1}^{4} \left|s_{k,1(t)}\right|^2$ and $S_2 = 2Re\left(s_{k,1(1)} s_{k,1(4)}{}^* - s_{k,1(2)} s_{k,1(3)}{}^*\right)$. Using simple algebraic manipulation (A.1) becomes:

$$det\left(\boldsymbol{S}_k{}^H \boldsymbol{S}_k\right) = \left(\left|s_{k,1(1)} - s_{k,1(4)}\right|^2 + \left|s_{k,1(2)} + s_{k,1(3)}\right|^2\right)^2 \left(\left|s_{k,1(1)} + s_{k,1(4)}\right|^2 + \left|s_{k,1(2)} - s_{k,1(3)}\right|^2\right)^2 \tag{A.2}$$

Replacing $s_{k,1(t)}$ in (A.2) with $\left(x_{k,1(t)} - \acute{x}_{k,1(t)}\right)$ full diversity is only achievable when the determinant equality in (A.2) is non-zero. This also implies that the diversity product given by $\zeta_c = \frac{1}{2}\min_{\acute{\mathbf{S}}_k \neq \mathbf{S}_k \forall \boldsymbol{\mathcal{V}}} \left|\det\left(\acute{\mathbf{S}}_k - \mathbf{S}_k\right)\right|^{\frac{1}{N}}$ is non zero, where $\boldsymbol{\mathcal{V}}$ is the set of all valid quasi-orthogonal matrices.

Appendix B

We now prove that the QOSF code in (5.11) achieves our targeted diversity order of $P\Gamma$ for any $(P+\Gamma) = 2^{r+1}, \forall\, P = \Gamma$, where r is a positive integer, and $\Gamma \leq L \ll N, L = min\{L_{SR}, L_{RD}\}$. Clearly, in order to achieve a diversity order of $P\Gamma$, there must be at least one non-zero block k of length $P\Gamma$ in$\left(\boldsymbol{\mathcal{V}} - \acute{\boldsymbol{\mathcal{V}}}\right)$, where $\boldsymbol{\mathcal{V}}$ and $\acute{\boldsymbol{\mathcal{V}}}$ are a pair of distinct codewords. In other words, we assume that at least$\left(\boldsymbol{\mathcal{V}}_k - \acute{\boldsymbol{\mathcal{V}}}_k\right) \neq 0$. This assumption does not decrease the rank of the matrix$\left(\boldsymbol{\mathcal{V}} - \acute{\boldsymbol{\mathcal{V}}}\right)$, and the minimum rank of $\left(\boldsymbol{\mathcal{V}} - \acute{\boldsymbol{\mathcal{V}}}\right)$ determines our achievable diversity order. We assume that there exists at least one block k of length $P\Gamma$ for which $\boldsymbol{\mathcal{V}}_k \neq \acute{\boldsymbol{\mathcal{V}}}_k$ or$\left(\boldsymbol{\mathcal{V}}_k - \acute{\boldsymbol{\mathcal{V}}}_k\right) \neq 0$ and the total number of sub-carriers $N > P\Gamma$. Denoting $\omega = e^{-j\frac{2\pi}{N}}$ and$|v_i - \acute{v}_i| = d_i$, the non-zero block of $\left(\boldsymbol{\mathcal{V}} - \acute{\boldsymbol{\mathcal{V}}}\right)$, given by $D\left(\boldsymbol{\mathcal{V}} - \acute{\boldsymbol{\mathcal{V}}}\right)$ can be decomposed as

$$D\left(\boldsymbol{\mathcal{V}} - \acute{\boldsymbol{\mathcal{V}}}\right) = \boldsymbol{W} \cdot \left(\boldsymbol{\mathcal{V}}_k - \acute{\boldsymbol{\mathcal{V}}}_k\right)$$

where $= \left[\boldsymbol{\omega}^{0^T}, \ldots, \boldsymbol{\omega}^{(L-1)^T}\right]^T$, $\boldsymbol{\omega} = \left[1, \omega^1, \ldots, \omega^{(P\Gamma-1)}\right]$

$\left(\boldsymbol{\mathcal{V}}_k - \acute{\boldsymbol{\mathcal{V}}}_k\right) = diag[\mathcal{G}(\mathbf{v}_1), \ldots, \mathcal{G}(\mathbf{v}_\Gamma)], \mathbf{v}_f = [d_1, \ldots, d_P]$, and $\mathcal{G}$ is a $P \times P$ identity matrix that maintains the quasi-orthogonal structure of the codewords. Thus

$$\left(\boldsymbol{\mathcal{V}}_k - \acute{\boldsymbol{\mathcal{V}}}_k\right) = diag[(d_1, d_2, \ldots, d_P)_1, (-d_2{}^*, d_1{}^*, \ldots, d_{P-1}{}^*)_2, \ldots, (d_1, d_2 \ldots, d_P)_\Gamma]$$

The matrix $D\left(\boldsymbol{\mathcal{V}} - \acute{\boldsymbol{\mathcal{V}}}\right)$ is a $P\Gamma \times P\Gamma$ matrix and $\boldsymbol{\omega}$ is of length $P\Gamma$. This implies that $D\left(\boldsymbol{\mathcal{V}} - \acute{\boldsymbol{\mathcal{V}}}\right)$ will contain $P\Gamma$ rows of non-zero elements. Using $\mathcal{G}\left(\mathbf{v}_f\right) = \mathbf{v}_f$ for ease of explanation, we have

$$D(\mathbf{V} - \mathbf{V}') = \begin{bmatrix} \mathbf{v}_1 & \mathbf{v}_1 & \cdots & \mathbf{v}_1 \\ \mathbf{v}_2 & \boldsymbol{\omega}\mathbf{v}_2 & \cdots & \boldsymbol{\omega}^{(\Gamma-1)}\mathbf{v}_2 \\ \vdots & \vdots & \ddots & \vdots \\ \mathbf{v}_{P\Gamma} & \boldsymbol{\omega}^{(P\Gamma-1)}\mathbf{v}_{P\Gamma} & \cdots & \boldsymbol{\omega}^{(P\Gamma-1)(\Gamma-1)}\mathbf{v}_{P\Gamma} \end{bmatrix}$$

where $\mathbf{v}_f$ is a $1 \times P$ vector containing elements $d_i = |v_i - \acute{v}_i|$, and v_i and $\acute{v}_i$ are made up of combined symbols v_i and $\acute{\mathrm{v}}_\iota$ respectively as discussed in Section II C. Our QOSF code has been constructed such that $|v_i - \acute{v}_\iota| \cdot \Phi = \left|(\mathrm{v}_i - \acute{\mathrm{v}}_\iota) + e^{j\theta_1}(\mathrm{v}_{i+1} - \acute{\mathrm{v}}_{\iota+1}) + \cdots + e^{j\theta_{\Gamma-1}}(\mathrm{v}_\Gamma - \acute{\mathrm{v}}_\Gamma)\right| \neq 0, \forall\, i \in \{1,3,\ldots,P\Gamma-1\}$ where $\Phi = diag\left[1, e^{j\theta_1}, \ldots, e^{j\theta_{P\Gamma-1}}\right]$. From Section III B we can also obtain $\left|v_j - \acute{v}_j\right| \cdot \Phi \neq 0, \forall\, j \in \{2,4,\ldots,\Gamma\}$. Thus minimum coding gain is achieved when either the odd entries of $D(\boldsymbol{\mathcal{V}} - \acute{\boldsymbol{\mathcal{V}}})$, given by $d_1, d_3, \ldots, d_{P-1}$ is set to zero, or the even entries $d_2, d_4, \ldots, d_P$ is set to zero. Assuming we set the even entries of $D(\boldsymbol{\mathcal{V}} - \acute{\boldsymbol{\mathcal{V}}})$ to zero, the non-zero odd entries of $D(\boldsymbol{\mathcal{V}} - \acute{\boldsymbol{\mathcal{V}}})$ can be expanded as

$$\bar{D}(\mathbf{V} - \mathbf{V}') = \begin{bmatrix} d_1 & 0 & \cdots & d_1 & 0 \\ 0 & d_1^* & \cdots & 0 & \boldsymbol{\omega}^{(\Gamma-1)} d_1^* \\ d_3 & 0 & \ddots & \boldsymbol{\omega}^{(\Gamma-1)} d_3 & 0 \\ \vdots & \vdots & \cdots & \vdots & \vdots \\ d_{P-1} & 0 & \cdots & \boldsymbol{\omega}^{(P\Gamma-1)(\Gamma-1)} d_{P-1} & 0 \\ 0 & d_{P-1}^* & \cdots & 0 & \boldsymbol{\omega}^{(P\Gamma-1)(\Gamma-1)} d_{P-1}^* \end{bmatrix}$$

Since $d_j \neq 0, \forall\, j \in \{1,2,\ldots,\mathrm{P}\}$, and $P = \Gamma$, we can get Γ linearly independent columns from the $P\Gamma \times P\Gamma$ matrix $\bar{D}(\boldsymbol{\mathcal{V}} - \acute{\boldsymbol{\mathcal{V}}})$with column indices $\sigma_j,\ j \in \{1,3,\ldots,P\Gamma-1\}$ and $\sigma_k,\ k \in \{2,4,\ldots,P\Gamma\}$. Therefore, $\bar{D}(\boldsymbol{\mathcal{V}} - \acute{\boldsymbol{\mathcal{V}}})$contains two sets of independent $\Gamma \times \Gamma$ sub-matrices. Let us denote $\bar{d}(\boldsymbol{\mathcal{V}} - \acute{\boldsymbol{\mathcal{V}}})_o$ as the $\Gamma \times \Gamma$ sub-matrix which contains the odd rows and odd columns of$\bar{D}(\boldsymbol{\mathcal{V}} - \acute{\boldsymbol{\mathcal{V}}})$, and $\bar{d}(\boldsymbol{\mathcal{V}} - \acute{\boldsymbol{\mathcal{V}}})_e$ as the $\Gamma \times \Gamma$ sub-matrix which contains the even rows and even columns of $\bar{D}(\boldsymbol{\mathcal{V}} - \acute{\boldsymbol{\mathcal{V}}})$. The $\Gamma \times \Gamma$ sub-matrix $\bar{d}(\boldsymbol{\mathcal{V}} - \acute{\boldsymbol{\mathcal{V}}})_o$ is constructed as

$$\bar{d}\,(\mathbf{V} - \mathbf{V}')_o = \begin{bmatrix} \bar{\mathbf{v}}_1 & \bar{\mathbf{v}}_1 & \cdots & \bar{\mathbf{v}}_1 \\ \bar{\mathbf{v}}_3 & \boldsymbol{\omega}^2 \bar{\mathbf{v}}_3 & \cdots & \boldsymbol{\omega}^{2(\Gamma-1)} \bar{\mathbf{v}}_3 \\ \vdots & \vdots & \ddots & \vdots \\ \bar{\mathbf{v}}_{P\Gamma-1} & \boldsymbol{\omega}^{(P\Gamma-2)} \bar{\mathbf{v}}_{P\Gamma-1} & \cdots & \boldsymbol{\omega}^{(P\Gamma-2)(\Gamma-1)} \bar{\mathbf{v}}_{P\Gamma-1} \end{bmatrix} \tag{B.1}$$

and $\bar{d}(\boldsymbol{\mathcal{V}} - \acute{\boldsymbol{\mathcal{V}}})_e$ is constructed as

$$\bar{d}\left(\mathbf{V}-\mathbf{V}'\right)_e = \begin{bmatrix} \overline{\mathbf{v}}_2 & \boldsymbol{\omega}\overline{\mathbf{v}}_2 & \cdots & \boldsymbol{\omega}^{(\Gamma-1)}\overline{\mathbf{v}}_2 \\ \overline{\mathbf{v}}_4 & \boldsymbol{\omega}^3\overline{\mathbf{v}}_4 & \cdots & \boldsymbol{\omega}^{3(\Gamma-1)}\overline{\mathbf{v}}_4 \\ \vdots & \vdots & \ddots & \vdots \\ \overline{\mathbf{v}}_{P\Gamma} & \boldsymbol{\omega}^{(P\Gamma-1)}\overline{\mathbf{v}}_{P\Gamma} & \cdots & \boldsymbol{\omega}^{(P\Gamma-1)(\Gamma-1)}\overline{\mathbf{v}}_{P\Gamma} \end{bmatrix} \quad \text{(B.2)}$$

where $\overline{\mathbf{v}}_f$ in (B.1) and (B.2) contain the odd entries and even entries of $\mathbf{v}_f$ respectively. Denote $\overline{\mathbf{V}}_o = [\overline{\mathbf{v}}_1, \overline{\mathbf{v}}_3, \ldots, \overline{\mathbf{v}}_{P\Gamma-1}]$ and $\overline{\mathbf{V}}_e = [\overline{\mathbf{v}}_2, \overline{\mathbf{v}}_4, \ldots, \overline{\mathbf{v}}_{P\Gamma}]$, the matrices $\bar{d}\left(\boldsymbol{\mathcal{V}}-\acute{\boldsymbol{\mathcal{V}}}\right)_o$ and $\bar{d}\left(\boldsymbol{\mathcal{V}}-\acute{\boldsymbol{\mathcal{V}}}\right)_e$ can be decomposed as follows:

$$\bar{d}\left(\boldsymbol{\mathcal{V}}-\acute{\boldsymbol{\mathcal{V}}}\right)_o = \overline{\mathbf{V}}_o \cdot \boldsymbol{W}_o$$

$$\bar{d}\left(\boldsymbol{\mathcal{V}}-\acute{\boldsymbol{\mathcal{V}}}\right)_e = \overline{\mathbf{V}}_e \cdot \boldsymbol{W}_e$$

where

$$\boldsymbol{W}_o = \begin{bmatrix} 1 & 1 & \cdots & 1 \\ 1 & \omega^2 & \cdots & \omega^{2(\Gamma-1)} \\ \vdots & \vdots & \ddots & \vdots \\ 1 & \omega^{(P\Gamma-2)} & \cdots & \omega^{(P\Gamma-2)(\Gamma-1)} \end{bmatrix}$$

$$\boldsymbol{W}_e = \begin{bmatrix} 1 & \omega & \cdots & \omega^{(\Gamma-1)} \\ 1 & \omega^3 & \cdots & \omega^{3(\Gamma-1)} \\ \vdots & \vdots & \ddots & \vdots \\ 1 & \omega^{(P\Gamma-1)} & \cdots & \omega^{(P\Gamma-1)(\Gamma-1)} \end{bmatrix}$$

The entries of $\boldsymbol{W}_o$ and $\boldsymbol{W}_e$ given by $W_{o(i)}$ and $W_{e(i)}$ respectively, increase geometrically along the rows and columns, thus $\boldsymbol{W}_o$ and $\boldsymbol{W}_e$ have the properties of a square Vandermonde matrix. The determinant of a square Vandermonde matrix can be expressed as [95, Section 6.1]

$$det(\boldsymbol{W}_o) = \prod_{1 \le i < j \le q} \left(W_{o(j)} - W_{o(i)}\right)$$

$$det(\boldsymbol{W}_e) = \prod_{1 \le i < j \le q} \left(W_{e(j)} - W_{e(i)}\right)$$

where $q = (\mathrm{P}\Gamma - 1)(\Gamma - 1)$. Since we have $\omega^n, n \in \{0,1,\dots,q\}$, then each of the entries $W_{o(i)}$ and $W_{e(i)}$ are distinct, that is $W_{e(i)} \neq W_{e(j)}$ and $W_{o(i)} \neq W_{o(j)}, \forall\, i \neq j$, and thus $det(\boldsymbol{W}_o) \neq 0$ and $det(\boldsymbol{W}_e) \neq 0$. We can now prove that $\bar{d}(\boldsymbol{\nu} - \acute{\boldsymbol{\nu}})_o$ and $\bar{d}(\boldsymbol{\nu} - \acute{\boldsymbol{\nu}})_e$ are full-rank matrices by showing that $det\left(\bar{d}(\boldsymbol{\nu} - \acute{\boldsymbol{\nu}})_o\right) \neq 0$ and $det\left(\bar{d}(\boldsymbol{\nu} - \acute{\boldsymbol{\nu}})_e\right) \neq 0$ as follows:

$$det\left(\bar{d}(\boldsymbol{\nu} - \acute{\boldsymbol{\nu}})_o\right) = det(\bar{\mathbf{V}}_o) det(\boldsymbol{W}_o)$$

$$= \prod_{f=1}^{P\Gamma-1} \bar{\mathbf{v}}_f \; det(\boldsymbol{W}_o)$$

$$det\left(\bar{d}(\boldsymbol{\nu} - \acute{\boldsymbol{\nu}})_e\right) = det(\bar{\mathbf{V}}_e) det(\boldsymbol{W}_e)$$

$$= \prod_{f=2}^{P\Gamma} \bar{\mathbf{v}}_f \; det(\boldsymbol{W}_e)$$

We already know that $\bar{\mathbf{v}}_f$ in (B.1) and (B.2) contain the odd entries and even entries of $\mathbf{v}_f$ respectively, that is $\bar{\mathbf{v}}_f = [d_1, d_{3,\dots}]$ for the odd entries and $\bar{\mathbf{v}}_f = [d_2, d_{4,\dots}]$ for the even entries, thus $\prod_{f=1}^{P\Gamma-1} \bar{\mathbf{v}}_f \neq 0$ and $\prod_{f=2}^{P\Gamma} \bar{\mathbf{v}}_f \neq 0$ since $d_j = |v_j - \acute{v}_j| \neq 0, \forall\, j \in \{1,3,\dots,P-1\}$ and $d_i = |v_i - \acute{v}_i| \neq 0, \forall\, i \in \{2,4,\dots,P\}$. We have already established that $det(\boldsymbol{W}_o) \neq 0$ and $det(\boldsymbol{W}_e) \neq 0$. Combining the above, it is clear that $det\left(\bar{d}(\boldsymbol{\nu} - \acute{\boldsymbol{\nu}})_o\right) \neq 0$ and $det\left(\bar{d}(\boldsymbol{\nu} - \acute{\boldsymbol{\nu}})_e\right) \neq 0$ and $\bar{d}(\boldsymbol{\nu} - \acute{\boldsymbol{\nu}})_o$ and $\bar{d}(\boldsymbol{\nu} - \acute{\boldsymbol{\nu}})_e$ are full-rank matrices. Based on these, $D(\boldsymbol{\nu} - \acute{\boldsymbol{\nu}})$ has minimum rank $P\Gamma$ and our QOSF code achieves diversity order of $P\Gamma$ for any $(P + \Gamma) = 2^{r+1}, \forall\, P = \Gamma$, where r is a positive integer, and$\Gamma \leq L \ll N, L = min\{L_{SR}, L_{RD}\}$.

REFERENCES

[1] K. K. Wong, and E. Elsheikh, "Optimized Cooperative Diversity for a Three-node Decode-and-Forward Relay Channels", IEEE 2nd International Symposium on Wireless Pervasive Computing: 5-7, San Juan, Puerto Rico, Piscataway, US, pp.296-301, February 2007.

[2] J. N. Laneman, and G.W. Wornell, "Energy-efficient Antenna Sharing and Relaying for Wireless Networks", IEEE Proceedings on Wireless Communications and Networking Conference, Vol.1, pp. 7–12, 2000.

[3] A. Sendonaris, E. Erkip and B. Aazhang, "User Cooperation Diversity–Part I: System Description", IEEE Transactions on Communications, Vol. 51, No. 11, pp 1927-1938, November 2003.

[4] A. Sendonaris, E. Erkip and B. Aazhang, "User Cooperation Diversity–Part II: Implementation Aspects and Performance Analysis", IEEE Transactions on Communications, Vol. 51, No.11, pp 1939-1948, November 2003.

[5] J. N. Laneman, D. N. C. Tse, and G. W. Wornell, "Cooperative Diversity in Wireless Networks: Efficient Protocols and Outage Behaviour", IEEE Transactions on Information Theory, Vol.50, pp.3062–3080, December 2004.

[6] T. M. Cover and A. A. El Gamal, "Capacity Theorems for the Relay Channel", IEEE Transactions on Information Theory, Vol. IT-25, pp. 572–584, September 1979.

[7] A. Sendonaris, E. Erkip, and B. Aazhang, "Increasing Uplink Capacity via User Cooperation Diversity," In Proceedings of IEEE International Symposium on Information Theory, pp. 156, August 1998.

[8] Z. Yi "Distributed Space-Time Block Codes in Wireless Cooperative Networks" PhD Thesis submitted to the Department of Electrical and Computer Engineering Queen's University, Canada, June 2009.

[9] P. Merkey and E. C. Posner, "Optimum Cyclic Redundancy Codes for Noisy Channels," IEEE Transactions on Information Theory, Vol. 30, No. 6, pp. 865–867, November 1984.

[10] A. K. Sadek, W. Su, and K. J. R. Liu, "Multi-node Cooperative Communications in Wireless Networks," IEEE Transactions on Signal Processing, Vol. 55, No. 1, pp. 341–355, January 2007.

[11] M. Yu and J. Li, "Is Amplify-and-Forward Practically Better Than Decode-and-Forward or Vice Versa?", Proceedings of IEEE International Conference on Acoustics, Speech, and Signal Processing, Vol.3, March 2005.

[12] T. E. Hunter and A. Nosratinia, "Diversity Through Coded Cooperation", IEEE Transactions on Wireless Communications, Vol. 5, No. 2, pp. 283-289, February 2006.

[13] A. Stefanov and E. Erkip, "Cooperative Coding for Wireless Networks", IEEE Transactions on Communications, Vol. 52, No. 9, September 2004.

[14] J. N. Laneman, "Network Coding Gain of Cooperative Diversity", IEEE Military Communications Conference, MILCOM, pp. 106-112, Vol. 1, October 2004.

[15] Y. Chen, S. Kishore, and J. Li, "Wireless Diversity through Network Coding", IEEE Wireless Communications and Networking Conference, WCNC, Las Vegas, pp. 1681 – 1686, April 2006.

[16] D. Chen and J. N. Laneman, "Modulation and Demodulation for Cooperative Diversity in Wireless Systems," IEEE Transactions on Wireless Communications, Vol. 5, pp. 1785–1794, July 2006.

[17] P. A. Anghel and M. Kaveh, "Exact Symbol Error Probability of a Cooperative Network in a Rayleigh-fading Environment," IEEE Transactions on Wireless Communications, Vol. 3, pp. 1416–1421, September 2004.

[18] J. N. Laneman, and G. W. Wornell, "Distributed Space-Time Coded Protocols for Exploiting Cooperative Diversity in Wireless Networks," IEEE Trans. Information Theory, Vol. 49, No. 10, pp. 2415–2525, October 2003.

[19] T. Hunter and A. Nosratinia, "Cooperation Diversity through Coding," IEEE International Symposium on Information Theory, Lausanne, Switzerland, p. 220, June 2002.

[20] M. Janani, A. Hedayat, T. E. Hunter, and A. Nosratinia, "Coded Cooperation in Wireless Communications: Space-time Transmission and Iterative decoding," IEEE Transactions Signal Processing, Vol. 52, No. 2, pp.362 – 371, February 2004.

[21] R. Ahlswede, N. Cai, S. Y. R. Li and R. W. Yeung, "Network Information Flow", IEEE Transactions on Information Theory, Vol. 46, No.4, pp. 1204-1216, 2000.

[22] J. N. Laneman, Cooperation in Wireless Networks: Principles and Applications, Chapter: Cooperative Diversity: Models, Algorithms, and Architectures pp. 163-188, Springer, 2006.

[23] M. N. Khormuji, and E. G. Larsson, "Cooperative Transmission Based on Decode-And-Forward Relaying with Partial Repetition Coding", IEEE Transactions on Wireless Communications, Vol.8, Issue 4, April 2009.

[24] S. Alamouti, "A Simple Transmit Diversity Technique for Wireless Communications," IEEE Journal on Selected Areas in Communications, Vol.16, pp. 1451–1458, August 1998

[25] V. Tarokh, N. Seshadri, and A. R. Calderbank, "Space-time codes forhigh data rate wireless communication: performance criterion and code construction," IEEE Transactions on Information Theory, vol. 44, pp. 744–765, 1998.

[26] V. Tarokh, H. Jafarkhani and A.R Calderbank, "Space Time Block Codes from Orthogonal Designs," IEEE Transactions on Information Theory, Vol. 45, No. 5, July 1999.

[27] Y. Jing and B. Hassibi, "Distributed space-time coding in wireless relay networks," IEEE Transactions on Wireless Communications, vol. 5, pp. 3524–3536, Dec. 2006.

[28] R. U. Nabar, H. Bolcskei and F. W. Kneubuhler, "Fading Relay Channels: Performance Limits and Space-time Signal Designs," IEEE Journal on Selected Areas in Communications, Vol. 22, pp. 1099–1109, August 2004.

[29] S. Barbarossa and G. Scutari, "Distributed Space-time Coding for Regenerative Relay Networks," IEEE Transactions on Wireless Communications, vol. 4, no. 5, pp. 2387-2399, September 2005.

[30] Y. Jing and H. Jafarkhani, "Distributed Differential Space-Time Coding for Wireless Relay Networks," IEEE Transactions on Communications, vol. 56, no. 7, pp. 1092-1100, July 2008.

[31] Y. Jing and H. Jafarkhani, "Using Orthogonal and Quasi-Orthogonal Designs in Wireless Relay Networks," IEEE Transactions on Information Theory, vol. 53, pp. 4106–4118, November 2007.

[32] G. Owojaiye, F. Delestre, and Y. Sun, "Source-assisting Strategy for Distributed Space-Time Block Codes," IEEE International Symposium on Wireless Communication Systems, pp. 174 – 178, York, England, November 2010.

[33] V. Erceg, D. G. Michelson, S.S. Ghassemzadeh, L. J. Greenstein, A. J. Rustako, P. B. Guerlain, M. K. Dennison, R. S. Roman, D. J. Barnickel, S. C. Wang, and R. R. Miller, "A Model for the Multipath Delay Profile of Fixed Wireless Channels," IEEE Journal on Selected Areas in Communications, Vol. 17, No. 3,pp. 399-410, March 1999.

[34] B. Vucetic, and J. Yuan, "Space-Time Coding", John Wiley and Sons, 2003.

[35] H. Jafarkhani, Space-Time Coding Theory and Practice, Chapter 5, Cambridge Academic Press, 2005.

[36] B. Sklar, "Rayleigh Fading Channels in Mobile Digital Communication Systems Part 2: Mitigation," IEEE Communications Magazine, July 1997.

[37] B. Sklar, "Rayleigh Fading Channels in Mobile Digital Communication Systems Part 1: Characterization," IEEE Communications Magazine, July 1997.

[38] L. Wang, W. Liu, and Y. Cheng, "Statistical Analysis of a Mobile-to-Mobile Rician Fading Channel Model," IEEE Transactions on Vehicular Technology, Vol. 58, No. 1, pp. 32-38, January 2009.

[39] B. Maham, A. Hjorungnesy, and G. Abreuz, "Distributed GABBA Space-time Codes with Complex Signal Constellations," 5th IEEE Sensor Array and Multi-channel Signal Processing Workshop, pp.118 – 121, July 2008.

[40] T. Cui, F. Gao, T. Ho and A. Nallanathan, "Distributed Space-Time Coding for Two-Way Wireless Relay Networks", IEEE Transactions on Signal Processing Vol. 57, Issue 2, pp. 658-671, February 2009.

[41] G. S. Rajan and B. S. Rajan, "Distributed Space-Time Codes for Cooperative Networks with Partial CSI", IEEE Wireless Communications and Networking Conference, March 2007.

[42] H. Jafarkhani, “A Quasi-orthogonal Space-time Block Code”, IEEE Transactions on Communications, Vol. 49, pp.1-4, January 2001.

[43] S. Sandhu and A. Paulraj, “Space-time Block Codes: A Capacity Perspective”, IEEE Communications Letters, Vol. 4, pp. 384-386, December 2000.

[44] Y. Jing and B. Hassibi, "Cooperative Diversity in Wireless Relay Networks With Multiple-Antenna Nodes," IEEE Proceedings of the International Symposium on Information Theory (ISIT '05), pp. 815-819, September 2005.

[45] F. Oggier and B. Hassibi, “An Algebraic Coding Scheme for Wireless Relay Networks with Multiple-Antenna Nodes”, IEEE Transactions on Signal Processing, Vol. 56, No. 7, July 2008.

[46] M. K. Simon, M.S. Alouini, Digital Communication over Fading Channel: A Unified Approach to Performance Analysis, John Wiley and Sons, 2000.

[47] A. Hottinen, O. Tirkkonen, and R. Wichman, Multi-Antenna Transceiver Techniques for 3G and Beyond, John Wiley and Sons, 2003.

[48] S. K. Kassim, M. Hayes, N.M. Eltayeb and J.A. Chambers, “Exploitation of Quasi-Orthogonal Space Time Block-codes in Virtual Antenna Arrays: Part II Monte Carlo-based Throughput Evaluation”, IEEE Vehicular Technology Conference, pp. 242 – 246, May 2008.

[49] K.G. Seddik, A. K. Sadek, A. S. Ibrahim, and K. J. R. Liu, “Design Criteria and Performance Analysis for Distributed Space-Time Coding”, IEEE Transactions on Vehicular Technology, Vol.57, No. 4, July 2008

[50] V. Tarokh, and H. Jafarkhani, “A Differential Detection Scheme for Transmit Diversity,” IEEE Journals on Selected Areas in Communications, pp. 1169–1174, July 2000.

[51] B. Hughes, "Differential space-time modulation," IEEE Transactions on Information Theory, Vol. 46, pp. 2567–2578, Nov. 2000

[52] S. Yiu, R. Schober, and L. Lampe, "Differential Distributed Space-Time Block Coding", in Proceedings of IEEE Pacific Rim Conference on Communications, Computers, and Signal Processing, pp. 53-56, August 2005

[53] S. H. Muhaidat, P. Ho and M. Uysal, "Distributed Differential Space-Time Coding for Broadband Cooperative Networks", IEEE Vehicular Technology Conference, April 2009.

[54] T. S. Rappaport, Wireless Communications: Principles and Practice, Prentice Hall, 1996.

[55] U. Madhow, Fundamentals of Digital Communication: Chapter 2.7, Cambridge University Press, 2008.

[56] Q. Zhao and H. Li, "Performance of Differential Modulation with Wireless Relays in Rayleigh Fading Channels," IEEE Communication Letters, vol.9, no.4, April 2005

[57] T. Kiran and B. Sundar Rajan, "Partially-coherent distributed space-time codes with differential encoder and decoder," IEEE Journal on Selected Areas in Communication, vol. 25, no. 2, pp. 426-433, Feb 2007.

[58] H. Wang and Z. Zhao, "Distributed differential space-time codes based on Weyl's reciprocity," IEEE International Symposium on Information Theory, ISIT pp 2828-2832, Seoul, Korea, Jun 2009.

[59] S. Ma and J. Zhang, "Non-coherent diagonal distributed space-time block codes for amplify-and-forward half-duplex cooperative relay channels," IEEE Transactions on Vehicular Technology, vol. 60, no.5, pp 2400-2405, Jun 2011.

[60] F. Oggier, and E. Lequeu, "Differential distributed space time coding based on Cayley codes," IEEE Transactions on Wireless Communications, vol. 8, no. 7, pp. 3808-3814, July 2009.

[61] Q. Zhao and H. Li, "Differential modulation for cooperative wireless systems," IEEE Transactions on Signal Processing, vol. 55, no. 5, pp. 2273-2283, May 2007.

[62] H. Jafarkhani and V. Tarokh, "Multiple transmit antenna differential detection from generalized orthogonal designs," IEEE Transactions on Information Theory, vol. 47, no. 6, pp. 2626–2631, September. 2001.

[63] G. Susinder Rajan, and B. Sundar Rajan, "Algebraic distributed differential space-time codes with low decoding complexity," IEEE Transactions on Wireless Communications, vol. 7, no. 10, pp. 3962-3971 October 2008.

[64] G. Susinder Rajan and B. Sundar Rajan, "Leveraging coherent distributed space-time codes for non-coherent communication in relay networks via training", IEEE Transactions on Wireless Communication, vol. 8, no. 2, pp. 683-688, February. 2009.

[65] G. Susinder Rajan and B. Sundar Rajan, "Non-coherent low-decoding-complexity space time codes for wireless relay networks", IEEE International Symposium on Information Theory, ISIT, pp 1521 – 1525, Nice, June 2007.

[66] V. Tarokh, H. Jafarkhani and A.R Calderbank, "Space Time Block Coding for Wireless Communications: Performance Results," IEEE Journal on Selected Areas in Communications, Vol. 17, No. 3, March 1999.

[67] E. Ayanoglu, E.G. Larsson, and E. Karipidis, "Computational complexity of decoding orthogonal space-time-block codes" IEEE Transactions on Communications, Vol.59 No. 4, pp. 936-941, April 2011.

[68] F. Oggier and B. Hassibi, "A coding scheme for wireless networks with multiple antenna nodes and no channel information," IEEE International Conference on Acoustics, Speech and Signal Processing, Vol. 3, pp. 413-416, Piscataway, NJ, April 2007.

[69] Z. Utkovski, G. Yammine and J. Lindner, "A distributed differential space-time coding scheme for two-way wireless relay networks," IEEE International Symposium on Information Theory, ISIT, pp 779-783, Seoul, Korea, Jun 2009.

[70] Y. Zhu and H. Jafarkhani, "Differential modulation based on quasi-orthogonal codes," IEEE Transactions on Wireless Communications, Vol. 4, No. 6, pp. 3018–3030, 2005.

[71] J. Liu and J. Li, "Packet design and signal processing for OFDM based mobile broadband wireless communication systems," IEEE Transactions on Mobile Computing, vol. 5, pp. 1133–1142, Sept. 2006.

[72] Q. Ma, C. Tepedelenlioglu, and Z. Liu, "Differential space-time-frequency coded OFDM with maximum multipath diversity," IEEE Transactions on Wireless Communications, vol. 4, no. 5, pp. 2232–2243, 2005.

[73] J. Flores, J. Sanchez, and H. Jafarkhani, "Differential quasi-orthogonal space-frequency trellis codes," IEEE Transactions on Wireless Communications, vol. 9, no. 12, Dec. 2010.

[74] T. Himsoon, W. Su, and K. J. R. Liu, "Single-block differential transmit scheme for broadband wireless MIMO-OFDM systems," IEEE Transactions on Signal Processing, vol. 54, no. 9, pp. 3305–3314, Sept. 2006.

[75] H. Li, "Differential space-time-frequency modulation over frequency selective fading channels," IEEE Communication Letters, vol. 7, no. 8, pp. 349–351, Aug. 2003.

[76] J. Xu, S. Zhu, and Z. Zhong, "Differential distributed space-frequency coding for broadband non-regenerative wireless relaying systems," IEEE Global Telecommunications Conference, pp. 1-6, 2008.

[77] W. Zhang, Y. Li, X. Xia, P.C. Ching, and K.B. Letaief, "Distributed space-frequency coding for cooperative diversity in broadband wireless Adhoc networks," IEEE Transactions on Wireless Communications, vol. 7, no. 3, pp. 995-1003, Mar. 2008.

[78] J. Wu, H. Hu, and M Uysal "High-rate distributed space-time-frequency coding for wireless cooperative networks," IEEE Transactions Wireless Communication, vol. 10, no. 2, pp. 614–625, Feb. 2011.

[79] W. Su and X. Xia, "Signal constellations for quasi-orthogonal space time block codes with full diversity," IEEE Transactions on Information Theory, vol. 50, no. 10, pp. 2331-2347, Oct. 2004.

[80] F. Fazel and H. Jafarkhani, "Quasi-orthogonal space-frequency and space-time-frequency block codes for MIMO OFDM channels," IEEE Transactions on Wireless Communications, vol. 7, no. 1, pp. 184-192, Jan. 2008.

[81] H. Zhang, D. Yuan, and H. Chen, "On Array-Processing-Based Quasi-Orthogonal Space–Time Block-Coded OFDM Systems," IEEE Transactions on Vehicular Technology, vol. 59, no.1, pp. 508-513, Jan. 2010.

[82] W. Su and K.J. Ray Liu, "Full-rate full-diversity space-frequency codes with optimum coding advantage" IEEE Transactions on Information Theory, vol. 51, no. 1, pp. 229-249, Jan. 2005.

[83] R. Bhatia, Positive Definite Matrices, Princeton Series in Applied Mathematics, 2007.

[84] A. Dogandzic, "Chernoff bounds on pairwise error probabilities of space–time codes," IEEE Transactions on Information Theory, vol. 49, no. 5, pp. 1327–1336, May 2003.

[85] K. G. Seddik and K. J. Ray Liu, "Distributed space-frequency coding over broadband relay channels," IEEE Transactions on Wireless Communications, vol.7, no.11, pp.4748-4757, Nov. 2008.

[86] H. Wang, X. Xia, and Q. Yin, "Distributed space-frequency codes for cooperative communication systems with multiple carrier frequency offsets," IEEE Transactions on Wireless Communications, vol. 8, no. 2, pp 1045-1055, Feb 2009.

[87] L. C. Tran and A Mertins, "Space-time-frequency code implementation in MB-OFDM UWB communications: Design criteria and performance," IEEE Transactions on Wireless Communications, vol. 8, no. 2, pp. 701–713, Feb. 2009.

[88] K. Lee, Y. Kim, and J. Kang, "A novel orthogonal space-time-frequency block code for OFDM systems," IEEE Communication Letters., vol. 13, no. 9, pp. 652–654, Sep. 2009.

[89] O. Oguz, A. Zaidi, J. Louveaux, and L. Vandendorpe, "Distributed space-time-frequency block codes for multiple-access-channel with relaying," IEEE Global Telecommunications Conference, pp. 1729-1733, Nov 2007.

[90] W. Yang, Y. Cai, and B. Zheng, "Distributed space-time-frequency coding for broadband wireless relay networks," IEEE Transactions on Vehicular Technology, vol. 61, no. 1, pp. 15 – 21, Jan 2012.

[91] S. Lee, S. Han, H. Ju, J. Lee, and D. Hong, "Group-wise distributed space-time-frequency coded OFDM over asymmetric frequency-selective AF relay channels," IEEE Vehicular Technology Conference (VTC Fall), pp. 1-5, 5-8 Sept. 2011.

[92] Z. Li and X. Xia, "A distributed differentially space-time-frequency coded OFDM for asynchronous cooperative systems with low probability of interception," IEEE Transactions on Wireless Communications, vol. 8, no. 7, pp. 3372-3379, July 2009.

[93] L.Y. Song and A. G. Burr, "Differential quasi-orthogonal space-time block codes," IEEE Transactions on Wireless Communications, vol. 6, no.1, pp.64–68, Jan. 2007.

[94] W. Su, Z. Safar, and K. J. Ray Liu, "Towards maximum achievable diversity in space, time, and frequency: performance analysis and code design," IEEE Transactions on Wireless Communications, vol. 4, no. 4, pp. 1847-1857, July 2005.

[95] R.A. Horn and C.R. Johnson, Topics in matrix analysis, Cambridge University Press, 1991.